UNVEILING THE POTENTIAL: EXPLORING GELATION MECHANISMS IN ALGINATE BEADS CROSSLINKED WITH CALCIUM, COPPER AND ZINC AND THEIR VERSATILE APPLICATIONS IN AGRICULTURE AND BIOMEDICINE

Belén Reig Vañó

UNIVERSITAT ROVIRA i VIRGILI

Unveiling the Potential: Exploring Gelation Mechanisms in Alginate Beads Crosslinked with Calcium, Copper and Zinc and their Versatile Applications in Agriculture and Biomedicine

BELÉN REIG VAÑÓ

DOCTORAL THESIS
2023

UNIVERSITAT ROVIRA I VIRGILI
UNVEILING THE POTENTIAL: EXPLORING GELATION MECHANISMS IN ALGINATE BEADS CROSSLINKED WITH CALCIUM,
COPPER AND ZINC AND THEIR VERSATILE APPLICATIONS IN AGRICULTURE AND BIOMEDICINE
Belén Reig Vañó

UNIVERSITAT ROVIRA I VIRGILI
UNVEILING THE POTENTIAL: EXPLORING GELATION MECHANISMS IN ALGINATE BEADS CROSSLINKED WITH CALCIUM,
COPPER AND ZINC AND THEIR VERSATILE APPLICATIONS IN AGRICULTURE AND BIOMEDICINE
Belén Reig Vañó

Unveiling the Potential: Exploring Gelation Mechanisms in Alginate Beads Crosslinked with Calcium, Copper and Zinc and their Versatile Applications in Agriculture and Biomedicine

Doctoral Thesis

by

Belén Reig Vañó

Supervisors:
Dr. Marta Giamberini
Dr. Bartosz Tylkowski

UNIVERSITAT ROVIRA i VIRGILI

Tarragona
2023

UNIVERSITAT ROVIRA I VIRGILI
UNVEILING THE POTENTIAL: EXPLORING GELATION MECHANISMS IN ALGINATE BEADS CROSSLINKED WITH CALCIUM,
COPPER AND ZINC AND THEIR VERSATILE APPLICATIONS IN AGRICULTURE AND BIOMEDICINE
Belén Reig Vañó

UNIVERSITAT ROVIRA i VIRGILI

Departament d'Enginyeria Química

Campus Sescelades

Avda. Països Catalans, 26

43007 Tarragona

Tel.: 977 55 97 87

Fax: 977 55 96 21

Marta Giamberini, Associate Professor at Rovira i Virgili University,
Departament d'Enginyeria Química.
Bartosz Tylkowski, Head of encapsulation and membrane technologies at the Chemical Technologies Unit at Eurecat.
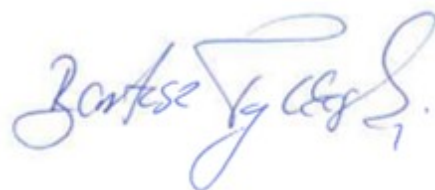
WE STATE that the present study, entitled "Unveiling the Potential: Exploring Gelation Mechanisms in Alginate Beads Crosslinked with Calcium, Copper, and Zinc and their Versatile Applications in Agriculture and Biomedicine" presented by Belén Reig Vañó for the award of the degree of Doctor has been carried out under our supervision at the Chemical Engineering Department at Rovira i Virgili University, and that it fulfils all the requirements to be eligible for the Doctor International Mention.

Tarragona, 31st of August of 2023

Supervisors of the Thesis
Dr. Marta Giamberini   Dr. Bartosz Tylkowski

UNIVERSITAT ROVIRA I VIRGILI
UNVEILING THE POTENTIAL: EXPLORING GELATION MECHANISMS IN ALGINATE BEADS CROSSLINKED WITH CALCIUM,
COPPER AND ZINC AND THEIR VERSATILE APPLICATIONS IN AGRICULTURE AND BIOMEDICINE
Belén Reig Vañó

Acknowledgements

Quiero agradecer en primer lugar a Marta Giamberini y Magdalena Olkiewicz por su apoyo. Sois y siempre seréis para mi un ejemplo a seguir tanto en lo profesional como en lo personal. También quiero agradecer a Anna Trojanowska y Monika Hapońska por ser mi brújula durante los primeros días que entraba al laboratorio y a lo largo de la tesis. Vuestra presencia y disposición fue clave para que me sintiera como en casa durante el principio de mi tesis. De igual forma quiero agradecer a mi supervisor Bartosz Tylkowski por depositar la confianza en mi y darme la oportunidad de llevar a cabo este proyecto.

Gracias también a las chicas de MEMTEC por su ayuda, Laura Carolina Valencia, Anna Mas, Yasmin Kabalan, Yaride Pérez, Iuliana Cota, y a Jordi Guardià; a los profesores Toni Reina, Alberto Puga y Ricard García-Valls por tan buenos consejos y a Xavier Montané por ayudarme durante los comienzos de mi tesis. Especialmente agradecida con Jonas Eissa Eleraky por su contundente apoyo a lo largo del proceso de esta tesis. Gracias por compartir tu alegría y optimismo conmigo.

Gràcies a les xiques de microscopia Rita Marimon, Mercé Moncusí, Núria Argany i Mariana Stefanova per la seua paciència i gran ajuda amenitzant totes i cadascuna de les hores que vaig passar al Servei.

GRÀCIES a la meua germana Aurora, la meua inspiració i el meu exemple d'esforç, disciplina i equilibri, i a mon pare Rafa, del qual vaig aprendre el que significa ser un bon líder. A les meues amigues i en especial a Fede Guerola per les llargues conversacions en els moments que més falta em vau fer. Vos vull molt. Thanks also to my flatmate and confidant Christine Justo. We always knew we would do it. Per últim, gràcies a Matheo López Pachón per la força que em vas donar per superar amb èxit el final d'aquesta etapa i per començar la següent.

I would like to express my gratitude to Professor Anna Bajek and Dr Łukasz Pokrywka from the Collegium Medicum im. Ludwika Rydygiera Bydgoszcz of Nicolaus Copernicu, Poland for welcoming me in their laboratory and enable the *in vitro* studies presented in this thesis to be possible. Additionally, thanks to Professor Magdalena Szczech from The Institute of Horticulture Research, Department of Microbiology and Rhizosphere in Skierniewice, Poland for the in collaboration that made possible to include the results regarding to Agriculture application.

Thanks also to my friends who critically read this thesis and helped me to correct language use: Matheo López Pachón, Jonas Eissa Eleraky, Mireia Sueca Comes and Łukasz Pokrywka.

Dedication

A ma mare Rosa Ana Vañó i al meu cosí Àlvar Aparisi per cuidarme ara i sempre.

Summary

Encapsulation technology has remarkably increased in the last years. It was initially created in the 1950s when dye-loaded beads were prepared for the production of carbonless copy paper. Nowadays, it is introduced as a ground-breaking field applied by many sectors such as Pharmaceutics, Agriculture and Biomedicine. Encapsulation is basically the process of coating substances within a shell or matrix, giving rise to capsules or spheres respectively. The coating material acts as a protective barrier and offers several advantages such as the controlled release, enhanced stability, improved bioavailability and targeted delivery of the encapsulated agents. These may include biologically active compounds (BACs), fragrances, cells, enzymes, and more.

One of the most interesting and extensively studied encapsulating material is alginate, which is a natural polysaccharide whose molecular structure consists of guluronic (G) and mannuronic (M) acid residues. Alginate beads may be prepared by ionotropic gelation, when an alginate aqueous solution undergoes gel formation upon exposure to a solution of polyvalent cations, or by acidic precipitation, which is a gelation process led by environmental pH values lower than the pKa of uronic residues. In the first case, the crosslinking mechanisms between cations and alginate chains have been generally described by the "egg-box" model, which suggests that negatively charged polymeric chains form electronegative cavities capable of hosting cations. Normally, counter-ions such as sodium are located in these cavities. However, during alginate gelation they might be replaced by multivalent ions.

In the first part of the thesis alginate hydrogel beads were prepared by ionotropic gelation employing a maturation time of 48h. Surprisingly, the characterization of the gelation conditions influencing the properties of resulting beads has been a neglected aspect in previous literature. However,

understanding the gelation process and the determinant factors that influence it, such as the crosslinker and its concentration, and the pH of the crosslinking bath, is important for numerous reasons, including tailoring the features of the resulting hydrogels and achieving a more effective and fruitful production.

The crosslinking agents investigated were calcium (Ca^{2+}), copper (Cu^{2+}) and zinc (Zn^{2+}). The chloride salts of these were present in the crosslinking bath at different concentrations: 0.5%, 2% and 10% (w/w). Generally, Ca^{2+} is the most frequently employed cation for alginate gelation and the most studied. Cu^{2+} was also introduced to supplement the previously reported comparisons between Ca- and Cu-based hydrogels with further assays. Nevertheless, Cu^{2+} is highly toxic under numerous contexts. In addition, Zn^{2+} was selected as an alternative to Cu^{2+} because it was considered a potential agent to obtain alginate hydrogels with unique properties required for diverse innovative applications.

The primary hypothesis was whether the crosslinking mechanism of each cation could be correlated with the physicochemical properties of the obtained hydrogels, specifically concerning the M fraction of the employed alginate. The interactions between alginate residues and the diverse cations were related with the characteristics of the obtained beads in terms of morphology, composition, binding amount and nature of the interactions involved, nanoscale structure and mechanical properties. Nevertheless, these are influenced not only by the properties of the ions involved but also by the composition and molecular weight distribution of alginate chains. Hence, alginate was first characterized by ^1H NMR and defined as high-M content. The physicochemical properties of the resulting hydrogels were thoroughly examined in our study, contributing to a better understanding of hydrogel formation, specifically concerning the M fraction of the employed alginate.

Based on the pH of the crosslinking baths, in case of Ca^{2+} and Zn^{2+} ionotropic gelation was basically considered the exclusive gelation mechanism, whereas in case of Cu^{2+} beads a hybrid system involving both ionotropic gelation along with acid precipitation was suggested when $CuCl_2$ concentration was higher than 2% (w/w). Morphological analysis revealed

very different surfaces and internal structures among the cryofractured beads, which evidenced the different crosslinking mechanisms of the three cations. Interestingly, Zn-based beads exhibited a well-defined core-shell structure, which enhances their potential for encapsulation purposes.

Mechanical characterization of the different beads combined with ESEM and microscopic observations demonstrated that in general Cu- and Zn-based systems exhibited better mechanical properties compared to Ca-based systems. This outcome can be reasonably expected due the presence of stronger and directional coordination bonds between the alginate units and the transition metals compared to the electrostatic interactions of alkaline earth metals. Besides, Ca-based beads exhibited an elastoplastic behaviour and high ductility.

The composition of hydrogel beads was investigated thought TGA. Notably, the number of uronate units per ion of Zn^{2+} remained constant within the range of concentrations studied, indicating a homogeneous coordination of uronate moieties with this cation. For Cu^{2+} the combination of ionotropic and acidic gelation elevated the number of uronate units per ion. Regarding the distinct compositions of Ca-beads, the differences might be associated to changes both in the alginate denticity and in the water molecules surrounding the cation. SAXS analysis revealed that pristine gel rod-like structure was only detected in beads obtained at lower cation concentrations. Based on FT-IR analyses, EXAFS data and beads' composition results, a hypothesis of bridging coordination was proposed for these systems.

Considering that encapsulation offers a physical barrier between the encapsulated agent and its environment, it is the most appropriate solution to protect BACs during storage and until its final use. Thus, in the second part of this thesis, alginate beads loaded with a grape seed phenolic extract were prepared employing Ca^{2+}, Cu^{2+} and Zn^{2+} as the crosslinkers, and morphologically characterized. However, any method to determine the encapsulation efficiency (EE) of BACs – by means of Folin-Ciocalteu, TGA nor HPLC, was consistent due to the formation of complexes between BACs and the crosslinking agents.

The third step of this thesis involved the assessment of the potential ben-

efits of the application of resulting beads in Agriculture and Biomedicine. On the one hand, in Agriculture, encapsulation technology offers advantages as sustainable delivery systems that effectively preserve and deliver active compounds to plants, preventing their environmental degradation and enabling sustained release. Hence, the effect of the encapsulated divalent ions (Ca^{2+}, Cu^{2+} and Zn^{2+}) released from beads on the germination and seedling growth of mustard seed was examined. The use of Ca-, Cu- and Zn-beads in soil solutions increased the concentration of respective cations. Zn-based beads raised available Cu^{2+} levels and vice versa, while Zn- and Cu-based beads lowered Ca^{2+} availability. Soil pH was crucial for cationic metal retention. The addition of perlite increased soluble cations. Cu^{2+} release inhibited germination and sprout biomass. Cu^{2+} and Zn^{2+} released from beads hindered radicle development. Ca^{2+} stimulated radicle elongation. Cu^{2+} initially increased cotyledon weight but became phytotoxic after 9 days. The results demonstrated the differential effects of cations on mustard seed germination, sprout biomass, radicle development and cotyledon weight, and provided valuable insights for agricultural practices involving the use of encapsulated cations.

On the other hand, alginate-based systems have been extensively employed for diverse Biomedical applications, including drug delivery, tissue engineering and cell encapsulation. Therefore, cell sensitivity and anti-cancer properties of the alginate beads, with and without BACs, were studied. Cytotoxicity assays were performed in different cell types: 3T3 mouse fibroblasts, T24 human urinary bladder cancer cells and SV-HUC-1 uroepitelium cells. Results revealed that the growth of 3T3 cells was not affected by Ca^{2+} nor BACs. Nevertheless, the viability of 3T3 cells was highly compromised by the extract of BACs-loaded Cu-beads. Surprisingly, at the lowest concentration, cell viability surpassed that of the control group. In SV-HUC-1 cells, the cytotoxic effects of Ca-beads extract were concentration-dependent and apparently associated with pH. Furthermore, the viability of SV-HUC-1 cells was drastically compromised at the minimum concentration of Zn-beads extract, particularly in the presence of BACs. The viability of T24 cells was negatively affected by the extracts derived from Ca-beads and BACs-loaded Ca-beads, with increasing Ca^{2+} concentrations. Interestingly, lower concentration of Cu-beads

extract seemed to promote progression of cancerous cells. Conversely, Zn-beads extract, with or without BACs, significantly reduced viability of T24 cells, except for the lowest concentration, where cell viability exceeded that of the control. Moreover, the presence of BACs in the extract led to enhanced survivability of T24 cells when compared to Zn^{2+} alone.

Therefore, these findings emphasize the dual potential of alginate beads. Firstly, they contribute to our understanding of the role of Ca^{2+}, Cu^{2+} and Zn^{2+} cations in plant growth and they highlight a sustainable and efficient strategy for enhancing crop yield, soil health and addressing environmental challenges. Simultaneously, alginate beads exhibit remarkable versatility and biocompatibility, making them valuable tools for biomedical applications. This binary utility reinforces the efficiency of alginate-based delivery systems, which not only ensure targeted beneficial effects but also promote the effectiveness of both agricultural and health-focused approaches. From Biomedicine to Agriculture, and beyond, the focus on alginate in encapsulation technology promises to continue driving innovation and shaping a more sustainable and advanced future.

Resumen

La tecnología de encapsulación ha aumentado notablemente en los últimos
años. Su origen se remonta a la década de 1950, cuando se producieron las
primeras cápsulas cargadas de colorante para la producción de papel au-
tocopiativo. Hoy en día, se presenta como un campo prometedor aplicado
por muchos sectores de la industria como la agricultura o la biomedicina.
La encapsulación es básicamente el proceso de contener sustancias dentro
de una caparazón o matriz, dando lugar a cápsulas o esferas respectiva-
mente. El material de recubrimiento actúa como barrera protectora y
ofrece varias ventajas, como la liberación controlada, una mejora de la es-
tabilidad, aumento de la biodisponibilidad y la administración selectiva de
los agentes encapsulados. Estos pueden incluir compuestos biológicamente
activos (BACs por sus siglas en ingles), fragancias, células, enzimas, y más.

Uno de los materiales de encapsulación más interesantes y estudiados es el
alginato, un polisacárido natural cuya estructura molecular está formada
por residuos de ácido gulurónico (G) y manurónico (M). Las cápsulas de
alginato pueden prepararse mediante gelificación ionotrópica, cuando una
solución acuosa de alginato transita en gel al exponerse a una solución de
cationes polivalentes, o mediante precipitación ácida, que es un proceso
de gelificación producto de valores de pH ambiental inferiores al pKa de
los residuos urónicos. En el primer caso, los mecanismos de entrecruza-
miento entre los cationes y las cadenas de alginato han sido generalmente
descritos mediante el modelo de "caja de huevos", que sugiere que las ca-
denas poliméricas cargadas negativamente forman cavidades electronega-
tivas capaces de albergar cationes. Normalmente, los contraiones, como
el sodio, se encuentran en estas cavidades. Sin embargo, durante la geli-
ficación del alginato pueden ser sustituidos por iones multivalentes.

En la primera parte de la tesis se prepararon cápsulas de alginato medi-
ante gelificación ionotrópica empleando un tiempo de maduración de 48h.
Sorprendentemente, el proceso de gelificación del alginato y su repercusión
en las características de las cápsulas resultantes no han sido estudiados en
profundidad ni caracterizados en la bibliografía existente. No obstante,
comprender los mecanismos de reticulación y los factores que determinan
la gelificación, como el agente reticulante, su concentración y el pH del

baño de reticulación, es importante por numerosas razones, entre ellas diseñar las características de los geles resultantes y lograr una producción más eficaz y fructífera.

Los agentes entrecruzantes investigados fueron el calcio (Ca^{2+}), el cobre (Cu^{2+}) y el zinc (Zn^{2+}). Las sales de cloruro de estos agentes estaban presentes en el baño de entrecruzamiento en diferentes concentraciones: 0.5%, 2% y 10% (p/p). En general, el Ca^{2+} además de ser el catión más estudiado, también es el más empleado para la gelificación del alginato. Asimismo se incluyó el Cu^{2+} para complementar las comparaciones previamente realizadas entre hidrogeles basados en Ca^{2+} y Cu^{2+} con ensayos adicionales. Sin embargo, el Cu^{2+} es altamente tóxico en numerosos contextos. Además, se seleccionó el Zn^{2+} como alternativa al Cu^{2+} porque se consideró un agente potencial para obtener hidrogeles de alginato con propiedades únicas y necesarias para diversas aplicaciones innovadoras.

La primera hipótesis fue si los diferentes mecanismos de gelificación de cada catión podían relacionarse con las propiedades fisicoquímicas de las cápsulas obtenidas, especialmente teniendo en cuenta la fracción de M del alginato empleado. Para ello, las interacciones entre los residuos de alginato y los diversos cationes se relacionaron con las características de las cápsulas obtenidas en términos de morfología, composición, cantidad de unión y naturaleza de las interacciones implicadas, estructura a nanoescala y propiedades mecánicas. Sin embargo, las propiedades fisicoquímicas de los hidrogeles no se ven influidas sólo por las propiedades de los iones implicados sino también por la composición y la distribución del peso molecular (Mw) del alginato. Por eso mismo, el alginato se caracterizó primero por RMN ^1H y se definió como de alto contenido en M o "high-M" en inglés. Las propiedades fisicoquímicas de las cápsulas resultantes se examinaron en profundidad, lo que contribuyó a una mejor comprensión de la formación de hidrogeles, específicamente en lo que respecta al alginato empleado con un alto contenido en M.

En función del pH de los baños de entrecruzamiento, en el caso del Ca^{2+} y el Zn^{2+} la gelificación ionotrópica se consideró básicamente como el mecanismo de gelificación exclusivo, mientras que en el caso de las cápsulas de Cu^{2+} se sugirió un sistema híbrido que implicaba tanto la gelificación

ionotrópica como la precipitación ácida cuando la concentración de $CuCl_2$ era superior al 2% (p/p). El análisis morfológico reveló superficies y estructuras internas muy diferentes entre las cápsulas criofracturadas, lo que evidenciaba los distintos mecanismos de reticulación de los tres cationes. Curiosamente, las cápsulas basadas en Zn presentaban una estructura de núcleo-cáscara bien definida, lo que aumenta su potencial para futuros fines de encapsulación.

La caracterización mecánica de las distintas cápsulas, combinada con las observaciones microscópicas y en ESEM, demostró que, en general, los sistemas basados en Cu^{2+} y Zn^{2+} presentaban mejores propiedades mecánicas que los basados en Ca^{2+}, probablemente debido a la presencia de enlaces de coordinación más fuertes y direccionales entre las unidades de alginato y los metales de transición, en comparación con las interacciones electrostáticas de los metales alcalinotérreos. Las cápsulas de Ca^{2+} mostraron un comportamiento elastoplástico y una elevada ductilidad.

La composición de las cápsulas se investigó mediante TGA. En particular, el número de unidades de uronato por ion de Zn^{2+} se mantuvo constante dentro del intervalo de concentraciones estudiado, lo que indica una coordinación homogénea de los residuos de uronato con este catión. En el caso del Cu^{2+}, la combinación de gelificación ionotrópica y ácida elevó el número de unidades de uronato por ion. En cuanto a las diversas composiciones de las cápsulas de Ca^{2+}, las diferencias podrían estar asociadas a cambios tanto en la denticidad del alginato como en las moléculas de agua que rodean al catión. El análisis SAXS reveló que la estructura prístina en forma de varilla de gel sólo se detectó en las cápsulas obtenidas a concentraciones más bajas de catión. A partir de los análisis FT-IR, los datos de EXAFS y los resultados de composición de las cápsulas, se propuso una hipótesis de coordinación tipo puente para estos sistemas.

Teniendo en cuenta que la encapsulación ofrece una barrera física entre el agente encapsulado y su entorno, es una solución adecuada para proteger BACs durante su almacenamiento y hasta su uso final. Así, en la segunda parte de esta tesis se prepararon cápsulas de alginato cargadas con un extracto fenólico de semilla de uva empleando Ca^{2+}, Cu^{2+} y Zn^{2+} como agentes entrecruzantes, y se caracterizaron morfológicamente. Sin

embargo, ningún método para determinar la eficiencia de encapsulación (EE) de los BACs - Folin-Ciocalteu, TGA ni HPLC, fue consistente debido a la formación de complejos entre los BACs y los cationes entrecruzantes.

El tercer paso de esta tesis consistió en la evaluación de los beneficios potenciales de las cápsulas obtenidas en aplicaciones de Agricultura y Biomedicina. Por un lado, en Agricultura, la tecnología de encapsulación ofrece sistemas de liberación sostenibles, que preservan y liberan compuestos activos a las plantas de manera efectiva, evitando su degradación y permitiendo la liberación controlada. De hecho, se examinó el efecto de la liberación de los iones encapsulados (Ca^{2+}, Cu^{2+} y Zn^{2+}) en la germinación y el crecimiento de plántulas de semillas de mostaza. El uso de las esferas de Ca^{2+}, Cu^{2+} y Zn^{2+} en las soluciones de suelo aumentó la concentración de los respectivos cationes. Las cápsulas con base de Zn^{2+} aumentaron los niveles disponibles de Cu^{2+} y viceversa, mientras que ambas redujeron la disponibilidad de Ca^{2+}. El pH del suelo fue crucial para la retención de metales catiónicos. La adición de perlita aumentó las cantidades de cationes solubles disponibles. La liberación de Cu^{2+} inhibió la germinación y la biomasa de los brotes. El Cu^{2+} y el Zn^{2+} liberados de las cápsulas mermaron el desarrollo de la radícula. El Ca^{2+} estimuló el alargamiento radicular. El Cu^{2+} inicialmente aumentó el peso del cotiledón pero se volvió fitotóxico después de 9 días. Los resultados demuestran los efectos diferenciales de los cationes en la germinación de la semilla de mostaza, la biomasa de los brotes, el desarrollo de la radícula y el peso de los cotiledones, y proporcionan conocimientos valiosos para las prácticas agrícolas que impliquen el uso de los cationes encapsulados.

Por otra parte, los sistemas de alginato han sido ampliamente empleados para diversas aplicaciones biomédicas, incluida la administración de fármacos, la ingeniería de tejidos y la encapsulación de células. Por ello, la sensibilidad celular y las propiedades anticancerígenas de las cápsulas de alginato, con y sin BACs, fueron evaluadas. Los ensayos de citotoxicidad MTT se hicieron en: fibroblastos 3T3 de ratón, células T24 de cáncer de vejiga urinaria humana y células SV-HUC-1 de uroepitelio. Los resultados indicaron que el crecimiento de las células 3T3 no se vio afectado por el Ca^{2+} ni por los BACs. No obstante, la viabilidad de las células 3T3 se vio muy comprometida por extracto de las cápsulas de Cu BACs 10%.

17

Sorprendentemente, a concentraciones más bajas, la viabilidad celular superó incluso la del grupo de control. En el caso de las células SV-HUC-1, los efectos citotóxicos del extracto de cápsulas de Ca^{2+} dependieron de la concentración y parecían estar asociados al valor de pH. Además, la viabilidad de las células SV-HUC-1 se vio drásticamente comprometida a concentración mínima de extracto de cápsulas de Zn^{2+}, efecto que se intensificó en presencia de BACs. La viabilidad de las células T24 se vio negativamente comprometida por los extractos derivados de las esferas de Ca^{2+} con y sin BACs, siendo el efecto más pronunciado a medida que aumentaba la concentración de Ca^{2+}. No obstante, el extracto de las cápsulas de Cu^{2+} no mostró toxicidad a concentraciones más bajas y, curiosamente, pareció promover la progresión de las células cancerosas. Por el contrario, el extracto de las cápsulas basadas en Zn^{2+}, con o sin BACs, disminuyó significativamente la viabilidad de las células T24, excepto a la concentración más baja en la que la viabilidad celular superó a la del control. De hecho, la presencia de BACs en el extracto dio lugar a una mayor supervivencia celular en comparación con el Zn^{2+} solo.

Por tanto, estos resultados exponen el doble potencial de las esferas de alginato. En primer lugar, contribuyen a nuestra comprensión del papel de los cationes Ca^{2+}, Cu^{2+} y Zn^{2+} en el crecimiento de las plantas y ponen de relieve una estrategia sostenible y eficiente para mejorar el rendimiento de los cultivos, la abundancia del suelo y hacer frente a los retos medioambientales. Al mismo tiempo, las cápsulas de alginato presentan una notable versatilidad y biocompatibilidad, lo que las convierte en valiosas herramientas para aplicaciones biomédicas. Esta utilidad refuerza la efectividad de los sistemas de administración basados en alginato, que no sólo garantizan efectos beneficiosos particulares sino que también promueven la eficacia de los enfoques tanto agrícolas como sanitarios. Desde la Biomedicina, pasando por la Agricultura, el alginato como tecnología de encapsulación promete seguir impulsando la innovación y dando forma a un futuro más sostenible y avanzado.

Resum

La tecnologia d'encapsulació ha augmentat notablement en els darrers anys. El seu origen es remunta a la dècada del 1950, quan es van preparar les primeres càpsules carregades de colorant per a la producció de paper autocopiatiu. Avui dia, es presenta com un camp prometedor aplicat per molts sectors de la indústria com ara l'Agricultura o la Biomedicina. L'encapsulació és bàsicament el procés de contenir substàncies dins una closca o matriu, donant lloc a càpsules o esferes respectivament. El material de recobriment actua com a barrera protectora i ofereix diversos avantatges, com l'alliberament controlat, una millora de l'estabilitat, l'augment de la biodisponibilitat i l'administració selectiva dels agents encapsulats. Aquests poden incloure compostos biològicament actius (BACs per les sigles en anglès), fragàncies, cèl·lules, enzims, i més.

Un dels materials d'encapsulació més interessants i estudiats és l'alginat, un polisacàrid natural l'estructura molecular del qual està composta per residus d'àcid gulurònic (G) i manurònic (M). Les càpsules d'alginat es poden preparar mitjançant gelificació ionotròpica, quan una solució aquosa d'alginat transita en gel a l'exposar-se a una solució de cations polivalents, o mitjançant precipitació àcida, que és un procés de gelificació dirigit per valors de pH ambiental inferiors al pKa dels residus urònics. En el primer cas, els mecanismes d'entrecreuament entre cations i les cadenes d'alginat s'han descrit generalment mitjançant el model de "caixa d'ous", que suggereix que les cadenes polimèriques carregades negativament formen cavitats electronegatives capaces d'allotjar cations. Normalment, els contraions, com ara el sodi, es troben en aquestes cavitats. No obstant, durant la gelificació de l'alginat aquests son substituïts pels ions multivalents.

A la primera part d'aquesta tesi es van preparar esferes d'alginat mitjançant gelificació ionotròpica, emprant un temps de maduració de 48h. Sorprenentment, el procés de gelificació i la seva repercussió en les característiques de les càpsules resultants no han estat estudiats en profunditat ni caracteritzats a la bibliografia existent. No obstant, comprendre els mecanismes de reticulació i els factors que determinen la gelificació, com l'agent reticulant, la seua concentració i el pH del bany de reticulació,

és important per nombroses raons, entre elles per dissenyar les característiques dels hidrogels resultants i aconseguir una producció més eficaç i fructífera.

Els agents entrecreuants investigats van ser el calci (Ca^{2+}), el coure (Cu^{2+}) i el zinc (Zn^{2+}). Al bany d'entrecreuament es trobaven les sals de clorur d'aquests cations en diferents concentracions: 0.5%, 2% i 10% (p/p). En general, a més de ser el més estudiat, el Ca^{2+} també és el catió més emprat per a la gelificació de l'alginat. També es va incloure el Cu^{2+} per complementar les comparacions prèviament realitzades entre hidrogels basats en Ca^{2+} i en Cu^{2+} amb assajos addicionals. No obstant això, el Cu^{2+} és altament tòxic sota nombrosos contextos. A més, es va seleccionar el Zn^{2+} com a alternativa al Cu^{2+} perquè es va considerar un agent potencial per obtenir hidrogels d'alginat amb propietats úniques i necessàries per diverses aplicacions innovadores.

La primera hipòtesi va ser si els mecanismes de gelificació de cada catió podien relacionar-se amb les propietats fisicoquímiques de les esferes obtingudes, especialment tenint en compte la fracció de M de l'alginat emprat. Per això, les diferents interaccions entre els residus d'alginat i els diversos cations es van relacionar amb les característiques de les càpsules obtingudes en termes de morfologia, composició, quantitat d'unió i naturalesa de les interaccions implicades, estructura a nanoescala i propietats mecàniques. Tot i això, les propietats fisicoquímiques dels hidrogels no es veuen influïdes només per les propietats dels ions implicats sinó també per la composició i la distribució del pes molecular (Mw) de l'alginat. Per això mateix, l'alginat es va caracteritzar primer per RMN ^1H i es va definir amb alt contingut en M o "high-M" en anglès. Les propietats fisicoquímiques de les esferes resultants es van examinar en profunditat, fet que va contribuir a una millor comprensió de la formació dels hidrogels, específicament pel que fa a l'alginat emprat amb un alt contingut en M.

En funció del pH dels banys d'entrecreuament, en el cas del Ca^{2+} i el Zn^{2+} la gelificació ionotròpica es va considerar bàsicament com el mecanisme de gelificació exclusiu, mentre que en el cas de les càpsules de Cu^{2+} es va suggerir un sistema híbrid que implicava tant la gelificació ionotròpica com la precipitació àcida quan la concentració de $CuCl_2$ era superior al 2% (p/p).

L'anàlisi morfològic va revelar superfícies i estructures internes molt diferents entre les càpsules criofracturades, cosa que evidenciava els diversos mecanismes de reticulació dels tres cations. Curiosament, les càpsules basades en Zn^{2+} presentaven una estructura de nucli-closca ben definida, cosa que augmenta el seu potencial per a futurs fins d'encapsulació.

La caracterització mecànica de les diferents esferes, juntament amb les observacions microscòpiques i d'ESEM, van demostrar que, en general, els sistemes basats en Cu^{2+} i Zn^{2+} presentaven millors propietats mecàniques que els basats en Ca^{2+}, probablement a causa de la presència d'enllaços de coordinació més forts i direccionals entre les unitats d'alginat i els metalls de transició, en comparació amb les interaccions electrostàtiques dels metalls alcalinoterris.

La composició de les esferes es va investigar mitjançant TGA. En particular, el nombre d'unitats d'uronat per ió de Zn^{2+} es va mantenir constant dins l'interval de concentracions estudiat, cosa que indica una coordinació homogènia dels residus d'uronat amb aquest catió. En el cas del Cu^{2+}, la combinació de gelificació ionotròpica i àcida va elevar el nombre d'unitats d'uronat per ió. Pel que fa a les diverses composicions de les càpsules de Ca^{2+}, les diferències podrien estar associades a canvis tant a la denticitat de l'alginat com a les molècules d'aigua que envolten el catió. A partir dels anàlisis FT-IR, les dades d'EXAFS i els resultats de composició de les càpsules, es va proposar una hipòtesi de coordinació tipus pont per a aquests sistemes.

Tenint en compte que l'encapsulació ofereix una barrera física entre l'agent encapsulat i el seu entorn, aquesta és una solució adequada per protegir BACs durant l'emmagatzematge i fins l'ús final. Així és que a la segona part d'aquesta tesi es van preparar càpsules d'alginat carregades amb un extracte fenòlic de llavor de raïm emprant Ca^{2+}, Cu^{2+} i Zn^{2+} com a agents entrecreuants i es van caracteritzar morfològicament. Tot i això, cap mètode per determinar l'eficiència d'encapsulació (EE) dels BACs - Folin-Ciocalteu, TGA ni HPLC, va ser consistent a causa de la formació de complexos entre els BACs i els cations entrecreuants.

El tercer pas d'aquesta tesi va consistir en l'avaluació dels beneficis potencials de les esferes obtingudes per aplicacions d'Agricultura i Biomedicina. D'una banda, en Agricultura, la tecnologia d'encapsulació ofereix sistemes d'alliberament sostenibles, per preservar i alliberar compostos actius a les plantes de manera efectiva, evitant-ne la degradació i permetent l'alliberament controlat. Per això, es va examinar l'efecte de l'alliberament dels ions encapsulats (Ca^{2+}, Cu^{2+} i Zn^{2+}) en la germinació i el creixement de plàntules de llavors de mostassa. Així és que l'ús de les esferes basades en Ca^{2+}, Cu^{2+} i Zn^{2+} en les solucions de sòl va augmentar la concentració dels cations respectius. Les càpsules amb base de Zn^{2+} van augmentar els nivells disponibles de Cu^{2+} i viceversa, mentre que les esferes amb base de Cu^{2+} i Zn^{2+} van reduir la disponibilitat de Ca^{2+}. El pH del sòl va ser la raó de la retenció de metalls catiònics. L'addició de perlita sí que va augmentar els cations solubles disponibles. L'alliberament de Cu^{2+} va inhibir la germinació i la biomassa dels brots. El Cu^{2+} i el Zn^{2+} alliberats de les càpsules van minvar el desenvolupament de la radícula. El Ca^{2+} va estimular l'allargament radicular. El Cu^{2+} inicialment va augmentar el pes del cotiledó però es va tornar fitotòxic després de 9 dies. Els resultats demostren els efectes diferencials dels cations en la germinació de la llavor de mostassa, la biomassa dels brots, el desenvolupament de la radícula i el pes dels cotilèdons i proporcionen idees valuoses per a les pràctiques agrícoles que impliquin l'ús dels cations encapsulats.

D'altra banda, els sistemes basats en alginat han estat àmpliament emprats per a diverses aplicacions biomèdiques, inclosa l'administració de fàrmacs, l'enginyeria de teixits i l'encapsulació de cèl·lules. Per això, la sensibilitat cel·lular i les propietats anticancerígenes de les esferes d'alginat, amb i sense BACs, van ser avaluades. Els assaigs de citotoxicitat MTT es van dur a terme en: fibroblasts 3T3 de ratolí, cèl·lules T24 de càncer de bufeta urinària humana i cèl·lules SV-HUC-1 d'uroepiteli. Els resultats indicaren que el creixement de les cèl·lules 3T3 no es va veure afectat per la concentració de Ca^{2+} ni pels BACs. Tot i això, la viabilitat de les cèl·lules 3T3 es va veure molt compromesa per l'extracte de càpsules BACs basades en Cu^{2+}. Sorprenentment, a la concentració més baixa, la viabilitat cel·lular va superar fins i tot la del grup control. En el cas de les cèl·lules SV-HUC-1, els efectes citotòxics de l'extracte de càpsules de Ca^{2+}

van ser dependents de la concentració i semblaven estar associats al pH. A més, la viabilitat de les cèl·lules SV-HUC-1 es va veure dràsticament compromesa a la concentració mínima d'extracte de càpsules de Zn^{2+}, efecte que es va intensificar en presència de BACs. La viabilitat de les cèl·lules T24 es va veure negativament afectada pels extractes derivats de les esferes de Ca^{2+} i d'aquestes esferes carregades de BACs, sent l'efecte més pronunciat a mesura que augmentava la concentració de Ca^{2+}. Curiosament, la dilució més baixa d'extracte de Cu^{2+} no va ser tòxica i, de fet, semblava promoure la progressió de les cèl·lules canceroses. Per contra, l'extracte de les esferes basades en Zn^{2+}, amb BACs o sense, va disminuir significativament la viabilitat de les cèl·lules T24, excepte en la concentració més baixa, en què la viabilitat cel·lular va superar la del control. A més, la presència de BACs a l'extracte va conduir a una supervivència cel·lular més gran en comparació del Zn^{2+} sol.

Per tant, aquests resultats exposen el doble potencial de les esferes d'alginat. En primer lloc, contribueixen a la nostra comprensió del paper dels cations Ca^{2+}, Cu^{2+} i Zn^{2+} en el creixement de les plantes i posen en relleu una estratègia sostenible i eficient per millorar el rendiment dels cultius, l'abundància del sòl i fer front als reptes mediambientals. Alhora, les càpsules d'alginat presenten una versatilitat i biocompatibilitat notables, fet que les converteix en eines valuoses per a aplicacions biomèdiques. Aquesta utilitat reforça l'eficiència dels sistemes d'administració basats en alginat, que no només garanteixen efectes beneficiosos específics sinó que també promouen l'eficàcia dels enfocaments agrícoles i sanitaris. Des de la Biomedicina, passant per l'Agricultura, l'alginat com a tecnologia d'encapsulació promet continuar impulsant la innovació i donant forma a un futur més sostenible i avançat.

Publications

- X. Montané, O. Kowalczyk, B. Reig-Vano, A. Bajek, K. Roszkowski, R. Tomczyk, W. Pawliszak, M. Giamberini, A. Mocek-Płóciniak and B. Tylkowski*, Current Perspectives of the Applications of Polyphenols and Flavonoids in Cancer Therapy, Molecules, 25, 3342 (2020)

- B. Reig-Vano, B. Tylkowski, X. Montané, M. Giamberini, Alginate-based hydrogels for cancer therapy and research, International Journal of Biological Macromolecules, 170, 424–436 (2021)

- X. Montané, K. Matulewicz, K. Balik, P. Modrakowska, M. Łuczak, Y. Pérez Pacheco, B. Reig-Vano, J.M. Montornés, A. Bajek, B. Tylkowski, Present trends in the encapsulation of anticancer drugs, Physical Sciences Reviews, 8, 327-344 (2023)

- B. Reig-Vano, C. Huck-Iriart, S. de la Flor, A. Trojanowska, B. Tylkowski, M. Giamberini, Structural and mechanical analysis on mannuronate-rich alginate gels and xerogels beads based on Calcium, Copper and Zinc as crosslinkers, International Journal of Biological Macromolecules, 246, 125659 (2023)

Book Chapter

- X. Montané, K. Matulewicz, K. Balik, P. Modrakowska, M. Łuczak, Y. Pérez Pacheco, B. Reig-Vano, J.M. Montornés, A. Bajek and B. Tylkowski, Present trends in the encapsulation of anticancer drugs, in book Medical Physics, Models and Technologies in Cancer Research, Eds. by A. Bajek, B. Tylkowski, 2021, ISBN: 9783110662290 , De Gruyter, Berlin, Boston, pp. 193-212

Congresses

- M. Giamberini, B. Tylkowski, M. Olkiewicz, B. Reig-Vano, K. Matulewicz and Ł. Kaźmierski, Chitosan/alginate based macrocapsules as an oral delivery system of DCA, 14th Mediterranean Congress of Chemical Engineering (MeCCE-14), Oral presentation, November 2020, Barcelona (Spain)

- B. Reig-Vano, M. Giamberini and B. Tylkowski, Alginate-based macrocapsules as an oral delivery system of grape seed polyphenols, 14th Mediterranean Congress of Chemical Engineering (MeCCE-14), Oral presentation, September 2021, Barcelona (Spain)

- B. Reig-Vano, M. Giamberini and B. Tylkowski, Alginate macrocapsules of phenolic compounds, 17th Doctoral Day at Rovira i Virgili University, Poster, May 2022, Tarragona (Spain)

- B. Reig-Vano, M. Giamberini, B. Tylkowski, S. de la Flor and A. Trojanowska, Relating Crosslinking Mechanism and Physicochemical Properties of Alginate Beads prepared with Calcium, Copper and Zinc, 18th Doctoral Day at Rovira i Virgili University, Poster, May 2023, Tarragona (Spain)

- B. Reig-Vano, M. Giamberini, B. Tylkowski, S. de la Flor, C. Huck-Iriart and A. Trojanowska, Insights in High-M content alginate hydrogels: Relating crosslinking mechanisms with resultant hydrogel's physicochemical features, 15th Mediterranean Congress of Chemical Engineering (MeCCE-15), Poster, February 2023, Barcelona (Spain)

Abbreviations

Alg — Alginate

G — Guluronic acid

M — Mannuronic acid

U — Uronates or uronic residues of mannuronic and guluronic acid

Ca^{2+} — Calcium ions

Cu^{2+} — Copper ions

Zn^{2+} — Zinc ions

MCl_2 — Salt chloride

$BACs$ — Biologically active compounds

TPC — Total phenol content

EE — Encapsulation efficiency

FC — Folin–Ciocalteu

GA — Gallic acid

Mo — Molybdenum

Na_2CO_3 — Sodium cabonate

$H_3PW_{12}O_{40}$ — Phosphotungstic acid

$H_3PMo_{12}O_{40}$ — Phosphomolybdic acid

FT-IR — Fourier-transform infrared

ATR — Attenuated total reflectance

$^1H\ NMR$ — Nuclear magnetic resonance

D_2O — Deuterium oxide

FG and FM — Molar fraction of monads

FGG, FMM, FGM and FMG — Molar fraction of diads

ESEM — Environmental scanning electron microscopy

EDX — Energy dispersive X-Ray spectroscopy

HPLC — High-performance liquid chromatography

ICP-OES — Inductively coupled plasma optical emission spectroscopy

MALDI-TOF — Matrix-Assisted Laser Desorption/Ionization Time-Of-Flight

MS — Mass spectrometry

ESI — Electrospray ionization

E — Young's modulus [Pa]

σ_b — Stress at break [Pa]

D — Diameter [m]

26

F Force [N]

ΔL Displacement [m]

ν Poisson ratio

Mw Molecular weight [g/mol]

W_m Water mass [g]; the weight loss until 170°C

NPs Nanoparticles

TGA   Thermogravimetric analyses

XRD   X-ray diffraction

WAXS   Wide angle X-ray diffraction

EXAFS   Extended X-ray absorption fine structure

SAXS   Small angle X-ray diffraction

λ Beam wavelength [cm^{-1}]

2θ Scattering angle [°]

R_g Radius of gyration of the scatterer [nm]

S Power law exponent at low angles

d Porod exponent

MTT 3-[4,5-dimethylthiazol-2-yl]-2,5 diphenyl tetrazolium bromide

$DMSO$ Dimethyl sulfoxide

HCl Hydrochloric acid

FBS   Fetal bovine serum

DMEM   Dulbecco's modified Eagle's medium

PBS   Phosphate-buffered saline

3T3   Primary mouse embryonic fibroblasts

T24   Human urinary bladder cancer cells

SV-HUC-1   Human uroepithelium cells

S Soil

SS Soil solution

$\mathring{A}$ Angstrom

A Area [m^2]

Ar Argon

°C   Celsius degree

cm Centimeter

eq Equation

g Gram

h Hour

min Minutes

mg Milligram

mL Milliliter

nm Nanometer

pH Potential of hydrogen

rpm Revolutions per minute

w Weight [kg]

z Charge

w/w Weight percentage

Contents

ii

List of Figures

List of Tables

Chapter 1

General introduction and objectives

1.1   Alginate

1.1.1   Chemical structure

Alginate (Alg) is a classification encompassing a whole family of natural polysaccharides, including alginic acid and Alg salts. These polymers consist of unbranched copolymers composed of $\beta(1{\rightarrow}4)$ linked β-D-mannuronic acid (M) and its C-5 epimer α-L-guluronic acid (G), which are the monomeric units. G and M monomers organize in a non-regular block-wise pattern where homosequences of consecutive M or G residues (M- and G-blocks) are interspersed with G/M heterosequences (Figure 1.1) [1, 2, 3]. The molecular weight (Mw) of Alg ranges from 32 to 400 kg/mol [2]. It is important to note that the Mw, composition, and hence, Alg features depend on the origin [1, 2, 4].
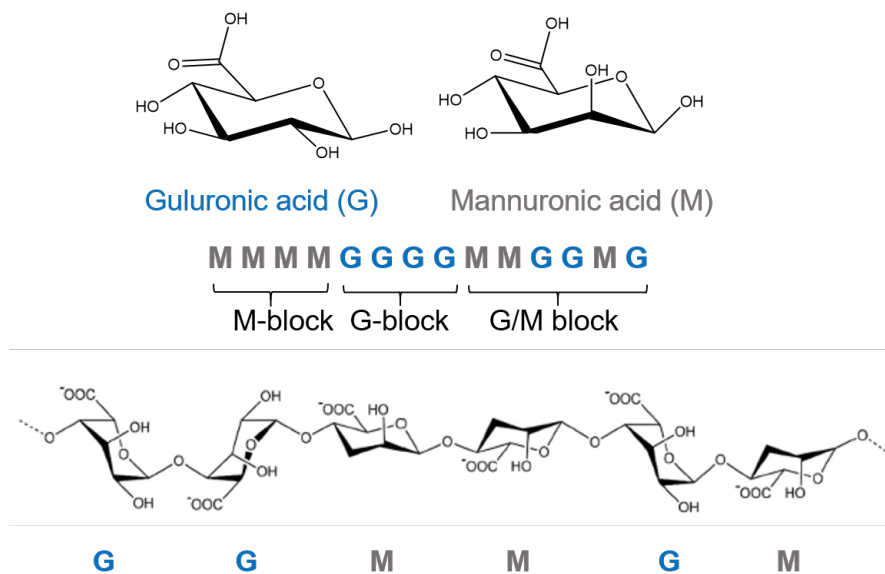
Figure 1.1: Chemical structure of Alg residues: mannuronic (M) and guluronic acid (G)

1.1.2   Sources and extraction

Alginates are found in a broad spectrum of brown algae such as *Macrocystis pyrifera, Laminaria hyperborea, Durvillaea Antarctica, Laminaria japonica, Laminaria digitate, Lessonia nigrescens, Ecklonia maxima, Ascophyllum nodosum* and *Sargassum* spp [2, 5]. For their extraction, counterions are firstly removed. Subsequently, alginic acid is neutralized and solubilized into Alg salts [6]. Sodium hydroxide or sodium carbonate might serve as alkali compounds that result in sodium Alg [4].

Alg is also biosynthesized as an exopolysaccharide by two different genera of bacteria: *Pseudomonas* and *Azotobacter* [7]. Alginates from *Azotobacter* have a great G-content and contribute to cysts, which are structures considerably resistant to desiccation [7]. In *Pseudomonas aeruginosa*, highly arranged Alg biofilms enable resistance against antibiotics while remaining undetected by the host immune system.

Bacteria produce high quality alginates compared to algae. They have superior properties and their structures are better characterized [4, 8]. Commonly, M/G ratio is higher too [3].

Nowadays, more than 200 different types of alginates are commercially available [1]. In spite of the heterogeneous composition, they normally proceed from farmed brown seaweeds. The specie and algae age is the main source of Alg variability [9].

2

1.2   Alginate gelation

The aqueous solution of Alg, also referred to as "sol" phase, is able to form stable hydrogels. The "sol" phase consists of closely linked Alg chains. The introduction of crosslinking agents enhances the linking process, resulting in the formation of the insoluble "gel" phase. This phenomenon is known as the "sol-to-gel" transition or Alg gelation [8, 10]. The formation of stable Alg hydrogels requires a minimum concentration of Alg 1% (w/w). These are capable of holding one hundred times their load in water by means of hydrogen bonding [1, 3].

Alginate gelation can be achieved through two distinct methods, resulting in either an ionic gel (ionotropic gelation) or an acidic gel (acid precipitation)[11].

The pKa values of G and M monomers are 3.65 and 3.38 respectively [11]. At higher pH values, the carboxyl groups undergo deprotonation, leading to repulsion between negatively charged polymeric chains. Alg is deprotonated across a broad range of pH values. Conversely, pH values lower than the pKa values result in protonation of carboxylates, leading to charge neutralization, chain aggregation, and acid precipitation [12]. A significant pH drop causes the precipitation of alginic acid aggregates, while a gradual decrease yields bulk formation of alginic acid gel. Acidic gels are primarily stabilized by hydrogen bonds, with M-blocks playing a crucial and necessary role in this process [11].

Alternatively, ionotropic gelation occurs when multivalent cations or cationic polymers present in the medium chelate the carboxyl moieties of uronic residues (U) [13]. Ionotropic gelation can be promoted by both external and internal mechanisms, depending on the source of the crosslinking agent [14]. As a matter of example, Figure 1.2 illustrates both gelation mechanisms involving Ca^{2+} ions.

External gelation occurs when multivalent cations from an external source diffuse through the "sol" phase. For instance, when a "sol" phase, normally in the form of droplets, is extruded into a crosslinking bath, it results in a "sol-to-gel" transition (Figure 1.2a). The crosslinking bath typically consists of an aqueous solution of a salt, such as calcium chloride. The crosslinking ions diffuse within the droplets, resulting in the formation of rounded gels with a uniform morphology. Due to the quick diffusion, the distribution of crosslinking agent is heterogeneous, with a higher concentration on the surface of the droplet compared to the inner parts. The concentration gradient depends on the diffusion kinetics [4, 11, 14]. Ionic crosslinking this process involves

ion exchange, and the gelation process is commonly described by the "egg-box" model [8, 10], as detailed in section 1.2.1.
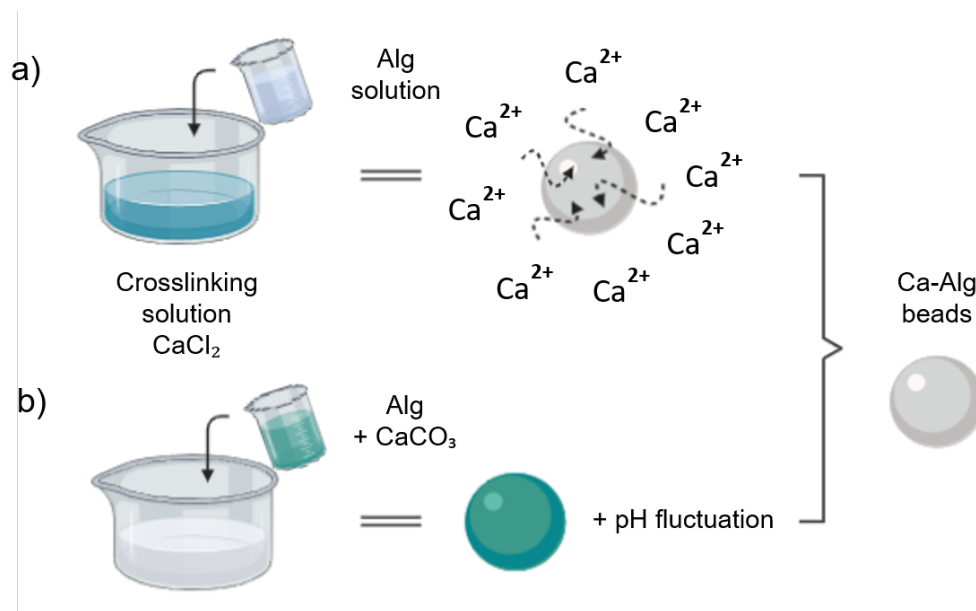
Figure 1.2: Schematic representation of a) external and b) internal gelation of Alg with Ca^{2+} ions.

The process of internal gelation involves the incorporation of an inactive form of the crosslinking agent within the "sol" phase. For example, some internal sources of calcium would be insoluble salts such as calcium tartrate, citrate, phosphate, oxalate and carbonate (Figure 1.2b). Gelation occurs through the activation of the crosslinker and cation release, enabled by the modulation of system properties such as pH and ion solubility [4]. Hydrogels obtained by internal gelation are homogeneous and display uniform ion distribution [6]. They are usually fragile and susceptible to being clustered [15, 16].

Ionotropic gelation is a fast, simple and cost-effective method carried out under gentle conditions [3, 14, 16]. Additionally, Alg gelation can be performed by gamma irradiation [17, 18] or by photo-crosslinking [5, 19]. Alg may be as well covalently crosslinked with agents such as glutaraldehyde [20, 21] or poly(ethylene glycol)-diamine [22]. In spite of enhancing the physicochemical properties of the hydrogels, reagents for covalent crosslinking might be noxious [1]. These methods can be combined with ionotropic crosslinking.

4

1.2.1   Alginate crosslinking and the "egg-box" model

When Alg chains contact the crosslinking cation, hydrogel forms and interactions evolve during the "maturation time". The interactions between the polymeric chains and multivalent cations have been always explained by the "egg-box" model (Figure 1.3). It suggests that G homosequences from adjacent chains form electronegative cavities, also known as "egg-box junctions", which have to ability to host multivalent cations [8]. Normally, counter-ions such as sodium are located in these cavities [6]. Nonetheless, during Alg gelation they might be replaced by multivalent ions whose size and charge also fit in [10]. The "egg-box" structure forms as a result of the ion exchange [8].

The coordination was supposed to be promoted by the oxygen atoms of carboxylic groups of cooperative G-blocks [11, 23] (Figure 1.3). Although only G-blocks were considered to take part in intermolecular crosslinking [1], MGM-blocks might contribute too though weak interactions [4, 5, 24].
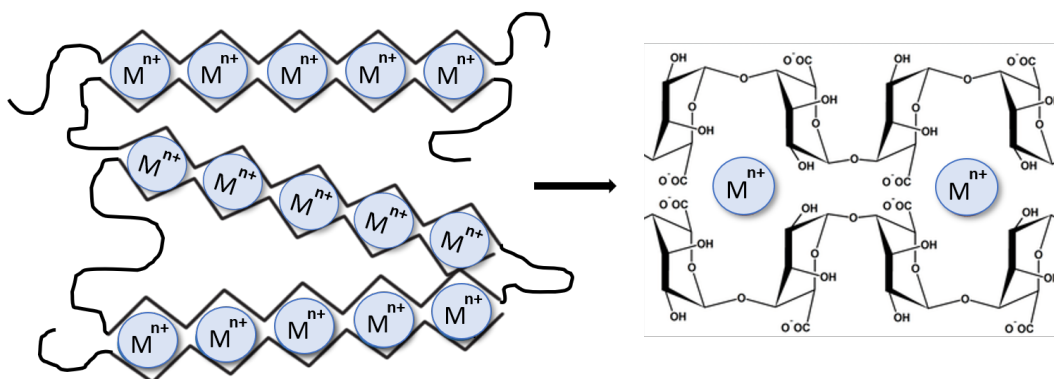
Figure 1.3: Schematic formulation of "sol-to-gel" transition and the "egg-box" model. G-blocks are represented by zig-zag portions whereas M-blocks and heterosequences are represented by the smooth parts of the polymeric chains

Gelation occurs when multivalent cations interact with the carboxylic groups of adjacent residues. The orientation of the Alg monomers plays a critical role in the gelation process. The horizontal alignment of M residues reduces the crosslinking probability, whereas the vertical orientation of G monomers increases the chances of interaction between adjacent units, promoting gelation [25]. As a result, Alg with higher M/G ratios will have a lower density of crosslinkers. Not only the Mw distribution but also the relative M/G ratio significantly influences the number of crosslinking

sites and, consequently, the physicochemical properties of hydrogels. These properties are further influenced by the characteristics of the crosslinking cation, such as valence and radius [11].

1.2.2   Ions employed as crosslinking agents

Alg gelation can be induced by various cations [6]. These crosslinking ions can be ranked based on their affinity to Alg: Mn < Zn, Ni, Co < Fe < Ca < Sr < Ba < Cd < Cu < Pb [11]. Among them, calcium (Ca) is the most commonly employed [4, 5, 16]. However, certain crosslinkers such as Cu, Pb, Cd, Sr and Ba, due to their high toxicity, are avoided for practical reasons [11].

The crosslinking mechanisms are considerably defined by the valency and radius of the cation [15]. Alg can be cross-linked by both bivalent and trivalent cations [14]. Nevertheless, chemical interactions are stronger with trivalent cations since they involve three carboxyl groups from different Alg chains instead of two [11]. Crosslinking with trivalent cations leads to the formation of stronger interactions and 3D networks [11].

The final characteristics of the hydrogel are influenced by the choice of crosslinker and the nature of its interactions with Alg [25]. The concentration of crosslinker also plays a role in determining the properties of the resulting hydrogels. Below a certain concentration threshold, crosslinking is ineffective, and gelation does not occur. As the concentration increases, the number of crosslinking bonds rises, resulting in significant effects. However, once the maximum degree of crosslinking is achieved, further increases in the concentration of the crosslinking agent may not yield significant differences [26]. Higher number of bonds leads to more compact hydrogels [26, 27].

All in all, features such as the size, surface characteristics and stability of the hydrogel are determined by the crosslinker [10, 28] and its concentration [29]. By tuning the appropriate crosslinker and its concentration, specific properties may be achieved. In this thesis, the focus was on the utilization of Ca^{2+}, Cu^{2+} and Zn^{2+} as crosslinking cations for Alg.

1.2.2.1   Calcium

Ca^{2+} is the most frequently employed ion for Alg gelation [4, 5, 16]. Specially, calcium chloride ($CaCl_2$) is employed as the Ca^{2+} source due to its high-water solubility, fast ionotropic gelation and non-toxicity [30].

Considering the gelation kinetics as an important parameter for hydrogel properties, slower gelation gives rise to improved organizations in regard to structure and mechanical integrity [31]. Soluble Ca^{2+} lead to quick but poorly oriented Alg gelation [1, 25, 32]. The fast crosslinking results in soft hydrogels [25]. Nevertheless, gelation rate can be tuned by factors such as Ca^{2+} concentration, pH and temperature [33, 34]. Reduced Ca^{2+} diffusion and delayed crosslinking rate might lead to more organized 3D networks and consequently, to improved physicochemical characteristics [35]. The surface morphology of Ca-Alg hydrogels is usually smooth, uniform and displays high porosity [3, 36].

Given that both affinity and Alg complexation are moderated, Ca^{2+} diffusion is continuous [36]. It has been evidenced that in Ca-based Alg hydrogels, the concentration of Ca^{2+} is higher on the surface that comes into contact with the crosslinking bath. Ca^{2+} diffuses among polymeric chains and interact with unoccupied binding sites. At the beginning, residues are unoccupied and Ca^{2+} quickly binds. Nevertheless, when the gel already forms and binding sites begin limited, Ca^{2+} ions must further diffuse. That is, crosslinking reaction progresses from the surface among the inner parts of the hydrogel. Ca^{2+} distribution is parabolic throughout the centre [36].

Increasing Ca^{2+} concentration in the crosslinking bath enlarges the concentration gradient, which favours diffusion [32]. Simultaneously, resistance to diffusion raises. The diffusional resistance has been proved to increase when $CaCl_2$ concentration is above 4% (w/v) and it is constant within the range from 1.3 to 4% (w/v) [32].

Although just G-blocks were considered to contribute in Alg gelation through intermolecular crosslinking with Ca^{2+} [1], MGM-blocks have been also evidenced to be involved through weak interactions [4, 5, 25]. At low concentration, G-blocks exhibit high affinity toward Ca^{2+}. At higher concentrations, Ca^{2+} ions might also bind to M-blocks and G/M heterosequences [37].

The binding of Ca^{2+} to G-blocks has been proved to be a multicoordination with the oxygen atoms of the carboxylate groups. At least eight adjacent G monomers are required for the establishment of firm junctions – "egg-box junctions" [11]. Computational models pointed Ca-Alg binding to be based only on electrostatic interactions

7

[37]. Hence, Ca^{2+} and oxygen orbitals do not overlap orbitals and remain localized around the cation center.

Ca^{2+} is an essential macronutrient involved in numerous cellular processes, signalling pathways and regulation of gene expression. In regard to plants, for instance, it contributes to significant functions including the maintenance of cell membrane structure and permeability, plant cell division and elongation, carbohydrate translocation and nitrogen metabolism [38, 39]. In addition, Ca^{2+} plays a regulatory role in signal transduction and nutrient absorption across the cell membrane [39, 40].

1.2.2.2 Copper

The strong Cu-Alg affinity leads to a fast and strong complexation [41]. The outermost part of the hydrogels normally consists of highly complexated Alg (almost precipitated), which seals the surface pores. Thus, low porosity structures are obtained [36]. The surface of the Cu-Alg hydrogels is very rough and comparable to a group of many small unrelated microgels probably as a consequence of inhomogeneous Cu^{2+} complexation [36].

In the case on hydrogel beads, the formation of a dense outer layer prevents Cu^{2+} diffusion toward the inner parts, which appear to lack material when observed under the microscope. Besides, the outer coat enhances the rigidity of the beads [42].

Some studies point Cu^{2+} concentration to be less determining for the resultant hydrogels properties, compared to Ca^{2+} [36, 42]. Following this premise, lower Cu^{2+} concentrations in comparison to Ca^{2+} seem to be enough to entirely complex the available U, probably due to the ten times higher affinity of Cu^{2+} in regard to Ca^{2+} [43].

The binding mechanism of Cu^{2+} to Alg is nonspecific [41]. Therefore, Cu^{2+} show a lack of selectivity for M or G residues. In addition, Cu^{2+} coordinate Alg by the formation of strong covalent bonds [37].

In vivo, Cu^{2+} is a trace metal which is part of several essential enzymes [44]. Cu^{2+} forms bioactive complexes with peptides and proteins [45]. Moreover, it exhibits angiogenic properties and plays a key role in bone formation [46]. Cu^{2+} supports the normal functioning of neutrophils and monocytes and modulates antimicrobial signalling in macrophages [47]. Additionally, Cu^{2+} is a micronutrient necessary during the primary phases of plant growth, contributing to the functionality of photosynthetic and respiratory electron transport chains. It also provides protective functions

against oxidative stress and contributes to cell wall metabolism [48, 49]. Furthermore, Cu^{2+} has been reported to possess bactericidal and antifungal activities [50, 51]. Hence, it has been traditionally employed for the extermination of several diseases in different crops. However, its extensive release intro the environment by human activities lead to environmental contamination.

The therapeutic concentration range of Cu^{2+} is relatively narrow and it results in powerful biological responses [45]. As a result, it has been employed in many Biomedical applications, including as a substitute of growth factors in tissue engineering, due to its stimulatory effect [52]. Intrauterine device can also incorporate Cu^{2+} to prevent pregnancy [53]. Nevertheless, exceeding the concentration limit can potentially lead to toxicity due to various mechanisms, such as the generation of reactive oxygen radicals, which can induce cellular damage. Additionally, Cu^{2+} can interfere with essential proteins that play critical roles in biological functions, causing the inactivation of enzymes and alterations in protein structure. Notably, elevated Cu^{2+} levels have been implicated in cancer progression, contributing not only to angiogenesis but also to proliferation and metastasis [54].

While Cu^{2+} is an essential component of plant growth media, participating in diverse biochemical and physiological pathways, its toxicity increases substantially at higher concentrations [55]. Therefore, it is crucial to regulate the dosage of Cu^{2+} during plant growth and development to mitigate excessive release into the environment. Encapsulation of Cu^{2+} within polymer matrix offers the potential for controlled release mechanism.

1.2.2.3 Zinc

Zn^{2+} has been pointed as a strong Alg crosslinker. It provides hydrogels with enough stability so as to sustain the release of encapsulated compounds under dissolution mediums [56]. As well as Cu^{2+}, Zn^{2+} ions complexate Alg chains through the formation of covalent-like coordinating bonds [37, 56, 57]. Hence, both Cu^{2+} and Zn^{2+} overlap with oxygen orbitals of uronates' carboxylic groups. The binding mechanism of Zn^{2+} is also nonspecific [41].

Zn^{2+} is required for the normal functioning of more than 300 enzymes and for the structural stability and expression of 2000 transcription factors [58]. It has antioxidant and anti-inflammatory capacity, through the modulation of oxidative stress and the production of ·OH scavengers [58]. Zn^{2+} displays immunomodulatory effects. It is essential for the development and regular activity of cells mediating innate immunity,

natural-killer cells, macrophages, neutrophils and T and B cells. It also enhances functions like phagocytosis and cytokines generation [59]. Zn^{2+} is known to inhibit NF-κB, which is a transcription factor that promotes the activation of gens responsible of malignant transformation, progression of cancer cells and drug resistance in several hematological and solid malignancies [60]. Zn^{2+} is an essential micronutrient that plays a crucial role in supporting optimal plant growth and development [58]. Zn fertilizers have gained significant interest in recent years, primarily due to the global incidence of Zn^{2+} deficiency in soils and the malnutrition issues derived, particularly prevalent in developing countries [61].

Zn^{2+} content within the organism remain constant despite excessive intake, by means of gastrointestinal adaptations regarding to Zn^{2+} absorption and excretion [56, 62]. Zn^{2+} deficiency might be a result of chelation in the intestines, which impedes absorption and may lead to immune dysfunctions and increased rate of tumor development [58]. In cancer patients, Zn^{2+} deficiency results in greater tumor size and tumor stage, shorter disease-free period and higher unplanned hospitalizations (extended duration and infection frequencies) [58].
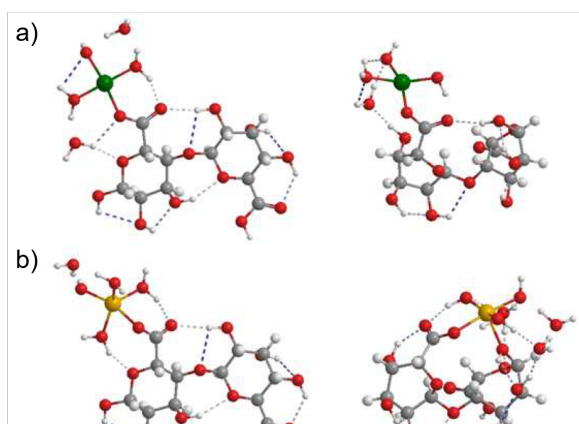
Figure 1.4: Computationally optimized complexes between a) Cu^{2+} and b) Zn^{2+} and an Alg chain simplified to one MM and GG disaccharide. The atoms are coloured according to atom type as follows: oxygen in red; carbon in grey; hydrogen in white; copper in green and zinc in yellow. Reprinted with permission from P. Agulhon, V. Markova, M. Robitzer, F. Quignard, and T. Mineva, "Structure of alginate gels: interaction of diuronate units with divalent cations from density functional calculations," Biomacromolecules, vol. 13. Copyright 2012. American Chemical Society.

1.3   Encapsulation

Encapsulation is the procedure of entrapping solid, liquid or gaseous substances into a coating material, giving rise to beads [63]. The first constituent may be called internal phase, payload, core material, fill or active agent, whereas the second component might be referred as encapsulating material, coat, shell, matrix, external phase, membrane, carrier material or wall. The nature of the encapsulated agent determines the properties of the encapsulating material.

Beads are defined as an internal phase that contains active compounds enveloped by encapsulating material. This material is typically synthetic or natural polymers [64]. Beads are classified as "spheres" if active compound is dispersed within spherical matrices, or "shell/core capsules" if the encapsulated compound is confined in the core and surrounded by a coating layer or shell (Figure 1.5) [6, 8, 14, 23, 65, 66, 67]. The term bead designates both capsules and spheres [65].

According to its size, beads are labeled as microbeads if their diameter ranges from 1 to 1000 μm, nanobeads if they measure from 10 to 1000 nm, and as macrocapsules if they are bigger than 1 mm [14, 23, 67]. Differences in size imply several consequences regarding to encapsulation efficiency, possible aggregation of beads and activity of the encapsulated compound [67].
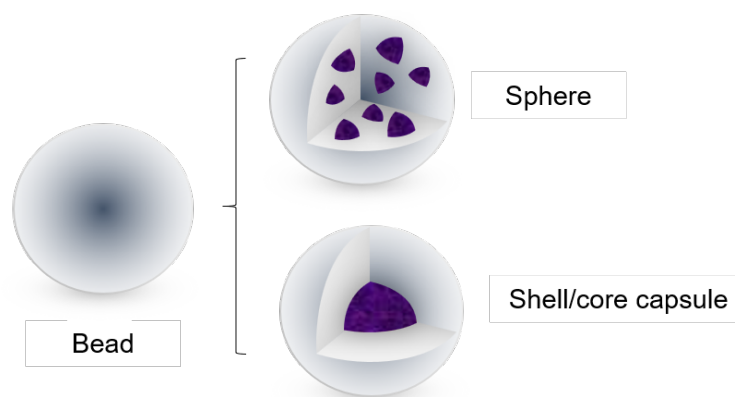
Figure 1.5: Beads classification in regard to the distribution of the encapsulated agent. The active compound is illustrated in purple whereas the spherical carrier matrix is represented in white

Encapsulation is frequently found in nature in form of egg, seeds, cells... Following the natural approach, encapsulation is mimicked as it offers a vast number of advantages, such as [5, 14, 64, 68, 69, 70]:

1. Protection of encapsulated compounds from environmental harmful agents, hazardous or toxic agents.

2. Improvement of encapsulated material stability and storage conditions.

3. Enhancement of its activity and/or shelf-life.

4. Creation of a novel product.

5. Transformation of fluids into solid systems such as powder, modulation of the colloidal and surface characteristics.

6. Control of beads' size and dispersibility.

7. Mask undesired properties of the encapsulated agent, such as the odour and taste.

8. Modulation and controlled release rate of the payload minimizing dose-related adverse effects. The release profile depends on the physicochemical features of the coating material. Release may be sustained, delayed or ordered if multiple compounds are encapsulated, according to the aimed needs of the application.

9. Targeted release of the encapsulated agent. The targeting ability is subjected to particle size, surface charge and hydrophobicity, and surface modification.

10. Bioavailability upgrade.

11. Achievement of efficient concentrations.

The release rate is tightly subject to the matrix composition. Hence, it defines the success of the delivery system. Both natural and synthetic polymers have been employed for encapsulation [71]. The following synthetic polymers have been used as delivery systems: ethylene-vinyl acetate (EVA) [72], poly(beta-amino esters) (PbAE) [73, 74] polycaprolactone (PCL) [75], poly(D,L-lactide–co–glycolide) (PLGA) [76], polyethylene glycol (PEG) [77], polyglycolic acid (PGA) [78], poly lactic acid (PLA) [79] and poly(vinyl alcohol) (PVA) [80, 81]. In addition, natural polymers that have been employed as encapsulating material are: on the one hand, polysaccharides such

as Alg [16], agarose [82], carrageenan [83], chitosan [84], cyclodextrins [85], dextran [86], fucoidan [87], hyaluronic acid [88], starch [89], pectin [90], polyhydroxybutyrate (PHB) [91] and poly(3-hydroxybutyrate-co-3-hydroxyvalerate) (PHBV) [92]; and on the other hand, proteins including albumin [93], collagen [94], keratin [95], gelatin [96] and gliadin [66, 67, 97].

1.3.1 Encapsulation methods

Beads might be prepared through diverse methodologies. Thus, the first step involves the formation of droplets, which can be achieved by extrusion, emulsion or spray-technologies (Figure 1.6) [63]. Extrusion, due to its simplicity, is commonly used together with ionotropic gelation to produce drug-loaded Alg beads [16]. In this technique, a polymeric solution is added drop wise to a crosslinking solution [16]. Electrodispersion and air atomization are two extrusion methods which enable the regulation of particle size through the application of electric or mechanical energy, respectively (Figure 1.6a) [8]. Electrodispersion employs pulsed electric fields to atomize a dispersed phase from a nozzle [3]. Air atomization utilizes pneumatic nozzles to generate uniform droplets using pressurized gas, typically air [3]. Ultimately, these droplets are introduced into a crosslinking bath containing an immiscible, isolating liquid where polymeric crosslinking occurs.

Emulsification techniques involve the formation of polymeric droplets within an emulsion system, followed by their subsequent gelation using a crosslinking agent (Figure 1.6b) [16]. In this process, beads are prepared within a non-aqueous continuous phase incorporating a surfactant as emulsifying agents [14]. Initially, the polymeric solution is dispersed and homogenized in an oil bath through low-energy or high-energy stirring methods such as sonication and microfluidics [3]. For instance, microfluidic technology is based on the diffusion of a dispersed phase through a microfluidic 'chip' reactor, which guarantees the production of uniform, highly monodispersed beads with high reproducibility and compliance [3]. In the next step, the gelling solution is gradually added to the emulsion and gelation occurs [11]. Emulsification is cost-effective method and yields homogeneous beads [8]. Factors such as the type and concentration of the emulsifier, the oil-to-polymer ratio and the homogenization shear influence the size distribution and diameter of the resulting beads [11, 16]. However, an additional centrifuging step is necessary to remove potential residual oil, surfactants and purify the final beads [8].

The principle of spray-drying involves the atomization of a dispersion phase, which undergoes a transformation to a dry state (Figure 1.6c). Subsequently, the dispersion is exposed to a hot gas in a closed-loop process to facilitate solvent evaporation and produce dry microbeads [8]. Additionally, this method can be performed in continuous, it is a simple and low-cost single-step method to produce dry beads.
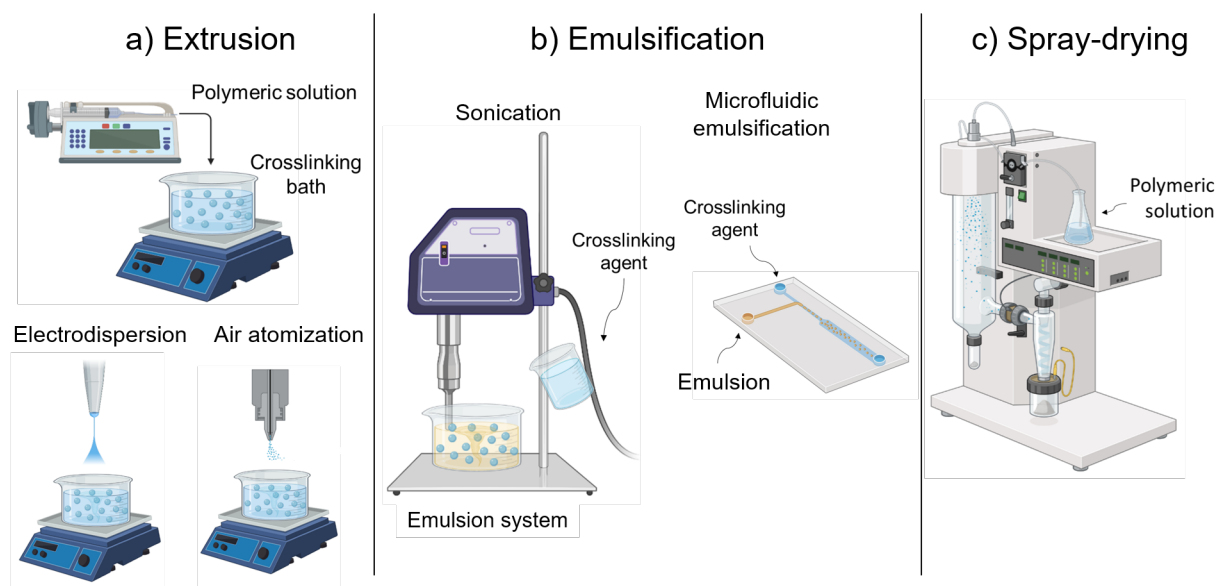
Figure 1.6: Representation of encapsulation methodologies: a) extrusion, b) emulsion and c) spray-drying techniques

Polymeric beads can also be prepared through polyelectrolyte complexation, wherein oppositely charged polyelectrolytes are combined lead by electrostatic interactions [97]. Ultimately, particles composed by polyelectrolyte multilayers are obtained. The properties of the resulting beads are influenced by various factors including pH, temperature and stirring speed.

The preparation method must be selected attending to certain conditions. The physicochemical properties of both, the encapsulated and encapsulating compounds will be determinant, as well as the desired beads size and physicochemical properties, payload application, industrial manufacturing and a suitable production cost [63]. It is also important to consider the chemical stability and biological activity of the encapsulated compound. Encapsulation efficiency must be high and the active compound release reproducible. Ideally, the process should be industrially scalable and organic solvent waste should be avoided or kept as low as possible [64]. The application of the delivery system is also an important factor to be considered. Usually, the more complex the method is, the smaller the obtained particles are.

14

1.4   Alginate beads

Production of Alg beads is simple and cost-effective. Certainly, Alg comprehends many benefits as it is obtained from natural renewable sources [5, 8], it is inexpensive and easy to obtain. Alg is considerably reactive and can be chemically derivatized. This fact allows obtaining Alg beads with particular characteristics for concrete applications [2, 8]. Alg is biocompatible and biodegradable. It is not irritant, toxic nor immunogenic [1, 8, 11, 16, 23]. When it is degraded, any harmful product nor cytotoxicity is produced. Kidneys are capable to efficiently remove alginates smaller than 50 kDa [3]. For all these arguments, Alg is undoubtedly the most vastly employed biopolymer for microencapsulation [23].

Encapsulation employing Alg involves two steps. First, the polymeric solution reaches the crosslinking bath and contacts the multivalent cation. Then, insoluble beads establish and evolve. At the beginning, beads may remain on the top of the bath solution until density increases and they sink. The required period until they reach the steady-state equilibrium is known as maturation time [36, 63].

Once formed, hydrogels retain a high water content. Water molecules keep trapped though hydrogen bonds [98]. However, during maturation time, syneresis takes place: beads contract due to external forces and water molecules are extruded out of the hydrogel structure [11, 99]. Syneresis is proportional to the strength of the interaction between crosslinker-uronates [27]. Remaining water molecules within the matrix arrange around both U and the crosslinking cations.

Draget et al. (2001) determined that the bigger the relative presence of heterosequences and the higher the Mw, the greater the syneresis. Low Mw Alg gave rise to stiffer structures, which opposed to contraction forces that prompted syneresis [100]. Results indicated the rise of junction zones to be key for syneresis driving force. In contrast, Donati et al. (2005) proposed that syneresis resulted from the depletion of storage modulus lead by the partial breakdown of the MG-MG junctions [29]. Helgerud et al. also pointed that syneresis was minor when Alg hydrogel was saturated with Ca^{2+} ions [99].

Gelation kinetics and stabilization time depend on the ion features and the ability to diffuse through the polymeric network, as well as on the polymer ability to be crosslinked. Final weight of beads not always depends on cation concentration [36].

Eventually, the disposition of Alg chains is determined by its hydration degree, hydrogen bonds and metallic bridges, and the relative M/G ratio. Actually, Alg beads display a re-swelling ability as a result of the modification of chain conformation led by the environmental pH [9]. Carboxylic groups of U remain protonated whether the pH is lower than pKa. Hence, polymeric chains tend to aggregate. In fact, at very low pH (< 2) Alg precipitates and forms very small, inelastic white beads also known as acidic gels. Whether the pH value is between 4 and 10, carboxylic groups deprotonate, repulsive forces rise and Alg chains stretch [36]. Therefore, pH values ultimately affects the release of the active agent from Alg beads.

Figure 1.7 displays the effects of different pH values on beads' behaviour. Once crosslinked, if carboxylic groups protonate, electrostatic repulsion reduces and Alg beads shrink (Figure 1.7a). Both the size of surface pores and the rate of drug delivery decrease. However, if pH value is above 7, carboxylates increase as well as repulsive forces. Beads swell and suface pores expand (Figure 1.7b). If pH is higher than 12, polymeric chains dissociate and result in a burst release of the encapsulated compound (Figure 1.7c) [36].
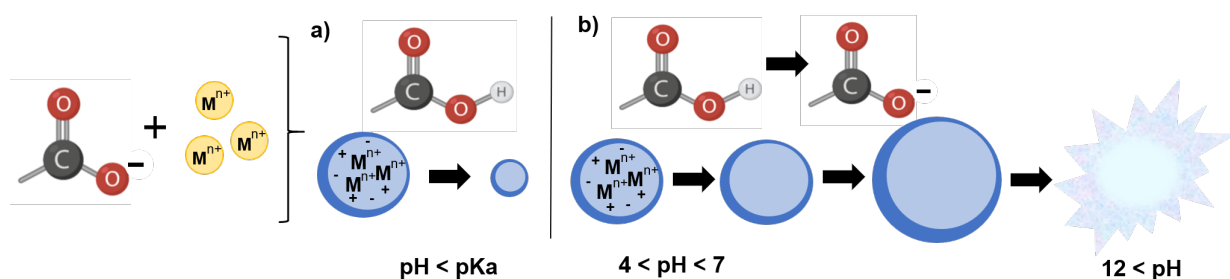
Figure 1.7: Sketch of carboxylate moieties of uronate residues in regard to environmental pH and repercussion on beads' swelling ability

1.4.1   Application of alginate beads

As previously mentioned, Alg beads provide advantages such as the protection of the core material from the surroundings and a controlled release of the active compounds. Nevertheless, the selection of an appropriate preparation methodology needs to meet certain requirements. The physicochemical properties of both the core material and the resulting beads as well as their application are important factors to be considered. Applications of Alg-based beads include:

- **Pharmaceutical application:** Alg has been employed for the encapsulation and delivery of drugs, vaccine, proteins and deoxyribonucleic acid (DNA) [16, 101, 102]. Physicochemical properties of Alg-based delivery systems might be modulated by the crosslinker nature and crosslinking degree [1, 9]. Release kinetics are depicted by the features of the encapsulated compound, surface pore size and the interactions between Alg chains and the active agent. In addition, supplementary properties like the antibacterial activity of Cu^{2+} and Zn^{2+} makes these hydrogels especially useful for their application as wound dressings [103, 104]. Actually, diverse Alg-based wound dressings are commercially available, such as: AlgiSite M™, Algicell™, Comfeel Plus™, Kaltostat™, SeaSorb®, Sorbsan™ and Tegagen™ [105].

- **Biomedical technology:** Giving the ability to retain large amounts of water and biological fluids, Alg hydrogels perfectly mimic biological tissues [14]. This is why they have been employed for tissue engineering and regenerative medicine, as 3D scaffolds that support cell growth, drug depots and as delivery systems for bioactive agents [16] and cell encapsulation [106] and transplantation [107], just as well as imaging [108], diagnosis tools and biosensing [109]. Injectable Alg and Alg-derived hydrogels have proved to be potential tools for therapy after myocardial infarction [110, 111] and for cancer treatment and research [112].

- **Cosmetic industry:** Alg based compounds have been applied as cosmetic additives [113] such as peeling products [114] and as substitutes to hyaluronic acids for submucosal injection [115].

- **Food technology:** Alg has been introduced in food supplemented with bioactive components and nutraceuticals (ingredients with potential health benefits) [116] and for food packaging, as an alternative to petroleum-based plastics [117, 118].

- **Agriculture:** Alg has been employed as biodegradable scaffold to encapsulate agrochemicals [119, 120] such as fertilizers [121, 122], pesticides [123, 124] and herbicides [125], and plant biostimulants [126, 127]. It has been used as well as soil conditioner for erosion control [128]. Conditioners are designed to improve the water retention of soil. Hence, Alg supposes a promising tool to achieve it.

17

- **Separation technology** Alg has been applied as an instrument to remove contaminants, such as heavy metals [129, 130], dyes [131], [132] and agrochemicals from aqueous solutions. Even some of the proposed Alg-based hydrogels could be reused.

Generally, the application of Alg-based hydrogels is possible because gelation occurs under mild conditions. Table 1.1 comprises some of the most recent Alg-based systems according to the employed crosslinker.

Normally, under physiological conditions Alg hydrogels are not stable for long-term application as they dissolve due to ion exchange with the ions in the surrounding media. Besides, Alg may promote aggregation of platelets and erythrocytes [1]. We could say that the main drawback of Ca-Alg hydrogels is the burst effect and fast release of encapsulated compounds [3]. Ca-Alg hydrogels may also be destabilized by Ca^{2+} chelators such as phosphates, lactates, citrates and carbonates [11]. When Ca^{2+} ions are released from the hydrogel matrix within an organism, homeostasis may be promoted [1]. Oppositely, the main drawback of Cu-Alg hydrogels is its toxicity under several contexts. Nevertheless, Zn^{2+} provides hydrogels with enough stability to sustain the release of the active agent under dissolution mediums [56].

This thesis deals with the study of Alg beads crosslinked with diverse divalent cations, namely Ca^{2+}, Cu^{2+} and Zn^{2+}. Interestingly, in our investigation we employed an unusually mannuronate-rich Alg, whose crosslinking mechanisms and networking features have not been analyzed, to the best of our knowledge. Moreover, we considered the application of the obtained beads in different fields such as Agriculture and Medicine. For this purpose, we also explored the encapsulation of natural, polyphenol-rich extracts into Alg beads.

18

Table 1.1: Application of Alg-based systems according to the employed crosslinker

Loaded Compound	Matrix	Crosslinker	Study aim	Results	References
Amygdalin	Alg and chitosan	Ca^{2+} - $CaCl_2$	Mucoadhesion and transmigration studies and *in vitro* assays on lung carcinoma H1299 cells	Improved mucoadhesion and transmigration. Promoted cellular uptake and cytotoxicity	[133]
Laccase	Alg	Cu^{2+} - $CuCl_2$	Optimization of laccase encapsulation	Enhanced encapsulation, stability, specific activity and degradation rate	[134]
Zinc insulin hexamer	Alg and maltodextrin	Zn^{2+} - $ZnCl_2$	Characterization of the insulin oral delivery system	Successful encapsulation, controlled release, bio-compatible and hypoglycemic effect in diabetic mice	[135]
Tea polyphenols	Alg and collagen hydrolysates	Ca^{2+} - $CaCl_2$	Co-encapsulation design to improve encapsulation efficiency and storage stability	Formula optimization; improved encapsulation rate and storage under harsh conditions	[136]
Cannabidiol	Alg	Zn^{2+} - $ZnSO_4$	Characterization of the release profile and *in vitro* and *in vivo* behaviour to be employed as wound dressing and for skin tissue engineering	Antibacterial and antioxidant activities. Enhancement of wound healing by modulating the inflammatory infiltration and improving collagen deposition, tissue granulation and angiogenesis	[137]
—	Alg and polyacrylamide	Ca^{2+} - $CaCl_2$ Zn^{2+} - $ZnCl_2$ Sr^{2+} - $SrCl_2$	Comparison of different divalent crosslinkers on antibacterial activity and wound healing process	Improved properties of Zn-based hydrogels: antibacterial activity, cell viability, mechanical strength and wound-healing process, promotion of fibroblast migration, angiogenesis and collagen deposition	[138]
Silver nanoparticles (NPs)	Alg	Zn^{2+} - $Zn(NO_4)_2$	Aerogel preparation, characterization and evaluation of catalytic behaviour and antibacterial properties of different compositions	Correlation between NPs and Zn^{2+} content, and their effects. Potential application for the reduction of the studied dyes and antibacterial properties	[139]
RL-QN15 (cyclic bioactive peptide)-loaded silica NPs	Alg	Zn^{2+} - $ZnCl_2$	Characterization of the hydrogel so as to be used as pro-regenerative dressing for chronic skin wound treatment	Slow release of loaded RL-QN15. Broad-spectrum antimicrobial activity. Promotion of rapid healing both *in vitro* and *in vivo* in methicillin-resistant *Staphylococcus aureus* biofilm-infected chronic wounds in mice	[140]
—	Alg, cationic starch and glycerol	—	Evaluation of the polyelectrolyte as antimicrobial food packaging material	Appropriate thermal, antimicrobial and surface properties to be used as films for food packaging	[141]
Amino acids-coated seeds	Alg and NPK solution	Cu^{2+} - $CuSO_4$ Mn^{2+} - $MnSO_4$ Ni^{2+} - $NiSO_4$	Development of a system that provides a source of fertilizing nutrients and biostimulants	Confirmed biostimulatory properties. Potential commercial application	[142]
Bacillus spp. XT13 and XT14	Alg	Ca^{2+} - $CaCl_2$	Optimization of a formulation with plant growth-promoting bacteria to increases the tolerance of Guinea grass to drought	Enhanced tolerance to water deficit. Potential strategy for climate change adaptation	[143]
Spirulina platensis	Alg	Ca^{2+} - $CaCl_2$	Enhancement of adsorption properties of microalgae using Alg hydrogels	Successful immobilization and effective removal of Pb^{2+} from aqueous solutions	[144]
Achromobacter spanius C1 and *Pseudomonas rhodesiae* C4	Alg	Ca^{2+} - $CaCl_2$	Optimization of the removal of a pesticide mixture of iprodione and chlorpyrifos from waste waters in a continuous system	Improved degradation of both pesticides. Establishment of a pesticide-containing waste waters treatment system	[145]

Bibliography

[1] K. Y. Lee and D. J. Mooney, "Alginate: Properties and biomedical applications," *Progress in Polymer Science*, vol. 37, no. 1, pp. 106–126, jan 2012.

[2] A. Sosnik, *Alginate Particles as Platform for Drug Delivery by the Oral Route: State-of-the-Art*, 2014, vol. 2.

[3] M. Lopes, "Preparation methods and applications behind alginate-based particles," *Expert opinion on drug delivery*, vol. 14, no. 6, p. 769–782, 2017.

[4] N. Pawar and K. J. Edgar, "Alginate derivatization: A review of chemistry, properties and applications," *Biomaterials*, vol. 33, no. 11, p. 769–782, 2012.

[5] A. Gonzalez-Pujana, G. Orive, J. L. Pedraz, E. Santos-Vizcaino, and R. M. Hernandez, "Alginate microcapsules for drug delivery," in *Alginates and their biomedical applications, Springer Series in Biomaterials Science and Engineering*.   Elsevier Ltd, 2012, vol. 11, pp. 67–100.

[6] D. Hudson and D. Margaritis, "Biopolymer nanoparticle production for controlled release of biopharmaceuticals," *Critical reviews in biotechnology*, vol. 34, no. 2, pp. 161–179, 2014.

[7] I. D. Hay, Z. U. Rehman, A. Ghafoor, and B. H. A. Rehm, "Bacterial biosynthesis of alginates," *J. Chem. Technol. Biotechno-Biotechnology*, vol. 85, no. 6, pp. 752–759, 2010.

[8] D. Dhamecha, R. Movsas, U. Sano, and J. U. Menon, "Applications of alginate microspheres in therapeutics delivery and cell culture: Past, present and future," *International journal of pharmaceutics*, vol. 569, p. 118627, oct 2019.

[9] S. M. J.S. Patil, M.V. Kamalapur and D. Kadam, "Ionotropic gelation and polyelectrolyte complexation, modulated drug delivery system: a review." *Digest Journal of Nanomaterials and Biostructures*, vol. 5, no. 1, pp. 241–248, mar 2010.

[10] R. Dorati, I. Genta, M. Ferrari, G. Vigone, V. Merico, S. Garagna, M. Zuc-
cotti, and B. Conti, "Formulation and stability evaluation of 3D alginate beads
potentially useful for cumulus–oocyte complexes culture," *Journal of Microen-
capsulation*, vol. 33, no. 2, pp. 137–145, jan 2016.

[11] S. H. Ching, N. Bansal, and B. Bhandari, "Alginate gel particles – A review
of production techniques and physical properties," *Critical Reviews in Food
Science and Nutrition*, vol. 57, no. 6, pp. 1133–1152, may 2015.

[12] C.-Y. Yu, H. Wei, Q. Zhang, X.-Z. Zhang, S.-X. Cheng, and R.-X. Zhuo,
"Effect of Ions on the Aggregation Behavior of Natural Polymer Alginate,"
J. Phys. Chem. B, vol. 113, no. 45, pp. 14 839–14 843, oct 2009. [Online].
Available: https://doi.org/10.10212Fjp906899j

[13] F. N. Sorasitthiyanukarn, C. Muangnoi, P. R. N. Bhuket, P. Rojsitthisak,
and P. Rojsitthisak, "Chitosan/alginate nanoparticles as a promising approach
for oral delivery of curcumin diglutaric acid for cancer treatment," *Materials
Science and Engineering: C*, vol. 93, pp. 178–190, dec 2018. [Online]. Available:
https://doi.org/10.10162Fj.msec.2018.07.069

[14] M. K. Mishra, Ed., *Handbook of encapsulation and controlled release.* CRC
Press, Taylor & Francis Group, CRC Press is an imprint of the Taylor & Francis
Group, an Informa business, 2016.

[15] B. S. Sapana P. Ahirrao, Paraag S. Gide and P. Sharma, "Ionotropic
Gelation: A Promising Cross Linking Technique for Hydrogels," *Journal
of Pharmaceutics and Nanotechnology*, vol. 2, pp. 1–6, dec 2014.
[Online]. Available: https://www.rroij.com/open-access/ionotropic-gelation-a-
promising-cross-linking-technique-for-hydrogels-.php?aid=34331

[16] N. T. T. Uyen, Z. A. A. Hamid, N. X. T. Tram, and N. Ahmad, "Fabrication
of alginate microspheres for drug delivery: A review," *International Journal
of Biological Macromolecules*, vol. 153, pp. 1035–1046, jun 2020. [Online].
Available: https://doi.org/10.10162Fj.ijbiomac.2019.10.233

[17] A. I. El-Batal, F. M. Mosallam, M. Ghorab, A. Hanora, M. Gobara,
A. Baraka, M. A. Elsayed, K. Pal, R. M. Fathy, M. A. Elkodous, and
G. S. El-Sayyad, "Factorial design-optimized and gamma irradiation-assisted
fabrication of selenium nanoparticles by chitosan and Pleurotus ostreatus

fermented fenugreek for a vigorous in vitro effect against carcinoma cells,"
International Journal of Biological Macromolecules, vol. 156, pp. 1584–1599,
aug 2020. [Online]. Available: https://doi.org/10.10162Fj.ijbiomac.2019.11.210

[18] M. Y. Abdelaal, E. A. Abdel-Razik, E. M. Abdel-Bary, and I. M. El-Sherbiny,
"Chitosan-based interpolymeric pH-responsive hydrogels for *in vitro* drug
release," *J. Appl. Polym. Sci.*, vol. 103, no. 5, pp. 2864–2874, 2006. [Online].
Available: https://doi.org/10.10022Fapp.25154

[19] S. R. Batool, M. A. Nazeer, D. Ekinci, A. Sahin, and S. Kizilel,
"Multifunctional alginate-based hydrogel with reversible crosslinking for
controlled therapeutics delivery," *International Journal of Biological
Macromolecules*, vol. 150, pp. 315–325, may 2020. [Online]. Available:
https://doi.org/10.10162Fj.ijbiomac.2020.02.042

[20] G. Chen, R. Wei, X. Huang, F. Wang, and Z. Chen, "Synthesis and
assessment of sodium alginate-modified silk fibroin microspheres as potential
hepatic arterial embolization agent," *International Journal of Biological
Macromolecules*, vol. 155, pp. 1450–1459, jul 2020. [Online]. Available:
https://doi.org/10.10162Fj.ijbiomac.2019.11.122

[21] H. Shen, F. Li, D. Wang, Z. Yang, C. Yao, Y. Ye, and X. Wang, "Chitosan-
alginate BSA-gel-capsules for local chemotherapy against drug-resistant breast
cancer," *Drug Des Devel Ther*, vol. 12, pp. 921–934, apr 2018. [Online].
Available: https://doi.org/10.21472Fddt.s158001

[22] F. Abasalizadeh, S. V. Moghaddam, E. Alizadeh, E. Akbari, E. Kashani,
S. M. B. Fazljou, M. Torbati, and A. Akbarzadeh, "Alginate-based hydrogels
as drug delivery vehicles in cancer treatment and their applications in wound
dressing and 3D bioprinting," *J Biol Eng*, vol. 14, no. 1, mar 2020. [Online].
Available: https://doi.org/10.11862Fs13036-020-0227-7

[23] B. Tylkowski and R. Jastrzab, "4. Smart Capsules for Lead Removal from
Industrial Wastewater," in *Lead: Its Effects on Environment and Health*,
A. Sigel, H. Sigel, and R. K. Sigel, Eds. De Gruyter, apr 2017, pp. 61–78.
[Online]. Available: https://doi.org/10.15152F9783110434330-004

[24] J. R. Rodrigues and R. Lagoa, "Copper Ions Binding in Cu-Alginate Gelation,"
Journal of Carbohydrate Chemistry, vol. 25, no. 2-3, pp. 219–232, may 2006.
[Online]. Available: https://doi.org/10.10802F07328300600732956

[25] J. K. Gandhi, E. C. Opara, and E. M. Brey, "Alginate-based strategies for therapeutic vascularization," *Therapeutic Delivery*, vol. 4, no. 3, pp. 327–341, mar 2013. [Online]. Available: https://doi.org/10.41552Ftde.12.163

[26] J. P. Senna, T. N. Barradas, S. Cardoso, T. C. Castiglione, M. J. Serpe, K. G. de Holanda e Silva, and C. R. E. Mansur, "Dual alginate-lipid nanocarriers as oral delivery systems for amphotericin B," *Colloids and Surfaces B: Biointerfaces*, vol. 166, pp. 187–194, jun 2018. [Online]. Available: https://doi.org/10.10162Fj.colsurfb.2018.03.015

[27] Ý. A. Mørch, I. Donati, B. L. Strand, and G. Skjåk-Bræk, "Effect of Ca^{2+}, Ba^{2+}, and Sr^{2+} on Alginate Microbeads," *Biomacromolecules*, vol. 7, no. 5, pp. 1471–1480, apr 2006. [Online]. Available: https://doi.org/10.10212Fbm060010d

[28] I. Machida-Sano, M. Hirakawa, H. Matsumoto, M. Kamada, S. Ogawa, N. Satoh, and H. Namiki, "Surface characteristics determining the cell compatibility of ionically cross-linked alginate gels," *Biomed. Mater.*, vol. 9, no. 2, feb 2014. [Online]. Available: https://doi.org/10.10882F1748-6041%2F9%2F2%2F025007

[29] I. Donati, S. Holtan, Y. A. Mørch, M. Borgogna, M. Dentini, and G. Skjåk-Bræk, "New Hypothesis on the Role of Alternating Sequences in Calcium-Alginate Gels," *Biomacromolecules*, vol. 6, no. 2, pp. 1031–1040, jan 2005. [Online]. Available: https://doi.org/10.10212Fbm049306e

[30] J.-Y. Leong, W.-H. Lam, K.-W. Ho, W.-P. Voo, M. F.-X. Lee, H.-P. Lim, S.-L. Lim, B.-T. Tey, D. Poncelet, and E.-S. Chan, "Advances in fabricating spherical alginate hydrogels with controlled particle designs by ionotropic gelation as encapsulation systems," *Particuology*, vol. 24, pp. 44–60, feb 2016. [Online]. Available: https://doi.org/10.10162Fj.partic.2015.09.004

[31] C. K. Kuo and P. X. Ma, "Ionically crosslinked alginate hydrogels as scaffolds for tissue engineering: Part 1. Structure, gelation rate and mechanical properties," *Biomaterials*, vol. 22, no. 6, pp. 511–521, mar 2001. [Online]. Available: https://doi.org/10.10162Fs0142-9612%2800%2900201-5

[32] A. Blandino, M. Macias, and D. Camtero, "Formation of calcium alginate gel capsules: influence of sodium alginate and $CaCl_2$ concentration on gelation kinetics," *J Biosci Bioeng*, vol. 88, no. 6, pp. 686–689, mar 1999. [Online]. Available: https://pubmed.ncbi.nlm.nih.gov/16232687/

[33] A. D. Augst, H. J. Kong, and D. J. Mooney, "Alginate Hydrogels as Biomaterials," *Macromol. Biosci.*, vol. 6, no. 8, pp. 623–633, aug 2006. [Online]. Available: https://doi.org/10.10022Fmabi.200600069

[34] J. P. Chen, L. Hong, S. Wu, and L. Wang, "Elucidation of Interactions between Metal Ions and Ca Alginate-Based Ion-Exchange Resin by Spectroscopic Analysis and Modeling Simulation," *Langmuir*, vol. 18, no. 24, pp. 9413–9421, oct 2002. [Online]. Available: https://doi.org/10.10212Fla026060v

[35] J. L. Drury, R. G. Dennis, and D. J. Mooney, "The tensile properties of alginate hydrogels," *Biomaterials*, vol. 25, no. 16, pp. 3187–3199, jul 2004. [Online]. Available: https://doi.org/10.10162Fj.biomaterials.2003.10.002

[36] N. M. Velings and M. M. Mestdagh, "Physico-Chemical Properties of Alginate Gel Beads," *Polymer Gels and Networks*, vol. 3, no. 3, pp. 311–330, oct 1995. [Online]. Available: https://doi.org/10.1016/0966-7822(94)00043-7

[37] P. Agulhon, V. Markova, M. Robitzer, F. Quignard, and T. Mineva, "Structure of Alginate Gels: Interaction of Diuronate Units with Divalent Cations from Density Functional Calculations," *Biomacromolecules*, vol. 13, no. 6, pp. 1899–1907, may 2012. [Online]. Available: https://doi.org/10.10212Fbm300420z

[38] Y. Xing, Z.-L. Zhu, F. Wang, X. Zhang, B.-Y. Li, Z.-X. Liu, X.-X. Wu, S.-F. Ge, and Y.-M. Jiang, "Role of calcium as a possible regulator of growth and nitrate nitrogen metabolism in apple dwarf rootstock seedlings," *Scientia Horticulturae*, vol. 276, 2021.

[39] V. Demidchik, S. Shabala, S. Isayenkov, T. A. Cuin, and I. Pottosin, "Calcium transport across plant membranes: mechanisms and functions," *The New phytologist*, vol. 220, no. 1, pp. 49–69, 2018.

[40] K. Thor, "Calcium-nutrient and messenger," *Frontiers in plant science*, vol. 10, p. 440, 2019.

[41] P. Agulhon, M. Robitzer, L. David, and F. Quignard, "Structural Regime Identification in Ionotropic Alginate Gels: Influence of the Cation Nature and Alginate Structure," *Biomacromolecules*, vol. 13, no. 1, pp. 215–220, dec 2011. [Online]. Available: https://doi.org/10.10212Fbm201477g

[42] J. M. C. Puguan, X. Yu, and H. Kim, "Characterization of structure, physico-chemical properties and diffusion behavior of Ca-Alginate gel beads prepared by different gelation methods," *Journal of Colloid and Interface Science*, vol. 432, pp. 109–116, oct 2014. [Online]. Available: https://doi.org/10.10162Fj.jcis.2014.06.048

[43] A. Haug, B. Larsen, O. Smidsrød, J. Møller, J. Brunvoll, E. Bunnenberg, C. Djerassi, and R. Records, "A study of the constitution of alginic acid by partial acid hydrolysis." *Acta Chem. Scand.*, vol. 20, pp. 183–190, 1966. [Online]. Available: https://doi.org/10.38912Facta.chem.scand.20-0183

[44] M. C. Linder and M. Hazegh-Azam, "Copper biochemistry and molecular biology," *The American journal of clinical nutrition*, vol. 63, pp. 797–811, 1996.

[45] D. C. Bassett, I. Madzovska, K. S. Beckwith, T. B. Melø, B. Obradovic, and P. Sikorski, "Dissolution of copper mineral phases in biological fluids and the controlled release of copper ions from mineralized alginate hydrogels," *Biomed. Mater.*, vol. 10, no. 1, dec 2014. [Online]. Available: https://doi.org/10.10882F1748-6041%2F10%2F12F015006

[46] J. P. Cattalini, J. Roether, A. Hoppe, F. Pishbin, L. H. Durand, A. Gorustovich, A. R. Boccaccini, S. Lucangioli, and V. Mouriño, "Nanocomposite scaffolds with tunable mechanical and degradation capabilities: co-delivery of bioactive agents for bone tissue engineering," *Biomed. Mater.*, vol. 11, no. 6, oct 2016. [Online]. Available: https://doi.org/10.10882F1748-6041%2F11%2F62F065003

[47] M. Serra, A. Columbano, U. Ammarah, M. Mazzone, and A. Menga, "Understanding metal dynamics between cancer cells and macrophages: Competition or synergism?" *Front. Oncol.*, vol. 10, apr 2020. [Online]. Available: https://doi.org/10.33892Ffonc.2020.00646

[48] K. Mikula, D. Skrzypczak, B. Ligas, and A. Witek-Krowiak, "Preparation of hydrogel composites using Ca^{2+} and Cu^{2+} ions as crosslinking agents," *Applied Sciences*, vol. 1, no. 6, may 2019. [Online]. Available: https://doi.org/10.10072Fs42452-019-0657-3

[49] M. Vinceković, S. Jurić, E. Đermić, and S. Topolovec-Pintarić, "Kinetics and mechanisms of chemical and biological agents release from biopolymeric microcapsules," *J. Agric. Food Chem.*, vol. 65, no. 44, pp. 9608–9617, oct 2017. [Online]. Available: https://doi.org/10.10212Facs.jafc.7b04075

[50] B. Dudová, D. Hudecová, R. Pokorný, M. Mikulášová, M. Palicová, P. Segla, and M. Melník, "Copper complexes with bioactive ligands," *Folia Microbiol*, vol. 46, no. 5, pp. 379–384, oct 2001. [Online]. Available: https://doi.org/10.10072Fbf02814425

[51] V. Lemoine, C. Bernard, C. Leman-Loubière, B. Clément-Larosière, M. Girardot, L. Boudesocque-Delaye, E. Munnier, and C. Imbert, "Nanovectorized Microalgal Extracts to Fight *Candida albicans* and *Cutibacterium acnes* Biofilms: Impact of Dual-Species Conditions," *Antibiotics*, vol. 9, no. 6, p. 279, may 2020. [Online]. Available: https://doi.org/10.33902Fantibiotics9060279

[52] C. Gérard, L.-J. Bordeleau, J. Barralet, and C. J. Doillon, "The stimulation of angiogenesis and collagen deposition by copper," *Biomaterials*, vol. 31, no. 5, pp. 824–831, feb 2010. [Online]. Available: https://doi.org/10.10162Fj.biomaterials.2009.10.009

[53] R. Kulier, P. O'Brien, F. M. Helmerhorst, M. Usher-Patel, and C. d'Arcangues, "Copper containing, framed intra-uterine devices for contraception," *Cochrane Database of Systematic Reviews*, oct 2007. [Online]. Available: https://doi.org/10.10022F14651858.cd005347.pub3

[54] Y. Li, "Copper homeostasis: Emerging target for cancer treatment," *IUBMB Life*, vol. 72, no. 9, pp. 1900–1908, jun 2020. [Online]. Available: https://doi.org/10.10022Fiub.2341

[55] D. Trigueros and S. Rossini-Oliva, "Tissue Distribution and Biochemical Changes in Response to Copper Accumulation in *Erica australis*," *Plants*, vol. 10, no. 7, 2021.

[56] N. S. Raut, P. R. Deshmukh, and M. J. Umekar, "Zinc cross-linked hydroxamated alginates for pulsed drug release," *International Journal of Pharmaceutical Investigation*, vol. 3, no. 4, pp. 194–202, dec 2013. [Online]. Available: https://www.ncbi.nlm.nih.gov/pmc/articles/PMC3853759/

[57] L. Iskandar, L. Rojo, L. D. Silvio, and S. Deb, "The effect of chelation of sodium alginate with osteogenic ions, calcium, zinc, and strontium," *J Biomater Appl*, vol. 34, no. 4, pp. 573–584, jul 2019. [Online]. Available: https://doi.org/10.11772F0885328219861904

[58] A. S. Prasad, "Biochemistry of zinc," *Springer*, vol. 11, no. 3, may 2013.

[59] A. H. Shankar and A. S. Prasad, "Zinc and immune function: the biological basis of altered resistance to infection," *The American Journal of Clinical Nutrition*, vol. 68, no. 2, pp. 447–463, aug 1998. [Online]. Available: https://doi.org/10.1093%2Fajcn%2F68.2.447s

[60] R. Uzzo, P. Leavis, W. Hatch, V. Gabai, N. Dulin, N. Zvartau, and V. Kolenko, "Zinc inhibits nuclear factor-kappa b activation and sensitizes prostate cancer cells to cytotoxic agents," *Clin Cancer Res*, vol. 8, no. 11, pp. 3579–3583, nov 2002. [Online]. Available: https://pubmed.ncbi.nlm.nih.gov/12429649/

[61] R. Prasad, Y. Shivay, and D. Kumar, "Interactions of Zinc with Other Nutrients in Soils and Plants - A Review," vol. 12, pp. 16–26, 2016.

[62] M. Taha, K. Aiedeh, Y. Al-Hiari, and H. Al-Khatib, "Synthesis of zinc-crosslinked thiolated alginic acid beads and their *in vitro* evaluation as potential enteric delivery system with folic acid as model drug," *Pharmazie*, vol. 60, no. 10, pp. 736–742, oct 2005. [Online]. Available: https://pubmed.ncbi.nlm.nih.gov/16259119/

[63] M. Borgogna, B. Bellich, and A. Cesàro, "Marine Polysaccharides in Microencapsulation and Application to Aquaculture: "From Sea to Sea"," *Marine Drugs*, vol. 9, no. 12, pp. 2572–2604, dec 2011. [Online]. Available: https://doi.org/10.3390%2Fmd9122572

[64] K. M. Manjanna, B. Shivakumar, and T. M. P. Kumar, "Microencapsulation: An acclaimed novel drug-delivery system for NSAIDs in arthritis," *Crit Rev Ther Drug Carrier Syst*, vol. 27, no. 6, pp. 509–545, 2010. [Online]. Available: https://doi.org/10.16152Fcritrevtherdrugcarriersyst.v27.i6.20

[65] M. Singh, K. Hemant, M. Ram, and H. Shivakumar, "Microencapsulation: A promising technique for controlled drug delivery," *Research in Pharmaceutical Sciences*, vol. 5, no. 2, pp. 65–77, 2010. [Online]. Available: https://www.ncbi.nlm.nih.gov/pmc/articles/PMC3093624/

[66] S. V. Bhujbal, P. de Vos, and S. P. Niclou, "Drug and cell encapsulation: Alternative delivery options for the treatment of malignant brain tumors," *Advanced Drug Delivery Reviews*, vol. 67-68, pp. 142–153, apr 2014. [Online]. Available: https://doi.org/10.10162Fj.addr.2014.01.010

[67] C. Y. Wong, H. Al-Salami, and C. R. Dass, "Microparticles, microcapsules and microspheres: A review of recent developments and prospects for oral delivery of insulin," *International Journal of Pharmaceutics*, vol. 537, pp. 223–244, feb 2018. [Online]. Available: https://doi.org/10.1016%2Fj.ijpharm.2017.12.036

[68] N. J. Zuidam and E. Shimoni, "Overview of microencapsulates for use in food products or processes and methods to make them," *Encapsulation Technologies for Active Food Ingredients and Food Processing*, pp. 3–29, jan 2009. [Online]. Available: https://doi.org/10.1007/978-1-4419-1008-02

[69] N. Zuidam and V. Nedovic, Eds., *Encapsulation Technologies for Active Food Ingredients and Food Processing*.   Springer New York, 2010, vol. 1.

[70] A. Kumari, S. K. Yadav, and S. C. Yadav, "Biodegradable polymeric nanoparticles based drug delivery systems," *Colloids and Surfaces B: Biointerfaces*, vol. 75, no. 1, pp. 1–18, jan 2010. [Online]. Available: https://doi.org/10.1016%2Fj.colsurfb.2009.09.001

[71] A. Nasir, A. Kausar, and A. Younus, "A review on preparation, properties and applications of polymeric nanoparticle-based materials," *Polymer-Plastics Technology and Engineering*, vol. 54, no. 4, pp. 325–341, oct 2014. [Online]. Available: https://doi.org/10.1080%2F03602559.2014.958780

[72] Z. Jin, K. Wu, J. Hou, K. Yu, Y. Shen, and S. Guo, "A PTX/nitinol stent combination with temperature-responsive phase-change 1-hexadecanol for magnetocaloric drug delivery: Magnetocaloric drug release and esophagus tissue penetration," *Biomaterials*, vol. 153, pp. 49–58, jan 2018. [Online]. Available: https://doi.org/10.1016%2Fj.biomaterials.2017.10.040

[73] C. G. Zamboni, K. L. Kozielski, H. J. Vaughan, M. M. Nakata, J. Kim, L. J. Higgins, M. G. Pomper, and J. J. Green, "Polymeric nanoparticles as cancer-specific DNA delivery vectors to human hepatocellular carcinoma," *Journal of Controlled Release*, vol. 263, pp. 18–28, oct 2017. [Online]. Available: https://doi.org/10.1016%2Fj.jconrel.2017.03.384

[74] Y. Liu, Y. Li, D. Keskin, and L. Shi, "Poly(β-amino esters): Synthesis, formulations, and their biomedical applications," *Adv. Healthcare Mater.*, dec 2018. [Online]. Available: https://doi.org/10.1002%2Fadhm.201801359

[75] P. Jiang, F. J. Chaparro, C. T. Cuddington, A. F. Palmer, M. P. Ohr, J. J. Lannutti, and K. E. Swindle-Reilly, "Injectable biodegradable bi-layered capsule for sustained delivery of bevacizumab in treating wet age-related macular degeneration," *Journal of Controlled Release*, vol. 320, pp. 442–456, apr 2020. [Online]. Available: https://doi.org/10.1016%2Fj.jconrel.2020.01.036

[76] C. Gong, X. Yu, B. You, Y. Wu, R. Wang, L. Han, Y. Wang, S. Gao, and Y. Yuan, "Macrophage-cancer hybrid membrane-coated nanoparticles for targeting lung metastasis in breast cancer therapy," *J Nanobiotechnol*, vol. 18, no. 1, jun 2020. [Online]. Available: https://doi.org/10.1186%2Fs12951-020-00649-8

[77] Y. Li, J. Lin, Z. Cai, P. Wang, Q. Luo, C. Yao, Y. Zhang, Z. Hou, J. Liu, and X. Liu, "Tumor microenvironment-activated self-recognizing nanodrug through directly tailored assembly of small-molecules for targeted synergistic chemotherapy," *Journal of Controlled Release*, vol. 321, pp. 222–235, may 2020. [Online]. Available: https://doi.org/10.1016%2Fj.jconrel.2020.02.025

[78] H.-C. Tsai, F. Maryani, C.-C. Huang, T. Imae, and J.-Y. Lin, "Drug-loading capacity and nuclear targeting of multiwalled carbon nanotubes grafted with anionic amphiphilic copolymers," *IJN*, pp. 4427–40, nov 2013. [Online]. Available: https://doi.org/10.2147%2Fijn.s53636

[79] M. Miranda, L. Silva, I. Carvalho, R. Amaral, M. de Paula, K. Swiech, J. Bastos, J. Paschoal, F. Emery, R. dos Reis, M. Bentley, and P. Marcato, "Targeted uptake of folic acid-functionalized polymeric nanoparticles loading glycoalkaloidic extract *in vitro* and *in vivo* assays," *Colloids and Surfaces B: Biointerfaces*, vol. 192, p. 111106, aug 2020. [Online]. Available: https://doi.org/10.1016%2Fj.colsurfb.2020.111106

[80] X. Chen, H. Qian, H. Qiao, B. Dong, E. Chen, D. Huang, T. Wang, and W. Chen, "Tumor-adhesive and pH-degradable microgels by microfluidics and photo-cross-linking for efficient antiangiogenesis and enhanced cancer chemotherapy," *Biomacromolecules*, vol. 21, no. 3, pp. 1285–1294, feb 2020. [Online]. Available: https://doi.org/10.1021%2Facs.biomac.0c00049

[81] M. S. Gularte, R. F. Quadrado, N. S. Pedra, M. S. Soares, N. P. Bona, R. M. Spanevello, and A. R. Fajardo, "Preparation, characterization and antitumor activity of a cationic starch-derivative membrane embedded

with a β-cyclodextrin/curcumin inclusion complex," *International Journal of Biological Macromolecules*, vol. 148, pp. 140–152, apr 2020. [Online]. Available: https://doi.org/10.1016%2Fj.ijbiomac.2020.01.104

[82] M. Hou, W. Liu, L. Zhang, L. Zhang, Z. Xu, Y. Cao, Y. Kang, and P. Xue, "Responsive agarose hydrogel incorporated with natural humic acid and MnO_2 nanoparticles for effective relief of tumor hypoxia and enhanced photo-induced tumor therapy," *Biomater. Sci.*, vol. 8, no. 1, pp. 353–369, 2020. [Online]. Available: https://doi.org/10.1039%2Fc9bm01472a

[83] X. Sun, C. Liu, A. Omer, L.-Y. Yang, and X. kun Ouyang, "Dual-layered pH-sensitive alginate/chitosan/kappa-carrageenan microbeads for colon-targeted release of 5-fluorouracil," *International Journal of Biological Macromolecules*, vol. 132, pp. 487–494, jul 2019. [Online]. Available: https://doi.org/10.1016%2Fj.ijbiomac.2019.03.225

[84] B. N. Matos, M. N. Pereira, M. de O. Bravo, M. Cunha-Filho, F. Saldanha-Araújo, T. Gratieri, and G. M. Gelfuso, "Chitosan nanoparticles loading oxaliplatin as a mucoadhesive topical treatment of oral tumors: Iontophoresis further enhances drug delivery *ex vivo*," *International Journal of Biological Macromolecules*, vol. 154, pp. 1265–1275, jul 2020. [Online]. Available: https://doi.org/10.1016%2Fj.ijbiomac.2019.11.001

[85] B. Tian, Y. Liu, and J. Liu, "Cyclodextrin as a magic switch in covalent and non-covalent anticancer drug release systems," *Carbohydrate Polymers*, vol. 242, p. 116401, aug 2020. [Online]. Available: https://doi.org/10.1016%2Fj.carbpol.2020.116401

[86] D. Li, T. Su, L. Ma, F. Yin, W. Xu, J. Ding, and Z. Li, "Dual-acidity-labile polysaccharide-di-drugs conjugate for targeted cancer chemotherapy," *European Journal of Medicinal Chemistry*, vol. 199, p. 112367, aug 2020. [Online]. Available: https://doi.org/10.1016%2Fj.ejmech.2020.112367

[87] C. Oliveira, N. M. Neves, R. L. Reis, A. Martins, and T. H. Silva, "A review on fucoidan antitumor strategies: From a biological active agent to a structural component of fucoidan-based systems," *Carbohydrate Polymers*, vol. 239, p. 116131, jul 2020. [Online]. Available: https://doi.org/10.1016%2Fj.carbpol.2020.116131

[88] I. S. Bayer, "Hyaluronic acid and controlled release: A review," *Molecules*, vol. 25, no. 11, p. 2649, jun 2020. [Online]. Available: https://doi.org/10.3390%2Fmolecules25112649

[89] H. Wei, W. Li, H. Chen, X. Wen, J. He, and J. Li, "Simultaneous Diels-Alder click reaction and starch hydrogel microsphere production via spray drying," *Carbohydrate Polymers*, vol. 241, p. 116351, aug 2020. [Online]. Available: https://doi.org/10.1016%2Fj.carbpol.2020.116351

[90] S. Minzanova, V. Mironov, D. Arkhipova, A. Khabibullina, L. Mironova, Y. Zakirova, and V. Milyukov, "Biological activity and pharmacological application of pectic polysaccharides: A review," *Polymers*, vol. 10, no. 12, p. 1407, dec 2018. [Online]. Available: https://doi.org/10.3390%2Fpolym10121407

[91] J. M. Korde and B. Kandasubramanian, "Microbiologically extracted poly(hydroxyalkanoates) and its amalgams as therapeutic nano-carriers in anti-tumor therapies," *Materials Science and Engineering: C*, vol. 111, p. 110799, jun 2020. [Online]. Available: https://doi.org/10.1016%2Fj.msec.2020.110799

[92] M. L. Tebaldi, A. L. C. Maia, F. Poletto, F. V. de Andrade, and D. C. F. Soares, "Poly(-3-hydroxybutyrate-co-3-hydroxyvalerate) (PHBV): Current advances in synthesis methodologies, antitumor applications and biocompatibility," *Journal of Drug Delivery Science and Technology*, vol. 51, pp. 115–126, jun 2019. [Online]. Available: https://doi.org/10.1016%2Fj.jddst.2019.02.007

[93] R. Borlan, A.-S. Tatar, O. Soritau, D. Maniu, G. Marc, A. Florea, M. Focsan, and S. Astilean, "Design of fluorophore-loaded human serum albumin nanoparticles for specific targeting of NIH:OVCAR3 ovarian cancer cells," *Nanotechnology*, vol. 31, no. 31, p. 315102, may 2020. [Online]. Available: https://doi.org/10.1088%2F1361-6528%2Fab8b90

[94] S. O. Correa, X. Luo, and C. B. Raub, "Microfluidic fabrication of stable collagen microgels with aligned microstructure using flow-driven co-deposition and ionic gelation," *J. Micromech. Microeng.*, vol. 30, jun 2020. [Online]. Available: https://doi.org/10.1088%2F1361-6439%2Fab8ebf

[95] L. Wang, J. Du, X. Han, J. Dou, J. Shen, and J. Yuan, "Self-crosslinked keratin nanoparticles for pH and GSH dual responsive drug carriers," *Journal of Biomaterials Science, Polymer Edition*, vol. 31, no. 15, pp. 1994–2006, jul 2020. [Online]. Available: https://doi.org/10.1080%2F09205063.2020.1788371

[96] M. T. Nazeri, S. Javanbakht, A. Shaabani, and M. Ghorbani, "5-aminopyrazole-conjugated gelatin hydrogel: A controlled 5-fluorouracil delivery system for rectal administration," *Journal of Drug Delivery Science and Technology*, vol. 57, p. 101669, jun 2020. [Online]. Available: https://doi.org/10.10162Fj.jddst.2020.101669

[97] J. Venkatesan, S. Anil, S.-K. Kim, and M. Shim, "Seaweed polysaccharide-based nanoparticles: Preparation and applications for drug delivery," *Polymers*, vol. 8, no. 2, p. 30, jan 2016. [Online]. Available: https://doi.org/10.33902Fpolym8020030

[98] B. H. Rehm and M. F. Moradali, Eds., *Alginates and Their Biomedical Applications*, ser. Springer Series in Biomaterials Science and Engineering. Singapore: Springer Singapore, 2018.

[99] T. Helgerud, O. Gserd, T. Fjreide, P. O. Andersen, and C. K. Larsen, "Alginates," *Food stabilisers, thickeners and gelling agents*, pp. 50–72, jan 2010. [Online]. Available: https://doi.org/10.33902Fpolym8020030

[100] K. I. Draget, O. Gåserød, I. Aune, P. O. Andersen, B. Storbakken, B. T. Stokke, and O. Smidsrød, "Effects of molecular weight and elastic segment flexibility on syneresis in Ca-alginate gels," *Food Hydrocolloids*, vol. 15, no. 4-6, pp. 485–490, jul 2001. [Online]. Available: https://doi.org/10.1016/S0268-005X(01)00046-7

[101] M. Szekalska, A. Puciłowska, E. Szymańska, P. Ciosek, and K. Winnicka, "Alginate: Current use and future perspectives in pharmaceutical and biomedical applications," *International Journal of Polymer Science*, vol. 2016, pp. 1–17, 2016. [Online]. Available: https://doi.org/10.1155%2F2016%2F7697031

[102] Q. He, T. Tong, C. Yu, and Q. Wang, "Advances in algin and alginate-hybrid materials for drug delivery and tissue engineering," *Marine Drugs*, vol. 21, no. 1, p. 14, dec 2022. [Online]. Available: https://doi.org/10.3390%2Fmd21010014

[103] M. A. Abureesh, A. A. Oladipo, Z. M. Mizwari, and E. Berksel, "Engineered mixed oxide-based polymeric composites for enhanced antimicrobial activity and sustained release of antiretroviral drug," *International Journal of Biological Macromolecules*, vol. 116, pp. 417–425, sep 2018. [Online]. Available: https://doi.org/10.1016%2Fj.ijbiomac.2018.05.065

[104] L. Sukhodub, M. Kumeda, L. Sukhodub, V. Bielai, and M. Lyndin, "Metal ions doping effect on the physicochemical, antimicrobial, and wound healing profiles of alginate-based composite," *Carbohydrate Polymers*, vol. 304, p. 120486, mar 2023. [Online]. Available: https://doi.org/10.1016%2Fj.carbpol.2022.120486

[105] B. Aderibigbe and B. Buyana, "Alginate in wound dressings," *Pharmaceutics*, vol. 10, no. 2, p. 42, apr 2018. [Online]. Available: https://doi.org/10.3390%2Fpharmaceutics10020042

[106] M. G. Funaro, K. V. Nemani, Z. Chen, Z. M. Bhujwalla, K. E. Griswold, and B. Gimi, "Effect of alginate microencapsulation on the catalytic efficiency andiin vitro/ienzyme-prodrug therapeutic efficacy of cytosine deaminase and of recombinantie. coli/iexpressing cytosine deaminase," *Journal of Microencapsulation*, vol. 33, no. 1, pp. 64–70, dec 2015. [Online]. Available: https://doi.org/10.3109%2F02652048.2015.1115902

[107] T. Andersen, P. Auk-Emblem, and M. Dornish, "3d cell culture in alginate hydrogels," *Microarrays*, vol. 4, no. 2, pp. 133–161, mar 2015. [Online]. Available: https://doi.org/10.3390%2Fmicroarrays4020133

[108] S. S. Lee, H. Kim, D. K. Sohn, J. B. Eom, Y. S. Seo, H. M. Yoon, and Y. Choi, "Indocyanine green-loaded injectable alginate hydrogel as a marker for precision cancer surgery," *Quant Imaging Med Surg*, vol. 10, no. 3, pp. 779–788, mar 2020. [Online]. Available: https://doi.org/10.21037%2Fqims.2020.02.24

[109] L. Zhao, S. Yin, and Z. Ma, "Casup2/sup-triggered pH-response sodium alginate hydrogel precipitation for amplified sandwich-type impedimetric immunosensor of tumor marker," *ACS Sens- Sensors*, vol. 4, no. 2, pp. 450–455, jan 2019. [Online]. Available: https://doi.org/10.1021 %2Facssensors.8b01465

[110] A. Hasan, A. Khattab, M. A. Islam, K. A. Hweij, J. Zeitouny, R. Waters, M. Sayegh, M. M. Hossain, and A. Paul, "Injectable hydrogels for cardiac tissue repair after myocardial infarction," *Adv. Sci.*, vol. 2, no. 11, p. 1500122, jul 2015. [Online]. Available: https://doi.org/10.1002%2Fadvs.201500122

[111] J. Leor, S. Tuvia, V. Guetta, F. Manczur, D. Castel, U. Willenz, Örs Petnehàzy, N. Landa, M. S. Feinberg, E. Konen, O. Goitein, O. Tsur-Gang, M. Shaul, L. Klapper, and S. Cohen, "Intracoronary injection of in situ forming alginate hydrogel reverses left ventricular remodeling

after myocardial infarction in swine," *Journal of the American College of Cardiology*, vol. 54, no. 11, pp. 1014–1023, sep 2009. [Online]. Available: https://doi.org/10.1016%2Fj.jacc.2009.06.010

[112] B. Reig-Vano, B. Tylkowski, X. Montané, and M. Giamberini, "Alginate-based hydrogels for cancer therapy and research," *International Journal of Biological Macromolecules*, vol. 170, pp. 424–436, feb 2021. [Online]. Available: https://doi.org/10.1016%2Fj.ijbiomac.2020.12.161

[113] S. B. Bae, H. C. Nam, and W. H. Park, "Electrospraying of environmentally sustainable alginate microbeads for cosmetic additives," *International Journal of Biological Macromolecules*, vol. 133, pp. 278–283, jul 2019. [Online]. Available: https://doi.org/10.10162Fj.ijbiomac.2019.04.058

[114] J. Kozlowska, W. Prus, and N. Stachowiak, "Microparticles based on natural and synthetic polymers for cosmetic applications," *International Journal of Biological Macromolecules*, vol. 129, pp. 952–956, may 2019. [Online]. Available: https://doi.org/10.10162Fj.ijbiomac.2019.02.091

[115] K. J. Kang, B.-H. Min, J. H. Lee, E. R. Kim, C. O. Sung, J. Y. Cho, S. W. Seo, and J. J. Kim, "Alginate hydrogel as a potential alternative to hyaluronic acid as submucosal injection material," *Dig Dis Sci*, vol. 58, no. 6, pp. 1491–1496, jan 2013. [Online]. Available: https://doi.org/10.10072Fs10620-012-2555-z

[116] J. M. Radhika Theagarajan, Sayantani Dutta and C. Anandharamakrishnan, "Alginates for food packaging applications," *Alginates: Applications in the biomedical and food industries*, no. 2, pp. 205–232, jan 2019.

[117] P. Cazón, G. Velazquez, J. A. Ramírez, and M. Vázquez, "Polysaccharide-based films and coatings for food packaging: A review," *Food Hydrocolloids*, vol. 68, pp. 136–148, jul 2017. [Online]. Available: https://doi.org/10.1016%2Fj.foodhyd.2016.09.009

[118] S. Benavides, R. Villalobos-Carvajal, and J. Reyes, "Physical, mechanical and antibacterial properties of alginate film: Effect of the crosslinking degree and oregano essential oil concentration," *Journal of Food Engineering*, vol. 110, no. 2, pp. 232–239, may 2012. [Online]. Available: https://doi.org/10.1016%2Fj.jfoodeng.2011.05.023

[119] E.-R. Kenawy and M. A. Sakran, "Controlled release formulations of agrochemicals from calcium alginate," *Ind. Eng. Chem. Res.*, vol. 35, no. 10, pp. 3726–3729, jan 1996. [Online]. Available: https://doi.org/10.10212Fie950448m

[120] F. A. Aouada and M. R. de Moura, "Nanotechnology applied in agriculture: Controlled release of agrochemicals," *Nanotechnologies in Food and Agriculture*, vol. 35, no. 10, pp. 113–118, jan 2015. [Online]. Available: https://doi.org/10.1007/978-3-319-14024-7$_5$

[121] M. González, M. Cea, J. Medina, A. González, M. Diez, P. Cartes, C. Monreal, and R. Navia, "Evaluation of biodegradable polymers as encapsulating agents for the development of a urea controlled-release fertilizer using biochar as support material," *Science of The Total Environment*, vol. 505, pp. 446–453, feb 2015. [Online]. Available: https://doi.org/10.10162Fj.scitotenv.2014.10.014

[122] I. M. Kadmiri, N. E. Mernissi, S. E. Azaroual, M. E. M. Mekhzoum, A. E. K. Qaiss, and R. Bouhfid, "Bioformulation of microbial fertilizer based on clay and alginate encapsulation," *Curr Microbiol*, vol. 78, no. 1, pp. 86–94, oct 2020. [Online]. Available: https://doi.org/10.1007%2Fs00284-020-02262-2

[123] S. Kumar, G. Bhanjana, A. Sharma, M. Sidhu, and N. Dilbaghi, "Synthesis, characterization and on field evaluation of pesticide loaded sodium alginate nanoparticles," *Carbohydrate Polymers*, vol. 101, pp. 1061–1067, jan 2014. [Online]. Available: https://doi.org/10.1016%2Fj.carbpol.2013.10.025

[124] Y.-L. Xie, W. Jiang, F. Li, Y. Zhang, X.-Y. Liang, M. Wang, X. Zhou, S.-Y. Wu, and C.-H. Zhang, "Controlled release of spirotetramat using starch–chitosan–alginate-encapsulation," *Bull Environ Contam Toxicol*, vol. 104, no. 1, pp. 149–155, nov 2019. [Online]. Available: https://doi.org/10.1007%2Fs00128-019-02752-5

[125] F. Artusio, D. Casà, M. Granetto, T. Tosco, and R. Pisano, "Alginate nanohydrogels as a biocompatible platform for the controlled release of a hydrophilic herbicide," *Processes*, vol. 9, no. 9, p. 1641, sep 2021. [Online]. Available: https://doi.org/10.3390%2Fpr9091641

[126] D. Jíménez-Arias, S. Morales-Sierra, P. Silva, H. Carrêlo, A. Gonçalves, J. F. T. Ganança, N. Nunes, C. S. S. Gouveia, S. Alves, J. P. Borges, and M. Â. A. P. de Carvalho, "Encapsulation with natural polymers to improve the properties of biostimulants in agriculture," *Plants*, vol. 12, no. 1, p. 55, dec 2022. [Online]. Available: https://doi.org/10.3390%2Fplants12010055

[127] R. S. Riseh, Y. A. Skorik, V. K. Thakur, M. M. Pour, E. Tamanadar, and S. S. Noghabi, "Encapsulation of plant biocontrol bacteria with alginate as a main polymer material," *IJMS*, vol. 22, no. 20, p. 11165, oct 2021. [Online]. Available: https://doi.org/10.3390%2Fijms222011165

[128] E. Manaila, G. Craciun, and I. C. Calina, "Sodium alginate-g-acrylamide/acrylic acid hydrogels obtained by electron beam irradiation for soil conditioning," *IJMS*, vol. 24, no. 1, p. 104, dec 2022. [Online]. Available: https://doi.org/10.3390%2Fijms24010104

[129] S. H. Park, K. Kim, J. H. Lim, and S. J. Lee, "Selective lithium and magnesium adsorption by phosphonate metal-organic framework-incorporated alginate hydrogel inspired from lithium adsorption characteristics of brown algae," *Separation and Purification Technology*, vol. 212, pp. 611–618, apr 2019. [Online]. Available: https://doi.org/10.1016%2Fj.seppur.2018.11.067

[130] N. Fatin-Rouge, A. Dupont, A. Vidonne, J. Dejeu, P. Fievet, and A. Foissy, "Removal of some divalent cations from water by membrane-filtration assisted with alginate," *Water Research*, vol. 40, no. 6, pp. 1303–1309, mar 2006. [Online]. Available: https://doi.org/10.1016%2Fj.watres.2006.01.026

[131] M. A. A. Aljar, S. Rashdan, and A. A. El-Fattah, "Environmentally friendly polyvinyl alcohol-alginate/bentonite semi-interpenetrating polymer network nanocomposite hydrogel beads as an efficient adsorbent for the removal of methylene blue from aqueous solution," *Polymers*, vol. 13, no. 22, p. 4000, nov 2021. [Online]. Available: https://doi.org/10.3390%2Fpolym13224000

[132] K. Akin, V. Ugraskan, B. Isik, and F. Cakar, "Adsorptive removal of crystal violet from wastewater using sodium alginate-gelatin-montmorillonite ternary composite microbeads," *International Journal of Biological Macromolecules*, vol. 223, pp. 543–554, dec 2022. [Online]. Available: https://doi.org/10.1016%2Fj.ijbiomac.2022.11.002

[133] R. Sohail and S. R. Abbas, "Evaluation of amygdalin-loaded alginate-chitosan nanoparticles as biocompatible drug delivery carriers for anticancerous efficacy," *International Journal of Biological Macromolecules*, vol. 153, pp. 36–45, 02 2020.

[134] S. Zhang, Z. Wu, G. Chen, and Z. Wang, "An improved method to encapsulate laccase from trametes versicolor with enhanced stability and catalytic activity," *Catalysts*, vol. 8, no. 7, p. 286, 2018. [Online]. Available: https://www.mdpi.com/2073-4344/8/7/286

[135] H. Cheng, H. Wu, T. Guo, H. Jin Park, and J. Li, "Zinc insulin hexamer loaded algi-
nate zinc hydrogel: Preparation, characterization and in vivo hypoglycemic ability,"
*European journal of pharmaceutics and biopharmaceutics : official journal of Arbeits-
gemeinschaft fur Pharmazeutische Verfahrenstechnik e.V*, vol. 179, pp. 173–181, 09
2022.

[136] Y. Feng, L. Niu, C. Sun, J. Tu, L. Yu, and J. Xiao, 2023.

[137] Z. Zheng, J. Qi, L. Hu, D. Ouyang, H. Wang, Q. Sun, L. Lin,
L. You, and B. Tang, "A cannabidiol-containing alginate based hydro-
gel as novel multifunctional wound dressing for promoting wound heal-
ing," *Biomaterials advances*, vol. 134, p. 112560, 2022. [Online]. Available:
https://www.sciencedirect.com/science/article/pii/S0928493121007001

[138] Q. Zhou, H. Kang, M. Bielec, X. Wu, Q. Cheng, W. Wei, and
H. Dai, "Influence of different divalent ions cross-linking sodium alginate-
polyacrylamide hydrogels on antibacterial properties and wound healing,"
Carbohydrate polymers, vol. 197, pp. 292–304, 2018. [Online]. Available:
https://www.sciencedirect.com/science/article/pii/S0144861718306325

[139] F. Benali, B. Boukoussa, N.-E.-H. Benkhedouda, A. Cheddad, I. Issam, J. Iqbal,
M. Hachemaoui, M. Abboud, and A. Mokhtar, 2022.

[140] P. Qin, J. Tang, D. Sun, Y. Yang, N. Liu, Y. Li, Z. Fu, Y. Wang, C. Li, X. Li,
Y. Zhang, Y. Liu, S. Wang, J. Sun, Z. Deng, L. He, Y. Wang, and X. Yang, 2022.

[141] F. Şen, İrem Uzunsoy, E. Baştürk, and M. V. Kahraman, "Antimicrobial agent-free
hybrid cationic starch/sodium alginate polyelectrolyte films for food packaging
materials," *Carbohydrate polymers*, vol. 170, pp. 264–270, 2017. [Online]. Available:
https://www.sciencedirect.com/science/article/pii/S0144861717304782

[142] D. Skrzypczak, Ł. Jarzembowski, G. Izydorczyk, K. Mikula, V. Hoppe, K. A. Mielko,
N. Pudełko-Malik, P. Młynarz, K. Chojnacka, and A. Witek-Krowiak, "Hydrogel
alginate seed coating as an innovative method for delivering nutrients at the early
stages of plant growth," *Polymers*, vol. 13, no. 23, 12 2021.

[143] J. Mendoza-Labrador, F. Romero-Perdomo, J. Abril, J.-P. Hernández, D. Uribe-
Vélez, and R. B. Buitrago, "Bacillus strains immobilized in alginate macrobeads
enhance drought stress adaptation of guinea grass," *Rhizosphere*, vol. 19, p. 100385,
2021.

[144] O. Purev, C. Park, H. Kim, E. Myung, N. Choi, and K. Cho, "Spirulina platensis im-
mobilized alginate beads for removal of pb(ii) from aqueous solutions," *International
journal of environmental research and public health*, vol. 20, no. 2, 2023.

[145] M. Levío-Raimán, C. Bornhardt, and M. C. Diez, "Biodegradation of iprodione and
chlorpyrifos using an immobilized bacterial consortium in a packed-bed bioreactor,"
Microorganisms, vol. 11, no. 1, 2023.

1.5   Thesis Objectives

The objectives of the thesis can be summarized as follows:

- Optimization of the beads production methodology. Technical factors such as Alg and crosslinker concentration, agitation speed and extrusion rate are considered. For the optimization process, Ca^{2+} is employed as crosslinking cation.

- Preparation of Alg beads with diverse crosslinking cations. On the one hand, we found interesting to supplement the existent comparison between Ca- and Cu-based Alg beads with further assays such as SAXS and EXAFS. On the other hand, Zn^{2+} is selected because we considered that its possibilities had not been yet fully explored and we saw in Zn^{2+} a potential agent to obtain Alg beads with unique properties required for diverse innovative applications.

- Establishing a relation between the physicochemical properties of the resulting beads and the crosslinking mechanisms of each cation in regard to the employed Alg.

- Encapsulation of a phenolic grape seed extract and characterization of the obtained beads in terms of morphology and encapsulation efficiency.

- Assessment of the potential benefits of the application of the alginate systems in Agriculture and Biomedicine. In first place, the influence of the cations Ca^{2+}, Cu^{2+} and Zn^{2+} released from the hydrogels and incubation time on the germination and seedling growth of mustard seed will be assessed. In second place, cell sensitivity and anti-cancer properties of the alginate systems, with and without BACs, will be evaluated by means of MTT cytotoxicity assays in 3T3, T24 and SV-HUC-1 cells.

Chapter 2

Materials and Methods

2.1   Materials

Sodium alginate was purchased from PanReac AppliChem (Barcelona, Spain). Calcium chloride anhydrous (Granular, 7.0 mm, 93.0%) and zinc chloride (reagent grade, 98%) were supplied by Sigma-Aldrich (Barcelona, Spain). Copper (II) chloride dihydrated (reagent grade, 98%) was acquired from Fisher scientific (Barcelona, Spain).

Bibraund Sterican 0.5 · 16 mm BL/BL 25 G · 5/8" needles and 10 mL NORM-JECT syringes were supplied by Sigma-Aldrich (Barcelona, Spain). Crystallizers (125 mm LBG 3.3) were obtained from Labbox (Barcelona, Spain).

Deuterium oxide (99.8%) (D_2O) was purchased from Sigma-Aldrich (Barcelona, Spain).

Standard calibrators pH 4 and pH 7 were obtained from Scharlab, Monobuf (Barcelona, Spain) and pH 10.01 from Fisher Scientific (Barcelona, Spain).

Vitaflavan (grape seed phenolic extract) from Les Dérivés Résiniques et Terpéniques (Dax, France) was a gift from Dr. Miquel Mulero Abellán (Nutrigenomics, Department of Biochemistry, Rovira i Virgili University).

Folin-Ciocalteu's reagent was supplied by PanReac AppliChem (Barcelona, Spain). Sodium carbonate anhydrous (White crystalline powder, 99.5%) was purchased from Fisher scientific (Barcelona, Spain). Gallic acid was acquired from Sigma (Barcelona, Spain).

Bidistilled water was produced in our laboratory.

Mustard *Brassica juncea* seeds were provided from Kampol PPHU (Rusiec, Poland). The soil used in the experiments was sandy-loam soil collected in the National Institute of Horticultural Research INHORT (Skierniewice, Poland) and contained: N-

NO_3- 53; P – 64; K – 107; Mg – 131 and Ca – 705 mg L^{-1} of soil. Perlite (3-6 mm) was obtained from Biovita (Poland).

3T3 NIH cell line (mouse embryonic fibroblasts) were purchased from the Interlab Cell Line Collection (ICLC) cell bank (San Martino Polyclinic Hospital, Genova, Italy). All reagents for cell cultures were supplied by Invitrogen (Massachusetts, USA). Multi well plates were obtained from Sarstedt (Nümbrecht, Germany). The MTT assay kit was purchased from Sigma-Aldrich (Gillingham, UK).

2.2   Methods

2.2.1   Preparation of polymeric solutions

2.2.1.1   Preparation of polymeric solution alginate 1.7% (w/w)

The studies are based on a polymeric solution consisting of alginate (Alg). To prepare the solution, 1.7 g of Alg are dissolved into distilled water under mild agitation. Subsequently, the solution's total mass is adjusted to 100 g using distilled water, resulting in a final concentration of Alg 1.7% (w/w). The polymeric solution is left for 24 h under gentle stirring (900 rpm) before its utilization in the experiments.

2.2.1.2   Preparation of polymeric solution alginate 1.7% (w/w) and grape seed phenolic extract

The polymeric solution comprising both Alg and grape seed phenolic extract (BACs) is prepared through the following procedure: First, 1.7 g of Alg is dissolved in distilled water (approximately reaching a mass of 40 g) and let under gentle stirring for 20 min. At the meantime, a water suspension containing 0.17 g of BACs in distilled water (20 g approximately) is prepared separately and subsequently mixed with the Alg solution. The final mass is then adjusted to 100 g using distilled, resulting in a final concentration of Alg 1.7% (w/w) and BACs 0.17% (w/w). The resulting polymeric solution is kept in dark under magnetic agitation (900 rpm) for 24 h at room temperature. Given their photosensitivity, all procedures implying BACs are conducted within brown-colored glass bottles.

This specific polymeric solution and the resultant beads are designated as BACs 10%, which depicts the relative concentration of BACs in relation to Alg. To obtain more concentrated polymeric solutions, the respective amounts of 0.34 g, 0.51 g, 0.68 g and 0.85 g of BACs are added. These polymeric solutions and the resulting beads are referred to as BACs 20%, BACs 30%, BACs 40% and BACs 50% respectively.

41

2.2.2   Preparation of hydrogels

2.2.2.1   Preparation of alginate beads

Calcium, copper and zinc (Ca-, Cu- and Zn-) beads are produced by external ionotropic gelation (Figure 2.1). Hence, 10 g of polymeric solution are extruded dropwise into a crosslinking bath under mild agitation (100 rpm) at room temperature. The extrusion is performed using a peristaltic pump (KDS 100 LEGACY SYRINGE PUMP, KDScientific, Massachusetts, USA) through a plastic syringe and a Sterican needle $0.5 \cdot 16$ mm BL/BL 25 G $\cdot$ 5/8" Bibraund (25G syringe needle) at an extrusion rate of 0.4 mL/min. The distance between the tip of the needle and the bath is maintained at 2.5 cm. The crosslinking bath consists of 200 g of an aqueous solution $CaCl_2$, $CuCl_2$ or $ZnCl_2$ (MCl_2) contained in a 125 mm crystallizer. After extrusion, the crystallizer is covered with Parafilm and left under magnetic stirring (100 rpm) for 48 hours at room temperature to allow for maturation. The formed beads are collected by filtration, washed with distilled water and dried in an oven at 40°C. After 24 h, they are stored in transparent flasks for further studies.
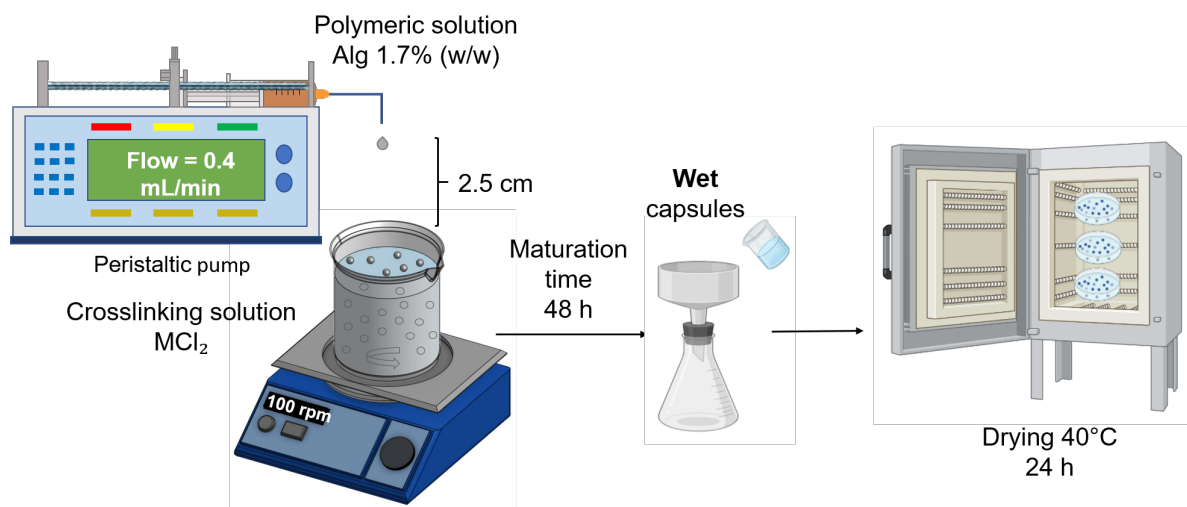
Figure 2.1: Set up of Alg beads preparation

2.2.2.2 Preparation of BACs-loaded alginate beads

The methodology followed to prepare BACs-loaded Alg beads is the same as previously reported in section 2.2.2.1 (Figure 2.1). Nevertheless, the system is protected from light with aluminium foil. The resultant beads also rest within the crosslinking bath under magnetic stirring (100 rpm) for 48 h to ensure complete beads' maturation. The resulting beads are collected by filtration and washed. They are dried in an oven at 40°C for 24 h and stored in brown colour flasks for further studies.

2.2.3 Alginate characterization

2.2.3.1 ^1H nuclear magnetic resonance

For the ^1H nuclear magnetic resonance (NMR), 20 mg of sodium Alg are dissolved in 1 mL of D_2O. The ^1H NMR spectra is recorded with a Varian Gemini 400 MHz NMR spectrometer (^1H – 400 MHz, tetramethylsilane; ^{13}C – 100 MHz, tetramethylsilane) (Agilent, California, USA) with a pulse delay time of 5 seconds. NMR is run at 70°C and presaturation is applied during the relaxation delay and mixing time with 25 Hz. Previously reported ^1H NMR spectra of sodium Alg is taken as a reference for the study of our sample.

2.2.3.2 Viscosity measurements

The viscosity of polymeric solution BACs 50% is measured with a rotational viscometer ROTAVISC lo-vi (IKA, Staufen, Germany) at room temperature, using spindle VOL-SP-13.5 and a speed of 50 rpm. Flow time values are superior to 5 minutes in all measurements. The error range under these conditions is 37.49 mPa.s.

2.2.4 Characterization of crosslinking bath

2.2.4.1 pH measurements

The pH measurements of the solutions are performed using an Orion 4-STAR plus pH/Conductivity benchtop meter (Thermo Scientific, Barcelona, Spain) with a model number 13-650-133. The calibration of the pH meter is conducted using buffer solutions with pH values of 4, 7, and 10.01 (Monobuf) in accordance with the ISO/IEC 17025 standard.

2.2.4.2   Inductively coupled plasma - Kinetics study

The objective of this kinetics study is to investigate the kinetics and isotherms of Zn^{2+} adsorption onto Alg beads. Therefore, Zn-Alg gelation assays are conducted using a 1.7% (w/w) polymeric solution of Alg, with a total volume of 50 g (distributed among four syringes, each containing 12.5 g). The Alg solution was added dropwise into a 1 L crystallizer containing a 0.5% (w/w) $ZnCl_2$ solution in MilliQ water. The evolution of Zn^{2+} concentration is monitored over a period of 48 h at room temperature. The beads are kept under continuous stirring at 100 rpm to ensure uniform distribution. The distance between the tip of the needle and the crosslinking bath is maintained at 2.5 cm. The extrusion is performed using a Sterican needle 0.5 · 16 mm BL/BL 25 G · 5/8" Bibraund (25G syringe needle) with an extrusion rate of 2 mL/min. Notably, the extrusion rate, the amount of polymeric solution used and the crosslinking bath volume are increased by five times compared to the preparation of beads described in section 2.2.2.1 in order to maintain a constant preparation time for the beads. For the analysis of Zn^{2+} concentration in the crosslinking bath,10 mL aliquots are withdrawn from the crosslinking bath at diverse time intervals. The concentration of Zn^{2+} is determined using inductively coupled plasma optical emission spectroscopy (ICP-OES) performed with a ICP-OES Spectro Arcos 160CCD instrument (Madrid, Spain). To prepare the samples for analysis, they are filtered and acidified with nitric acid at a concentration 1% (v/v). A four-point standard curve from 0.8 to 80 mM Zn^{2+} is employed to quantify the concentration of Zn^{2+} in the crosslinking bath.

2.2.5   Characterization of beads

2.2.5.1   Microscopes

The dimensional distribution and morphology of wet and dried beads is studied using an optical microscope LEICA DM 2500 (Leica microsystems, Wetzlar, Germany). Images of SV-HUC-1 and T24 cells are captured using an inverted, phase contrast microscope Olympus CKX53

2.2.5.2   Environmental scanning electron microscopy and energy dispersive X-Ray spectroscopy

The morphology and internal structure of dry beads is examined using environmental scanning electron microscopy (ESEM) with a FEI ESEM Quanta 600 (Eindhoven, Netherlands). The analyses are performed under low vacuum conditions at an electron beam intensity of 10-15 kV, employing various magnifications. The associated

energy dispersive X-Ray spectroscopy (EDX) detector is utilized to determine the distribution of cations within the beads. For sample preparation, the beads are mounted onto metal stubs using two-sided adhesive carbon tape. Cross-sections are obtained by cutting dry beads into slices employing liquid nitrogen and a surgical blade. A total of 4-5 beads are analysed per condition, considering different crosslinking agents and concentrations, to ensure representative observations and accurate conclusions.

2.2.5.3   Cryofracture

The evolution of beads' inner structure during maturation time is assessed through cryofracture analysis. For this purpose, wet beads are collected at various time intervals: 1 h, 6 h, 24 h and 48 h after preparation. Cryogenic preparation is carried out under vacuum in a cryopreparation system Epredia cryostat, CryoStar NX50 (Fisher Scientific, Massachusetts, USA). The cryofracture process involves the immersion of a small number of wet beads into liquid nitrogen, which induces a freeze-fracture in the beads. Subsequently, the selected beads are transferred to a cold metal block and maintained at low temperatures while being sliced using two precooled needles. This process results in the creation of free-break surfaces.

To prepare the samples for ESEM analysis, the obtained beads are attached to an aluminium stab with carbon adhesive and then coated with a thin gold layer (approximately 200–400 Å thick) through sputter-coating (30 mA, 3 min, 5 kV, 50 pA) using an ion sputter instrument model SCD 040 (Bal-Tec, Balzers, Liechtenstein). To ensure reliable observations and accurate results, approximately 4-5 beads are observed and analyzed for each condition, considering different crosslinking agents and concentrations.

2.2.5.4   Thermogravimetric analysis

Thermogravimetric analyses (TGA) are performed to investigate the thermal stability and final composition of Alg beads. The TGA experiments are conducted using a Mettler-Toledo TGA/SDTA 851e thermobalance (Mettler-Toledo Inc., Schwerzenbach, Switzerland). For each TGA test, approximately 18 mg of sample are utilized. The analyses are performed in a dynamic mode, operating in the temperature range from 30°C to 800°C in air with a gas flow rate of 50 mL/min and a heating rate of 10°C/min. Before initiating the TGA analysis, samples are subjected to isothermal holding at 30°C for 15 min. This step is carried out to eliminate any superficial water present in the samples.

2.2.5.5   Attenuated total reflectance-assisted Fourier transform infrared spectroscopy

The binding nature of cations−uronic acid residues interactions is evaluated using Fourier-transform infrared (FT-IR) spectroscopy. Samples are analysed using an FT-IR spectrometer 680 Plus (Jasco Analitica Spain, Madrid, Spain) by attenuated total reflectance (ATR). To evaluate the binding interactions, samples of sodium Alg powder and Alg beads crosslinked with $CaCl_2$, $CuCl_2$ or $ZnCl_2$ at a concentration of 0.5%, 2% and 10% (w/w) are used. Sodium Alg is employed as a reference in the analysis. Thus, one single dry bead at once is placed between the diamond crystal and the ATR accessory. Spectra is run in transmission mode with 32 scans and a resolution of ± 4 cm^{-1}, monitoring a wavenumber range from 400 to 4000 cm^{-1}. IR data is recorded and managed using OPUS software from Bruker. Baseline is corrected and smoothed.

Basis of FT-IR

The principle underlying FT-IR spectroscopy lies in the interaction between infrared (IR) radiation, represented as a sinusoidal electromagnetic wave, and molecules like Alg, cations and water. When these molecules interact with IR radiation, they undergo distinct vibrational modes, which correspond to specific wavelengths in the IR spectra (as detailed in Table 4, Chapter 3). Vibrational excitation occurs if the interaction between the electric field and molecules possesses sufficient energy. Consequently, this excitation leads to alterations in the dipole moment of the charged system. To induce this vibrational excitation, the frequency of the IR radiation must match the frequency of the vibrating mode.

In FT-IR spectroscopy, various types of molecular vibrations can be observed, such as symmetric or asymmetric stretching of bond lengths and bending of angles, which are considered IR active. For instance, Figure 2.2 displays a representation of a) symmetric and b) asymmetric stretching vibrations of a carboxylate [1].

The principal IR spectroscopy techniques are two: transmission (measurement of the quantity of transmitted radiation through the sample) and reflection (determination of the reflected light after surface impinging) [1]. Given that IR radiation just penetrates the samples from 1 to 10 μm, the obtained information of the reflectance might be an estimation of the beads' closest surface area.
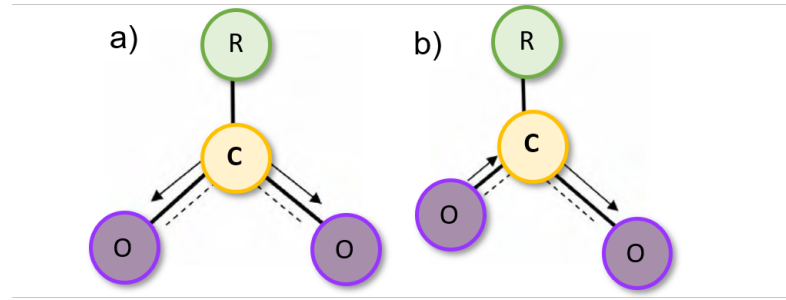
Figure 2.2: Sketch of a) symmetric and b) asymmetric stretching vibrations of a carboxylate

2.2.5.6   Compression tests - Mechanical properties

Dynamic mechanical analysis in compression is performed to assess the effect of crosslinker type and concentration on beads' mechanical properties. The analysis is conducted using a dynamic-mechanical thermal analyser DMAQ800 (TA Instruments, Delaware, USA). The compression tests are performed in static mode, utilizing a compression clamp with a 15 mm diameter plate. Compression strength is determined at 25°C with a ramp force of 2 N/min. During the test, both the compressive extension and reactive force are recorded using TA analysis software. To ensure reliability and accuracy, the compression approach is tested on a minimum of ten beads with the same experimental conditions, and the statistical results are subsequently reported.

The diameter (D) of dry beads is measured using a Mitutoyo 547 digital Thickness Gage for precise measurements, which provides a resolution of 0.01 mm and an accuracy of ± 20 μm. To evaluate the failure behaviour of each bead, photographs are taken before and after the compression test using a Digital Microscope Leica DMS1000.

The force (F) versus displacement (ΔL) curve is obtained for each tested bead. On the one hand, the calculation of the stress at break (σ_b) is based on the compression and crush of the beads and the quantification of the resultant stress. To evaluate the stress at break (if capsules shatter), it is assumed that the contact surface is the transverse circular section. Thus, equation 2.1 is applied.

$$\sigma_{brake} = \frac{F_{break}}{\left(\dfrac{\pi}{4}D^2\right)} \tag{2.1}$$

On the other hand, Young's modulus (E) is calculated from the linear part of the curve $F - (\Delta L/2)^{3/2}$ applying the Hertz theory [2] and a Poisson ratio of 0.5 [3, 4]. Certain assumptions need to be considered to comprehend this theory:

1. The matter of the contacting beads is homogeneous. If the condition is not met, it is assumed to be homogeneous to suit the mechanical behavior analysis.

2. The outer layer of the contacting beads is smooth enough for the tangential forces to be annulled.

Young modulus is quantified using the expression:

$$F = \frac{4}{3}D^{\frac{1}{2}}\frac{E}{1-\nu^2}(\frac{\Delta L}{2})^{\frac{3}{2}} \tag{2.2}$$

, where:

- F depicts the force exerted during the compression (N).

- D regards to the deformation (m) described as the range between the piston at a given deformation and the initial position in contact with the bead.

- ν refers to the Poisson ratio.

- ΔL refers to the displacement.

2.2.6   X-ray diffraction (XRD)

2.2.6.1   Wide angle XRD

The composition of beads and TGA residues is determined by wide angle X-ray diffraction (WAXS). Tests are made using a diffractometer D8-Advance (Bruker-AXS, Billerica, Massachusetts, USA) with vertical theta-theta goniometer, incident- and diffracted-beam Soller slits of 2.5°, a fixed 0.5° receiving slit and an automatic Air-scattering knife on the sample surface. The angular 2θ range is between 0.5° and 50° for beads and between 5° and 80° in case of TGA residues. Data is collected with an angular step of 0.02° at a step/time of 0.5 seconds. Cuk_α radiation is obtained from a copper X-ray tube operated at 40 kV and 40 mA. Diffracted X-rays are detected with a PSD detector LynxEye-XE-T with an opening angle of 2.94°. Sample is deposited on a low-background support (Si(510)).

The diffractograms are recorded and interpreted with the software DIFFRAC.EVA 5.2 from Bruker.axs and the database PDF-2 release 2018 from ICDD (International Center for Diffraction Data).

2.2.6.2   Small angle XRD

In situ Small angle X-ray scattering (SAXS) measurements are performed in the BL11 NCD-SWEET beamline from the ALBA Synchrotron Light source, Barcelona, Spain (project ID 2022097172). Alg xerogels are placed between Kapton tape. The incoming beam energy is set at 15 keV with a sample detector distance of 3600 mm. 2D patterns are recorded in a Pilatus 1M (Dectris, Switzerland) detector. Patterns are recorded during 1 and 30 seconds integration, where no radiation damage effects are observed during measurements. Isotropic 2D patterns are integrated using pyFAI library [5] where the obtained q-rage is between 0.07 and 3.5 nm^{-1} where $q = (\frac{4\pi}{\lambda})sin(\theta)$ with λ incoming beam wavelength and 2θ the scattering angle.

SAXS models

After drying/aging the beads evolve to compact structures where part of the beam showed some degree of crystallinity. The formation of small crystalline structures affected the low angle region with the appearance of a power Law of ca 4 (smooth surface crystals) and a clear diffraction peak between 1.4 and 1.65 nm^{-1} depending on the sample (4.5-3.8 nm expressed in $d_{spacing} = \frac{2\pi}{q}$). However, part of the remaining original structure obtained from the hydrogel could be observed.

Since previews reports in Alg based hydrogels showed a rod-like structure [6], we approximated this object thought a semi-empirical Guinier-Porod function [7] which is given by a split function which contains a Guinier and a Porod function:

$$GP(q, R_g, s, d) = \begin{cases} \dfrac{1}{q^s}exp(-\dfrac{R_g^2 q^2}{3-s}), & \text{if } q \leq Q_1 \\[3mm] \dfrac{D}{q^d}, & \text{if } q \geq Q_1 \end{cases} \tag{2.3}$$

, where:

- D is calculated such that the Guinier and the Porod function presents continuity at the boundary point Q_1 as its first derivative.

- R_g is the radius of gyration of the scatterer.

- S refers to the power law exponent at low angles, which is 1 for rod-like structures.

- d concerns to the Porod exponent.

49

The parameter "s" is set as larger compact structures were recognized, which supported the scattered intensity recorded. The Q_1 value is defined as:

$$Q_1 = \frac{1}{R_g}\left[\frac{(d-s)(3-s)}{s}\right]^{\frac{1}{2}} \qquad (2.4)$$

In the present data, a Porod exponent of 4 (attributed to smooth surface) was observed. This exponent corresponds with the power law at medium regimes described by other authors (usually called $\alpha 2$) [6, 8, 9], however exponents near 4 were observed in low pH hydrogels [8], moreover it is expected that the drying process made the structure more compact, hence, this parameter was kept fixed in order to decrease the number of fitting variables. The final model considered a rod-like structure (eq. 2.5):

$$I(q) = C_1 P_{GP}(q, R_g) + C_2 G(q, qc_1, FWHM_1) + C_3 G(q, qc_2, FWHM_2) + \frac{c_3}{q^p} \qquad (2.5)$$

, where:

- C_1, C_2, C_3, C_4 are scalars.

- qc_1 and $FWHM_1$ are the position and width of a Gaussian function for the diffraction peak.

- qc_2 and $FWHM_2$ are the position and width of the amorphous material (background at high angles).

- p is the power law function for the background at very low angles (ca 4).

Eventually, Patterns were analyzed using an in-house written program in Python 3.8 using the lmfit library for least-square procedures [9].

2.2.6.3   Extended X-ray absorption fine structure

Extended X-ray absorption fine structure (EXAFS) measurements are performed at the BL16-NOTOS beamline at ALBA synchrotron Light Source in Barcelona, Spain (project ID 2021025034). The EXAFS spectra of the Cu, Zn k-edges are recorded at room temperature in transmission mode with three ion chambers as detectors with gas mixture optimized to improve the measured signal. Third ionization chamber is used to measure the Cu and Zn metallic references simultaneously with the sample for energy calibration. The samples are placed between Kapton windows. The EX-AFS data are extracted from the measured absorption spectra by standard methods

using the LARCH software, which is part of the IFFEFIT package. The structural parameters (coordination numbers, bond lengths, and their mean squared disorders) are obtained by a nonlinear least-squares fit of the EXAFS signal in R-space. The theoretical scattering path amplitudes and phase shifts for all the paths used in the fits are calculated using the FEFF code. The k-range is set from 3 to 14 $\mathring{A}^{-1}$ and the Fourier transforms are fitted in different regions. The passive reduction factor S0 is restrained to a value of 0.90 for Zn and 0.88 for Cu. This value is obtained from fitting the EXAFS spectrum of a metallic Zn and Cu foils respectively and by constraining the coordination number of each metallic component.

2.2.7   Folin–Ciocalteu colorimetric assay

Polyphenols are quantified following Folin–Ciocalteu (FC) colorimetric assay as previously assessed by Singleton et al. [10] with minor modifications. A sample aliquot of 0.5 mL is mixed with 0.5 mL of FC reagent and 10 mL of water in a 22 mL amber vial. After 5 min, 8 mL of Na_2CO_3 7.5 % (w/w) aqueous solution are added to the vial and mixed. Following 2 h incubation at room temperature, absorbance is read at 765 nm in a UV-1800 Spectrophotometer (Shimadzu, Kyoto, Japan). UV/Vis data is recorded with UVprobe software version 2.52 supplied by Shimadzu. Analysis are conducted in triplicate.

Basis of Folin–Ciocalteu assay

Folin–Ciocalteu (FC) Assay is a widely used analytical method based on a commercially available FC reagent, originally developed by Otto Folin and Vintilă Ciocâlteu. FC reagent is composed of a mixture of complexes of phosphotungstic acid ($H_3PW_{12}O_{40}$) and phosphomolybdic acid ($H_3PMo_{12}O_{40}$) [11]. These complexes enable a redox reaction between the FC reagent and the phenolic compounds present in a basic medium, resulting in the formation of a blue–coloured chromophore with an absorption peak at 765 nm [12].

The oxygen uptake by phenolic compounds occurs rapidly near or above their pK value, which is typically around pH 10. In a basic medium, the phenolic compounds undergo deprotonation, generating phenolate anions that can reduce the FC reagent [13]. Hence, this reaction occurs in the presence of an alkaline reagent - Na_2CO_3.

It is widely accepted that molybdenum (Mo) serves as the electron acceptor from the phenolic compounds. Consequently, the phenols reduce Mo^{6+} to Mo^{5+}, leading to a noticeable change in colour from intense yellow (Mo^{6+}) to blue (Mo^{5+}), resulting in an increase in absorbance (Figure 2.3) [14]. This absorbance variation can be easily

measured using a UV/Vis spectrophotometer and is directly proportional to the total phenol content (TPC). To quantify the TPC, the absorbance of the sample is related to the absorbance of a standard antioxidant, which typically is gallic acid, expressing the results in terms of gallic acid equivalents [15]. Nevertheless, other standards like catechin, caffeic acid, chlorogenic acid, or ferulic acid may be employed [16, 17].
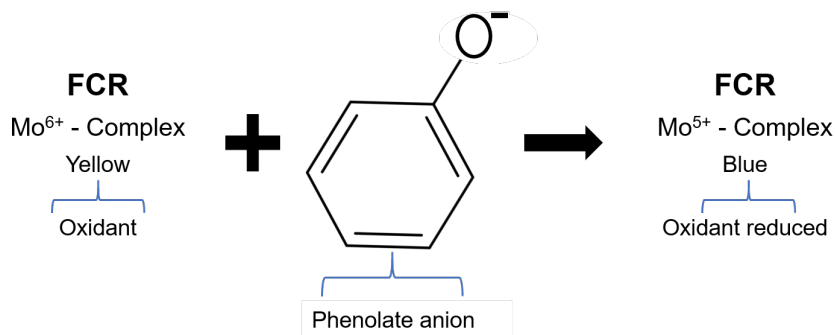
Figure 2.3: Reduction reaction of FC reagent during polyphenols quantification

2.2.7.1   Total phenolic content

For the calculation of the total phenolic content (TPC) in the grape seed extract (BACs), the sample contains 10 mg of BACs diluted in 100 mL of MilliQ water. External calibration is performed with gallic acid (GA) dissolved in MilliQ water. A six-point standard curve from 0.092 to 0.46 mg GA/mL is employed to quantify the TPC of the sample. The obtained calibration curve is:

$$Abs765nm = 2.40 \cdot GA\%(w/w) - 0.028 \qquad R^2 = 0.99 \qquad (2.6)$$

2.2.7.2   Encapsulation efficiency

The amount of BACs entrapped into the Alg beads is determined indirectly by the quantification of the TPC remaining in the crosslinking bath after beads maturation time, which are not encapsulated.

The encapsulation efficiency (EE) is calculated using the following equation:

$$EE(\%) = \frac{L_0 - L}{L_0} 100 \tag{2.7}$$

, where L_0 is the initial TPC in the extruded polymeric solution (theoretical load) and L is the TPC present in the crosslinking bath after preparing the beads.

TPC is calculated following the FC method as previously described in section 2.2.7. A six-point standard curve is established with GA diluted in $CaCl_2$ or $CuCl_2$ 2% (w/w).

2.2.8   Matrix-assisted laser desorption/ionization time-of-flight mass spectrometry

Matrix-assisted laser desorption/ionization time-of-flight mass spectrometry (MALDI-TOF) analysis is conducted using an Agilent 1200 liquid chromatograph coupled to a 6210 Time of Flight (TOF) mass spectrometer from Agilent Technologies (Waldbronn, Germany), with an electrospray ionization (ESI) source interface for the acquisition of mass spectra. The fragmentator voltage is maintained at 120 V. Samples are directly injected into the system with a flow rate of 0.6 mL/min, employing a mobile phase consisting of a 50% acetonitrile/methanol mixture.

Raw data from the mass spectrometry analysis are processed using the 'find-by-formula' algorithm available in the Agilent Profinder B.06 software. This algorithm generates a score based on the similarities between the sample spectra and a reference formula, which has been previously adjusted in consideration of the expected compounds. The top matching results, indicated by the formulas with the highest scores, are then displayed. Subsequently, the identified formulas are cross-referenced with the corresponding polyphenols using a database exported from Phenol-Explorer 3.0 [18].

2.2.8.1   Identification of polyphenols

The BACs formula is characterized from a sample that consists of 100 mg of BACs diluted in distilled water at a final concentration of 0.1% (w/w).

2.2.8.2   Release assay

The BACs release is assessed from the extract of 200 mg of beads after 24h in contact with distilled water.

2.2.9   High-performance liquid chromatography

The detection of GA is performed using a reverse phase high-performance liquid chromatography (HPLC) employing an Agilent 1100 system equipped with a C18 column. The mobile phase utilized in this analysis is a composition of ammonium acetate, water and acetonitrile, with a ratio 1:83:16 (pH 4.3). The flow rate of the mobile phase is set at 0.6 mL/min, and the UV detection is performed at a wavelength of 270 nm. In a related study performed by Silva et al.[19] triethylammonium phosphate was employed instead of ammonium acetate. The pH of the mobile phase was adjusted to 4.3 using acetic acid.

2.2.10   *In vitro* cell culture

Cells are cultured in Dulbecco's Modified Eagle's Medium (DMEM)/F-12 (50:50 1X) supplemented with 10% fetal bovine serum (FBS) at a volume of 45 mL per 500 mL of medium. Additionally, the culture medium is supplemented with antibiotics, including penicillin, streptomycin and amphotericin B at a concentration of 5 μL per 500 mL. The cell culture is maintained within a humidified incubator HERA cell supplied by Kendro Laboratory Products Gmbh (Hanau, Germany) at a temperature of 37°C and in an atmosphere with 5% CO_2.

2.2.10.1   Cell passage

Cells are seeded in a 75 cm^2 flask and passaged upon reaching 90% confluence through a gentle trypsinization process. During the passage, the cells are initially washed with 2 mL of PBS to eliminate cellular debris. Subsequently, PBS is removed and 1-2 mL of trypsin is added. The flask is incubated for a maximum of 3-5 min. Under microscopic observation, the detachment of cells from the flask's surface is checked. Following this, 1-2 mL of fresh medium is introduced to finish the trypsinization process. Using a pipette, the detached cells are transferred to a 15 mL falcon tube. The falcon tube is then centrifuged at 15000G for 5 min at 22°C. Eventually, supernatant is discarded and 2 mL of fresh culture media is added to resuspend the cells.

2.2.10.2   Cell count

After the passage, the number of cells in the 2 mL of culture media is quantified. For this purpose, 15 μL of resuspended cells are sampled from the falcon tube and mixed with 15 μL of trypan blue in a Neubauer glass (Figure 2.4). The cell count is determined by calculating the average number of cells observed in at least 4 big squares of the Neubauer glass. Each big square comprises 16 smaller squares - 1 mm^2.
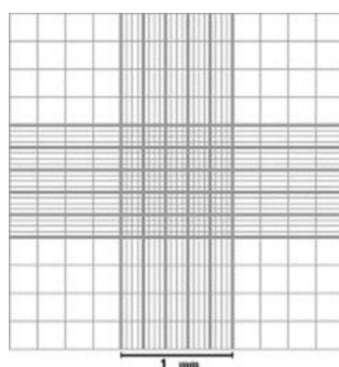
Figure 2.4: Neubauer chamber

2.2.10.3   Preparation of beads' extracts

Various extracts are prepared using different quantities of Alg beads. Initially, the beads are immersed in 1.5 mL of acidic media (HCl 1M X10, pH 2) and incubated for a duration of 2 h. Then, the acidic media is replaced with 2.5 mL of fresh culture media, and the beads are further incubated for 24 h. Eventually, the mixture is centrifuged at 350 G for 3 min , resulting in the separation of the supernatant, which represents the extract. The obtained extract is then tested on cells at varying concentrations, namely 100%, 10%, 1% and 0,1% to estimate the appropriate starting dose for the following cytotoxicity assays. The extract is diluted using fresh culture media during these tests.

2.2.10.4   MTT assay

The MTT method is used to assess cellular viability and cytotoxicity. It involves the use of (3-[4,5-dimethylthiazol-2-yl]-2,5 diphenyl tetrazolium bromide) - MTT. The experimental procedure begins by seeding cells in 96-well flat-bottom plates at a density of 5000 cells per well. After 24h, the culture medium is replaced with 100 µl of extracts obtained from the beads. The cells are then incubated for 24h with

the corresponding treatment. As a positive control, some wells are left with culture media only (no treatment). Afterwards, each well is washed with 100 μl of phosphate-buffered saline (PBS) and incubated for 5 min. After this incubation period, PBS is discarded, and 50 μl of MTT solution (at a concentration of 5 mg/mL) is added to each well. The cells are then incubated in the dark for 2 hours. After the MTT incubation, the MTT solution is replaced with 100 μl of dimethyl sulfoxide (DMSO). This step helps dissolve the formazan crystals produced by viable cells during the MTT reaction. Finally, the cell viability is assessed by measuring the absorbance of each well at two wavelengths, at 570 nm and 655 nm, using a spectrophotometer (Varioskan, Thermo Fisher Scientific, Barcelona, Spain) and analyzing the data with Scanlt 5.0 software. All experimental conditions were tested at least in quintuplicate.

Basis of MTT assay

The MTT assay is based on the enzymatic activity of mitochondrial dehydrogenases, which are (NAD(P)H-dependent cellular oxidoreductase enzymes). These enzymes facilitate the reduction of MTT (yellow colored) to formazan as depicted in Figure 2.5 [20]. Enzymatic catalysis only occurs in viable cells. Hence, healthy and normally growing cells display higher rates of MTT reduction compared to inactive or dead cells. As a result of this reduction reaction, insoluble formazan crystals are formed. Subsequently, they are solubilized using DMSO, leading to the development of a purple color, which is monitored spectrophotometrically at 565 nm. Absorbance at 565 nm is normalized with reference wavelength at 655 nm to minimize the influence of non-specific absorption. MTT is usually removed before adding DMSO in order to withdraw the unbound MTT, which can also interfere in the spectrophotometric analysis. Cells die during the MTT conversion to formazan.
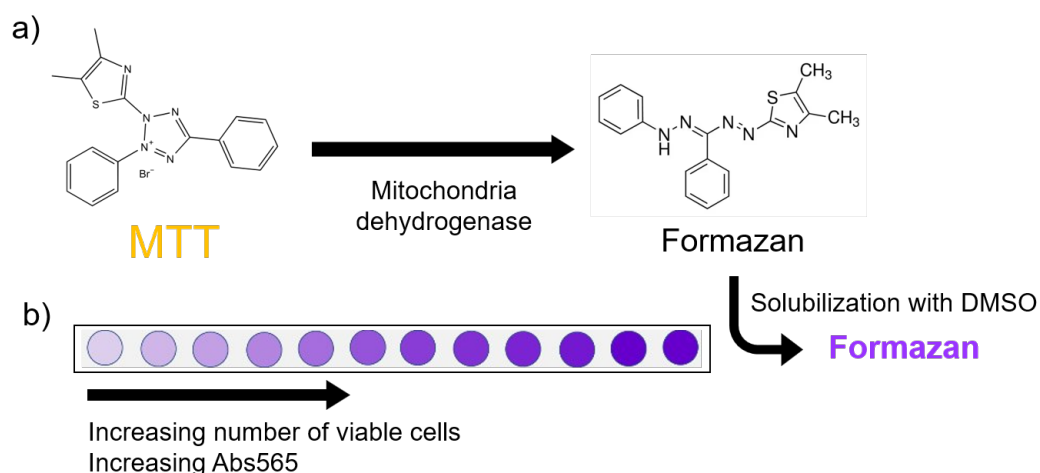
Figure 2.5: Metabolism of MTT to formazan salt by viable cells shown in a) chemical reaction and in b) wells with cells seeded

2.2.11   Crop application

2.2.11.1   Preparation of soil solution

The soil solution is prepared by thoroughly mixing 6 kg of soil with 6 L of water and repose it at ambient temperature for 24 h. Subsequently the solution is filtrated to discard soil particles and distributed into 50 mL falcon tubes. To each tube, 0.5 g of beads prepared with MCl_2 0.5% (w/w) is added. The control consists of soil solution without capsules (SSControl). Three tubes are prepared for each treatment – SS-Ca, SS-Cu and SS-Zn. The tubes are incubated at 25°C in the dark for 3, 6 and 9 days.

2.2.11.2   Assessment of beads' effect on mustard plant

To investigate the effect of the encapsulated cations on the plants two type of tests are carried out: mustard germination tests and mustard seedling growth tests.

2.2.11.2.1 Germination tests

The tests are performed in Petri plates, lined with disks of filter paper soaked with soil solution added with the capsules prepared with MCl_2 0.5% (w/w). After 3 days of incubation, and then after 6 and 9 days, the soil solution with capsules in falcon tubes is vortexed and 2 mL is poured into Petri plate (90 mm diam.) lined with sterile cellulose filter paper (Figure 2.6). Six plates are prepared for each type of soil/capsule formulation at each incubation time. Afterwards, fifteen mustard (*Brassica juncea*) seeds are settled on the filter paper in each plate. Hence, the plates with the seeds are

incubated in a growth chamber (SANYO MRL-351H, Japan) for 14 h of light at 20°C and 10 h of darkness at 18°C for a total of 10 days. After incubation, mustard sprouts are counted to determine germination. The sprouts are then removed from the plates and radicle length and weight, shoot weight, and total weight are measured. Each test is repeated one time under the same conditions.
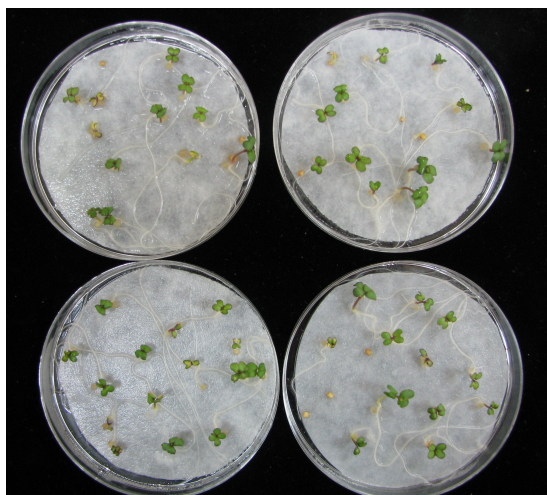
Figure 2.6: Set up of mustard germination tests performed in *Brassica juncea* seeds with SSControl

2.2.11.2.2 Mustard seedling growth assessment

The same soil, as for preparation of the soil solution for germination tests, is used in the experiment on the effect of cations release from the capsules on the growth of mustard seedlings. For this experiment, the soil is mixed with perlite 3-6 mm (Biovita, Poland) at a volume ratio 3:1, and distributed into plastic containers (11x17x5 cm), 600 g of the soil mixture per container. In addition, 6 g of the capsules (1%) are added per container and thoroughly mixed. The soil without capsules is prepared as a control – Scontrol. The soil in each container is moistened to achieve approximately 60% moisture content. Closed containers are incubated at ambient temperature for 7 and 14 days. The next step of this experiment is performed with the use of Phytotoxkit (TI-GRET, Poland), which is intended for phytotoxicity screening of chemicals, leachates in soil or in other solid, bulk materials (Figure 2.7). The evaluation is carried out in special, transparent, plastic plates (21x15.5x0.5 cm), divided to two chambers, one of which is filled with soil sown with test plant seeds. Construction of the plates allows direct observation and measurement of the length of the testing plants.
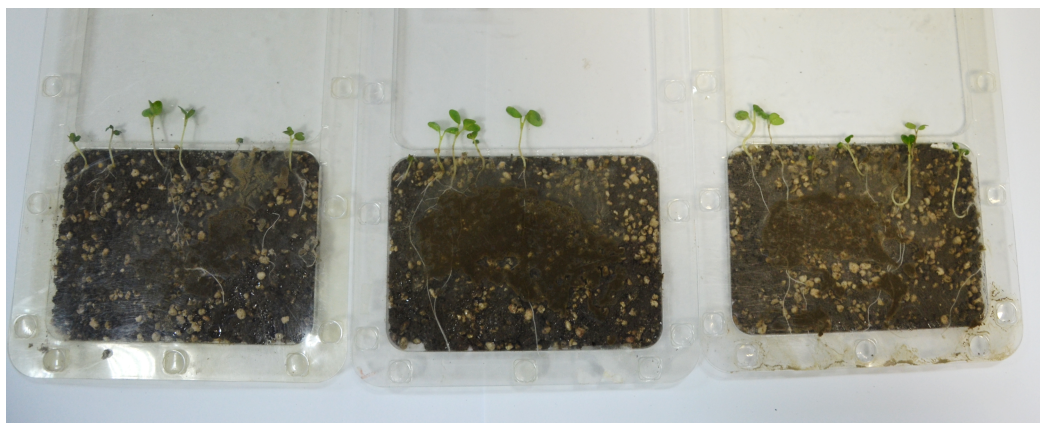
Figure 2.7: Phytotoxkit for mustard seedling growth test performed in *Brassica juncea* with SControl

Therefore, after one week of incubation, 180 g of the soil containing the capsules is taken from each container and divided among three Phytotoxkit plates (each plate containing 60 g of soil) – S-Ca, S-Cu and S-Zn. Ten seeds of mustard *B. juncea* are then sown into each plate. The plates are incubated in the growth chamber for 14 h in the light at 20°C, and 10 h in dark at 18°C. The same is repeated after 14 days of soil incubation in the containers. The Phytotoxkit plates are incubated for 10 days. Thereafter, mustard seedlings are extracted carefully and following parameters are measured: radicle length and weight, shoot weight, total plant weight. The tests are repeated once at the same conditions.

2.2.11.3   Chemical analysis

The soil solutions incubated with studied capsules, as well as the bulk soil added with these capsules, are subjected to chemical analysis. For soil solutions, three samples (20 mL) of each solution are taken after 3, 6 and 9 days of incubation and analysed for the content of available forms of Ca^{2+}, Cu^{2+} and Zn^{2+}. For bulk soil mixed with the capsules, the samples (50 g) are taken after 7, and then after 14 days of incubation, and studied for available forms of mentioned above elements. The samples for each treatment are analysed in triplicates.

Determination of Ca^{2+}, Cu^{2+} and Zn^{2+} in the soil solutions is directly performed using an ICP-OES plasma spectrometer model Optima 2000 DV (Perkin-Elmer) at specific wavelengths: 317.933 nm for Ca^{2+}, 327.393 nm for Cu^{2+} and 206.200 nm for Zn^{2+}.

For determination of plant-available forms of these cations in the soil samples is conducted using the methods outlined by Nowosielski (1978), which are widely employed in the network of Chemical and Agricultural Stations in Poland for diagnostic purposes. For Ca^{2+} analysis, the soil is extracted with acetic acid solution 0.03 N at a volume ratio of soil:acetic acid solution 20 g:200 mL, and mixed on a rotary stirrer for 30 min. After filtration, the Ca^{2+} concentration is measured by ICP at the wavelength described above. In the case of Cu^{2+} and Zn^{2+}, the soil is extracted with Lindsey solution based on EDTA and citric acid at a volume ratio of 25:100 mL. After mixing on a rotary stirrer and filtration, these elements contents are determined with ICP at mentioned wavelengths.

2.2.11.4   Statistical analysis

Data from the experiments are tested for normality of distribution and homogeneity of variance using Shapiro-Wilk and Lavenea tests, respectively. An analysis of variance is then performed in a two-factor model with the variance due to the repetition of experiments extracted. If significance is found for the effects tested, the means are compared using Duncan's test. Calculations are performed in the statistical package STATISTICA v. 13 (Dell Inc. 2016).

Bibliography

[1] A. Davoodi, "Mechanistic studies of localized corrosion of al alloys by high resolution *in-situ* and *ex-situ* probing techniques," Ph.D. Thesis, Universitetsservice US-AB, Stockholm, 2008.

[2] H. Hertz, "Ueber die berührung fester elastischer körper," *Journal für die reine und angewandte Mathematik*, no. 92, pp. 156–171, 1881.

[3] C. X. Wang, C. Cowen, Z. Zhang, and C. R. Thomas, "High-speed compression of single alginate microspheres," *Chemical Engineering Science*, vol. 60, no. 23, pp. 6649–6657, 2005.

[4] K. Kim, J. Cheng, Q. Liu, X. Y. Wu, and Y. Sun, "Investigation of mechanical properties of soft hydrogel microcapsules in relation to protein delivery using a mems force sensor," *Journal of biomedical materials research. Part A*, vol. 92, no. 1, pp. 103–113, 2010.

[5] G. Ashiotis, A. Deschildre, Z. Nawaz, J. P. Wright, D. Karkoulis, F. E. Picca, and J. Kieffer, "The fast azimuthal integration python library: pyfai," *Journal of applied crystallography. Part 2*, vol. 48, pp. 510–519, 2015.

[6] A. Posbeyikian, E. Tubert, A. Bacigalupe, M. M. Escobar, P. R. Santagapita, G. Amodeo, and M. Perullini, "Evaluation of calcium alginate bead formation kinetics: An integrated analysis through light microscopy, rheology and microstructural saxs," *Carbohydrate polymers*, vol. 269, p. 118293, 2021.

[7] B. Hammouda, "A new guinier–porod model," *Journal of applied crystallography*, vol. 43, no. 4, pp. 716–719, 2010.

[8] I. Zazzali, T. R. Aguirre Calvo, V. M. Pizones Ruíz-Henestrosa, P. R. Santagapita, and M. Perullini, "Effects of ph, extrusion tip size and storage protocol on the structural properties of ca(ii)-alginate beads," *Carbohydrate polymers*, vol. 206, pp. 749–756, 2019.

[9] M. Newville, T. Stensitzki, D. B. Allen, and A. Ingargiola, "Lmfit: Non-linear least-square minimization and curve-fitting for python," *Astrophysics Source Code Library*, record ascl:1606.014, p. ascl:1606.014, 2016.

[10] V. L. Singleton, R. Orthofer, and R. M. Lamuela-Raventós, "Analysis of total phenols and other oxidation substrates and antioxidants by means of folin-ciocalteu reagent," *Methods in Enzymology*, vol. 299, pp. 152–178, 1999.

[11] *Production and Management of Beverages.* Elsevier, 2019.

[12] L. M. Magalhães, M. A. Segundo, S. Reis, and J. L. F. C. Lima, "Methodological aspects about *in vitro* evaluation of antioxidant properties," *Analytica chimica acta*, vol. 613, no. 1, pp. 1–19, 2008.

[13] L. K. MacDonald-Wicks, L. G. Wood, and M. L. Garg, "Methodology for the determination of biological antioxidant capacity *in vitro*: a review," *Journal of the Science of Food and Agriculture*, vol. 86, no. 13, pp. 2046–2056, 2006.

[14] R. L. Prior, X. Wu, and K. Schaich, "Standardized methods for the determination of antioxidant capacity and phenolics in foods and dietary supplements," *Journal of agricultural and food chemistry*, vol. 53, no. 10, pp. 4290–4302, 2005.

[15] T. Katsube, H. Tabata, Y. Ohta, Y. Yamasaki, E. Anuurad, K. Shiwaku, and Y. Yamane, "Screening for antioxidant activity in edible plant products: comparison of low-density lipoprotein oxidation assay, dpph radical scavenging assay, and folin-ciocalteu assay," *Journal of agricultural and food chemistry*, vol. 52, no. 8, pp. 2391–2396, 2004.

[16] A. Karadag, B. Ozcelik, and S. Saner, "Review of methods to determine antioxidant capacities," *Food Analytical Methods*, vol. 2, no. 1, pp. 41–60, 2009.

[17] F. Shahidi and Y. Zhong, "Measurement of antioxidant activity," *Journal of Functional Foods*, vol. 18, pp. 757–781, 2015.

[18] J. A. Rothwell, J. Perez-Jimenez, V. Neveu, A. Medina-Remón, N. M'hiri, P. García-Lobato, C. Manach, C. Knox, R. Eisner, D. S. Wishart, and A. Scalbert, "Phenol-explorer 3.0: a major update of the phenol-explorer database to incorporate data on the effects of food processing on polyphenol content," *Database: the journal of biological databases and curation*, 2013.

[19] J. Silva, P. Vanat, D. Marques-da Silva, J. R. Rodrigues, and R. Lagoa, "Metal alginates for polyphenol delivery systems: Studies on crosslinking ions and easy-to-use patches for release of protective flavonoids in skin," *Bioactive materials*, vol. 5, no. 3, pp. 447–457, 2020.

[20] A. Bahuguna, I. Khan, V. K. Bajpai, and S. C. Kang, "Mtt assay to evaluate the cytotoxic potential of a drug," *Bangladesh Journal of Pharmacology*, vol. 12, no. 2, 2017.

Chapter 3

Structural and mechanical analysis on alginate hydrogel beads. Influence of calcium, copper and zinc as crosslinking agents at diverse concentrations

3.1   Introduction

The understanding of gelation and crosslinking mechanism of alginate (Alg) is fundamental, not only to modulate but also to anticipate the physicochemical properties of hydrogels. The prediction of hydrogel's behaviour is crucial for its application in approaches that require beads with specific features. By understanding the behaviour of Alg hydrogels and the factors that influence gelation, such as crosslinker type, concentration and pH of the crosslinking bath, one could select the most suitable formulation for a given application, design the composition that would give the expected results and define the optimal manufacturing process.

Understanding the properties of hydrogels is essential for ensuring quality and safety. For instance, when employed as delivery systems, the behaviour of Alg hydrogels under different environments can determine the encapsulation efficiency of a certain active compound, a targeted and controlled drug delivery, the release rate, and the achievement of the therapeutic dose. When employed in tissue engineering, hydrogel features that depict the degradation rate and the support of cell growth determine the success of the approach. The knowledge of these properties could prevent

64

the failure of therapies and upgrade medical treatments.

Lastly, the characteristics of hydrogels provide essential information for the design of innovative devices and complex structures that will function as aimed under certain situations. Understanding the physicochemical properties of hydrogels may also result in the development of unique materials and original technologies with improved properties. By knowing the underlying parameters that depict the features of Alg hydrogels, new materials could be developed with enhanced strength, ductility, targeted activity, and other properties that could generate revolutionary and upgraded products.

In this chapter diverse crosslinkers and concentrations were employed to obtain Alg beads with varied properties. Hence, $CaCl_2$, $CuCl_2$, and $ZnCl_2$, also referred as MCl_2, were employed as crosslinking agents at concentrations of 0.5%, 2% and 10% (w/w). The aim of the current chapter was to thoroughly examine the interactions between Alg residues and these cations in order to get quantitative data on the nature and amount of binding. Hence, the effects and distinctions between the crosslinking mechanism of these three crosslinking cations and Alg were examined.

Due to the limited understanding of Zn^{2+} role in the process of Alg crosslinking, we were very optimistic for this cation. Indeed, Zn^{2+} is a vital component of our body since it is involved in several cellular processes, including cell proliferation, differentiation and wound healing [1]. Its antioxidant, anti-inflammatory and anti-microbial properties have also been demonstrated. Zn^{2+} is a viable option for medical devices due to its affordability and availability. In fact, Zn-based beads showed promising qualities for potential uses such as delivery methods [2] or for accelerating the healing process of wounds [3]. Zn is a soft metal, and it may form coordinative covalent-like connections with the carboxylates groups of Alg, creating hydrogels that are stronger and more stable than those made with Ca^{2+}, enabling a more precise drug delivery.

Our aim was to gain a deeper knowledge on the characteristics and possible applications of Alg with High-M content so that they can be used more widely. Given that the mannuronic fraction of the studied Alg is a key element in cation-uronate interactions and the properties of resulting hydrogels, the first step addressed Alg characterization. In addition, considering that the pH value is the primary divergence between acidic or ionotropic gelation, it was contemplated when comparing characterization results, mainly of Cu-beads.

We hypothesized that the physicochemical characteristics of the obtained beads might be connected to the crosslinking mechanisms of each cation. Therefore, beads were characterized in terms of morphology (ESEM), interactions involved between the cations and uronate residues (FT-IR), composition of Alg beads (TGA) and mechanical properties in compression tests, as well as nanoscale structure (SAXS). These properties were connected to the diverse gelation processes and conditions. Our analyses were all performed on xerogels, in contrast to the literature, where the published structural determinations concerned aerogels.

3.2   Results

3.2.1   Optimization and set up of beads' preparation process

Calcium, copper and zinc (Ca-, Cu- and Zn-) beads were produced by external ionotropic gelation as previously described in Chapter 2, section 2.2.2. Initial parameters for beads preparation were depicted in previous experiments performed in our research group (data not published). As a general procedure, 10 g of polymeric solution Alg 1.7% (w/w) were extruded drop-wise into a crosslinking bath under agitation (500 rpm) with an extrusion rate of 0.4 mL/min. The crosslinking bath was composed of 200 g of aqueous solution $CaCl_2$ 2% (w/w). Nevertheless, this methodology was further optimized.

The first parameter in being adjusted was the crosslinking bath: $CaCl_2$ concentration, the final mass of crosslinking solution, size of the crystallizer and stirring speed. Thus, the mass of the crosslinking bath remained the same (200 g) but the stirring rate was reduced as it had not any significant effects on beads' morphology (data not shown). The distance between the tip of the needle and the crosslinking solution was kept constant at 2.5 cm. The selected concentrations of $CaCl_2$ was 2% (w/w) as higher concentration led to beads' aggregation (Figure 3.1a and 3.1b).

Additionally, diverse Alg concentrations were tested: 2.1%, 1.7% and 0.6% (w/w) (Figure3.1b, 3.1c and 3.1d). The selected concentration of Alg was 1.7% (w/w) as lower concentration resulted in tear-shaped beads (Figure 13.1c) and no significant differences were observed between polymeric solution Alg 2.1 (w/w) (Figures 3.1b and 3.1d). However, the employment of lower amount of Alg implies the reduction of production costs. Higher extrusion rates were also contemplated. Nonetheless, a faster flow of polymeric solution resulted in tear-shaped beads (Figures 3.1e and 3.1f).
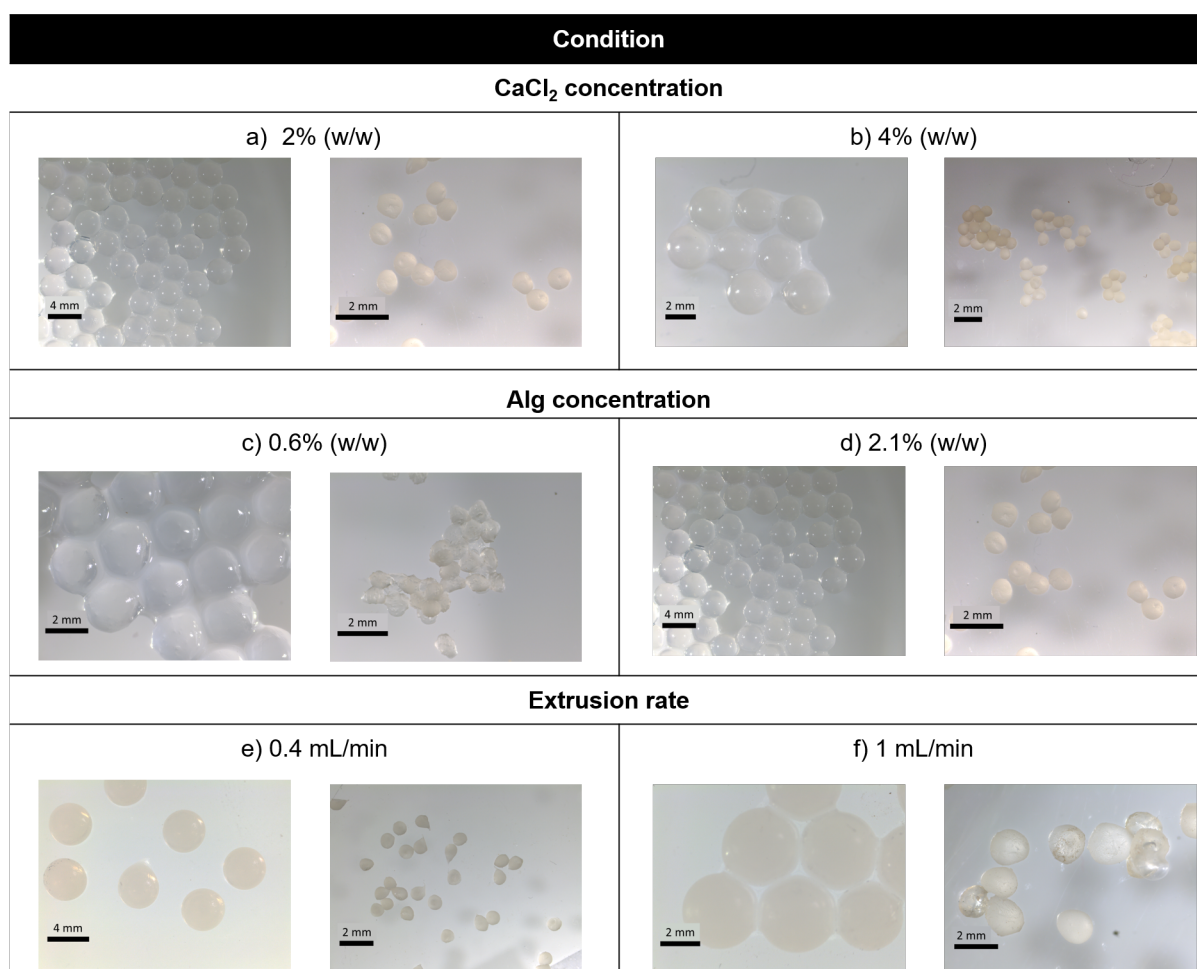
Figure 3.1: Parameters modified during optimization of beads' preparation process and resultant beads

When the Alg polymeric solution was extruded into the divalent cation solution, Alg gelation immediately occurred and beads formed. Beads density gradually rose during the so-called maturation time. The duration of this stage is determined by the cation nature, the pH value of the crosslinking bath, ionic strength and, occasionally, its concentration [4, 5].

The maturation time of beads was set to 48h. This time is remarkably longer compared to most studies reported in the literature, in which 3h to 24h are usually spent. It is important to notice that the evolution of these systems is gradual and considerably slow: the crosslinking reaction that results in gel formation progresses across the hydrogel, from the outer to the inner part, at the same time that syneresis occurs. For this reason, beads may require reasonably extended times to reach the steady-state equilibrium point. Summing up, the optimized conditions used for beads preparation were:

- Concentration of polymeric solution Alg 1.7% (w/w).

- Coagulation or crosslinking bath: 200 g of MCl_2 0.5%, 2% and 10% (w/w), where M is: Ca, Cu or Zn.

- Stirring rate of 100 rpm.

- Extrusion rate of 0.4 mL/min.

3.2.2 Alginate characterization

The composition and molecular weight (Mw) distribution of the employed Alg were characterized by ^1H nuclear magnetic resonance (NMR). Alginates are usually hydrolyzed previously to ^1H NMR in order to diminish their Mw. However, in this case pretreatment was not required as a good spectral resolution was achieved probably because of the low Mw of the employed Alg. NMR analysis was conducted at 70 °C in order to reduce the viscosity of the analysed sample, hence to obtain narrower line-widths peaks and lower noise [6].

In the literature, studies on Alg hydrogels classify materials with a broad range of M/G ratio, typically ranging from approximately 0.5 to 1.6, as High-G content or Low-G (or High-M) content Alg, respectively [7, 8, 9]. It is of great importance to determine the composition of the Alg under investigation in order to establish correlations between its composition and the gelling, structural, and mechanical properties in the presence of the different considered cations. The M/G ratio was determined by ^1H NMR spectroscopy following the method described by Belattmania et al. [10].

Alg spectra (Figure 3.2) displayed characteristic frequencies of M and G residues contributions [10, 11]. The three specific ^1H NMR peaks were focused on for the determination of the sequence within the sodium (Na-)Alg polymeric chain: (Peak I) the peak attributed to H-5 of guluronic acid residues in the homopolymeric G blocks at 4.5–4.6 ppm, (Peak II) the overlapped peaks of anomeric hydrogens of mannuronic acids (M1) and the H-5 of alternating blocks (GM-5) at 4.6–5.3 ppm, and (Peak III) the peak of anomeric hydrogen of guluronic acid residues (G) at 5.4–5.6 ppm (Figure 3.3, Table 3.1).
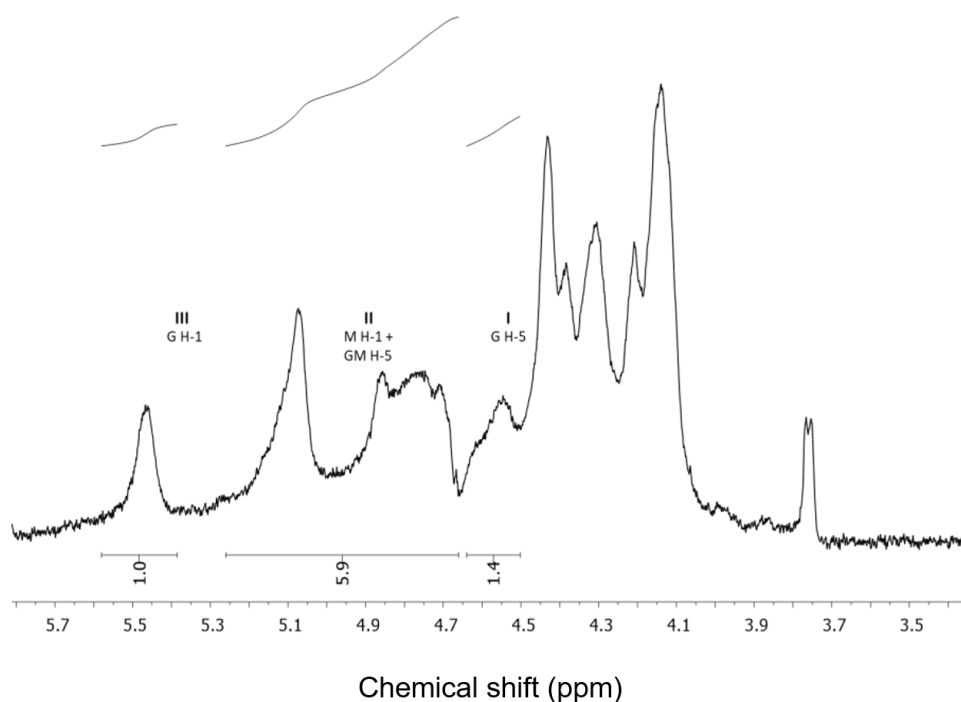
Figure 3.2: ^1H NMR spectra of Na Alg using D_2O as a solvent, recorded at 70°C with a presaturation of 25 Hz
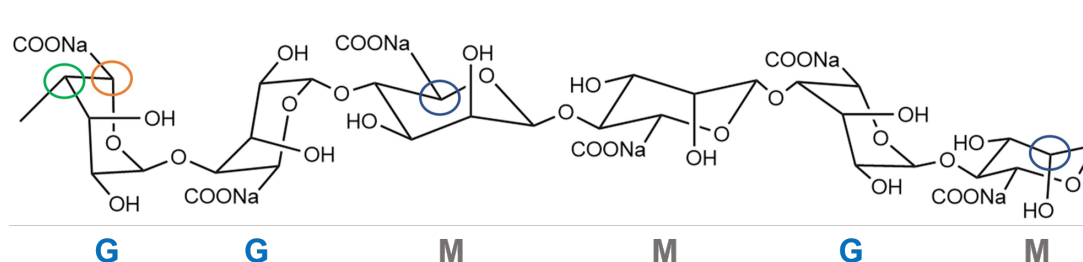
Figure 3.3: Representative structure of Alg $\beta(1\rightarrow4)$ linked β-D-mannuronic acid (M) and β-L-guluronic acid (G) monomers and schematic representation of G-dimers, M-dimers and G/M heterosequence. Peak I, Peak II and Peak III identified in the ^1H NMR spectra are indicated by yellow, blue and green circles, respectively

The calculation of the M/G ratio and the molar fractions of monads (FG, FM), and diads (FMM, FGG, FGM, FMG) sequences was based on the areas of abovementioned three peaks by employing the formula given by Grasdalen et al. [12] as previously applied by Belattmania et al. [10]. Calculations revealed an unusual high molar fraction of M content, as M/G ratio values ranged from 6.3 to 6.39 (Table 3.1). The monad molar fraction for M was FM= 0.86, whereas for G, FG= 0.14. The diads fractions were as follows: FMM= 0.81; FGG= 0.19; FGM= 0.05. Therefore, FMM homosequences were remarkably higher compared to FGG homopolymeric and heteropolymeric fractions (FGM = FMG).

Table 3.1: Composition data of Alg samples according to ^1H NMR results

NMR Data	Value
Peak I	1
Peak II	5.93
Peak III	1.37
FG=AI/(AII + AIII)	0.14
FM=1 - FG	0.86
FGG=AIII/(AII + AIII)	0.19
FGM = FMG = FG - FGG	0.05
FMM=FM - FMG	0.81
M/G=(1 - FG)/FG	6.30
η=FMG/(FM · FG)	0.43

The description of Alg sequence was further completed by the η parameter, which evaluated the distribution of G and M residues within the sequences. In fact, η values < 1 would correspond to the abundance of homopolymeric blocks, $\eta = 1$ for completely random distribution and $1 < \eta < 2$ for alternate-like sequence of MG and GM residues [12]. The value of η was 0.43-0.45, which determined the abundance of homopolymeric blocks. The employed Na Alg was rich in M-blocks.

Based on these results, the calculated M/G ratio gave an unprecedentedly high value of 6.08, indicating a remarkable predominance of MM blocks and classifying the analysed Alg as Low-G or High-M content. As previously mentioned, the distribution of M and G units has a significant impact on the gelling properties. According to the "egg-box" model, the exceptional dominance of M units in Alg should drastically reduce ionic binding and create hydrogels with entangled networks of relatively long and elastic M segments. Thus, the resulting hydrogel was expected to be more dynamic and to have higher porosity and permeability in comparison to hydrogels produced from High-G content Alg [13].

Generally, Alg with High-M content generates more elastic hydrogels as a result of the low charge density and ineffective electrostatic interactions, which result in reduced ionic binding between M-rich polymeric chains [14, 15]. In addition, given the open flat geometry of M residues, a greater number of chain associations and architectures are plausible [16]. This can also be the reason for the broad peaks in the ^{1}H NMR spectra [6]. High degree of hydrogen bonding has been found in M-rich Alg structures, which may lead to self-assembled Alg chains [16]. The electrostatic interactions of M-rich chains may be influential whether the molecular mass is higher.

Therefore, in order to explain the overall behaviour of the Alg under study, it was reasonable to assume that MM dimers were predominant over GM, MG, or, more negligible, GG dimers. For simplicity, the saccharide units are generally referred to as U (uronic residues).

3.2.3   Characterization of the crosslinking bath

In order to accurately determine the pH of the coagulation bath, monitor its evolution among time and assess the characteristics of the resulting gels, the same quantity of polymeric solution (Alg 1.7% (w/w)) was extruded into crosslinking baths containing varying concentrations of MCl_2 (0.5%, 2% and 10% (w/w)). The gelation of Alg took place under all conditions. Hence, the concentration of cations in the crosslinking bath exceeded the theoretical needed amount to compensate for the Na^+ to M^{2+}

exchange, specifically when the (M^{2+}/Na^+) ratio surpassed 0.5. Nevertheless, it should be considered that the diverse concentrations of M^{2+} result in different pH values of the crosslinking baths, which are reported in Table 3.2.

Table 3.2: Values of pH as measured in the crosslinking bath containing $CaCl_2$, $CuCl_2$ and $ZnCl_2$ at different concentrations before Alg extrusion and after 0h, 24h and 48h

Concentration	pH0	pH t= 0h	pH t= 24h	pH t= 48h
$CaCl_2$ 0.5% (w/w)	7.89	7.60	8.3	6.47
$CaCl_2$ 2% (w/w)	7.99	-	-	-
$CaCl_2$ 10% (w/w)	10.31	10.8	7.43	7
$CuCl_2$ 0.5% (w/w)	4.49	4.37	4.37	4.35
$CuCl_2$ 2% (w/w)	4.1	-	-	-
$CuCl_2$ 10% (w/w)	2.98	2.96	2.99	3
$ZnCl_2$ 0.5% (w/w)	6.93	6.58	6.19	6.34
$ZnCl_2$ 2% (w/w)	6.32	-	-	-
$ZnCl_2$ 10% (w/w)	5.31	5.57	5.56	5.47
Alg 1.7% (w/w)	7.15		7.16	After 2 weeks

These pH values can be interpreted based on the different reactions that take place between the cation and water [17]. Indeed, when $CaCl_2$ is employed as crosslinking agent:

$$Ca^{2+} + H_2O \leftrightharpoons CaOH^+ + H^+ \qquad k = 10^{-12.6} \tag{3.1}$$

$$H^+ + Cl \longrightarrow Cu(OH)_2 \qquad k = 10^7 \tag{3.2}$$
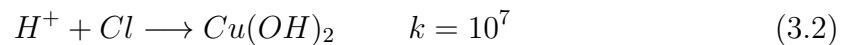
The combination of both equations (3.9) and (3.2) results in an increase of $[OH^-]$ concentration, leading to alkaline pH values. Hence, considering the pKa of alginic acid, which is approximately 3.4 [18], it can be observed that the pH of the crosslinking bath was higher than the pKa of M and G units at any investigated $CaCl_2$ concentration regime. Therefore, in this case, ionotropic gelation was expected to take place exclusively.

Oppositely, when $CuCl_2$ is employed as crosslinker, giving the strong Lewis acid character of Cu^{2+}, the following reactions occur:

$$Cu^{2+} + OH^- \longrightarrow CuOH^+ \qquad k = 10^{6.3} \tag{3.3}$$

$$Cu^{2+} + 2OH^- \longrightarrow Cu(OH)_2 \qquad k = 10^{12.8} \tag{3.4}$$

Reactions (3.3) and (3.4) increase $[H_3O^+]$ concentrations and shift the pH values towards acidic values (Table 3.2). As a result, both alginic acid precipitation as well as ionotropic gelation were expected to occur. Specifically, the ratio [alginic acid]/[Alg] at 0.5%, 2% and 10% (w/w) $CuCl_2$ concentration was about 0.081, 0.20 and 2.6, respectively. Hence, when the $CuCl_2$ concentration in the crosslinking bath was 10% (w/w), acidic precipitation of Alg might be predominant. Nevertheless, the beads formed with $CuCl_2$ 2% (w/w) may be a hybrid system of Cu-Alg/alginic acid.

If $ZnCl_2$ is employed as crosslinker, analogous reactions to (3.3) and (3.4) take place:

$$Zn^{2+} + OH^- \longrightarrow Zn(OH)^+ \qquad k = 10^5 \tag{3.5}$$

$$Zn^{2+} + 2OH^- \longrightarrow Zn(OH)_2 \qquad k = 10^5 \tag{3.6}$$

However, giving that Zn^{2+} is a milder Lewis-acid, the pH value of the crosslinking bath is slightly acidic (Table 3.2) [19]. Therefore, even in the most concentrated Zn^{2+} crosslinking bath (10% (w/w)), the ratio [alginic acid]/[Alg] is 0.012. Ionotropic gelation was expected to be predominant.

3.2.4   Preparation of alginate beads

The experimental procedure followed to prepare Alg beads is depicted in Chapter 2, Section 2.2.2. Figures 3.4, 3.5 and 3.6 display optical microscopy images of the resulting beads among maturation time.

When the polymeric solution was extruded into the crosslinking solution containing divalent cations, bead formation took place immediately. Subsequently, the density of the beads gradually increased during the maturation process, which was influenced by factors such as the type and concentration of cation, pH of the coagulation bath, and ionic strength [4, 5]. In this study, the maturation time for the Alg beads lasted for 48h, which was notably longer than most studies reported in the literature (ranging from 3h to 24h). Furthermore, it must be considered that the evolution of these systems is slow since crosslinking reactions that determine gel formation proceed from the outer to the inner part of the beads, accompanied by syneresis. Thus, longer maturation times were expected to achieve steady-state equilibrium of beads, particularly when a high amount of cation was employed.
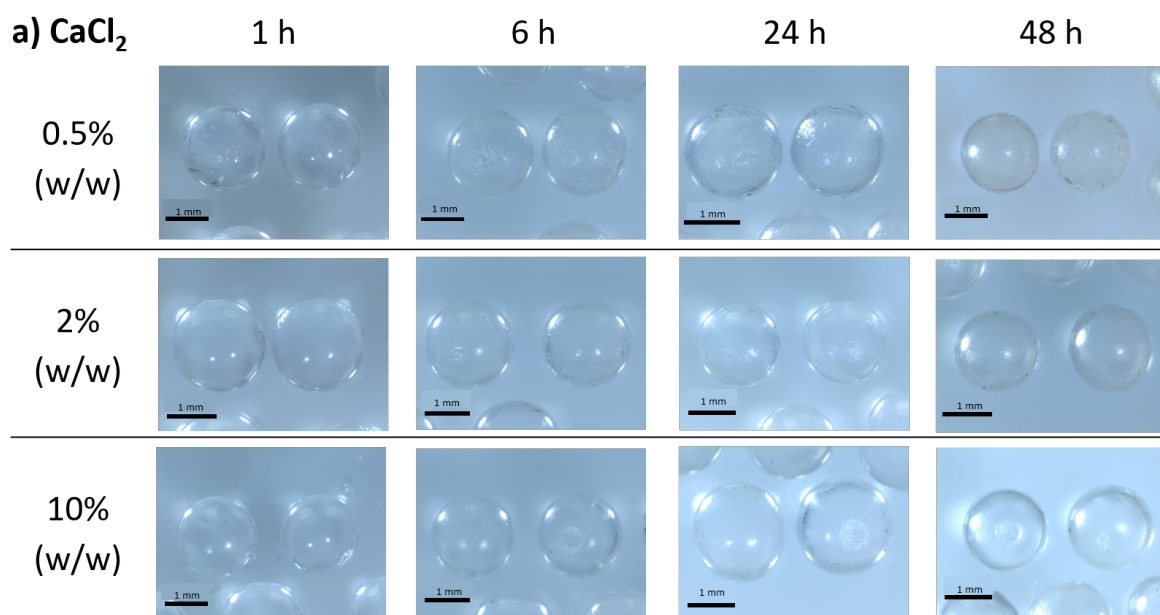
Figure 3.4: Loupe micrographies of Alg beads crosslinked with $CaCl_2$ 0.5%, 2% and 10% (w/w) after 1h, 6h, 24h and 48h maturation
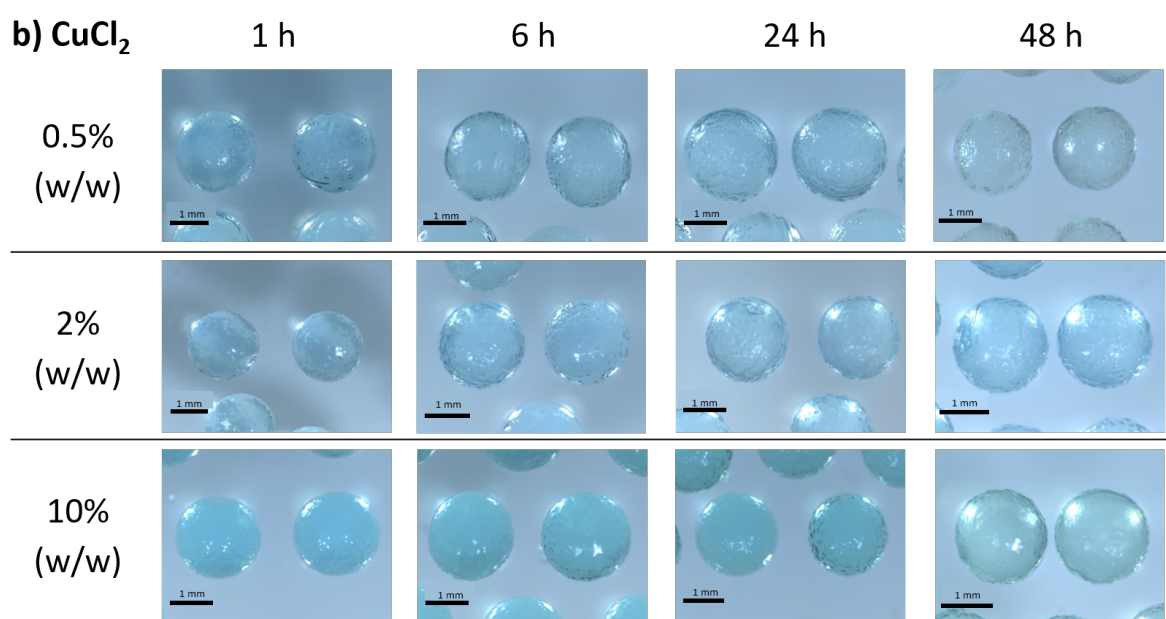
Figure 3.5: Loupe micrographies of Alg beads crosslinked with $CuCl_2$ 0.5%, 2% and 10% (w/w) after 1h, 6h, 24h and 48h maturation
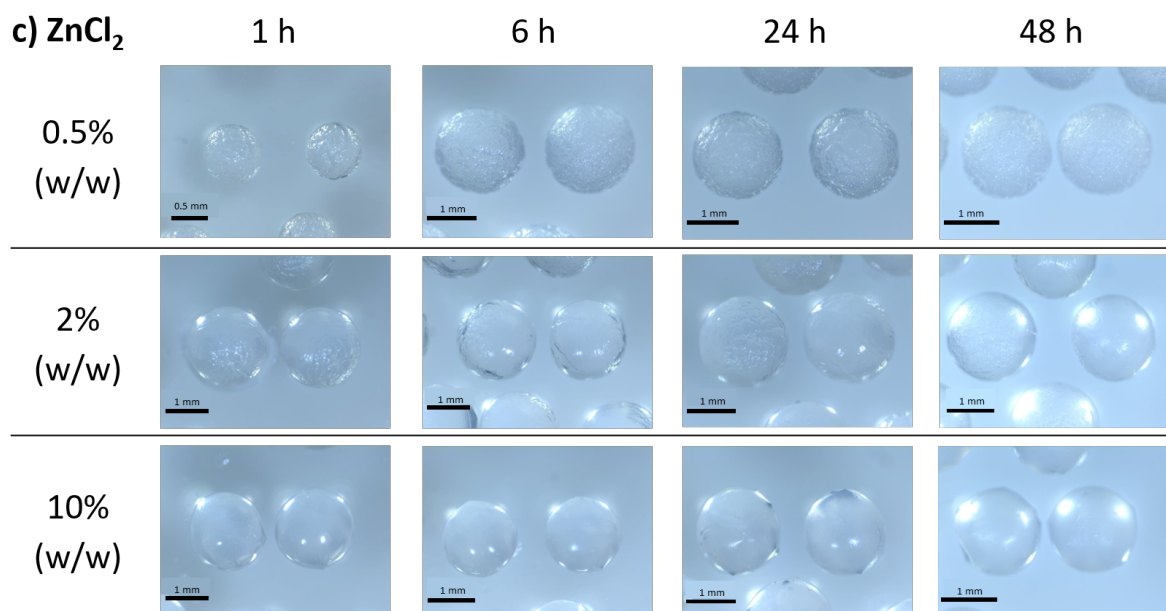
Figure 3.6: Loupe micrographies of Alg beads crosslinked with $ZnCl_2$ 0.5%, 2% and 10% (w/w) after 1h, 6h, 24h and 48h maturation

In order to establish the duration of maturation time, the diameter of wet beads was monitored throughout the crosslinking process up until 48h. Findings are presented in Figure 3.7.

Principally, and as expected owing to syneresis, the diameter of the beads generally decreased during maturation time (Figure 3.7). This was because the solvent was expelled from the hydrogel, which shrinks. A stable dimensional situation was apparently reached after 48h, since no significant variation in beads' diameters was observed beyond this time point.

Additional studies were carried out by FT-IR analysis at different maturation time intervals to confirm the suitability of the 48-hour maturation time for bead formation and development.

FT-IR has already been utilized in the literature to investigate the coordination properties of metal-Alg complexes, through the evaluation of the difference between the symmetric and asymmetric vibrational modes of the carboxylate groups ($\Delta \nu$) of the resulting beads [9, 20]. The comparison between the $\Delta \nu$ values of the ionically-crosslinked Alg and those of the uncrosslinked Na Alg should provide information regarding the nature of metal coordination. As a result, $\Delta \nu$ may be used as a probe of beads' maturation, when reaching a constant $\Delta \nu$ value implies that a stable coordination has been established and that the proper maturation stage has been achieved.

As an example, Figure 3.8 displays the FT-IR spectra ranging from 600 to 4000 cm^{-1} of Ca-, Cu-, and Zn-based Alg beads, prepared with a 0.5% (w/w) MCl_2 solution and after 48h of maturation. For comparison, the spectrum of Na Alg is also presented. Moreover, the $\Delta \nu$ values for the various cations at the lowest 0.5% (w/w) and highest 10% (w/w) MCl_2 concentrations obtained at different maturation times are also shown in Table 3.3. We focus on the trends displayed in Table 3.3, while a fuller discussion of the final $\Delta \nu$ values obtained, together with Figure 3.8, is found in Section 3.2.7.

The $\Delta \nu$ values reported in Table 3.3 indicated that after 48h of maturation time, stable values were generally reached. The only exception was the condition of $ZnCl_2$ 0.5% (w/w), where $\Delta \nu$ exhibited a very small modification and seemed to stabilize after 24h. Nevertheless, a maturation time of 48h was selected for all the investigated systems in order to standardize the beads' preparation process.

76
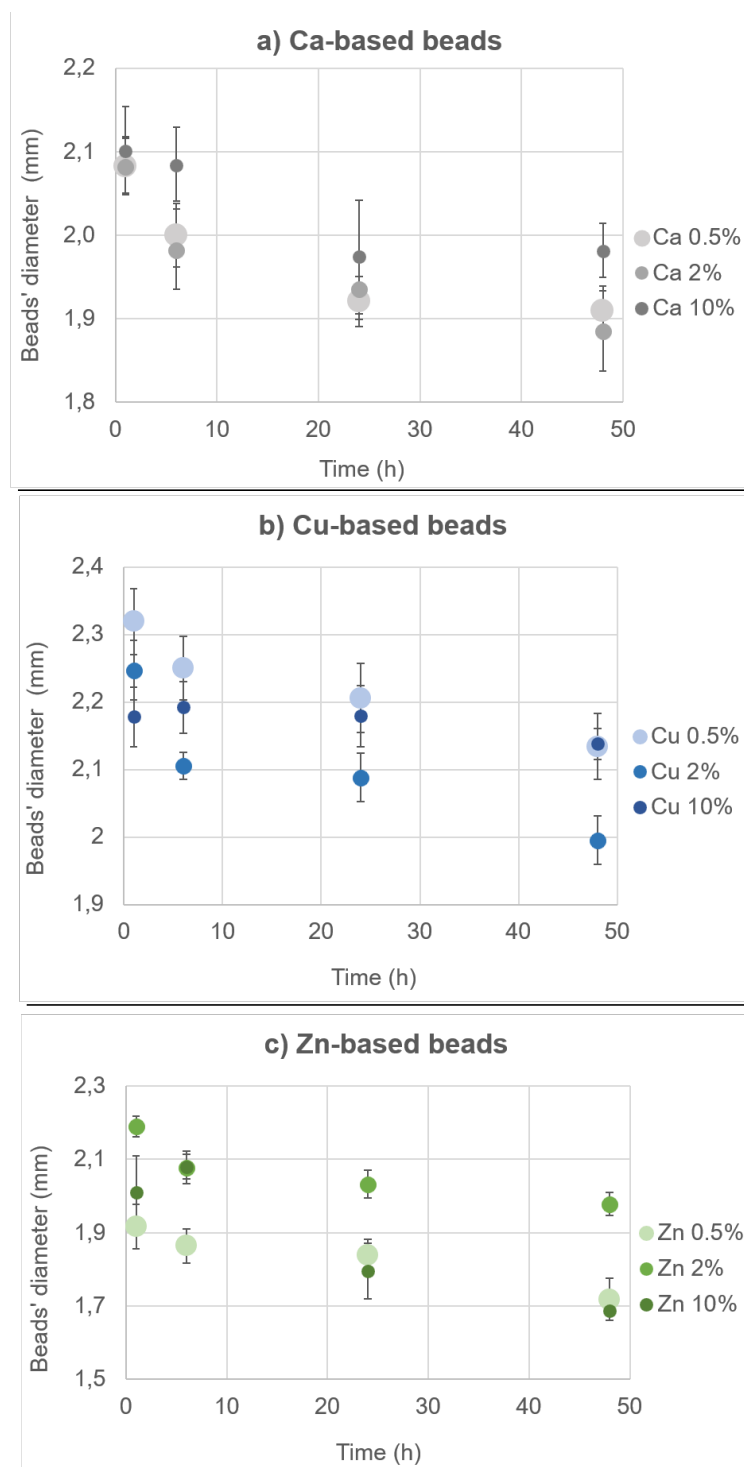
Figure 3.7: Average and standard deviation of beads' diameter among maturation time for a) Ca-, b) Cu- and c) Zn-based Alg hydrogels obtained from crosslinking baths containing MCl_2 0.5%, 2% and 10% (w/w)
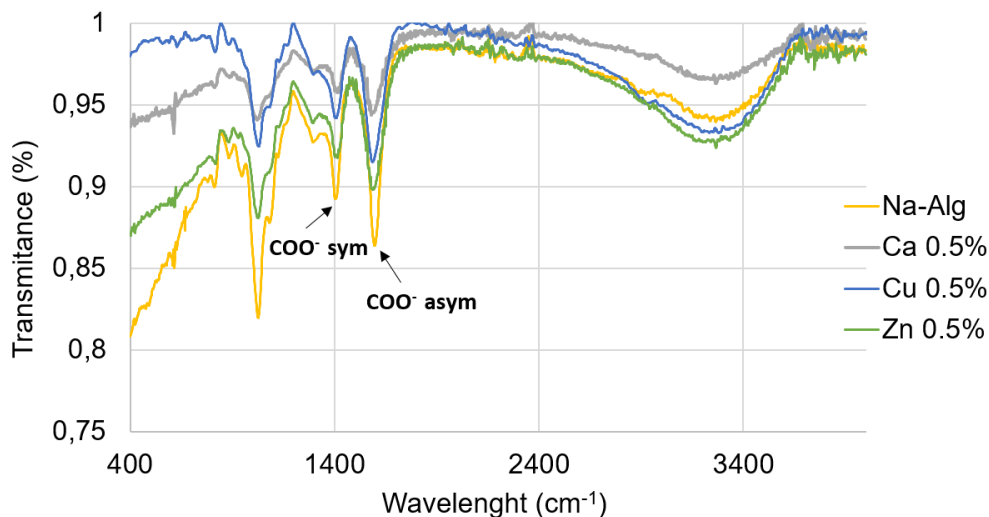
Figure 3.8: FT-IR spectrum between 600 and 4000 cm^{-1} of Na Alg, and of Ca-, Cu- and Zn-based Alg beads prepared from MCl_2 0.5% (w/w) after 48h maturation time. Bands corresponding to both asymmetric and symmetric vibrational modes of carboxylate groups are indicated

Table 3.3: Differences between the asymmetric and symmetric vibrational modes of carboxylate groups ($\Delta\nu$) in Na Alg and Alg beads prepared with MCl_2 0.5% and 10% (w/w) aqueous solution at different maturation times. (*) Powder sample

		Maturation time (h)			
		1	6	24	48
Sample		$\Delta\nu$ (cm^{-1})			
Na Alg*		190			
$CaCl_2$	0.5% (w/w)	174	174	165	165
	10% (w/w)	175	154	150	150
$CuCl_2$	0.5% (w/w)	170	174	180	180
	10% (w/w)	158	161	180	180
$ZnCl_2$	0.5% (w/w)	178	176	176	176
	10% (w/w)	140	177	172	172

3.2.5   Structure of alginate beads

Bead formation occurs instantaneously if the concentration and inherent viscosity of the polymeric solution surpass a specific threshold value, which depends on the crosslinking cation used [7]. Indeed, beads formation is subjected to the integrity of the droplets when they meet the cation solution, with the entanglements of the polymeric chains playing a crucial role in this process. In our study, the Alg solution employed, characterized by an apparent viscosity of 866 mPas and an Alg concentration of 17 g/L, was able to produce stable beads with each of the three cations (Ca^{2+}, Cu^{2+} and Zn^{2+}) at the lowest concentration employed (0.5% (w/w)) (Figure 3.9), which is consistent with the trends reported in the literature [7]. Subsequently, the beads underwent the maturation phase in which the gel beads' evolution progressed from the outer surface to the inner part of the beads.

Figure 3.9 displays ESEM images of dry beads prepared by extrusion of polymeric solution into a crosslinking bath 0.5% (w/w) MCl_2, after 48h of maturation time and dried in an oven at 40°C for 24h. Thus, stable beads were formed in all three cases. The most visible differences were observed in the outer morphology of the beads: the surface of the Ca-beads was smooth and uniform (Figure 3.9a), whereas those of the Cu-beads were vastly rough and irregular, resembling to the aggregation of numerous microgels (Figure 3.9b). For Zn-crosslinked beads, this effect was even more pronounced (Figure 3.9c). These differences could be attributed to variations in the crosslinking mechanisms.

Hence, when the outer surface of the polymeric drop came into contact with the cation solution, stronger interaction was established between Alg and Cu^{2+} or Zn^{2+}, compared to Ca^{2+}. This gave rise to the development of a rigid wall of highly complexated Alg around the beads, which impeded the diffusion of Cu^{2+} and Zn^{2+} toward the core of the bead. On the contrary, Ca^{2+} diffusion was expected to be more homogeneous, producing denser and more regular beads. Previous studies on macromolecule diffusion and adsorption, as well as volume reduction during maturation of Ca- and Cu-based beads, support this hypothesis [21, 22].

Ca-beads' surface smoothed and beads' size rose with increasing $CaCl_2$ concentration (Figure 3.10a and 3.11a).

Compared to Cu 0.5% beads, spiked points were observed in the surface of Cu 2% beads (Figure 3.10b). These skewers could be associated to highly complexated Alg and/or the accumulation of Cu^{2+} ions as skewers were not usual at the lowest concentration. In fact, the higher the Cu^{2+} concentration, the greater number of skewers (Figure 3.11b).

The surface of Zn-beads was rougher when prepared with $ZnCl_2$ 0.5% (w/w) though it smoothed with the highest $ZnCl_2$ concentration (Figure 3.10c and 3.11c). Probably, a faster gelation and the stronger diffusion driving force of higher Zn^{2+} concentrations prevented Alg diffusion through the crosslinking bath.

During the maturation step, beads' density rises and syneresis occurs. The evolution of the beads takes place from the surface to the inside of the hydrogels. Therefore, maturation is a slow phenomenon that depends on the cation diffusion through the initially precipitated Alg layers. Consequently, it affects the final morphology and internal structure of the beads. Ultimately, a stable state is established.

MCl$_2$ 0.5% (w/w)

a) Ca^{2+} — b) Cu^{2+} — c) Zn^{2+}

Size = 0.47 ± 0.03 mm — Size = 0.44 ± 0.02 mm — Size = 0.43 ± 0.01 mm
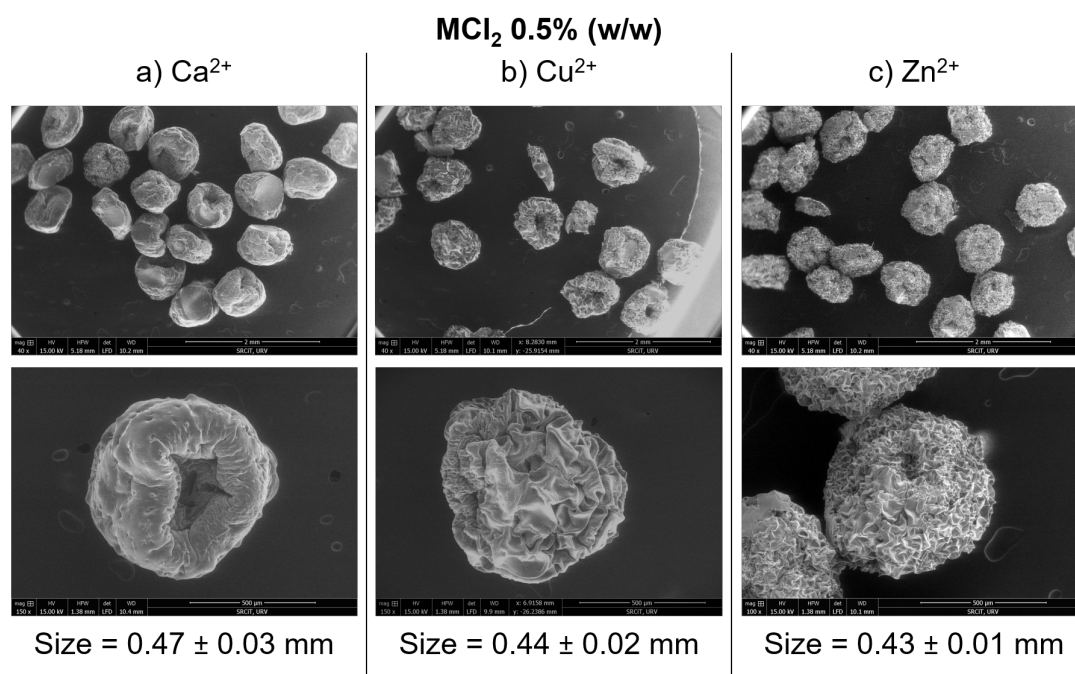
Figure 3.9: ESEM images of Alg beads crosslinked with MCl_2 0.5% (w/w) where M is: a) Ca, b) Cu and c) Zn, after 48h maturation time and dried at 40°C for 24h. Top: general view; bottom: detail of a single bead

80

MCl$_2$ 2% (w/w)

| a) Ca^{2+} | b) Cu^{2+} | c) Zn^{2+} |

| Size = 0.54 ± 0.07 mm | Size = 0.47 ± 0.07 mm | Size = 0.54 ± 0.03 mm |
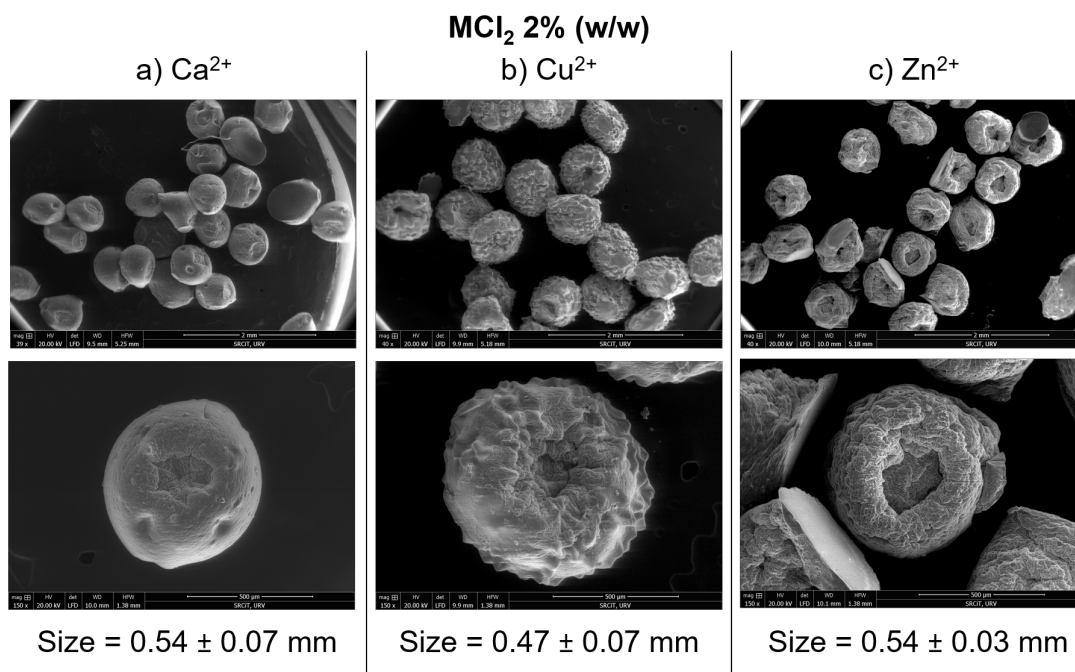
Figure 3.10: ESEM images of Alg beads crosslinked with MCl_2 2% (w/w) where M is: a) Ca, b) Cu and c) Zn, after 48h maturation time and dried at 40°C for 24h. Top: general view; bottom: detail of a single bead

MCl$_2$ 10% (w/w)

| a) Ca^{2+} | b) Cu^{2+} | c) Zn^{2+} |

| Size = 0.54 ± 0.02 mm | Size = 0.47 ± 0.01 mm | Size = 0.46 ± 0.03 mm |
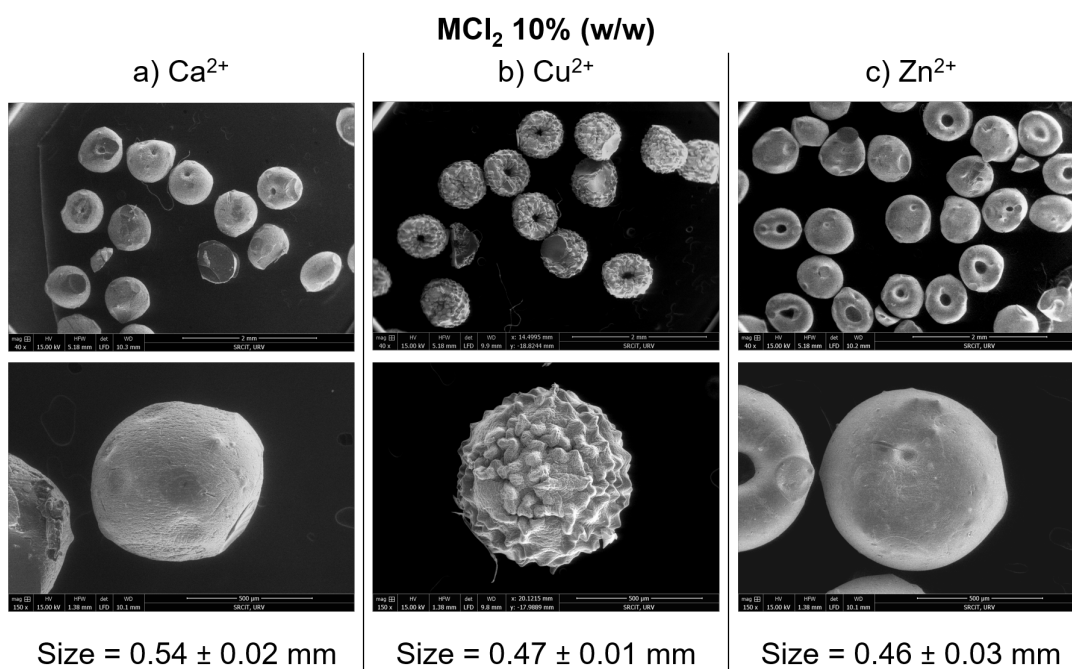
Figure 3.11: ESEM images of Alg beads crosslinked with MCl_2 10% (w/w) where M is: a) Ca, b) Cu and c) Zn, after 48h maturation time and dried at 40°C for 24h. Top: general view; Bottom: detail of a single bead

81

To explore the beads' homogeneity and get insight into their formation mechanism, the development of the beads obtained at different cation concentrations was tracked over time. Hence, beads were withdrawn from the crosslinking bath at different maturation times, cryofractured and their cross-sections observed by ESEM.

Regarding the size of beads prepared with MCl_2 0.5% (w/w), Ca-beads' size decreased after 6h of maturation (Figure 3.11a). However, this effect was not clearly evident in Cu-beads (Figure 3.11b). This was consistent with the findings of Velings et al. [4], who described a greater volume decrease in Ca-beads compared to Cu-beads. They determined that low $CuCl_2$ concentrations (0.05 M) were already enough to complex all the U sites of Alg hydrogels (2% (w/w)). Hence, the $CuCl_2$ concentration did not influence any of the studied beads' properties (beads' weight ratio). They also pointed the presence of completely complexated Alg (almost precipitated) in the outermost part of the beads due to the strong Cu-Alg affinity. This outer coat sealed the surface pores preventing the diffusion of further Cu^{2+} toward the centre of the beads. The wall provided rigidity and avoided volume reduction, which could be related with syneresis restriction.

Figure 3.12 reveals the evolution of beads prepared with MCl_2 0.5% (w/w) among maturation time. All MCl_2 0.5% (w/w) systems showed a change in the internal morphology after 48h, confirming that this period was reasonably requested for reaching the steady state of the bead. Probably longer times would not have resulted in any morphological variations.

Although the cross-section of Ca-based beads could not be distinctly seen after maturation time, it was evidenced that Cu- and Zn-based beads had a less dense core compared to Ca-based beads. This supports the previously suggested crosslinking mechanism.

In the case of Ca-beads, the low concentration of Ca^{2+} enabled Alg diffusion through the crosslinking bath as the gelation was not fast enough [23]. Thus, beads' surface was rough at first and it flattened during maturation time. The final smooth surface may be a result of the ionic character of the interaction between Ca^{2+} and U. This interaction was not strong and hence, modifications and reorganization might be allowed.

The main difference between Ca- and Zn-beads was the rougher surface of Zn-beads. This was possibly associated to the smaller molarity of Zn^{2+} in the crosslinking bath as well as the weaker interaction with U, which gave rise to a slower Zn^{2+} diffusion and Alg gelation. Perhaps for the same reason Zn-beads might be smaller.

Two factors must be considered when concentration of the crosslinking cation is increased. Firstly, the Alg gelation in the outer layers is expected to have more crosslinking points, making a more rigid wall and less permeable to cations' diffusion, potentially preventing the inner gel from growing uniformly. Secondly, the concentration difference between the cation in the crosslinking bath and the inner part of the bead also increases, potentially favouring cation diffusion toward the centre of the bead. As a result, the final beads' morphology is determined by the balance of these two contrary elements.

Figure 3.13 relates to beads prepared with MCl_2 2% (w/w). Regarding the internal morphology and its progression over time, the micrographies show that there was not any relevant variation between Ca-beads prepared with $CaCl_2$ 0.5% or 2% (w/w). Cu-beads became denser, developing in a "spongy" manner. Zn-beads still had a remarkable shortage of material in the core of the beads. The results suggested that in the case of Cu^{2+}, the diffusion took precedence over wall stiffness, but in the case of Zn^{2+}, the rigid wall prevented Zn^{2+} diffusion. This divergence may be manifested as well in the mechanical properties of the beads.

The pictures of the beads prepared with MCl_2 10% (w/w) displayed in Figure 3.14 evidenced that the surface of Ca-beads was still very smooth, whereas Cu-beads' one was highly uneven. This was reasonable given that in the latter sample, acidic gelation may predominate over ionotropic gelation. Surprisingly, Zn-beads displayed a smooth surface, implying that the diffusion force resulting from the concentration difference promoted cation diffusion through the outer wall of the beads.

The evolution of the inner part of Ca-beads from an empty core to a multi-layered and denser one was evidenced. Blandino et al. already pointed Ca^{2+} diffusion resistance to be effective when $CaCl_2$ was employed at a concentration higher than 4% (w/v). They already indicated the formation of a denser membrane of highly complexated Alg [24]. Probably, the formation of the thicker wall resulted in an initial resistance to Ca^{2+} diffusion and an empty core, which was compensated over the time as cations were able to diffuse towards the beads.

The same occurred with Zn-beads, whose core was compartmentalized, and surface evened out over the time. Nonetheless, denser regions coexisted simultaneously with more empty ones after maturation time, resulting in an irregular inner morphology. Ca- and Cu-based beads likewise had a multi-layered core. These seemed to be more occupied of polymer, which appeared more uniformly distributed.

In case of Cu-beads a rough surface, strongly layered core and spongy structures in the beads' walls were evidenced. Numerous spiked points were observed in the inner walls and surface, which supported their association to highly complexated Alg. Furthermore, the spongy structures could as well be associated to highly complexated Alg and/or the accumulation of Cu^{2+} ions as they were not as usual in beads prepared with lower concentrations of $CuCl_2$. All these findings evidenced the unbalanced Alg complexation. The resistance to Cu^{2+} diffusion, resulting from Alg gelation, was not sufficient to organize the intense Cu^{2+} diffusion, resulting from the concentration difference. Hence, the outer wall formed but the diffusion driving force overpassed this constriction. This presumably also led to Alg sweep among the inner parts of beads. Thus, the core becomes more intricate among the time.
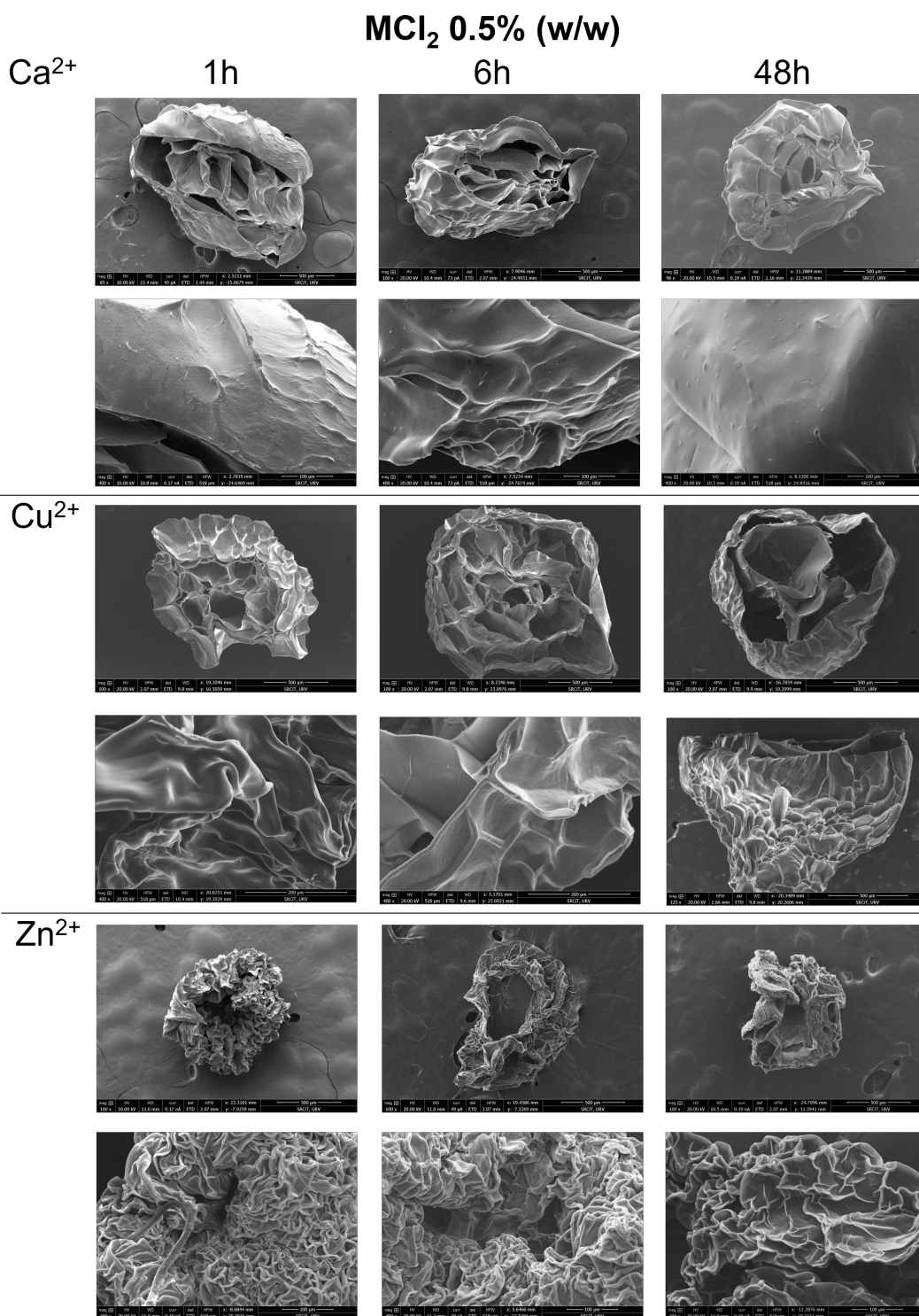
Figure 3.12: ESEM micrographies of the cross-sections and surface of Alg beads crosslinked with MCl_2 0.5% (w/w) after 1h, 6h and 48h maturation
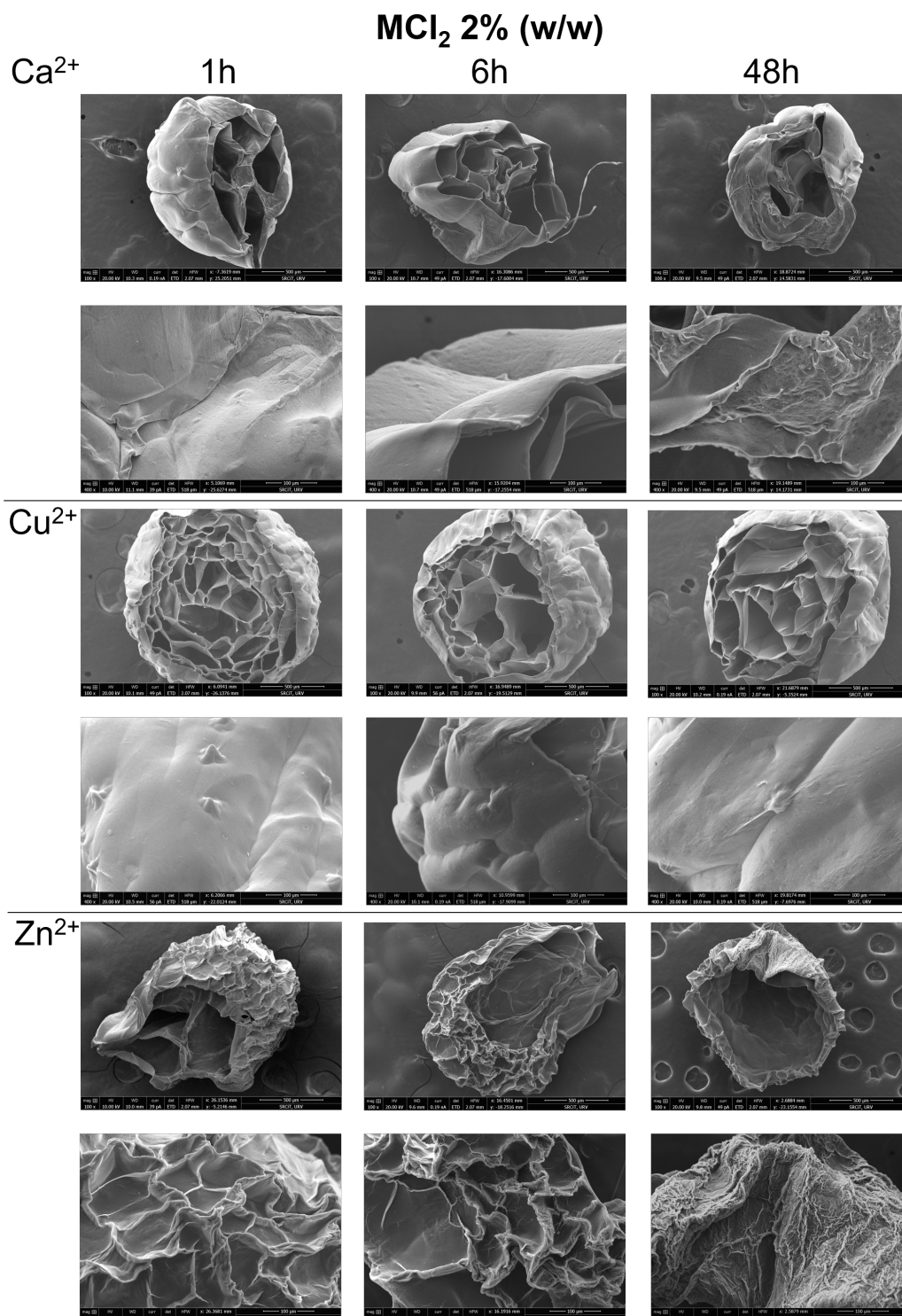
Figure 3.13: ESEM micrographies of the cross-sections and surface of Alg beads crosslinked with MCl_2 2% (w/w) after 1h, 6h and 48h maturation
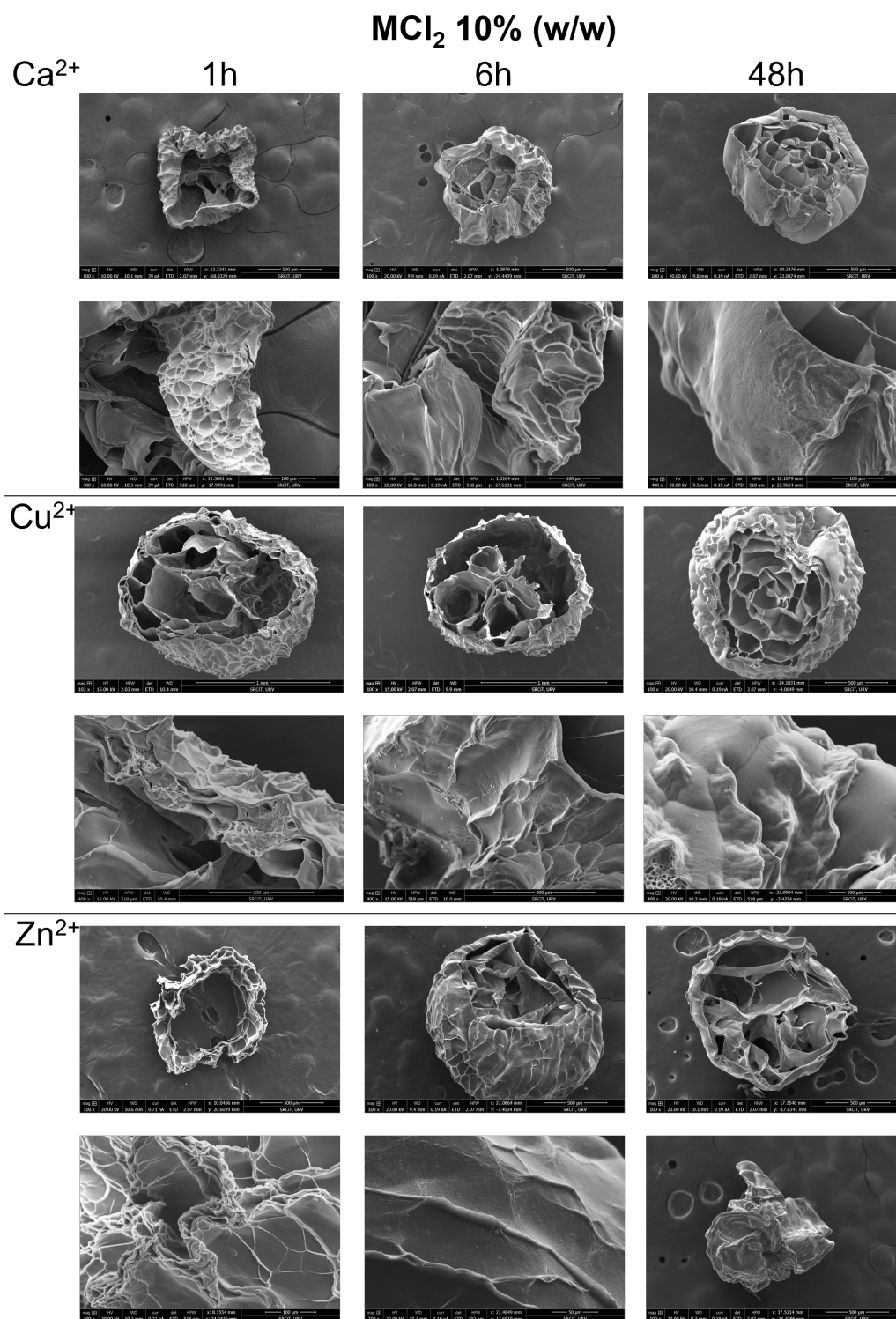
Figure 3.14: ESEM micrographies of the cross-sections and surface of Alg beads crosslinked with MCl_2 10% (w/w) after 1h, 6h and 48h maturation

3.2.6   Composition of alginate beads

The thermogram of Alg/M^{2+} beads prepared with MCl_2 0.5%, 2% and 10% (w/w) respectively are displayed in Figure 3.15. The progress of temperature together with the mass loss was estimated from the residual mass (%) vs. temperature (°C) curves.

Thermogravimetric analysis in air enabled the estimation of the metal load of each sample through the residue at 800°C. Calcination of M^{2+}-beads in oxidizing environment resulted in the formation of the corresponding metal oxides, as determined by wide angle X-ray diffraction (XRD) (Data not shown). The metal amount was calculated from the residual mass at 800°C, which corresponded to the oxide content. Hence, the equation previously reported by Agulhon et al. was employed (eq. 3.7) to estimate the metal load of each sample [25]:

$$M^{2+}(mol) = Residue(g) \cdot \frac{M_W M^{2+} \left(\frac{g}{mol}\right)}{M_W M^{2+} oxide \left(\frac{g}{mol}\right)} \tag{3.7}$$

, where:

- M^{2+} is the metal load of beads in mol.

- $M_W M^{2+}$ is its molar mass.

- $M_W M^{2+}$ oxide is the molar mass of CaO, CuO and ZnO, which is 56.07 g/mol, 63.55 g/mol and 65.38 g/mol, respectively.

TGA also allowed the estimation of the number of U that corresponded per cation (eq. 3.8), as well as the water content of the metal/Alg beads.

$$n_{\frac{U}{C}} = \frac{[100 - M^{2+}\left(\%(w/w)\right) - Water\left(\%(w/w)\right) \; evaporated \; until \; 170°C] / M_{w_u}}{\frac{M^{2+}\left(\%(w/w)\right)}{M_{w_{M^{2+}}}}} \tag{3.8}$$

, where:

- $n_{\frac{U}{C}}$ is the number of U residues per cation.

- $M^{2+}\left(\%(w/w)\right)$ is the percentage of metal in beads.

- M_{w_u} is the molar mass of U residues (176 g/mol).

- $M_{w_{M^{2+}}}$ is the molar mass of the metal.
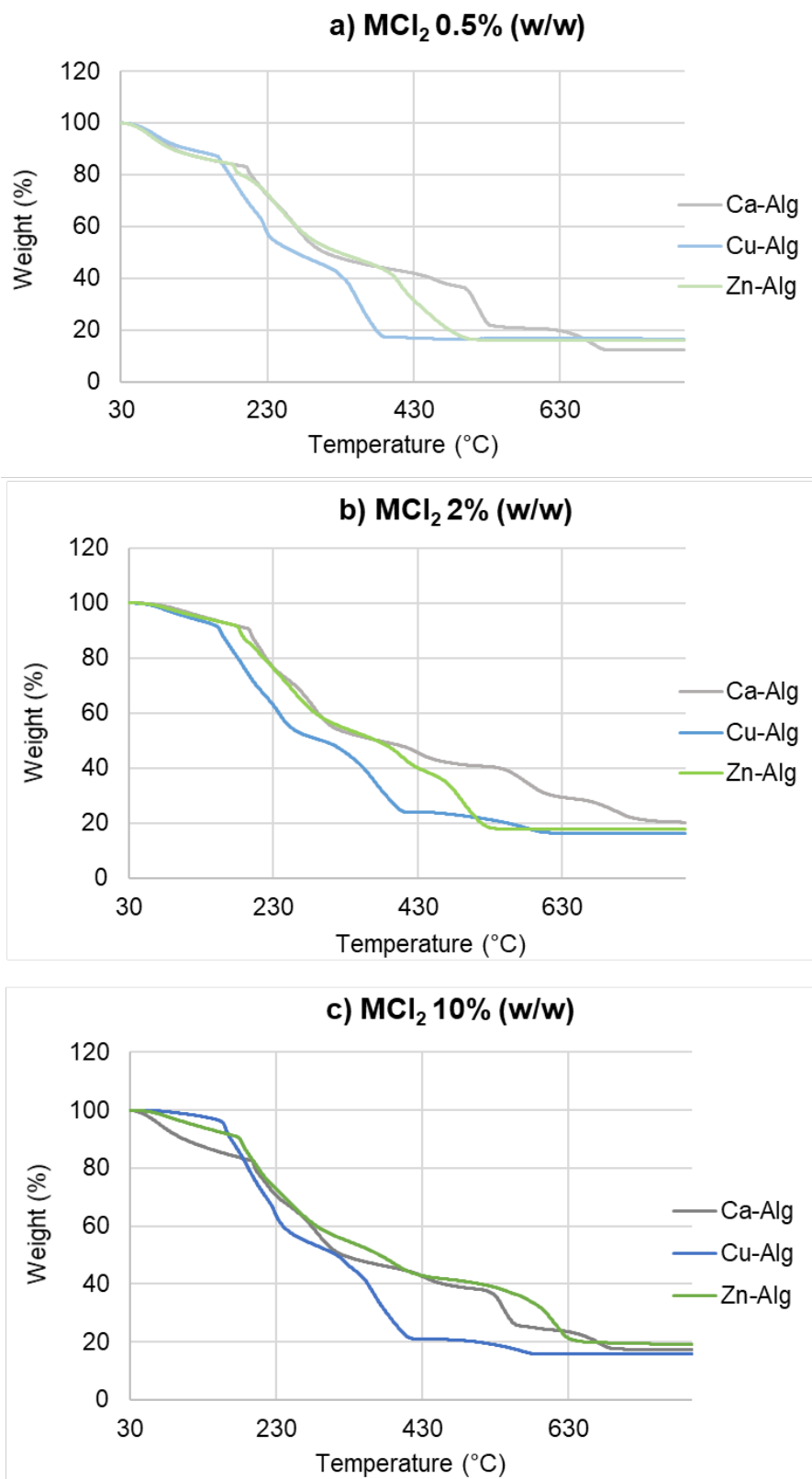
Figure 3.15: Thermogram of Alg M^{2+}-beads obtained with MCl_2 a) 0.5%, b) 2% and c) 10% (w/w) where M is: Ca (grey), Cu (blue) and Zn (green)

Results of both the number of U per cation $(n_{\frac{U}{C}})$ and the number of water molecules per cation $(n_{\frac{w}{C}})$ are displayed in Table 3.4. Giving that calculations of $n_{\frac{U}{C}}$ involved the deduction of the amount of water in beads, which could not be accurately defined, this parameter may be considered as an estimation, as well as $n_{\frac{w}{C}}$. Even if these numbers were not very rigorous, they provided some qualitative estimations about the systems under investigation.

Table 3.4: Number of uronate units per cation $(n_{\frac{U}{C}})$ and number of water molecules per cation $(n_{\frac{w}{C}})$ in the corresponding beads

Sample	Residue (%)	$n_{\frac{U}{C}}$	$n_{\frac{w}{C}}$
$CaCl_2$ 0.5%	12.14	2	4.4
$CaCl_2$ 2%	20.21	1.2	1.8
$CaCl_2$ 10%	17.28	1.3	3.4
$CuCl_2$ 0.5%	16.58	2	2.9
$CuCl_2$ 2%	16.36	2	3.9
$CuCl_2$ 10%	15.75	2.3	2.1
$ZnCl_2$ 0.5%	16.11	2	4.5
$ZnCl_2$ 2%	17.81	2	2.6
$ZnCl_2$ 10%	18.93	2	2.7

In general, the decomposition of Ca beads occurred in three steps: dehydration (from 30°C to 163-195°C depending on the crosslinking cation employed), Alg decomposition, which may lead to H_2O, CH_4, CO_2 and carbonaceous residues formation (170-340°C), and oxidation of previously formed intermediate carbonaceous char material (400-800°C). Hence, three characteristic regions of weight loss may be differentiated. The second thermal event divided into two main peaks, which demonstrated a more complex weight loss pattern. Both peaks corresponded to the destruction and disintegration of glycosidic bonds [26]. Probably the second thermal event may also involve the partial evaporation of residual water. Both second and third regions were most likely partially merged. Obtained TGA curves agreed with previous findings [26].

The thermograms of Cu- and Zn- beads displayed a simpler thermal decomposition in regard to Ca-beads. Primarily, the thermal event related to the degradation of glycosidic bonds in Cu- and Zn beads took place at lower temperature, as well as the oxidation of previously formed carbonaceous char material. The higher the concentration of Zn^{2+} and Cu^{2+}, the higher temperatures to oxidize the carbonaceous char

material. The thermal decomposition pattern obtained for Cu beads corresponded with previous findings [27].

The $n_{\frac{U}{C}}$ calculated for a 0.5% (w/w) concentration was 2 regardless the crosslinker (Table 3.4). The number of water molecules per cation ($n_{\frac{w}{C}}$) was similar for Ca- and Zn-beads which was 4.4 and 4.5, respectively. The number of water molecules decreased to 2.9 for Cu-beads.

In the case of a MCl_2 concentration of 2% (w/w), the $n_{\frac{U}{C}}$ was 2 for Cu- and Zn-beads but it was smaller for Ca-beads, which was 1.2 (Table 3.4). Cu-beads presented the greater number of $n_{\frac{w}{C}}$, followed by Zn- and Ca- beads. The determined values were 3.9, 2.6 and 1.8, respectively. The fact that the residue of Ca-beads was the largest whereas $n_{\frac{U}{C}}$ was the smallest suggested the presence of Ca^{2+} ions despite they may not interact with U residues probably due to the fast and disorganized diffusion.

Agulhon et al. determined by means of computational techniques that the interactions between U and alkaline earth metals (Ca^{2+}) was essentially electrostatic, whereas the interactions with transition metals (Cu^{2+} and Zn^{2+}) involved the formation of strong covalent-coordination bonds [25]. Additionally, Katz et al. found through the study of protein crystal structures and *ab initio* computing that the coordination number of Ca^{2+} in crystalline structures normally varied between 6 and 8. Indeed, oxygen is the usual ligand and interacts with the carboxyl groups of Alg residues in an unidentate or bidentate way, as well as a minimum of one molecule of water [28]. In the case of mannuronate dimers, however, DFT-based calculations revealed that two Ca^{2+}-O distances corresponded to the oxygen of water molecules and that the addition of water molecules did not substantially affected the Ca^{2+}-O distances in regard to water-free configurations [25]. Therefore, the variability in $n_{\frac{U}{C}}$ and $n_{\frac{w}{C}}$ with the diverse Ca^{2+} concentrations may be due to alterations of both the Alg denticity and the number of water molecules surrounding the Ca^{2+} ions.

The value of $n_{\frac{U}{C}}$ was equal to 2 when $CuCl_2$ concentration 0.5 and 2% (w/w). This estimation matched the predicted theoretical value for complete complexation of Alg with divalent cations. Nevertheless, this number rose if Cu^{2+} was available in excess. Moreover, it is significant to recall that when Cu-beads were prepared in a crosslinking bath $CuCl_2$ 10% (w/w), acidic precipitation was most probably to occur due to the pH of the crosslinking bath (Table 3.2). Hence, the amount of Cu ions estimated for the calculation of the $n_{\frac{U}{C}}$ parameter might at least partially belong to uncoordinated cations that were "trapped" during acidic precipitation into the acidic

hydrogel. In the case of Zn-beads, the value of $n_{\frac{U}{C}}$ was 2 regardless the initial $ZnCl_2$ concentration. This result pointed a homogeneous Alg coordination to Zn^{2+}.

3.2.7 FT-IR analysis

3.2.7.1 Main vibrational modes

As was already cited in Section 3.2.4, metal-carboxylate interactions in the complex with Alg may be studied using FT-IR spectroscopy [9, 20, 29, 30]. Table 3.5 describes the main absorption frequencies that may be found in the IR spectra of Alg beads, displayed in Figure 3.16, and the correlation with the molecular vibrations involved. In Table 3.6 the values of $\nu(COO^-)asym$ and $\nu(COO^-)sym$ are displayed for each crosslinking cation and concentration.

The study of the main peaks obtained from the IR spectra of -beads (Figure 3.16) indicated that:

1. All IR spectra exhibited absorbance bands at 3273 cm^{-1}, 1596 cm^{-1}, 1407 cm^{-1}, 1112 cm^{-1}, 1026 cm^{-1}, 883 cm^{-1}, 812 cm^{-1} and 738 cm^{-1} approximately. Especially, the frequency at 738 cm^{-1} was fairly accurate and replicated among all samples.

2. In line with the NMR characterization, in all samples the band associated to mannuronate residues (812-814 cm^{-1}) was pronounced, whereas the band correlated to guluronate residues (around 730 cm^{-1}) was not visible at all. This finding confirmed the predominance of M units in the employed Alg.

3. The band assigned to the C-OH stretching vibration (at 1080 cm^{-1}) was accentuated for the sample of Na Alg, while it was considerable broader and smaller in the samples of crosslinked Alg, indicating that the hydroxyl oxygen participated in the coordination with the divalent cations [31, 32].

4. $\nu(COO^-)asym$ and $\nu(COO^-)sym$ remained fairly constant among the diverse crosslinker conditions, unlike different crosslinkers. These results pointed to the diverse crosslinking mechanisms as different and specific anionic groups contributed in each complex M^{2+}-Alg [6].

5. Differences between spectra of the diverse crosslinkers were mainly due to $\nu(COO^-)asym$ and $\nu(COO^-)sym$ absorbance bands. Cu-beads displayed the lowest $\nu(COO^-)asym$ and $\nu(COO^-)sym$, whereas Ca-beads displayed the highest $\nu(COO^-)sym$.

6. All $\nu(COO^-)asym$ values were lower than the obtained for Na Alg. These findings evidenced an improved symmetry of Ca, Zn and Cu-complexes in regard to Na Alg. The greatest difference was for Cu-beads.

7. The space between the $\nu(COO^-)sym$ and $\nu(COO^-)asym$ was notably larger for Na Alg compared to crosslinked Alg. It could be explained by the enhanced symmetry of the cation-Alg complex because of crosslinking.
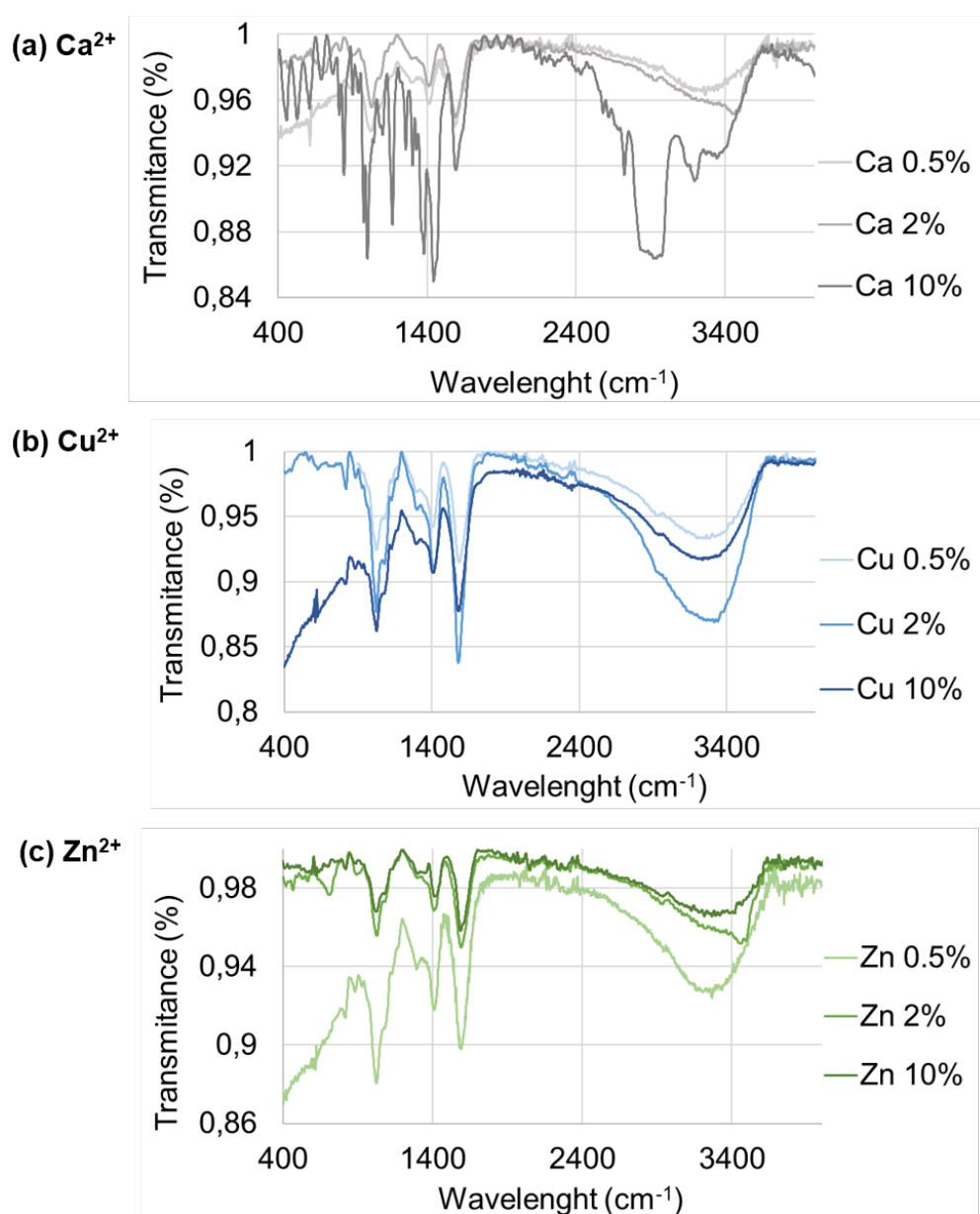
Figure 3.16: FT-IR spectra of M^{2+}-beads obtained with MCl_2 0.5%, 2% and 10% (w/w) where M is: a) Ca, b) Cu and c) Zn

93

Table 3.5: Interpretation of the main absorption wavelengths of the IR spectra of M^{2+}-Alg beads and the associated molecular vibrations [9, 10, 15, 33, 34]

Band	Corresponding to:	
3245-3273 cm^{-1}	–OH stretching vibration	ν(OH)
2936-2978 cm^{-1}	–C–H stretching vibrations of saturated aliphatic species	ν(CH)-anomer
1580-1600 cm^{-1}	Symmetric –COO stretching vibration of carboxylate groups	$\nu(COO^-)sym$
1407-1427 cm^{-1}	Asymmetric –COO stretching vibration of carboxylate groups	$\nu(COO^-)asym$
1102-1073 cm^{-1}	–C–O stretching vibration of the pyranosyl ring	
1025 cm^{-1}	Stretching of C–O groups	
962-928 cm^{-1}	C–O stretching of uronates	
871-883 cm^{-1}	C1–H mannuronic acid deformation	
815-833 cm^{-1}	Attributed to M residues	
787 cm^{-1}	Assigned to G residues	

Table 3.6: Values of asymmetric and symmetric stretching vibration of carboxylate groups ($\nu(COO^-)asym$ and ($\nu(COO^-)sym$) of M^{2+}-beads prepared with different concentrations of MCl_2

	$\nu(COO^-)asym$	$\nu(COO^-)sym$	$\Delta\nu(COO^-)$
Na Alg	1596	1404	190
$CaCl_2$ 0.5% (w/w)	1580	1415	165
$CaCl_2$ 2% (w/w)	1588	1417	171
$CaCl_2$ 10% (w/w)	1600	1423	177
$CuCl_2$ 0.5% (w/w)	1587	1407	180
$CuCl_2$ 2% (w/w)	1584	1405	179
$CuCl_2$ 10% (w/w)	1587	1407	180
$ZnCl_2$ 0.5% (w/w)	1590	1414	176
$ZnCl_2$ 2% (w/w)	1588	1408	180
$ZnCl_2$ 10% (w/w)	1587	1415	172

3.2.7.2   Binding modes - carboxyl group coordination to cations

The binding mode or type of coordination between the crosslinking cations and Alg residues may be evaluated through the difference between the asymmetric and symmetric vibrational modes of carboxylate groups, $\Delta\nu(COO^-)$ in the crosslinked beads. The kind of metal coordination was determined by comparing the $\Delta\nu(COO^-)$ of uncrosslinked Na Alg with the $\Delta\nu(COO^-)_{complex}$ obtained from beads' evaluation. Therefore, the separation of these bands gave rise to the following interpretation [35]: $\Delta\nu(COO^-)_{complex} \ll \Delta\nu(COO^-)_{Na}$ corresponds to bidentate chelating coordination; $\Delta\nu(COO^-)_{complex} \sim \Delta\nu(COO^-)_{Na}$ corresponds to bidentate bridging coordination; $\Delta\nu(COO^-)_{complex} \gg \Delta\nu(COO^-)_{Na}$ corresponds to unidentate coordination.

Providing that Alg chains consist of two different uronic acids - M and G, more than one type of cation-carboxylate coordination may be feasible [6]. For example, the type of complexation of a Ca ion located between two chains of M- and G-blocks has been previously studied with computational methods [36]. Results demonstrated that Ca^{2+} linked in an unidentate interaction to one of the chains and in a bidentate type to the other (Figure3.17b, c and d). Otherwise, Cu^{2+} bound urontaes in a complete bidentate chelating interaction (Figure3.17c).
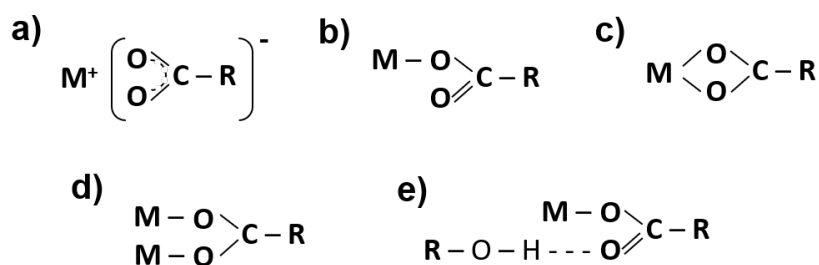
Figure 3.17: Binding modes between M^{2+}-carboxyl group of uronates as proposed by Agulhon et al.: a) anionic or uncoordinated; b) unidentate; c) bidentate chelating; d) bidentate bridging and; e) pseudo-bridging unidentate type [36]

The coordination of G-blocks with metal ions has been reported to be a bidentate chelating type (Figure 3.17c) [37]. Nevertheless, the complexation with M-blocks depends on the radius and affinity of the crosslinking cation [37]. M residues are highly flexible and generally arrange randomly. In addition, not all carboxyl groups of the M-blocks may be linked by hydrogen bonds, as $\nu(OH)$ value keeps constant regardless the crosslinker and concentration.

Primarily, the $\Delta\nu(COO^-)$ value of Ca-, Zn- and Cu-beads was inferior to $\Delta\nu(COO^-)_{Na}$ Alg. Since this difference was smaller than 200 cm^{-1}, the type of coordination would correspond to a bidentate chelating type, according to previous studies [37, 38]. In a bidentate chelating interaction, the cation is known to interact equally with the two oxygen atoms of the carboxylate (Figure 3.17c). Nevertheless, results reported in previous sections demonstrated the presence of water molecules within the hydrogel network; the shift of $\nu(OH)$ through lower frequencies after crosslinking as an enhanced contribution of -OH groups to H-bond network; and $\Delta\nu(COO^-)$ values closer to 200 cm^{-1} suggested that 'pseudo-bridging' unidentate type could be the dominant (Figure 3.17e) [39]. In the bridging form, the two carboxyl oxygens interact with two M^{2+} ions (Figure 3.17d). In the 'pseudo-bridging' form, one carboxyl oxygen interacts with a cation while the other oxygen establishes hydrogen bonds with adjacent OH- groups belonging to water molecules [39]. In contrast, the "egg-box" model depicts this type of coordination for the polyguluronate-M^{2+} complex. Nevertheless, in our situation, the M-rich Alg may lead to a different arrangement, making the calculated $\Delta\nu(COO^-)_{complex}$ also consistent with a different binding mode such as bidentate bridging type.

Considering the determined number of U per cation (Table 3.4), as well as the findings from FT-IR and EXAFS analysis, for the 0.5% Cu- and Zn-beads it was proposed that each divalent cation was surrounded by four CO, with each group originating from a distinct carboxyl group within the Alg structure. In this configuration, the cation would function as a tetrafunctional "crosslinking agent" for the M-rich Alg, as depicted in Figure 3.18. Additional coordination positions could potentially be occupied by hydroxyl groups from U or water molecules. This hypothesis may hold true for higher concentrations of Zn. However, due to the situation of an hybrid system in the case of Cu, predicting its coordination is more challenging.
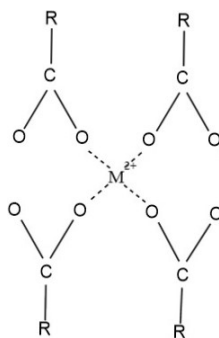
Figure 3.18: Schematic representation of the bridging coordination hypothesized for Alg beads obtained from $CuCl_2$ and $ZnCl_2$ 0.5% (w/w)

Eventually, according to Fuks et al., a slight increase of the $\Delta\nu(COO^-)_{complex}$ value with the increasing inversed cationic radii might be related with a rise of the symmetry and a balance of the bond lengths [38]. Therefore, it could be stated that the most symmetric interaction between carboxyl oxygens would occur when Zn^{2+} was employed as crosslinking agent, followed by Cu^{2+} and Ca^{2+}. In addition, the shift of the vibrational frequencies of a determined condition (crosslinker and concentration) in time tended to lower energies. This could be a consequence of reaching the equilibrium state. It seemed that $\Delta\nu(COO^-)asym$ varied more than $\Delta\nu(COO^-)sym$ until equilibrium was reached.

3.2.8   Mechanical characterization

All the systems under investigation were mechanically characterized in compression mode after drying at 40°C for 24h. The corresponding values of Young Modulus (E) and Strength at break (σ_b) for each system are displayed in Figure 3.19. Figure 3.20 corresponds to stress–strain curves of the investigated conditions. Moreover, Figure 3.21 shows the fracture pictures of the beads after compression tests. Two factors were considered while discussing these findings: 1) the composition of the material, which depicts the number of crosslinking sites in the hydrogel and the strength of the interactions established; and 2) the morphology of the bead, which influences the resistance of the outer wall and crack propagation under compression force.

Uniaxial compression tests of beads after drying at 40°C for 24h revealed that most of the stress–strain curves were not linear even over the first millimetres (Figure 3.20). The E of the tested beads did not increase linearly with increasing cation concentration.

It was observed when the beads prepared with MCl_2 0.5% (w/w) were compared that the Ca-based system was the less stiff and robust (Figure 3.19). Based on the rheological behavior of Ca-systems, interaction between Ca^{2+}-Alg were proved not to be permanent but to move or break under shearing instead [8]. In fact, the micrographs of 0.5% (w/w) samples after mechanically tested showed that Ca-beads flattened out rather than breaking under the applied stress (Figure 3.21). Ca-beads displayed an obvious elastoplastic behavior, as represented by the load-displacement curves (Figure 3.20). This was also consistent with the reported final inner morphology of Ca-beads (Figure 3.12-3.14), which displayed a compact core with several planes that provided support to withstand the compression stress.

97

When Ca 0.5% beads were tested, ductility was high and they crushed with practically no cracks. The stress failure value was not significant enough since only two capsules fractured (Figure 3.19a). Cu- and Zn-based systems, on the other hand, exhibited superior mechanical qualities (Figure 3.19b and c). When $CuCl_2$ 0.5% (w/w) was employed, the obtained material was highly rigid. The resistance was elevated and only few beads broke. When $ZnCl_2$ 0.5% (w/w) was utilized, the obtained beads were resistant and comparatively ductile. The curve described a deformable material (Figure 3.20a). Beads did not break easily, with almost no cracks nor pieces. Probably, this was due to the presence of stronger and more directional coordination bonds between the cations and Alg U. Giving that both systems had a relatively empty core, their mechanical resistance might be primary due to the outer shell.

The images of the outer layer reported by ESEM (Figure 3.12-3.14) showed that Zn-beads had a thicker shell, which might explain their high E and σ_b values. While Cu-beads completely fractured, cracks were seen in the structure of Zn-beads (Figure 3.21). The difference in the fracture process was certainly represented by the load-displacement curves.

Regarding the samples prepared with MCl_2 2% (w/w), Ca 2% beads were less ductile than Ca 0.5% beads. The level of resistance to plasticization was lower. Young's modulus values were greater. They were the most rigid of Ca beads (Figure 3.19). This was expected since bigger cation concentrations leads to further crosslinking points with Alg, which increase the rigidity of the bead. It was reflected in the beads' fracture behavior as small cracks appeared before failure, as well as in the load-displacement curve (Figures 3.20 and 3.21). In fact, the shift in the slope of the curve manifested the formation of these cracks, while still displaying elastoplastic properties. The core of the beads seemed fairly comparable to that of the Ca 0.5% beads (Figure 3.12), which supported flattening rather than full bead failure.

In the case of Cu 2% beads, they were slightly more ductile and with lower resistance (they have less strength) (Figure 3.19). It should be noted that at the pH measured for the $CuCl_2$ 2% (w/w) bath, a hybrid system was expected to form, in which around 20% of the U residues were present in the acidic form and did not complexate Cu^{2+}. The inner part of Cu 2% beads looked denser compared to Cu 0.5% beads (Figure 3.12), which was consistent with the micrography of shattered samples (Figure 3.21) and the load-displacement curve (Figure 3.20). Cu 2% samples fractured with tiny cracks while preserving mechanical integrity. Beads broke and

split in two large pieces. The variation in the slope indicated the higher ductility of Cu 2% beads.

In regard to Zn 2% beads, samples proved to be more rigid and less deformable than Zn 0.5% beads (Figure 3.19), likely because the outer wall was thinner. The images of Zn-beads tested revealed that the resistance was fairly similar as they completely broke into large pieces (Figure 3.21), which may be explained by the empty core-shell structures shown in Figure 3.13.

When beads were prepared with $CaCl_2$ 10% (w/w), the load-displacement behavior of Ca 10% beads was comparable to that one of Ca 2% samples (Figure 3.20). Both E and σ_b values were higher probably due to the increase in the number of crosslinking sites (Figure 3.19). The slope of the load-displacement curve with higher metal loads was modified as cracks appeared at higher stress levels compared to Ca 0.5% and 2% beads (Figure 3.21). The images of the shattered samples revealed that beads significantly flattened before the appearance of cracks. Hence, beads obtained with $CaCl_2$ 10% (w/w) demonstrated a clearly ductile behavior. This fact was consistent with the cross-section ESEM images (Figure 3.13). The cracks were more visible in this case. Ca 10% beads displayed a similar behavior to Ca 0.5% beads but the first ones were more rigid and less ductile (Figure 3.19).

Beads obtained with $CuCl_2$ 10% (w/w) were strongly rigid compared to Cu 2% beads (Figure 3.19). Thus, load-displacement curves were notably dissimilar but comparable to Cu 0.5% beads, showing a more fragile mechanical behavior (Figure 3.20). This would correspond to the rather regular and compact core (Figure 3.14). It is important to highlight that a hybrid gel, which consists of alginic acid and Cu-Alg, undoubtedly formed in this case. In addition, Cu 10% beads were crushed with visible and complete fractures (Figure 3.21), which was also related to a denser and homogeneous core.

Zn 10% beads were less rigid and resistant. However, E and σ_b values were very scattered (Figure 3.20c), evidencing the inhomogeneity of the internal structure. This was corroborated by the ESEM pictures of the cross-section of Zn-beads (Figure 3.14), in which denser parts coexisted with more empty zones. Furthermore, the surface coat displayed very different thicknesses. As a result, giving that the mechanical behavior is strongly dependent on the contact region where the compression test is effected, the values of mechanical results were more scattered. Hence, the estimated mean value of E and σ_b was low but the deviation was very high. The pictures of the

shattered beads (Figure 3.21) reinforced the dispersed measurements as a portion of the samples totally broke into many pieces whereas other beads broke in two.
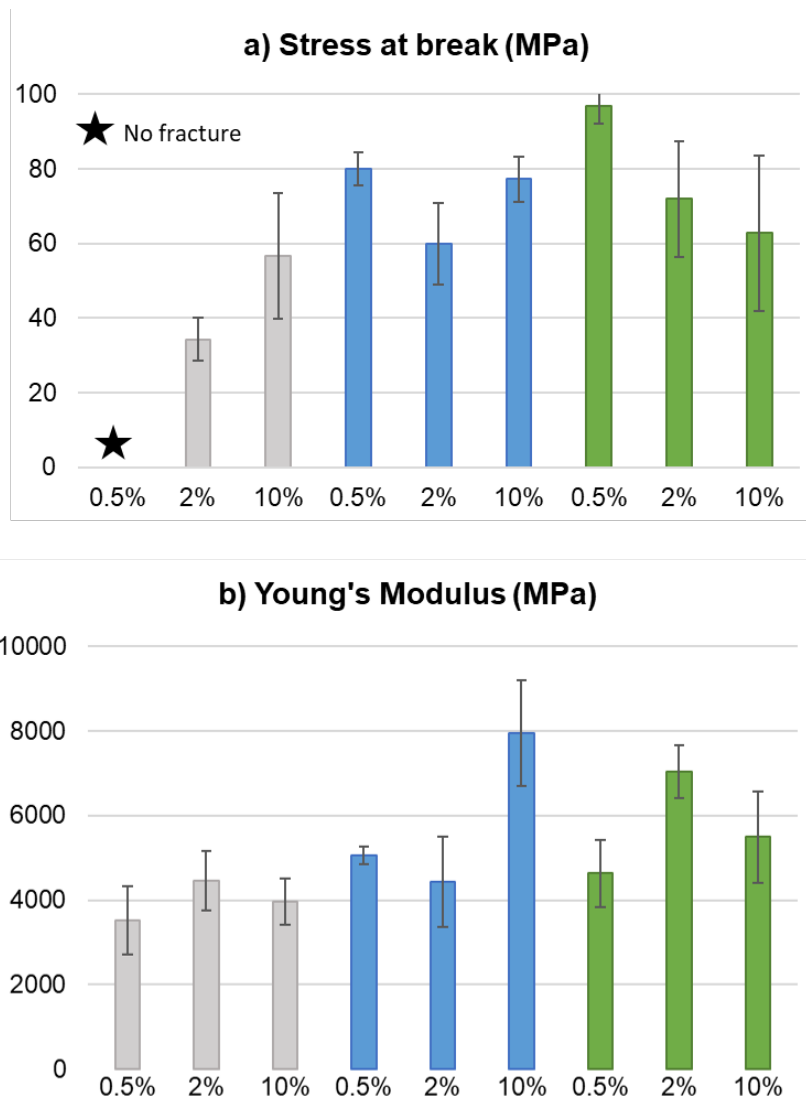
Figure 3.19: a) Strength at break (σ_b), and b) Young Modulus (E) of M^{2+}-Alg beads obtained at different MCl_2 concentrations after 48h maturation and drying at 40°C for 24h. Grey bars refer to beads prepared with $CaCl_2$, blue bars refer to $CuCl_2$ and green bars to $ZnCl_2$

100
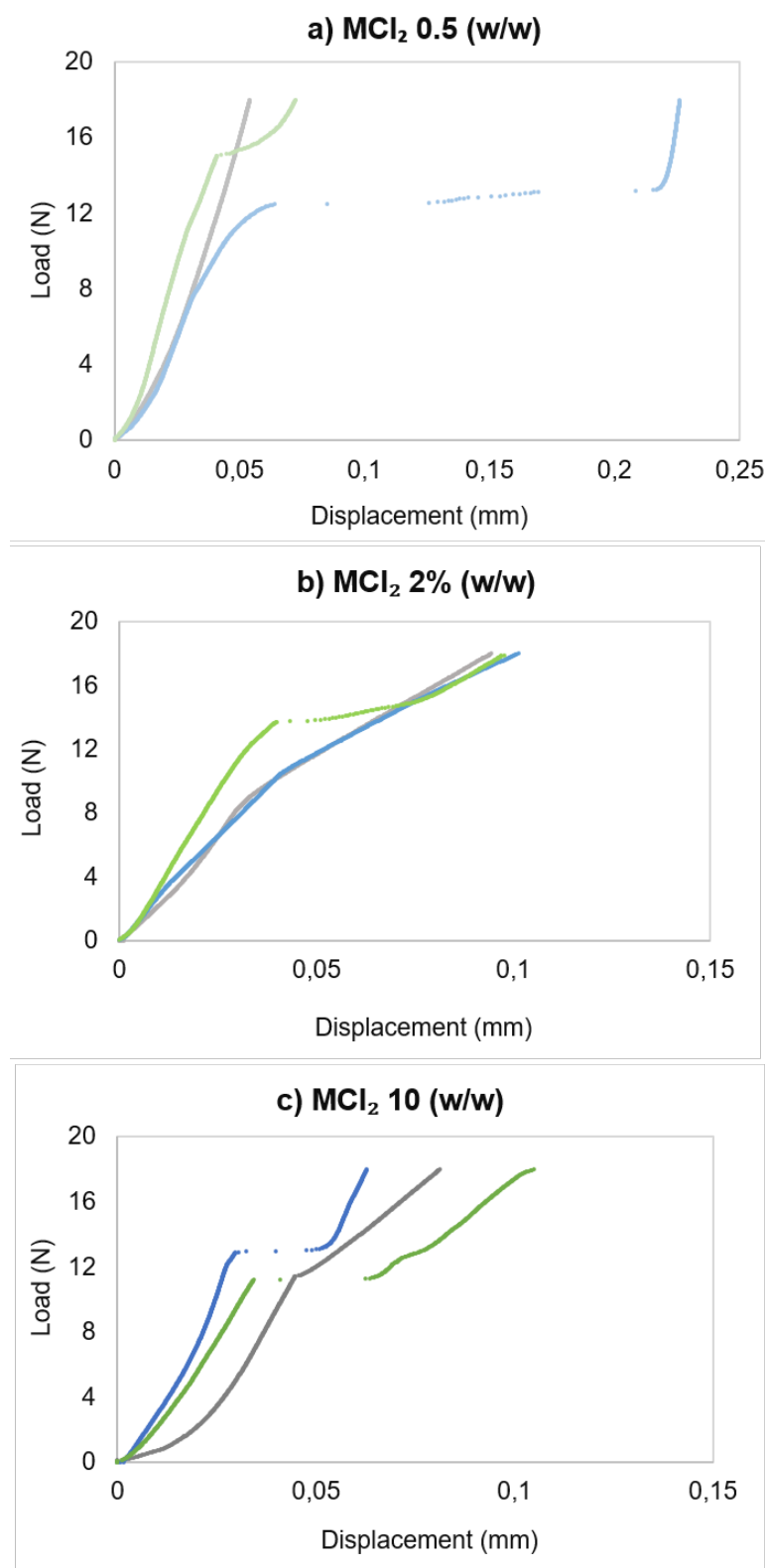
Figure 3.20: Load-displacement curves of the compression tests for beads prepared with MCl_2 a) 0.5%; b) 2% and c) 10% (w/w) where M is: Ca (grey), Cu (blue) and Zn (green)
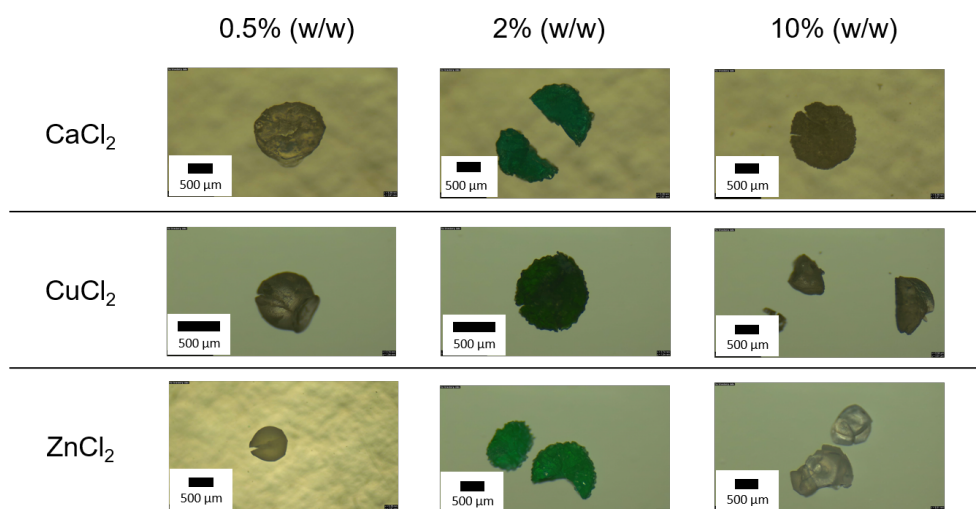
Figure 3.21: Images taken from the failure samples after the compression test

3.2.9 SAXS analysis

Figure 3.22 displays the SAXS patterns of the M^{2+}-beads prepared with MCl_2 0.5%, 2% and 10% (w/w) in logarithmic scale. Part of the beams exhibited some degree of crystallinity, pointing beads to transform into compact structures after drying or aging. All models had a linear slope equal to -4 (matching to a power law of q^{-4}), which corresponds with the presence of large and compact structures with smooth surfaces [40]. This effect could be attributed to the packing of the polysaccharides when the gel is dry to consolidate the bead. Nevertheless, low metal loads (0.5% (w/w)) displayed also a reminiscence of the rod-like structure previously reported for these Alg hydrogels, suggesting an increase in the densely packed domains amount in the order: Ca<Cu<Zn [25].

The fitting process yield the rod-like contribution, and it is illustrated as a dashed line (Figure 3.22). A shift in these contribution to the lower angles means an increase in the structure size. Hence, Ca-based hydrogels exhibited smaller rod diameters compared to Cu or Zn, while the $d_{spacing}$ parameter, which was obtained from the Bragg peak position at q range between 1 and 2 nm^{-1}, showed the contrary tendency. Only the contribution of Bragg peak correlation was detected in the analysis. Additionally, Wide Angle X-Ray Scattering (WAXS) patterns were measured, revealing that the samples were predominantly amorphous, with only a slight presence of long spacing correlation.
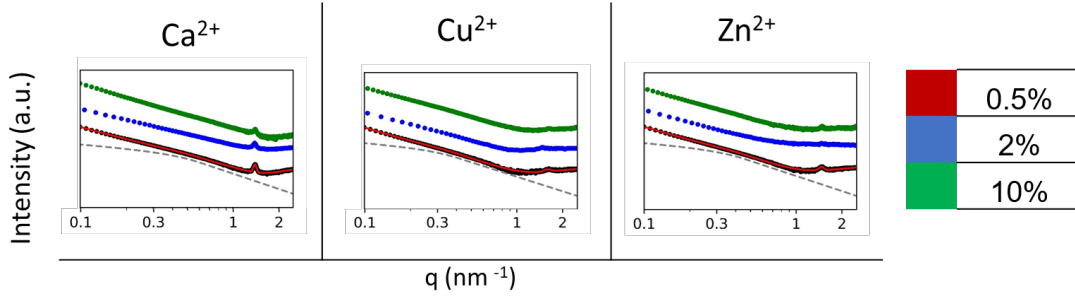
Figure 3.22: SAXS patterns expressed in loglog scale for M^{2+}-Alg hydrogels where M^{2+} refers to: a) Ca^{2+}, b) Cu^{2+} and c) Zn^{2+}. In each panel, from the bottom to the top beads prepared with MCl_2: 0.5% (red), 2% (blue) and 10% (w/w) (green), respectively. The continuous line is the fitting results for MCl_2 0.5% (w/w) whereas the dashed line represents the rod-like structure contribution to the total intensity

Table 3.7 shows the fitting results for the studied samples at 0.5% (w/w) MCl_2. The diameter of the rod-like structure was the same order of magnitude as for previously described M-Alg hydrogels and aerogels [25]. Nonetheless, according to our results, the diameter of Ca-beads was smaller than the diameter of Cu-beads.

Table 3.7: Structural parameters obtained from SAXS pattern fittings for MCl_2 0.5% (w/w) samples and diameter of dry bead as measured by digital Thickness Gage. The rod-like structure diameter was calculated as $Diameter = 2\sqrt{2}Rg$

Cation	Rod Rg (nm)	Rod diameter (nm)	$d_{spacing}$ (nm) Bragg peak	Q_{rod}/Q_{dp}	Bead diameter (mm)
Ca^{2+}	3.10 ± 0.01	8.77 ± 0.03	4.49	8.65	0.47 ± 0.03
Cu^{2+}	3.37 ± 0.01	9.53 ± 0.03	4.27	6.66	0.44 ± 0.01
Zn^{2+}	4.24 ± 0.03	11.99 ± 0.09	3.85	5.92	0.42 ± 0.01

The Q_{rod}/Q_{dp} relationship displayed in Table 3.7 quantifies the arbitrary scale relationship between the rod-like structure quantity regarding the densely packing domains one by the calculation of the invariant Q [40] and taking account the rod-like function and the Gaussian contribution invariant of the diffraction peak [41]:

$$Q_{rod}/Q_{dp} = \frac{C_1 \int_0^\infty P_{GP}(q, R_G)q^2 dq}{C_2 \int_0^\infty G(q, qc_1, FWHM_1)q^2 dq} \tag{3.9}$$

103

When the Q_{rod} / Q_{dp} variable is reduced, the average amount of densely packed nanodomains – crystallinity – of the structure increases in regard to the remaining rods. In addition, the rise in average crystallinity matched the decrease of beads' size (Figures 3.9-3.11). This consequence was likely the result of a more compact configuration at the microscopic level.

Once the MCl_2 concentration in the crosslinking bath was increased to 2% or 10% (w/w) (Figure 3.21), the rod-like structure nearly fade. Possibly, the influence of the compacted content concealed the intensity of the few remaining rods as more numerous and larger configurations scatter more than smaller ones [40]. The diffraction peak could be identified in these samples, but the relationship between the peak intensity and MCl_2 concentration was not evident enough. Nonetheless, the results evidenced that exclusively the Alg beads prepared with the lowest concentration of cation retained part of the pristine gel. When the cation concentration increased, structures compacted on aging. Hence, reorganization of the hydrogel, aging and drying processes were all affected by diverse factors such as polysaccharides charge, which was affected by the pH of the medium, and ionic strength. As a result, the interpretation of the behaviour of these complex structures was challenging.

3.2.10 Extended X-ray absorption fine structure (EXAFS)

EXAFS analysis was applied to study the coordination environment of Cu- and Zn-based hydrogels. The X-Ray absorption near edge (XANES) Spectra is displayed in Figure 3.23. It could be observed that the shape and features were maintained with the diverse metal concentrations. It suggested that the local environment remained similar despite the metal load in the bead.

Moreover, the strong peak near the absorption edge was less intense for Cu 10% samples compared to Cu 0.5% samples, which probably was due to saturation effects in the detector. As a result, only samples prepared with $CuCl_2$ 0.5% (w/w) were analysed by EXAFS.

The FFT derived from EXAFS spectra in radial distribution for Cu- and Zn- 0.5% beads, acquired from the interval 3-14-1 K space is displayed in Figure 3.24. Hence, according to the transformed patterns, oxide particles were not generated during the aging process nor precipitation of $ZnCl_2$ nor $CuCl_2$. The fact that the position of the main peak matched with the acetate references (Figures 3.24c and 3.24d) suggested that the properties involved organic environments connected by M-O bonds. Given

that there were no previous evidences nor references of the local environment, oxygens were assumed to be the closest atoms to crosslinking cations.

Therefore, an individual M-O path with Cu formiate dihydrate and two pathways for Zn oxalate were applied to fit the coordination shell. The LARCH database enabled the obtention of the initial estimation. In the case of Cu^{2+} samples, a single option was considered for the primary coordination shell, with a coordination number of 4.3 ± 0.4, a Cu-O bond length of 1.960 ± 0.003 Å, and a Debye-Waller factor of $6x10^{-3}$. In fact, DFT-based calculations on MM dimers already predicted a coordination number of 4 for Cu^{2+} complex, and a bond distance between 1.99-2.19 Å [36].

Alternatively, in Zn^{2+} samples two different oxygen bonds were expected to be established with Zn: the first with a coordination number of 4.0 ± 0.2, a Zn-O bond length of 2.051 ± 0.006 Å, and a Debye-Waller factor of $7x10^{-3}$; and the second with a coordination number of 1.1 ± 0.1, a Zn-O bond length of 2.34 ± 0.02 Å, and a Debye Waller factor of 0.01. The potential presence of a labile water molecule in the coordination sphere of Zn^{2+} was suggested in the second path. This result implied that in Zn-beads prepared with $ZnCl_2$ 0.5% (w/w), each Zn^{2+} coordinated four oxygens from U and one molecule of water. Indeed, the fitting obtained following this assumption generated fairly satisfactory results. Moreover, Agulhon et al.'s [36] also calculated the coordination number for Zn^{2+} to be 5. Whether water molecules were present, unidentate type binding and antiparallel orientation of mannuronic residues should take place, as stated by these authors.
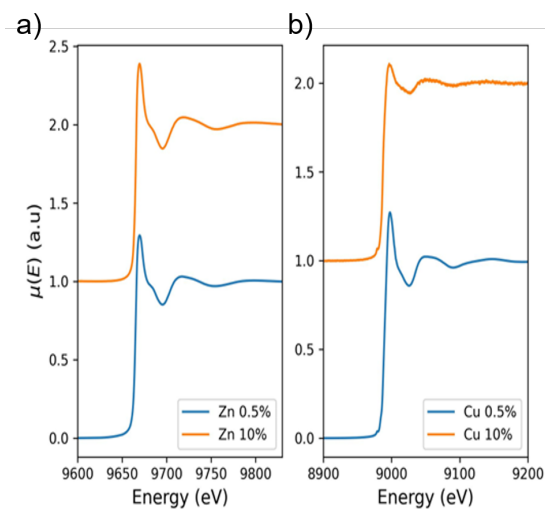
Figure 3.23: X-Ray Absorption Near Edge Spectra for a) Zn- and b) Cu-beads prepared with MCl_2 0.5% and 10% (w/w)
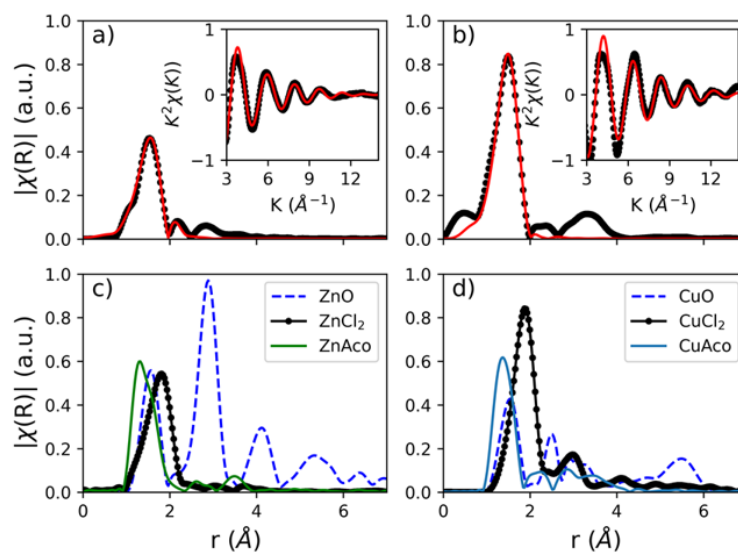
Figure 3.24: Fourier transform of the EXAFS spectra for a) Zn- and b) Cu-beads prepared with MCl_2 0.5% (w/w). References are also plotted for comparative analysis: c) ZnO, $ZnCl_2$ and Zn^{2+} acetate (ZnAco) and d) CuO, $CuCl_2$ and Cu^{2+} acetate (CuAco)

106

3.2.11   Study of Zn^{2+} gelation

Figure 3.25 illustrates the evolution of the interactions between U and Zn^{2+} during the preparation and maturation of Alg beads in a crosslinking bath of $ZnCl_2$ 0.1% and 0.5% (w/w). Hence, it reveals that at the beginning of beads' formation, a higher number of Alg units interacted per mol of Zn compared to the following time points. Both studied concentrations displayed the same tendency (Figure 3.25). Therefore, initially Alg was very concentrated and gelation must be local. Figure 3.12c evidenced the formation of an initial thin shell in Zn 0.5% beads, which was not compact and reorganized among time. Certain period of time was required for an optimal organization. Unfortunately, the core of beads prepared with $ZnCl_2$ 0.1% (w/w) could not be clearly observed as they deformed during cryofracture manipulation (Figure 3.26). Nevertheless, a core-shell structure was discerned previously to cryofracture when beads were still wet.

The resistance to Zn^{2+} diffusion was not strong in either of the employed $ZnCl_2$ concentrations. However, the lowest concentration depicted a more homogeneous diffusion likely due to the softer resistance of Alg gellified layers (Figure 3.25a). In addition, the time needed to achieve an optimal coordination state (constant number of $n_{\frac{U}{C}}$) appeared shorter for a concentration of $ZnCl_2$ 0.1% (w/w). Although taking longer, the optimal coordination state was achieved in both cases and the number of Alg units per mol of Zn resulted to be 2 (Table 3.8).
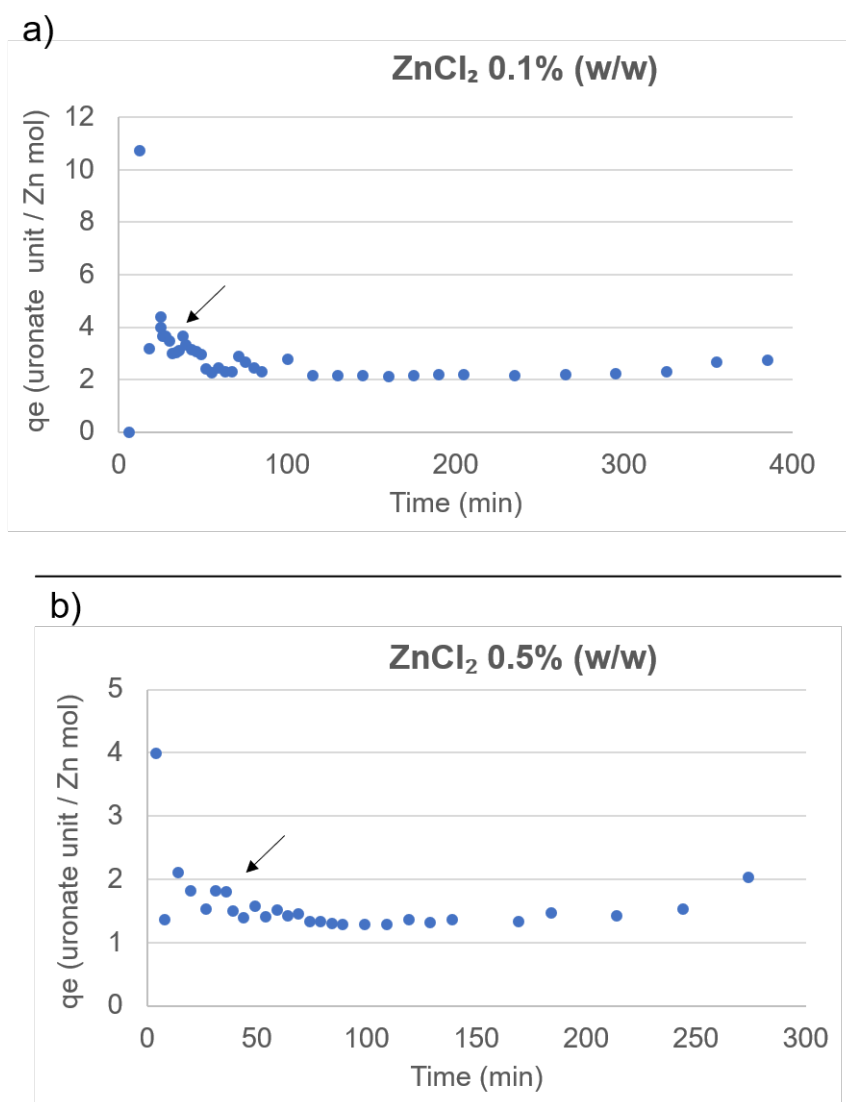
Figure 3.25: Evolution of Alg units bound per mol of Zn^{2+} during the preparation and maturation of Alg beads with $ZnCl_2$ a) 0.1% and b) 0.5% (w/w). The last drop of polymeric solution is extruded at time a) 19 min and b) 39 min and it is indicated by the arrows

ZnCl$_2$ 0.1% (w/w)
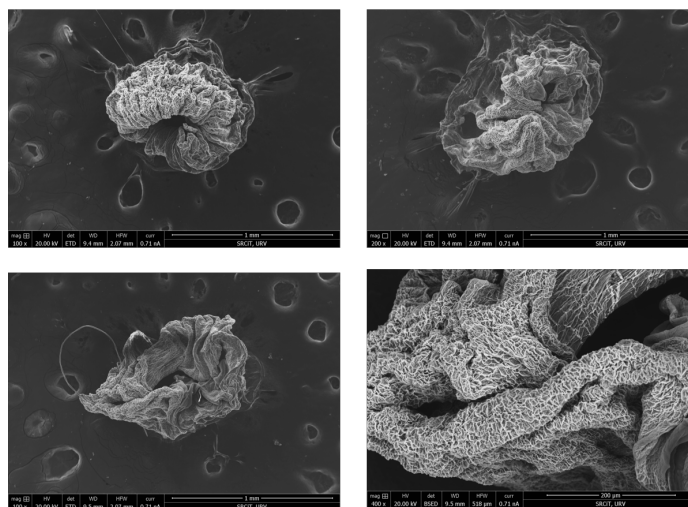
Figure 3.26: ESEM micrographies of cryofractured Zn-beads crosslinked with $ZnCl_2$ 0.1% (w/w) after 48h maturation

Table 3.8: Number of uronate units per cation $(n_{\frac{U}{C}})$ of Alg beads prepared with $ZnCl_2$ 0.1% and 0.5% (w/w) determined by TGA

Compund	Residue (%)	n$_{\frac{U}{C}}$
$ZnCl_2$ 0.1%	17.78	2
$ZnCl_2$ 0.5%	16.11	2

3.3   Conclusions

- The determination of Alg composition is crucial in order to compare the gelling, structural and mechanical properties of hydrogels prepared with diverse cations. Crosslinking mechanisms of Alg with divalent cations has been normally explained by the "egg-box" model. Nevertheless, it highlights the crucial role of G-blocks to promote gelation whereas M-blocks or G/M heterosequences are more relegated.

- In this chapter, M-rich Alg was crosslinked with Ca^{2+}, Cu^{2+} or Zn^{2+} cations at diverse concentrations. The preparation process of Alg hydrogels was optimized in regard to the concentration of Alg and metal chloride in the crosslinking bath, extrusion rate and set up. Moreover, the time employed for beads' maturation -

109

48h, was remarkably longer than the time employed in the most part of previous studies - 3-24h. Given that cations' diffusion towards the beads and the evolution of these systems is quite slow, we considered longer times to be necessary to reach the steady-state equilibrium.

- Generally, Alg with high-M content generates more elastic hydrogels compared to G-rich Alg [14]. This is due to the low charge density and ineffective electrostatic interactions between M-rich polymeric chains [15]. In addition, given the open and flat geometry of M residues [16], a greater number of chain associations and architectures are plausible. In addition, the broad peaks in the ^1H NMR spectra were likely a result of this fact [6]. Moreover, high degree of hydrogen bonding has been found in M-rich Alg structures, which may lead to self-assembled Alg chains [16].

- The resulting hydrogels were characterized in terms of morphology (ESEM, SAXS and EXAFS), composition (TGA and WAXRD), mechanical properties and interactions between U and different cations (FT-IR). Based on the pH values of the crosslinking baths, when Ca^{2+} and Zn^{2+} were employed as crosslinking agents, only ionotropic gelation gave rise to beads' formation. Nevertheless, in case of Cu^{2+}, a hybrid system of ionotropic gelation and acid precipitation was proposed to lead to beads formation.

- The ESEM pictures revealed the wide variety of surfaces and inner morphologies of cryofractured beads, consistent with the distinct gelation mechanisms of each crosslinking cation. In all cases, Alg gelation was conditioned by both, the stiffness and permeability of the outer wall, as well as on the concentration of the crosslinker in the coagulation bath. Notably, Zn-based beads displayed a more defined core-shell structure, which enhanced their potential for future applications. Ca-beads resulted to be the less resistant and the most ductile hydrogels. These elastoplastic behaviour, which progressively diminished with rising the metal load, could be attributed to the ionic nature of Ca^{2+} interaction [36]. The cracks after the beads' crush would evidence the presence of the same charges very close in the space. Alternatively, Cu- and Zn-beads were the same resistant. Indeed, both have been proved to coordinate with Alg by the formation of strong covalent bonds [34, 36]. Zn-beads resulted to be more resistant than Ca-beads probably due to the employed Alg. Normally, Zn^{2+} displays the lowest Alg affinity. Nevertheless, Ca^{2+} exhibits high affinity toward G-rich

110

Alg chains while Zn^{2+} interaction is unspecific [36]. Zn^{2+} binds randomly with GG-block, MM-blocks and MG-blocks [6]. Therefore, the interaction of Zn^{2+} with M-rich Alg was more favourable compared to Ca^{2+}. Probably, the obtained Ca-beads had similar properties as Zn-beads because of the lack of Ca crosslinking points [6]. Otherwise, the M/G ratio of Alg did not concern the level of crosslinking nor Zn^{2+} crosslinking points [6]. Nevertheless, Cu complexation is always going to be strong due to the high Alg affinity and the lack of selectivity for the diverse U [36]. The observations made with ESEM supported the results of mechanical analysis and pointed Cu- and Zn-based systems in general to have better mechanical properties than Ca-based one. In the case of Zn-based hydrogels, increasing Zn^{2+} concentration led to a rise in rigidity and eventually on the strength. However, the highly inhomogeneous inner structure of Zn 10% beads resulted in scattered values of E and σ_b. In the instance of Cu-beads, increasing the Cu^{2+} concentration resulted in a greater E although the ultimate σ_b did not certainly change. As the pH value of the coagulation bath was under the Alg pKa, the interpretation of this hybrid acidic-ionic system may be challenging.

- From the TGA results, it is relevant that the calculated number of U per Zn^{2+} ion was 2 regardless of the studied concentration. This evidences a homogenous coordination between Alg and this cation. The composition of Ca- and Cu-beads, on the other hand, was influenced by the concentration of crosslinker. In the case of Ca-beads, the variation of beads' composition could be attributed to alterations in the Alg denticity as well as in the number of water molecules surrounding the Ca^{2+} ion. In regard to Cu-beads, it is likely that the number of U per cation increased because of the combination of ionotropic and acidic gelation.

- The nature of metal-Alg interactions was studied by means of FT-IR. It was based on the comparison of the diverse $\Delta\nu$, which is the difference between the asymmetric and symmetric vibrational modes of carboxyl groups [9], of the crosslinked and uncrosslinked Na Alg. Therefore, the resulting values of $\Delta\nu(COO^-)_{complex} > \Delta\nu(COO^-)_{Na}$ pointed, according to the literature [9], to a "pseudo-bridged" unidentate interaction, in which one oxygen in the carboxylate interacts with the cation whereas the other oxygen establishes a hydrogen bond with a neighbouring hydroxyl group.

- SAXS research revealed that only the beads formed at lower cation concentrations had pristine gel rod-like structure. The degree of crystallinity was correlated to bead's size. Thus, the most crystalline structure was identified in the most compact Zn beads.

- EXAFS technique was applied to analyse the coordination environment of Cu- and Zn-beads and determined that no oxide particles were generated during the beads manufacturing procedure. It should be noted that the coordination number was 4.3 ± 0.4 for Cu 0.5% beads, whereas each Zn^{2+} ion could coordinate 4 oxygens from an U as well as one molecule of water. These results are supported by Density Functional Calculations (DFT) on Cu^{2+} or Zn^{2+} and dimannuronate complexes, as well as by ICP results, which indicate that the optimal coordination state - the number of Alg units per mol of Zn^{2+}, is 2 regardless the $ZnCl_2$ concentration.

- These findings suggest that Zn-based hydrogels display features that might be useful for future innovative applications. Zn^{2+} gave rise to beads with superior mechanical qualities and a core-shell structure, which is very suitable for the microencapsulation of active compounds. Nonetheless, when compared to Ca^{2+} and Cu^{2+}, the gelation mechanism of Zn^{2+} has not been as frequently studied. Firstly, the lack of selectivity and creation of strong coordination interactions with the carboxyl groups of the Alg residues result in stronger and more stable hydrogels, in contrast with Ca^{2+} [34, 36]. In addition, the reduced affinity of Alg for Zn^{2+} may be seen as a benefit as the crosslinking process could be tuned more easily, potentially allowing the formation of more complex structures. Moreover, Zn^{2+} is an essential element, which is involved in many cellular processes such as cell growth, differentiation, and enhancement of wound healing [1]. Zn^{2+} has shown to have antioxidant and anti-inflammatory properties [1]. Although having strong antibacterial characteristics, Cu-based hydrogels demonstrated cytotoxicity to human cells, which restricts their use [42].

Bibliography

[1] A. S. Prasad, *Biochemistry of Zinc*, ser. Biochemistry of the Elements Ser. New York, NY: Springer, 2013, vol. 11. [Online]. Available: https://ebookcentral.proquest.com/lib/kxp/detail.action?docID=6583565

[2] H. Cheng, H. Wu, T. Guo, H. Jin Park, and J. Li, "Zinc insulin hexamer loaded alginate zinc hydrogel: Preparation, characterization and *in vivo* hypoglycemic ability," *European journal of pharmaceutics and biopharmaceutics: official journal of Arbeitsgemeinschaft fur Pharmazeutische Verfahrenstechnik e.V*, vol. 179, pp. 173–181, 2022.

[3] Z. Zheng, J. Qi, L. Hu, D. Ouyang, H. Wang, Q. Sun, L. Lin, L. You, and B. Tang, "A cannabidiol-containing alginate based hydrogel as novel multifunctional wound dressing for promoting wound healing," *Biomaterials advances*, vol. 134, p. 112560, 2022.

[4] N. M. Velings and M. M. Mestdagh, "Physico-chemical properties of alginate gel beads," *Polymer Gels and Networks*, vol. 3, pp. 311–330, 1995.

[5] T. Ramdhan, S. H. Ching, S. Prakash, and B. Bhandari, "Time dependent gelling properties of cuboid alginate gels made by external gelation method: Effects of alginate-$CaCl_2$ solution ratios and pH," *Food Hydrocolloids*, vol. 90, pp. 232–240, 2019.

[6] L. Iskandar, L. Rojo, L. Di Silvio, and S. Deb, "The effect of chelation of sodium alginate with osteogenic ions, calcium, zinc, and strontium," *Journal of biomaterials applications*, vol. 34, no. 4, pp. 573–584, 2019.

[7] C. Ouwerx, N. Velings, M. Mestdagh, and M. Axelos, "Physico-chemical properties and rheology of alginate gel beads formed with various divalent cations," *Polymer Gels and Networks*, vol. 6, no. 5, pp. 393–408, 1998.

[8] M. Mancini, M. Moresi, and R. Rancini, "Mechanical properties of alginate gels: empirical characterisation," *Journal of Food Engineering*, vol. 39, no. 4, pp. 369–378, 1999.

[9] S. K. Papageorgiou, E. P. Kouvelos, E. P. Favvas, A. A. Sapalidis, G. E. Romanos, and F. K. Katsaros, "Metal-carboxylate interactions in metal-alginate complexes studied with FTIR spectroscopy," *Carbohydrate Research*, vol. 345, no. 4, pp. 469–473, 2010.

[10] Z. Belattmania, S. Kaidi, S. El Atouani, C. Katif, F. Bentiss, C. Jama, A. Reani, B. Sabour, and V. Vasconcelos, "Isolation and FTIR-ATR and ^{1}H NMR Characterization of Alginates from the Main Alginophyte Species of the Atlantic Coast of Morocco," *Molecules (Basel, Switzerland)*, vol. 25, no. 18, 2020.

[11] H. M. Jensen, F. H. Larsen, and S. B. Engelsen, "Characterization of Alginates by Nuclear Magnetic Resonance (NMR) and Vibrational Spectroscopy (IR, NIR, Raman) in Combination with Chemometrics," *Methods in molecular biology (Clifton, N.J.)*, vol. 1308, pp. 347–363, 2015.

[12] H. Grasdalen, B. Larsen, and O. Smidsrød, "A p.m.r. study of the composition and sequence of uronate residues in alginates," *Carbohydrate Research*, vol. 68, no. 1, pp. 23–31, 1979.

[13] P. E. Ramos, P. Silva, M. M. Alario, L. M. Pastrana, J. A. Teixeira, M. A. Cerqueira, and A. A. Vicente, "Effect of alginate molecular weight and M/G ratio in beads properties foreseeing the protection of probiotics," *Food Hydrocolloids*, vol. 77, pp. 8–16, 2018.

[14] S. H. Ching, N. Bansal, and B. Bhandari, "Alginate gel particles: A review of production techniques and physical properties," *Critical reviews in food science and nutrition*, vol. 57, no. 6, pp. 1133–1152, 2017.

[15] A. Dodero, S. Vicini, M. Alloisio, and M. Castellano, "Sodium alginate solutions: correlation between rheological properties and spinnability," *Journal of Materials Science*, vol. 54, no. 10, pp. 8034–8046, 2019.

[16] J. Brus, M. Urbanova, J. Czernek, M. Pavelkova, K. Kubova, J. Vyslouzil, S. Abbrent, R. Konefal, J. Horský, D. Vetchy, J. Vysloužil, and P. Kulich, "Structure and Dynamics of Alginate Gels Cross-Linked by Polyvalent Ions Probed via Solid

State NMR Spectroscopy," *Biomacromolecules*, vol. 18, no. 8, pp. 2478–2488, 2017.

[17] F. Burriel-Martí, *Quimica analitica cualitativa.* Madrid, España: Thomson, 2008.

[18] A. Haug, S. E. Rasmussen, R. C. Sheppard, W. G. Terry, B. Sjöberg, and J. Toft, "Dissociation of alginic acid," *Acta Chemica Scandinavica*, vol. 15, pp. 950–952, 1961.

[19] N. G. Gaylord and J. B. Neilands, "Organic sequestering agents. s. chaberek and a. e. martell. wiley, new york, 1959. xv + 616 pp. \$25.00," *Journal of Polymer Science*, vol. 45, no. 146, pp. 550–551, 1960.

[20] C. Sartori, D. S. Finch, B. Ralph, and K. Gilding, "Determination of the cation content of alginate thin films by FTi.r. spectroscopy," *Polymer*, vol. 38, no. 1, pp. 43–51, 1997.

[21] C.-Y. Yu, H. Wei, Q. Zhang, X.-Z. Zhang, S.-X. Cheng, and R.-X. Zhuo, "Effect of ions on the aggregation behavior of natural polymer alginate," *The journal of physical chemistry. B*, vol. 113, no. 45, pp. 14 839–14 843, 2009.

[22] A. Łetocha, M. Miastkowska, and E. Sikora, "Preparation and characteristics of alginate microparticles for food, pharmaceutical and cosmetic applications," *Polymers*, vol. 14, no. 18, 2022.

[23] E.-S. Chan, T.-K. Lim, W.-P. Voo, R. Pogaku, B. T. Tey, and Z. Zhang, "Effect of formulation of alginate beads on their mechanical behavior and stiffness," *Particuology*, vol. 9, no. 3, pp. 228–234, 2011.

[24] A. Blandino, M. Macías, and D. Cantero, "Formation of Calcium Alginate Gel Capsules: Influence of Sodium Alginate and $CaCl_2$ Concentration on Gelation Kinetics," *Journal of Bioscience and Bioengineering*, vol. 88, no. 6, pp. 686–689, 1999.

[25] P. Agulhon, M. Robitzer, L. David, and F. Quignard, "Structural regime identification in ionotropic alginate gels: influence of the cation nature and alginate structure," *Biomacromolecules*, vol. 13, no. 1, pp. 215–220, 2012.

[26] B. Tomadoni, M. F. Salcedo, A. Y. Mansilla, C. A. Casalongué, and V. A. Alvarez, "Macroporous alginate-based hydrogels to control soil substrate moisture: Effect on lettuce plants under drought stress," *European Polymer Journal*, vol. 137, p. 109953, 2020.

[27] R. Horga, F. Di Renzo, and F. Quignard, "Ionotropic alginate aerogels as precursors of dispersed oxide phases," *Applied Catalysis A: General*, vol. 325, no. 2, pp. 251–255, 2007.

[28] A. K. Katz, J. P. Glusker, S. A. Beebe, and C. W. Bock, "Calcium ion coordination: A comparison with that of beryllium, magnesium, and zinc," *Journal of the American Chemical Society*, vol. 118, no. 24, pp. 5752–5763, 1996.

[29] J. P. Chen, L. Hong, S. Wu, and L. Wang, "Elucidation of Interactions between Metal Ions and Ca Alginate-Based Ion-Exchange Resin by Spectroscopic Analysis and Modeling Simulation," *Langmuir*, vol. 18, no. 24, pp. 9413–9421, 2002.

[30] T. Dudev and C. Lim, "The effect of metal binding on the characteristic infrared band intensities of ligands of biological interest," *Journal of Molecular Structure*, vol. 1009, pp. 83–88, 2012.

[31] Y. Liu, J. Zhao, C. Zhang, H. Ji, and P. Zhu, "The flame retardancy, thermal properties, and degradation mechanism of zinc alginate films," *Journal of Macromolecular Science, Part B*, vol. 53, no. 6, pp. 1074–1089, 2014.

[32] X. Zhang, L. Wang, L. Weng, and B. Deng, "Strontium ion substituted alginate–based hydrogel fibers and its coordination binding model," *Journal of Applied Polymer Science*, vol. 137, no. 16, p. 48571, 2020.

[33] J. Coates, "Interpretation of infrared spectra, a practical approach," in *Encyclopedia of analytical chemistry*, R. A. Meyers, Ed.   Chichester: Wiley, 2000.

[34] N. S. Raut, P. R. Deshmukh, and M. J. Umekar, "Zinc cross-linked hydroxamated alginates for pulsed drug release," *International Journal of Pharmaceutical Investigation*, vol. 3, pp. 194–202, 2013.

[35] K. Nakamoto, *Theory and applications in inorganic chemistry*, 6th ed., ser. Infrared and Raman spectra of inorganic and coordination compounds.   Hoboken: Wiley, 2009, vol. / Kazuo Nakamoto ; Pt. A.

[36] P. Agulhon, V. Markova, M. Robitzer, F. Quignard, and T. Mineva, "Structure of alginate gels: interaction of diuronate units with divalent cations from density functional calculations," *Biomacromolecules*, vol. 13, no. 6, pp. 1899–1907, 2012.

[37] Q. Wang, L. Zhang, Y. Liu, G. Zhang, and P. Zhu, "Characterization and functional assessment of alginate fibers prepared by metal-calcium ion complex coagulation bath," *Carbohydrate polymers*, vol. 232, p. 115693, 2020.

[38] L. Fuks, D. Filipiuk, and M. Majdan, "Transition metal complexes with alginate biosorbent," *Journal of Molecular Structure*, vol. 792-793, pp. 104–109, 2006.

[39] M. Nara, H. Torii, and M. Tasumi, "Correlation between the Vibrational Frequencies of the Carboxylate Group and the Types of Its Coordination to a Metal Ion: An *ab initio* Molecular Orbital Study," *The Journal of Physical Chemistry*, vol. 100, no. 51, pp. 19 812–19 817, 1996.

[40] A. Craievich, *Small-Angle X-ray Scattering by Nanostructured Materials.* Springer International Publishing, 05 2016, pp. 1–46.

[41] N. Torasso, A. Vergara-Rubio, P. Rivas-Rojas, C. Huck-Iriart, A. Larrañaga, A. Fernández-Cirelli, S. Cerveny, and S. Goyanes, "Enhancing arsenic adsorption via excellent dispersion of iron oxide nanoparticles inside poly(vinyl alcohol) nanofibers," *Journal of Environmental Chemical Engineering*, vol. 9, no. 1, p. 104664, 2021.

[42] W. Klinkajon and P. Supaphol, "Novel copper (ii) alginate hydrogels and their potential for use as anti-bacterial wound dressings," *Biomedical materials (Bristol, England)*, vol. 9, no. 4, p. 045008, 2014.

Chapter 4

Analysis of preparation and characterization of BACs-loaded alginate beads

4.1   Introduction

Polyphenols are secondary metabolites synthesised by a wide variety of plants. They are phytochemicals - non-nutrient plant chemicals with inherent health benefits [1]. Hence, these biologically active compounds (BACs) are known to potentially reduce the risk of chronic diseases such as cardiovascular diseases, type II diabetes and cancers [2]. Polyphenols' synthesis is thought to have been acquired by plants during evolution in order to accommodate to the ecosystem [3]. They are often employed as a defence mechanism against biotic (phytoalexins and anti-feedants) and abiotic stress (protection against ultraviolet light and antioxidants), as well as an interaction mechanism [4, 5]. Not only does the variety and abundance of plant phenolics depend on the specie but also, in the land where it is grown, the season, the foliage conditions, the extraction process, and quantification and determination method [6].

The chemical structure of polyphenols contains unsaturated bonds (Figure 4.1) that make them susceptible to pH alterations, photolysis, enzymatic activity, temperature, water, oxidants and the presence of metal ions [2, 7]. They might be deteriorated as a consequence of their strong antioxidant potential. Despite the challenge to preserve their stability and bioavailability, the promising results for preventing diseases of polyphenols kept the interest for these compounds [2]. Hence, the stability of polyphenols should be preserved in order to maintain their structure and bioactivity. This should also be considered when assessing the evolution of polyphenols within a system.
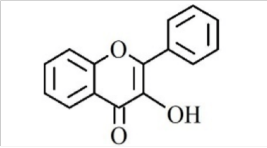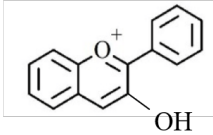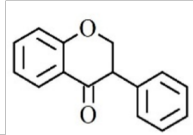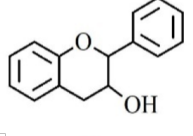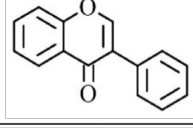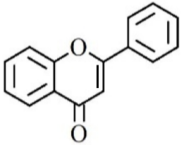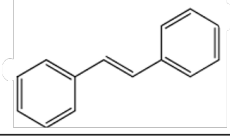
Compound group	General structural formula	Representatives
Flavonols		Quercetin
Anthocyanidins		Cyanidine
Isoflavonoids		Isoflavone, genistein
Flavanols		Catechin, epicatechin
Flavonones		Hesperetin, naringenin
Flavons		Apigenin
Stilbene		Resveratrol

Note: The leftmost column spans "Flavonoids" across the first six rows and "Stilbenoid" for the last row.

Figure 4.1: Structure of the main types of polyphenols

119

Encapsulation may provide a protective effect to the encapsulated agents. Incorporation of polyphenols into polymer matrices is an attractive approach to preserve their functionality. Encapsulation of polyphenols has already been proven to support their stability and bioavailability [2, 8]. It may improve the long term storage stability, prevent oxidation, decrease the reduction of volatile substances, simplify the manipulation, promote or avoid the union with other excipients, and regulate polyphenols content within a system [8]. Encapsulation of polyphenols has already been applied to cover their astringent and bitter taste [9]. In case of oral delivery systems, encapsulation may protect polyphenols from gastrointestinal fluid during digestion and preserve their bioactivity [9, 10]. Encapsulation might be an effective strategy for controlled release and targeted delivery, in order to increase full potential and beneficial health effects of these phytochemicals.

The development of new biomaterials incorporating polyphenols is growing at a steady pace. For instance, the review article written by Shavandi et al. [11] gathers the most novel applications of these systems, which have been employed as antibacterial coatings for bone replacement [12], as multifunctional hydrogels for sutureless wound closure [13], and as coordination nanomaterials for combination therapy in cancer treatment [14, 15]. Moreover, diverse delivery systems have been proved to enhance the bioavailability and anticancer efficiency of the encapsulated polyphenols [16].

Despite its advantages as encapsulating material [17, 18, 19, 20, 21, 22], Alg matrices have been scarcely applied for polyphenols' encapsulation. Among its remarkable benefits, including its biocompatibility and biodegradability, Alg ameliorates the stability of encapsulated polyphenols [23]. Some examples of previously encapsulated plant extracts and polyphenols within Alg (combined or alone) are:

- Curcumin encapsulated within: galactosylated Alg [24]; Fe_3O_4 nanoparticles with Alg–chitosan shell [25]; Fe_3O_4–Alg core with BSA-poly(3-acrylami do-propyl)trimethylammonium chloride shell (p(APTMACl)) [26]; and Alg and gum arabic [27].

- Quercetin-loaded Alg-chitosan nanoparticles [28].

- Green tea polyphenols in Alg-Poly(vinyl alcohol) (PVA) matrix [29].

- Limonin and nomilin (triterpenoids) in Alg-zein complexes [30].

- *Clitoria ternatea* petal flower extract [2].

- Thyme (*Thymus serpyllum*) aqueous extract [31].

- Pomegranate peel's (*Punica granatum*) polyphenol extract [32].

- Yerba mate (*Ilex paraguariensis*) extract [33].

- BRS Violet grape pomace extract [22].

- Extracts of medicinal herbs such as nettle (*Urtica dioica*), hawthorn (*Crategus laevigata*), raspberry leaf (*Rubus idaeus*), olive leaf (*Olea europea*), yarrow (*Achillea millefolium*) and ground ivy (*Glechoma hederacea*) in Alg–chitosan microbeads [34].

- Icariin [35] and chlorogenic acid [36] incorporated into chondrocytes-seeded Alg hydrogels.

- Catechin-loaded Alg-chitosan scaffolds with chondrocytes seeded [37].

Encapsulation of plant phenolics and extracts within Alg-based beads proved to successfully improve their light and thermal stability and slowed the degradation rate [2, 22]. The stability of BACs during processing and storage and their bioavailability were also enhanced [2, 8, 9, 28, 38].

In the present chapter the attempts of Vitaflavan encapsulation are reported. Vitaflavan is a branded grape seed phenolic extract derived from red grapes, which is known for their antioxidant properties [39]. It is employed as a dietary supplement or nutraceutical, due to the potential health-promoting effects of the BACs comprised on its formula. Previous studies suggested that BACs may protect the human organism from oxidative stress, prevent hypertension, diminish systemic inflammation and improve cardiovascular capacity [40].

First, the preparation methodology of BACs-loaded Alg microbeads was optimized. Secondly, the resulting beads were characterized in terms of morphology though optical microscopy and ESEM. Analysis were also performed to determine the encapsulation efficiency by Folin-Ciocalteu (FC) assay, HPLC and TGA, as well as to establish the release profile of the encapsulated compounds in water by MALDI-TOF. Additionally, the BACs formula was characterized and the stability of polyphenols within the encapsulating system was assessed in order to preserve their structure and bioactivity during and after encapsulation.

4.2   Results

4.2.1   Study of the encapsulating agent

4.2.1.1   Characterization of BACs formula

The powerful antioxidant activity of Vitaflavan is supported by its formulation, which comprises several BACs. The total phenolic content in the grape seed extract was determined following the FC colorimetric assay though the calibration curve based on gallic acid (GA) dissolved in MilliQ water (Chapter 2, eq. 6). The total phenolic content was $62.81 \pm 3.62\%$ of the total extract weight.

The polyphenolic constituents of Vitaflavan were already characterized by Sánchez-Patán et al. [41]. Their findings revealed that flavan-3-ols were the main components, including the non-galloylated monomers (+)-catechin and (-)-epicatechin (42.2%), (-)-epigallocatechin gallate (7.8%), non-galloylated dimeric procyanidins B1, B2, B3, B4 (42.1%), galloylated dimeric procyanidins B2-3-O-gallate and B2-3'-O-gallate (1.0%), and trimeric procyanidins C1 and T2 (4.1%). In addition, non-flavonoid compounds such as GA, represented 2.7% of total quantified phenolic compounds.

The formula of the employed grape seed phenolic extract was characterized by MALDI-TOF mass spectrometry (MS). The obtained MS spectra is displayed in Figure 4.2 and the identified compounds are reported in Table 4.1. The characterization of Vitaflavan performed by Esteban-Fernández et al. also served as a reference for the investigations conducted in this chapter [42].

Table 4.1: Compounds and corresponding peaks of the MS spectra of BACs aqueous solution identified by the database Phenol-Explorer 3.0

Compound	Peak (m/z)
4-Ethylphenol	122.55
Salicylic acid monohydrate	156.98
4-amino-2-phenylphenol	185.53
Caffeic acid monohydrate	198.01
Acetyl eugenol	206.05
-	226.56
Catechin and/or epicatechin	291.08
Gallic acid 4-O-glucoside, carnosic acid and/or galloyl glucose	332.06
Hydrated form of previous ones	350.08
Procyanidin B1, B2, B3 and/or B4	579.14
Procyanidin B2-3'-O-gallate and/or B2-3'-O-gallate	730.15
Procyanidin C1 or T2	866.20

Considering the list provided by Esteban-Fernández et al., it is observed that some compounds are not detected in our sample, namely epicatechin-3-O-gallate and p-coumaric acid. However, additional compounds are identified in the extract that we employ such as acetyl eugenol, gallic acid 4-O-glucoside, carnosic acid and/or galloyl glucose (Table 4.1). Moreover, several abundant peaks are detected during the analysis that are not present in the database exported from Phenol-Explorer 3.0. These peaks are identified at m/z values of 122.55, 156.98, 185.53, 198.01, 226.56 and 350.08 (Figure 4.2). A comparison with literature data suggests the attribution of these peaks to: 4-Ethylphenol (122.55), salicylic acid monohydrate (156.98), 4-amino-2-phenylphenol (185.53), caffeic acid monohydrate (198), while the peak at 226 could not be identified. However, it must be mentioned that the detected signals could correspond to the combination of the different compounds with diverse number of water molecules, together with Na^+, Ca^{2+}, K^+ or NH_4^+ cations present in the matrix, making the unequivocal attribution a hard task. For the same consideration, the identification of m/z values exceeding 350 was challenging as they were presumed to correspond to complex compositions of BACs along with the aforementioned cations and water molecules.
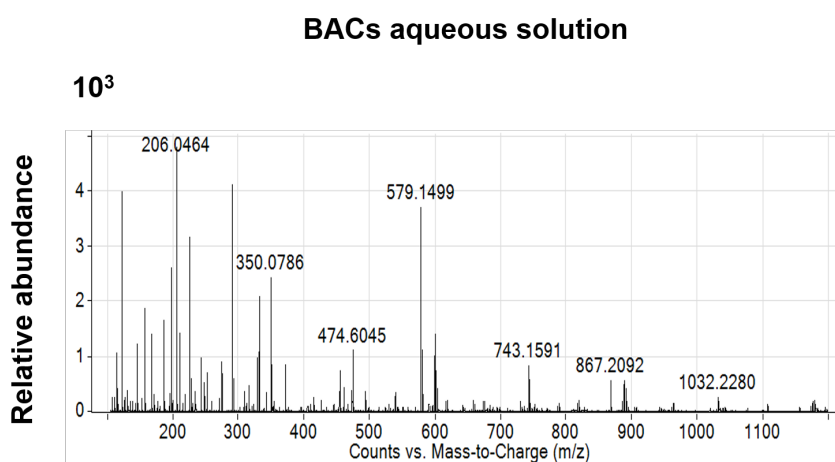
Figure 4.2: Characterization of BACs stability in the crosslinking bath - Effect of light and atmosphere

4.2.1.2   Assessment of BACs stability under encapsulating conditions

The stability and antioxidant capacity of BACs are supposed to depend on diverse factors such as temperature, light, storage conditions and pH (if dissolved). BACs comprised in the phenolic extract are likely to be unstable. Hence, the effect of light and atmosphere on BACs' stability was analysed. Namely, the UV/Vis spectra of an aqueous solution of BACs was recorded after 48 h under inert atmosphere of argon (Ar) or under open atmosphere in dark and unprotected from light. Spectra are shown in Figure 4.3.

It can be observed that the spectra variance between samples kept in open atmosphere is likely not significant enough (Figure 4.3b). It suggests that BACs stability is not conditioned by neither the inert atmosphere nor by the light exposure. Therefore, samples are expected to be stable in aqueous solution under the crosslinking bath conditions.
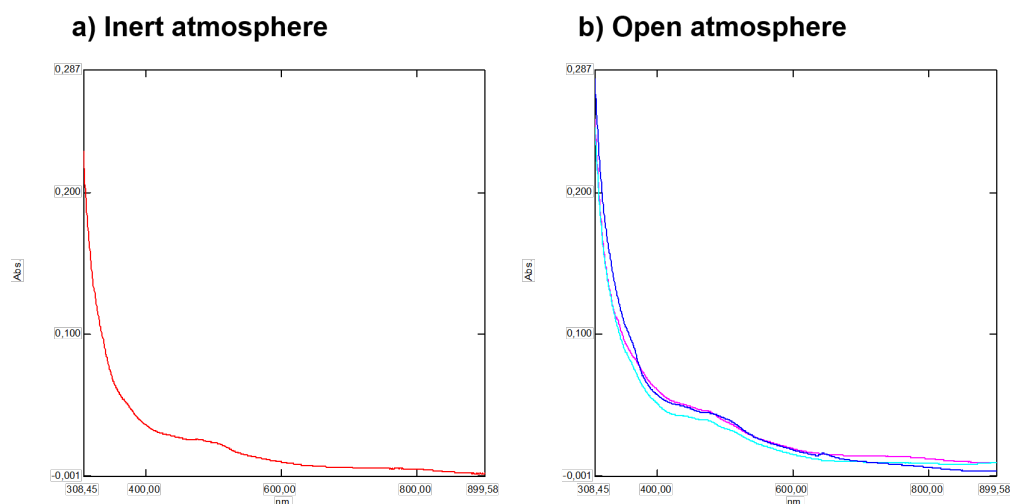
Figure 4.3: Absorption spectra of BACs aqueous solutions after 48h under a) inert atmosphere of Ar (red) and b) under open atmosphere in dark (blue) and unprotected from light (pink)

In fact, previous studies pointed the presence of co-pigments to inhibit the effects of UV degradation and stabilize the polyphenols in plant extracts [5]. Co-pigmentation is the association of components that contribute with each other by means of Van der Waals forces and hydrophobic interactions. For instance, Pedro et al. proved that co-pigmentation protects anthocyanins from nucleophilic attack of water molecules [43]. In this experiment diverse co-pigments, including glucose, phytic and GA, were added to a black rice extract (*Oryza sativa*) exposed to light. Among

124

them, GA provided the greatest increment of anthocyanins' half-life time. This observation suggests that certain co-pigments, which can be present in the plant extract, may play a crucial role in inhibiting the effects of UV degradation and effectively stabilize the polyphenols [5].

4.2.2 Encapsulation of BACs

4.2.2.1 Assessment of different preparation methods for BACs 10% polymeric solution

The preparation of BACs 10% polymeric solution was optimized in order to achieve the highest BACs encapsulation efficiency. Three different methodologies were assessed:

- Sample P0 = Not dissolved Alg (1.7 g Alg in 70 g of water) + 0.17 g of BACs dissolved in 28 g of water. Final mass adjusted to 100 g

- Sample P1 = Dissolved Alg (1.7 g Alg + 80 g of water + 20 min under agitation) + 0.17 g of BACs dissolved in 10 g of water. Final mass adjusted to 100 g

- Sample P2 = Not dissolved Alg (1.7 g) + BACs (0.17 g) + water up to 100 g

BACs 10% beads were prepared following the methodology previously described in Chapter 2, Section 2.2.2. utilizing a crosslinking bath of $CaCl_2$ 2% (w/w). The corresponding samples are shown in Figure 4.4. The formation of aggregates in the crosslinking bath is revealed in sample P2 due to the poor BACs dissolution in the polymeric solution, while no evident differences are observed between samples P0 and P1. Nevertheless, the following polymeric solutions containing BACs are prepared according to P1 procedure in order to assure homogeneity.

Sample

| P0 | P1 | P2 |
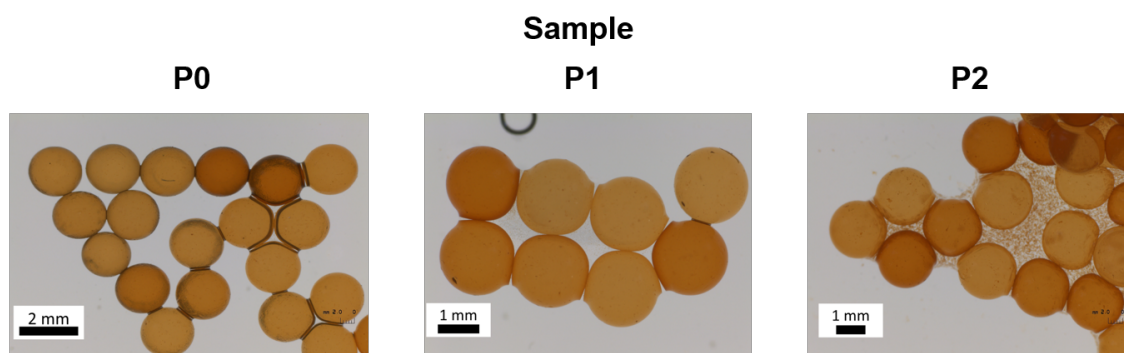
Figure 4.4: Loupe images of wet BACs 10% beads prepared with $CaCl_2$ 2% (w/w) and three polymeric solutions prepared with different methodologies P0, P1 and P2

4.2.2.2   Morphological characterization of BACs-loaded beads

As a first attempt, we tried to encapsulate BACs in Alg using Ca^{2+} as crosslinker, which has been widely reported and therefore, it could be considered as a reference. Moreover, we also tried to introduce Cu^{2+} as crosslinker, though its use in polyphenols encapsulation has been unadvised. For instance, Da Silva et al. suggested to avoid Cu ions in biomaterials intended for the encapsulation of polyphenols as it might be incompatible with some of these compounds even at low concentrations [44]. The interactions between Cu^{2+} and polyphenols (in the presence of bicinchoninic acid in a buffered medium pH 7) has been demonstrated to lead to Cu^{2+} reduction to Cu^+. Nevertheless, since we were interested also in agricultural applications, where Cu^{2+} has been widely used as a fertilizer and for the treatment of plant diseases, the use of Cu-based beads was also considered. Eventually, we produced Zn-based beads due to its novelty and potential applications in Biomedicine, personal care products and as an alternative to Cu-based beads in Agriculture.

The mean size of empty dry Alg beads was 0.54 ± 0.07 mm, 0.47 ± 0.07 mm and 0.54 ± 0.03 mm, when prepared with $CaCl_2$, $CuCl_2$ and $ZnCl_2$ 2% (w/w), respectively (Chapter 3, Section 3.2.5). On the other hand, BACs 10% dry beads exhibited sizes of 0.62 ± 0.04 mm, 0.78 ± 0.1 mm and 0.74 ± 0.05 mm when prepared with $CaCl_2$, $CuCl_2$ and $ZnCl_2$ 2% (w/w), respectively. These results suggest that the BACs loading process affects the size of beads, as reasonably expected. Figure 4.5 illustrates the structure of BACs 10% dry beads prepared with $CaCl_2$, $CuCl_2$ and $ZnCl_2$ 2% (w/w).

126

Ca-based BACs 10% beads are globular and display a homogeneous surface (Figure 4.5a). Flat and highly irregular beads with a rougher surface are observed when Cu^{2+} is employed as cross-linking agent (Figure 4.5b). The beads' surface is even rougher when Zn^{2+} is utilized as cross-linking cation (Figure 4.5c). These findings align with the ESEM pictures corresponding to empty Ca-, Cu- and Zn-beads. However, a core-shell structure could not be evidenced in any case. EDX observations revealed a homogeneous distribution of the cations within the beads.

a) Ca-BACs 10% beads
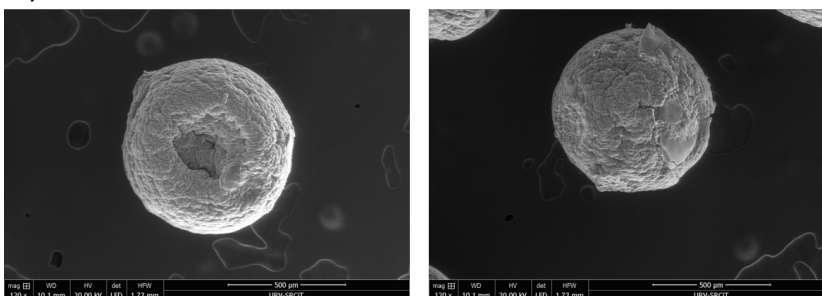
b) Cu-BACs 10% beads
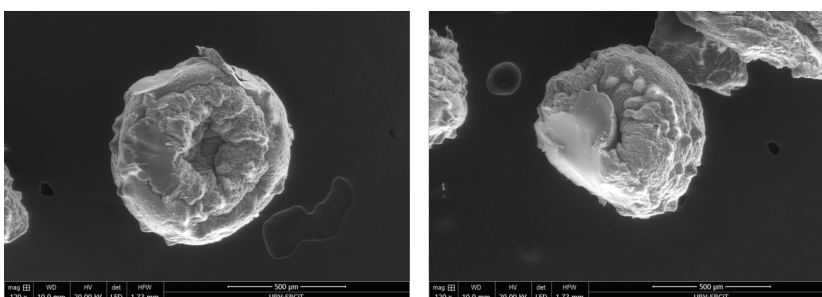
c) Zn-BACs 10% beads
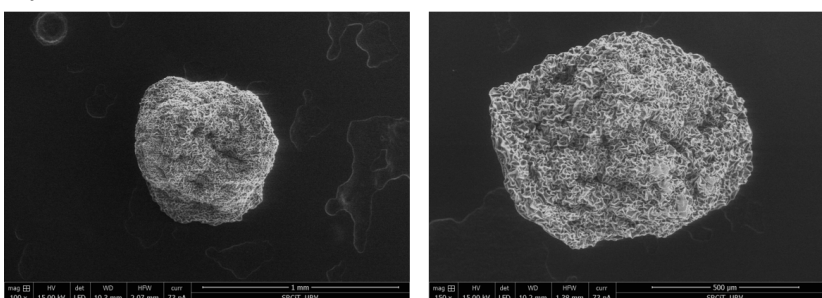
Figure 4.5: ESEM images of dry BACs 10% beads prepared with a) $CaCl_2$, b) $CuCl_2$ and b) $ZnCl_2$ 2% (w/w)

4.2.3   Determination of encapsulation efficiency

The determination of the quantity of BACs loaded within the beads is referred to as encapsulation efficiency (EE). This parameter provides information about the amount of BACs entrapped within the beads, thereby reflecting the efficiency of the preparation method. In this section, we tried to define a methodology to assess the EE by diverse techniques, testing various polymeric solutions and concentrations of BACs, crosslinking agents and concentrations of cations.

4.2.3.1   Analysis of encapsulation efficiency by FC colorimetric assay

When FC reagent is employed to measure the concentration of polyphenols in a sample, absorbance at 765 nm (Abs765) is recorded after following the FC colorimetric assay (Chapter 2, Section 2.2.7). In order to correlate the Abs765 to the polyphenol concentration, a calibration curve based on GA is established. Therefore, in order to test qualitatively whether the investigated metal chlorides (MCl_2) have an effect on the calibration curve, a stock solution of the calibration standard was dissolved in MilliQ water and further diluted in aqueous solutions of: $CuCl_2$, $CaCl_2$ and $ZnCl_2$ 0.5% and 10% (w/w). Then, the absorption spectra were recorded and are displayed in Figure 4.6.
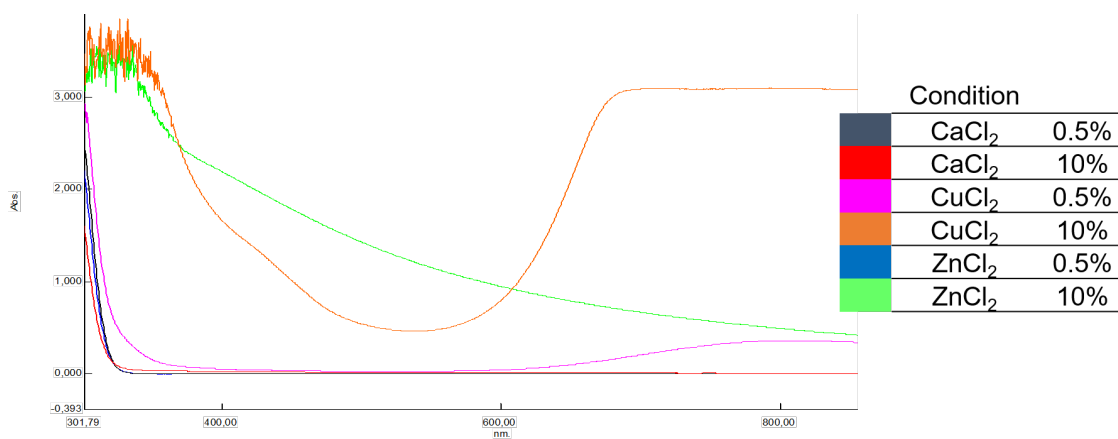
Figure 4.6: Absorption spectra of GA dissolved in aqueous solutions of MCl_2 0.5% and 10% (w/w)

Figure 4.6 evidences that $CaCl_2$ solution does not alter GA absorption spectra regardless of the concentration. Nonetheless, GA spectra is modified by both $CuCl_2$ 0.5% and 10% (w/w). Evidently, higher $CuCl_2$ concentrations have greater effects. GA spectra is altered only by 10% (w/w) $ZnCl_2$ concentration. Indeed, when 10% (w/w) $ZnCl_2$ was added to the GA stock solution, the sample became turbid. Actually, it has been reported that complexes can be formed by polyphenols in the presence of divalent cations [44]. Indeed, Figure 4.7 evidences the formation of complexes when BACs are added to an aqueous solution of $CaCl_2$ and $CuCl_2$ 10% (w/w). The formation of chelates between GA and divalent cations could be responsible for the alterations in GA absorption spectra.
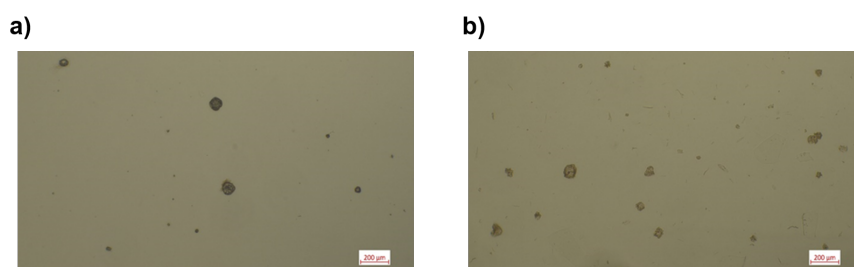
Figure 4.7: Micrographies of BACs in a) $CaCl_2$ and b) $CuCl_2$ aqueous solution
.

As a further proof, we investigated the spectra of BACs aqueous solutions in the presence of $CuCl_2$. They are displayed in Figure 4.8. It can be observed that BACs are affected by the amount of $CuCl_2$. The higher the $CuCl_2$ concentration, the greater the increase of absorbance values between 550 and 1100 nm.
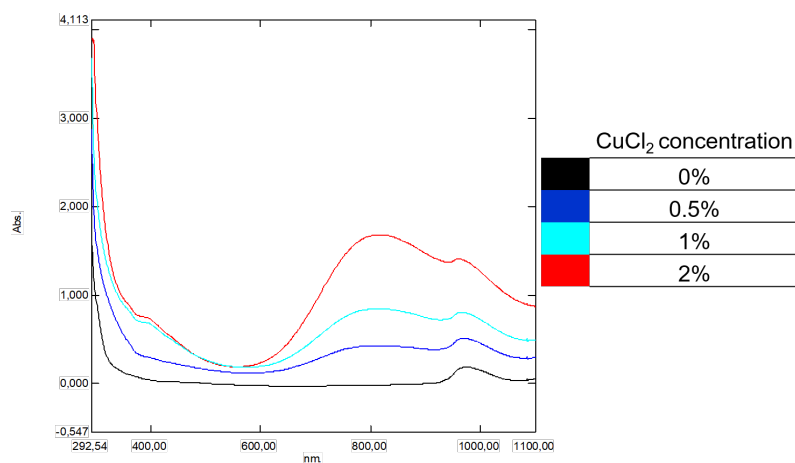
Figure 4.8: Effect of $CuCl_2$ concentration on the absorbance spectra of BACs' aqueous solution

In addition, for the following experiment we tried to quantify the effect of the MCl_2 presence on the BACs determination by FC method. For this, a stock solution of BACs was dissolved in MilliQ water at a concentration of 1.7 mg/mL and further diluted in MilliQ water or aqueous $CaCl_2$ solutions to a concentration of 0.085 mg/mL. After the FC colorimetric assay, the Abs765 was recorded and BACs concentration was calculated according to diverse calibration curves of GA diluted in MilliQ water (eq. 4.1), $CaCl_2$ 0.5% (eq. 4.2) or 10% (w/w) (eq. 4.3). The obtained results are displayed in Table 4.2.

$$Abs765 = 2.40 \cdot GA\%(w/w) - 0.028 \quad R^2 = 0.99 \tag{4.1}$$

$$Abs765 = 2.29 \cdot GA\%(w/w) + 0.068 \quad R^2 = 0.99 \tag{4.2}$$

$$Abs765 = 26.25 \cdot GA\%(w/w) - 0.058 \quad R^2 = 0.99 \tag{4.3}$$

Table 4.2: Abs765 values of BACs in MiliQ water or $CaCl_2$ 2% (w/w) aqueous solution and BACs concentration (expressed as mg GA equivalent/mL) determined though different calibration curves of GA diluted in: MilliQ water, $CaCl_2$ 0.5% (w/w) or $CaCl_2$ 10% (w/w)

		Pattern curve employed		
		MilliQ	$CaCl_2$ 0.5% (w/w)	$CaCl_2$ 10% (w/w)
Sample	**Abs 765**	**BACs concentration (mg GA eq./mL)**		
BACs in MilliQ	0.245	0.087	0.077	0.012
BACs in $CaCl_2$ 2% (w/w)	0.31	0.114	0.105	0.014

Abs765 is greater when BACs are diluted in $CaCl_2$ 2% (w/w) compared to MilliQ water (Table 4.2.3.1). In addition, BACs concentration calculated with the pattern curve based on GA in MilliQ water is greater compared to BACs concentration when diluted in $CaCl_2$ 0.5% (w/w) (eq. 4.2). The concentration difference concerning the employed calibration curve is remarkably different when $CaCl_2$ 10% (w/w) calibration curve is employed (eq. 4.3). These findings evidence the Ca^{2+} interference with FC reagent at high $CaCl_2$ concentrations.

Therefore, the quantification of BACs through the FC method, was not appropriate in this case due to the presence of high amounts of cations in the crosslinking bath.

4.2.3.2   Analysis of encapsulation efficiency by HPLC

Given the difficulties to find a reliable method to quantify the EE of BACs, we attempted to evaluate the EE through HPLC. Thus, as a model, a simplified system wherein the polymeric solution consisted of 50% GA was studied instead of the complex mixture of BACs. Beads were prepared utilizing $CaCl_2$ and $ZnCl_2$ at concentrations of 0.5% and 10% (w/w). Samples were collected from the residual crosslinking baths after the determined maturation time. A calibration curve was established for GA diluted in MilliQ water (eq. 4.4).

$$HPLC\ signal/a.u.\ at\ 270\ nm\ = 28.83\ GA\ (ppm) - 131.74 \qquad (4.4)$$

For sake of comparison, EE values were also calculated for the same samples by the FC method. The EE values of both FC and HPLC assays are displayed in Table 4.3.

Table 4.3: Encapsulation efficiency (EE) determined by FC assay and HPLC of GA50% beads prepared with $CaCl_2$ and $ZnCl_2$ at a concentration of 0.5% and 10% (w/w)

	EE (%)	
	FC assay	HPLC
$CaCl_2$ 0.5% (w/w)	5.23	2.19
$CaCl_2$ 10% (w/w)	96.01	2.82
$ZnCl_2$ 0.5% (w/w)	90.99	0.25
$ZnCl_2$ 10% (w/w)	92.66	71.31

In case of FC methodology, GA concentration and corresponding EE were calculated using the standard curves of GA dissolved in $CaCl_2$ 0.5% (w/w) (eq. 4.2), $CaCl_2$ 10% (w/w) (eq. 4.3), $ZnCl_2$ 0.5% (w/w) (eq. 4.5) and $ZnCl_2$ 10% (w/w) (eq. 4.6), respectively.

$$Abs765 = 24.19 \cdot GA\%(w/w) + 0.068 \quad R^2 = 0.99 \qquad (4.5)$$

$$Abs765 = 22.56 \cdot GA\%(w/w) + 0.095 \quad R^2 = 0.99 \qquad (4.6)$$

Based on the results in Table 4.3, it is observed that the EE defined by HPLC is lower compared to the FC assay, especially when $CaCl_2$ 10% and $ZnCl_2$ 0.5% (w/w) are employed as crosslinkers. One possible explanation for this disparity is the potential amplification of the FC reagent signal in presence of high concentrations of $CaCl_2$ and $ZnCl_2$, as previously seen (Figure 4.8). Nevertheless, $ZnCl_2$ 0.5% (w/w) was not pointed to alter GA absorption spectra. Alternatively, it is plausible that the HPLC signal of GA may have been diminished by these cations.

To investigate these hypotheses, samples of GA dissolved in MilliQ water, $CaCl_2$ and $ZnCl_2$ 10% (w/w) are further analysed by HPLC (Figure 4.9). The retention time of GA is constant regardless of the sample. The results reveal that the identification of GA is not influenced by the presence of $CaCl_2$ 10% (w/w), while the GA signal is diminished by the presence of $ZnCl_2$ 10% (w/w).
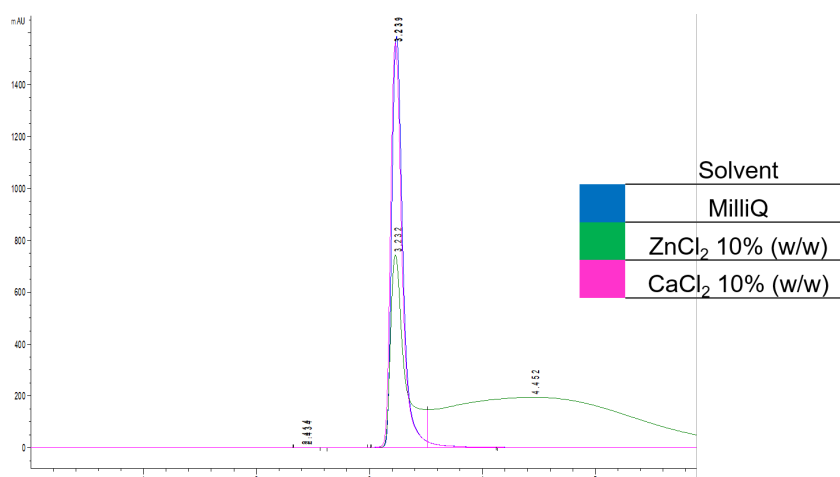
Figure 4.9: HPLC spectrum of a sample of GA dissolved in MilliQ water, $CaCl_2$ or $ZnCl_2$ 10% (w/w)

Therefore, in the case of $ZnCl_2$, not only is the GA signal diminished in HPLC analyses but the FC reagent signal is also increased, as illustrated in Figure 4.6. The reduction in GA signal could potentially be attributed to the formation of chelates, which are evidenced by the broad peak observed in the green spectra at a retention time of 4.45 minutes (Figure 4.9).

In the case of $CaCl_2$ 10% (w/w), the results obtained by HPLC are inconclusive, as GA encapsulation seemed to be ineffective whereas the FC method indicates an EE value of 96%. Therefore, neither HPLC quantification seemed to be adequate to estimate the EE.

4.2.3.3   Analysis of encapsulation efficiency by TGA

As previously mentioned, the EE measures the quantity of the BACs entrapped within the beads and thus, describes the efficiency of the preparation method and crosslinking cation. In this study, three crosslinkers, namely Ca^{2+}, Cu^{2+} and Zn^{2+}, are utilized at diverse concentrations. However, calculating the EE of BACs when Cu^{2+} is employed as the crosslinking cation presents challenges using the FC assay due to Cu^{2+} reduction and BACs complexation. Similarly, either FC nor HPLC methodology provided with conclusive EE values for Ca- and Zn-based systems. To address this, we attempted to estimate the EE by means of TGA in oxidizing atmosphere (air). Initially, we approximated the EE by analysing TGA data of BACs-loaded beads prepared with $CaCl_2$ 2% (w/w). Therefore, the first step involves the determination of the quantity of Ca^{2+} (mol) in 100 g of BACs-loaded beads based on the residue at 800°C and eq. 4.7:

$$Ca^{2+}(mol) = \frac{\text{Residue (g)} \cdot \text{Mw } Ca^{2+}(g/mol)}{\text{Mw CaO (g/mol)}} \qquad (4.7)$$

, where Ca^{2+} is the metal load in mol of 100 g of BACs-loaded beads, Mw Ca^{2+} is its molar mass, which is 40.08 g/mol, and Mw Ca^{2+} oxide is the molar mass of CaO, which is 56.07 g/mol.

The composition of the residue after TGA in air is determined as CaO by wide angle X-ray diffraction (WAXS) (Data not shown). In second place, the calculation of the mass of Alg (eq. 4.8) is derived from the determined quantity of Ca^{2+} mol (n_{Ca}), assuming the same coordination number ($n_{U/Ca}$) previously calculated for empty Ca-beads (Chapter 3, Section 3.2.6), according to:

$$Alg(g) \; in \; 100 \; g \; of \; BACs - loaded \; beads = (n_{Ca} \cdot n_{U/Ca}) \cdot Mw_u \qquad (4.8)$$

, where Mw_u is the molar mass of uronate residues, which is 176 g/mol. As a result:

$$BACs(g) \; in \; 100 \; g \; of \; BACs-loaded\, beads = 100 \; g \; -W_m- \; Alg(g) - Ca^{2+}(g) \quad (4.9)$$

, where W_m corresponds to water mass; the weight loss until 170°C in grams.

In last place, considering the mass of polymeric solution extruded prior to taking the respective samples, which consists of Alg and BACs at a specific percentage relative to Alg (theoretical BACs), EE could be defined as follows:

$$EE = \frac{\text{BACs (g) based on TGA data}}{\text{Theoretical BACs (g)}} \qquad (4.10)$$

133

Thermal degradation curves for BACs-loaded Ca-beads prepared with diverse polymeric solutions are displayed in Figure 4.10. Hence, they were analysed and the obtained values of EE are also displayed.

However, the quantification of Alg percentage within Ca-beads yielded values that progressively decreased with increasing BACs content, reaching even negative values, which suggests a potential overestimation of Alg content, likely due to the calculation being based on Ca^{2+} mol. In other words, the detected Ca content from the residue at 800°C is not only involved in the complexation with Alg, but also with BACs. The chelation of Ca^{2+}, as well as of the other divalent cations, represents a limitation that interferes with the determination of the EE using TGA.
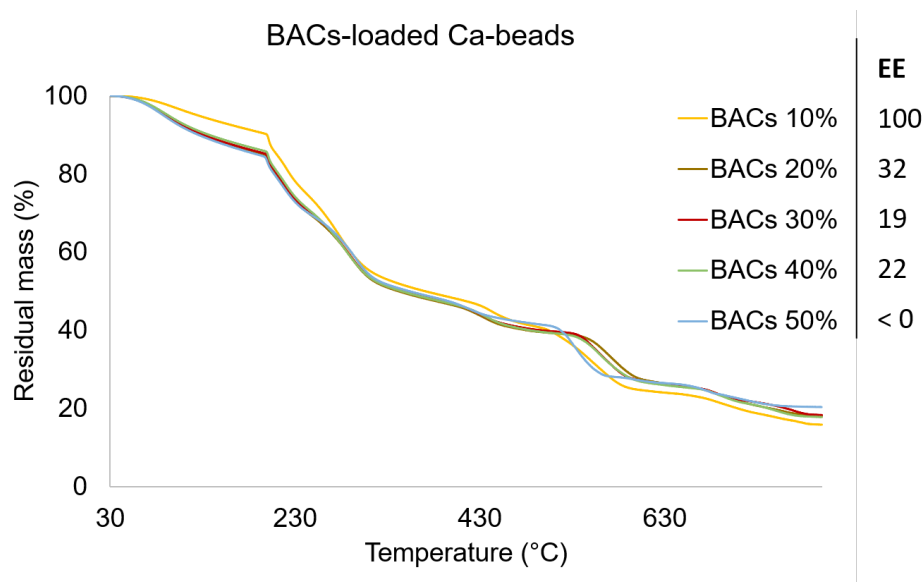
Figure 4.10: TG curves under air flow of 50 mL/min and a heating rate of 10°C/min, of BACs-loaded Alg beads prepared with $CaCl_2$ 2% (w/w) and polymeric solutions BACs 10%, 20%, 30%, 40% and 50% and resulting EE values

4.2.4 Release studies

Although we could not determine the EE of BACs, we considered relevant to assess, at least qualitatively, their release in water. Therefore, we investigated the delivery behavior of diverse BACs-loaded beads - BACs 10%, BACs 20% and BACs 30% beads, through MALDI-TOF MS. Hence, beads were immersed in MilliQ water and, after 24h, a sample was taken and directly injected into the MALDI-TOF. The obtained peaks were qualitatively compared with the ones present in the original BACs extract. Results are shown in Table 4.4. Nevertheless, one should remember that the

134

BACs entrapped fraction does not necessarily comprise all the compounds originally contained in the extract.

Table 4.4: Peaks obtained from the MS spectra of BACs extract and BACs 10%, BACs 20% and BACs 30% beads after 24h in MilliQ water; and the corresponding assignments. N.A. depicts not assigned peaks

Peak (m/z)	Assigned compound	Extract	BACs 10%	BACs 20%	BACs 30%
115.96	N.A.		X	X	X
122.55	4-Ethylphenol and/or 4-hydroxybenzaldehyde and/or benzoic acid	X	X	X	X
143.06	N.A.		X		
156.99	Salicylic acid monohydrate and/or 1,4-Naphtoquinone	X	X	X	X
185.53	N.A.	X			
197.00	Gallic acid ethyl ester and/or	X	X	X	X
198.01	syringic acid and/or caffeic acid monohydrate		X		
200.01	N.A.		X	X	X
206.05	Acetyl eugenol	X			
216.02	Bergapten and/or xanthotoxin		X		
226.56	N.A.	X			
266.89	N.A.			X	
268.88	Formononetin and/or coumestrol			X	X
291.08	Catechin and/ or epicatechin	X	X		
307.91	N.A.			X	X
332.06	Gallic acid 4-O-glucoside, carnosic acid and/or galloyl glucose	X			
730.15	Procyanidin B2-3'-O-gallate and/or B2-3'-O-gallate	X			

In any case, it is evident that primarily smaller molecules, which are probably less prone to complexation and are expected to diffuse easier, are the ones being delivered (Figure 4.4). The hindered release of BACs, which remain confined within the Alg matrix, is likely attributed to their complexation. Consequently, the release of BACs after 24h in MilliQ water is limited. Further investigations should be performed, for instance, at different pH, to determine whether complex stability can be reduced and/or diffusion through Alg can increase so that release can be enhanced.

4.3   Conclusions

- The stability of BACs was evaluated under different conditions, including the exposure to an inert atmosphere and light. Neither the presence of an inert atmosphere nor light exposure demonstrated a significant impact on the stability of BACs.

- The HPLC method employed to determine the encapsulation efficiency (EE) of BACs demonstrated inconsistency. It revealed the formation of chelates between GA and $ZnCl_2$ at a concentration of 10% (w/w).

- Calculations based on thermogravimetric analysis (TGA) data for determining the EE led to an overestimation of the alginate (Alg) content. This overestimation was attributed to the excess of cations that did not interact with the polymer chains. Consequently, accurate calculation of the EE was not achievable.

- It is crucial to invest additional efforts in finding alternatives to accurately quantify the amount of BACs entrapped within Alg beads, considering their complexation with Ca^{2+}, Cu^{2+} and Zn^{2+} cations in the crosslinking bath. Furthermore, investigating how BACs' complexation affects their encapsulation, whether it enhances or inhibits it, would be of significant interest.

- Release assays aimed to examine the behavior of BACs-loaded Ca-beads and the release tendencies of BACs. MS primarily identified small molecules. Peaks with m/z values greater than 350 were challenging to identify and were presumed to correspond to complex compositions of various BACs with water molecules, along with Na^+, Ca^{2+}, K^+ or NH_4^+ cations. As a result, the release of BACs was impeded and only small molecules, which have lower tendencies to form complexes and are easier to be released from the Alg matrix, were detected.

- Summing up, due to the complexation of BACs with cations, Alg may not be the ideal material for their encapsulation as the presence of crosslinking cations is necessary for the production of Alg beads.

Bibliography

[1] M. K. Singh, S. K. Singh, A. Kumar, B. A. Kehinde, I. Majid, and V. Nanda, *Functional and preservative properties of phytochemicals*, B. Prakash, Ed. Academic Press, 2020.

[2] P. Pasukamonset, O. Kwon, and S. Adisakwattana, "Alginate-based encapsulation of polyphenols from *Clitoria ternatea* petal flower extract enhances stability and biological activity under simulated gastrointestinal conditions," *Food Hydrocolloids*, vol. 61, pp. 772–779, 2016.

[3] B. R. Lichman, G. T. Godden, and C. R. Buell, "Gene and genome duplications in the evolution of chemodiversity: perspectives from studies of lamiaceae," *Current opinion in plant biology*, vol. 55, pp. 74–83, 2020.

[4] A. Sugiyama, "Flavonoids and saponins in plant rhizospheres: roles, dynamics, and the potential for agriculture," *Bioscience, biotechnology, and biochemistry*, vol. 85, no. 9, pp. 1919–1931, 2021.

[5] I. Volf, I. Ignat, M. Neamtu, and V. Popa, "Thermal stability, antioxidant activity, and photo-oxidation of natural polyphenols," *Chemical Papers*, vol. 68, no. 1, 2014.

[6] D. C. Marino, L. Z. L. Sabino, J. Armando, A. D. A. Ruggiero, and H. D. Moya, "Analysis of the polyphenols content in medicinal plants based on the reduction of Cu(II)/bicinchoninic complexes," *Journal of agricultural and food chemistry*, vol. 57, no. 23, pp. 11 061–11 066, 2009.

[7] M. V. Galmarini, C. Maury, E. Mehinagic, V. Sanchez, R. I. Baeza, S. Mignot, M. C. Zamora, and J. Chirife, "Stability of individual phenolic compounds and antioxidant activity during storage of a red wine powder," *Food and Bioprocess Technology*, vol. 6, no. 12, pp. 3585–3595, 2013.

[8] D. F. Rocha-Parra, M. C. Lanari, M. C. Zamora, and J. Chirife, "Influence of storage conditions on phenolic compounds stability, antioxidant capacity and colour of freeze-dried encapsulated red wine," *LWT*, vol. 70, pp. 162–170, 2016.

[9] V. Nedovic, A. Kalusevic, V. Manojlovic, S. Levic, and B. Bugarski, "An overview of encapsulation technologies for food applications," *Procedia Food Science*, vol. 1, pp. 1806–1815, 2011.

[10] A. Munin and F. Edwards-Lévy, "Encapsulation of natural polyphenolic compounds: A review," *Pharmaceutics*, vol. 3, no. 4, pp. 793–829, 2011.

[11] A. Shavandi, A. E.-D. A. Bekhit, P. Saeedi, Z. Izadifar, A. A. Bekhit, and A. Khademhosseini, "Polyphenol uses in biomaterials engineering," *Biomaterials*, vol. 167, pp. 91–106, 2018.

[12] A. Sayed Abdelgeliel, S. Ferraris, A. Cochis, S. Vitalini, M. Iriti, H. Mohammed, A. Kumar, M. Cazzola, W. M. Salem, E. Verné, S. Spriano, and L. Rimondini, "Surface Functionalization of Bioactive Glasses with Polyphenols from *Padina pavonica* Algae and *in situ* Reduction of Silver Ions: Physico-Chemical Characterization and Biological Response," *Coatings*, vol. 9, no. 6, p. 394, 2019.

[13] X. Du, Le, Wu, H. Yan, L. Qu, L. Wang, X. Wang, S. Ren, D. Kong, and L. Wang, "Multifunctional hydrogel patch with toughness, tissue adhesiveness, and antibacterial activity for sutureless wound closure," *ACS biomaterials science engineering*, vol. 5, no. 5, pp. 2610–2620, 2019.

[14] L. Shan, G. Gao, W. Wang, W. Tang, Z. Wang, Z. Yang, W. Fan, G. Zhu, K. Zhai, O. Jacobson, Y. Dai, and X. Chen, "Self-assembled green tea polyphenol-based coordination nanomaterials to improve chemotherapy efficacy by inhibition of carbonyl reductase 1," *Biomaterials*, vol. 210, pp. 62–69, 2019.

[15] J. Wang, W. Sang, Z. Yang, Z. Shen, Z. Wang, O. Jacobson, Y. Chen, Y. Wang, M. Shao, G. Niu, Y. Dai, and X. Chen, "Polyphenol-based nanoplatform for MRI/PET dual-modality imaging guided effective combination chemotherapy," *Journal of materials chemistry. B*, vol. 7, no. 37, pp. 5688–5694, 2019.

[16] R. Lagoa, J. Silva, J. R. Rodrigues, and A. Bishayee, "Advances in phytochemical delivery systems for improved anticancer activity," *Biotechnology advances*, vol. 38, p. 107382, 2020.

[17] Kuen Yong Lee and David J. Mooney, "Alginate: Properties and biomedical applications," *Progress in polymer science*, vol. 37, no. 1, pp. 106–126, 2012.

[18] B. Tylkowski and R. Jastrzab, "4. Smart Capsules for Lead Removal from Industrial Wastewater," pp. 61–78, apr 2017.

[19] S. H. Ching, N. Bansal, and B. Bhandari, "Alginate gel particles: A review of production techniques and physical properties," *Critical reviews in food science and nutrition*, vol. 57, no. 6, pp. 1133–1152, 2017.

[20] N. T. T. Uyen, Z. A. A. Hamid, N. X. T. Tram, and N. Ahmad, "Fabrication of alginate microspheres for drug delivery: A review," *International Journal of Biological Macromolecules*, vol. 153, pp. 1035–1046, jun 2020.

[21] D. Dhamecha, R. Movsas, U. Sano, and J. U. Menon, "Applications of alginate microspheres in therapeutics delivery and cell culture: Past, present and future," *International journal of pharmaceutics*, vol. 569, p. 118627, 2019.

[22] E. Bruno Romanini, L. Misturini Rodrigues, A. Finger, T. Perez Cantuaria Chierrito, M. Da Regina Silva Scapim, and G. Scaramal Madrona, "Ultrasound assisted extraction of bioactive compounds from BRS Violet grape pomace followed by alginate-Ca^{2+} encapsulation," *Food Chemistry*, vol. 338, p. 128101, 2021.

[23] I. Esparza, M. J. Cimminelli, J. A. Moler, N. Jiménez-Moreno, and C. Ancín-Azpilicueta, "Stability of phenolic compounds in grape stem extracts," *Antioxidants (Basel, Switzerland)*, vol. 9, no. 8, 2020.

[24] P. R. Sarika, N. R. James, P. R. A. Kumar, and D. K. Raj, "Galactosylated alginate-curcumin micelles for enhanced delivery of curcumin to hepatocytes," *International journal of biological macromolecules*, vol. 86, pp. 1–9, 2016.

[25] W. Song, X. Su, D. A. Gregory, W. Li, Z. Cai, and X. Zhao, "Magnetic alginate/chitosan nanoparticles for targeted delivery of curcumin into human breast cancer cells," *Nanomaterials*, vol. 8, no. 11, 2018.

[26] S. Amani, Z. Mohamadnia, and A. Mahdavi, "pH-responsive hybrid magnetic polyelectrolyte complex based on alginate/BSA as efficient nanocarrier for curcumin encapsulation and delivery," *International journal of biological macromolecules*, vol. 141, pp. 1258–1270, 2019.

[27] A. Hassani, S. Mahmood, H. H. Enezei, S. A. Hussain, H. A. Hamad, A. F. Aldoghachi, A. Hagar, A. A. Doolaanea, and W. N. Ibrahim, "Formulation, characterization and biological activity screening of sodium alginate-gum arabic nanoparticles loaded with curcumin," *Molecules*, vol. 25, no. 9, 2020.

[28] D. Aluani, V. Tzankova, M. Kondeva-Burdina, Y. Yordanov, E. Nikolova, F. Odzhakov, A. Apostolov, T. Markova, and K. Yoncheva, "Evaluation of bio-compatibility and antioxidant efficiency of chitosan-alginate nanoparticles loaded with quercetin," *International journal of biological macromolecules*, vol. 103, pp. 771–782, 2017.

[29] G. Chen, L. He, P. Zhang, J. Zhang, X. Mei, D. Wang, Y. Zhang, X. Ren, and Z. Chen, "Encapsulation of green tea polyphenol nanospheres in PVA/alginate hydrogel for promoting wound healing of diabetic rats by regulating PI3K/AKT pathway," *Materials science & engineering C: Materials for biological applications*, vol. 110, p. 110686, 2020.

[30] G. F. M. Bautista, M. L. P. Vidallon, K. C. Salamanez, and E. B. Rodriguez, "Nanodelivery system based on zein-alginate complexes enhances *in vitro* chemo-preventive activity and bioavailability of pomelo [*Citrus maxima* (burm.) merr.] seed limonoids," *Journal of Drug Delivery Science and Technology*, vol. 54, p. 101296, 2019.

[31] R. Stojanovic, A. Belscak-Cvitanovic, V. Manojlovic, D. Komes, V. Nedovic, and B. Bugarski, "Encapsulation of thyme (*Thymus serpyllum* L.) aqueous extract in calcium alginate beads," *Journal of the Science of Food and Agriculture*, vol. 92, no. 3, pp. 685–696, 2012.

[32] W. Zam, G. Bashour, W. Abdelwahed, and W. Khayata, "Alginate-pomegranate peels' polyphenols beads: effects of formulation parameters on loading efficiency," *Brazilian Journal of Pharmaceutical Sciences*, vol. 50, no. 4, pp. 741–748, 2014.

[33] L. M. Llive, M. Perullini, P. R. Santagapita, A. Schneider-Teixeira, and L. De-ladino, "Controlled release of fertilizers from Ca(II)-alginate matrix modified by yerba mate (*Ilex paraguariensis*) waste," *European Polymer Journal*, vol. 138, p. 109955, 2020.

[34] A. Belščak-Cvitanović, R. Stojanović, V. Manojlović, D. Komes, I. J. Cindrić, V. Nedović, and B. Bugarski, "Encapsulation of polyphenolic antioxidants from

medicinal plant extracts in alginate–chitosan system enhanced with ascorbic acid by electrostatic extrusion," *Food Research International*, vol. 44, no. 4, pp. 1094–1101, 2011.

[35] P. Wang, F. Zhang, Q. He, J. Wang, H. T. Shiu, Y. Shu, W. P. Tsang, S. Liang, K. Zhao, and C. Wan, "Flavonoid Compound Icariin Activates Hypoxia Inducible Factor-1α in Chondrocytes and Promotes Articular Cartilage Repair," *PloS one*, vol. 11, no. 2, p. e0148372, 2016.

[36] X. Cheng, K. Li, S. Xu, P. Li, Y. Yan, G. Wang, Z. Berman, R. Guo, J. Liang, S. Traore, and X. Yang, "Applying chlorogenic acid in an alginate scaffold of chondrocytes can improve the repair of damaged articular cartilage," *PloS one*, vol. 13, no. 4, p. e0195326, 2018.

[37] M. Türk, S. Karahan, M. Çinar, S. Küçük, and G. Ç. Dinçel, "Characterization of chondrocytes cultured on catechin-loaded alginate-chitosan scaffolds," *Artificial cells, nanomedicine, and biotechnology*, vol. 41, no. 4, pp. 240–248, 2013.

[38] N. D. A. Arriola, P. I. Chater, M. Wilcox, L. Lucini, G. Rocchetti, M. Dalmina, J. P. Pearson, and R. D. de Mello Castanho Amboni, "Encapsulation of *stevia rebaudiana Bertoni* aqueous crude extracts by ionic gelation - effects of alginate blends and gelling solutions on the polyphenolic profile," *Food Chemistry*, vol. 275, pp. 123–134, 2019.

[39] Z. Rasines-Perea and P.-L. Teissedre, "Grape polyphenols' effects in human cardiovascular diseases and diabetes," *Molecules (Basel, Switzerland)*, vol. 22, no. 1, 2017.

[40] N. A. Al-Awwadi, C. Araiz, A. Bornet, S. Delbosc, J.-P. Cristol, N. Linck, J. Azay, P.-L. Teissedre, and G. Cros, "Extracts enriched in different polyphenolic families normalize increased cardiac NADPH oxidase expression while having differential effects on insulin resistance, hypertension, and cardiac hypertrophy in high-fructose-fed rats," *Journal of agricultural and food chemistry*, vol. 53, no. 1, pp. 151–157, 2005.

[41] F. Sánchez-Patán, C. Cueva, M. Monagas, G. E. Walton, G. R. Gibson, P. J. Martín-Álvarez, M. Victoria Moreno-Arribas, and B. Bartolomé, "Gut microbial catabolism of grape seed flavan-3-ols by human faecal microbiota. Targetted analysis of precursor compounds, intermediate metabolites and end-products," *Food Chemistry*, vol. 131, no. 1, pp. 337–347, 2012.

[42] A. Esteban-Fernández, I. Zorraquín-Peña, M. D. Ferrer, A. Mira, B. Bartolomé, D. González de Llano, and M. V. Moreno-Arribas, "Inhibition of oral pathogens adhesion to human gingival fibroblasts by wine polyphenols alone and in combination with an oral probiotic," *Journal of agricultural and food chemistry*, vol. 66, no. 9, 2018.

[43] A. C. Pedro, D. Granato, and N. D. Rosso, "Extraction of anthocyanins and polyphenols from black rice (*Oryza sativa* L.) by modeling and assessing their reversibility and stability," *Food Chemistry*, vol. 191, pp. 12–20, 2016.

[44] J. Silva, P. Vanat, D. Marques-Da-Silva, J. R. Rodrigues, and R. Lagoa, "Metal alginates for polyphenol delivery systems: Studies on crosslinking ions and easy-to-use patches for release of protective flavonoids in skin," *Bioactive materials*, vol. 5, no. 3, pp. 447–457, 2020.

Chapter 5

Application of alginate beads in Agriculture and Biomedicine

5.1   General introduction of alginate beads applications

The latest projections by the United Nations suggest that the world's population could grow to around 8.5 billion in 2030 and 9.7 billion in 2050. It is predicted to reach a peak of around 10.4 billion people during the 2080s and to remain at that level until 2100 [1]. Thus, on the one hand, it is widely recognized that global agricultural productivity must increase to feed a rapidly growing world population. Therefore, sustainable crop production needs to be secured and enhanced. On the other hand, the high rate of population growth affects long-range planning of community health and medical facilities, which will require the improvement of treatment outcomes in many ways such as the enhancement of therapeutic efficacy while reducing toxicity, patient compliance and entirely new medical treatments [2, 3]. Therefore, urgent measures must be taken to address these challenges and ensure the provision of enough food and healthcare services to the expanding global community. Thus, the aim of the work described in this chapter was to investigate the potential benefits of Alg beads application in Agriculture and Biomedicine fields. The studies presented in this chapter were carried out in collaboration with The National Institute of Horticulture Research, Department of Microbiology and Rhizosphere in Skierniewice, Poland and with The Collegium Medicum im. Ludwika Rydygiera Bydgoszcz of Nicolaus Copernicus University, Department of Urology and Andrology, Torun, Poland. The samples studied are summarized in Table 5.1.

143

Table 5.1: Samples analyzed in the study outlined in Chapter 5, classified based on their designated applications

Sample	Crosslinking bath	Maturation time	BACs concentration
Agriculture application			
Ca-beads	$CaCl_2$ 0.5% (w/w)	48h	-
Cu-beads	$CuCl_2$ 0.5% (w/w)	48h	-
Zn-beads	$ZnCl_2$ 0.5% (w/w)	48h	-
Biomedicine application			
Cytotoxicity			
BACs 10% Ca-beads	$CaCl_2$ 2% (w/w)	48h	0.17% (w/w)
BACs 10% Cu-beads	$CuCl_2$ 2% (w/w)	48h	0.17% (w/w)
Anti-cancer properties			
Ca-beads	$CaCl_2$ 2% (w/w)	48h	-
Zn-beads	$ZnCl_2$ 2% (w/w)	48h	-
BACs 10% Zn-beads	$ZnCl_2$ 2% (w/w)	48h	0.17% (w/w)

5.2 Introduction to applications of alginate beads in Agriculture

The main aim of the research presented in this chapter was to investigate the effect of encapsulated divalent ions: Ca^{2+}, Cu^{2+} and Zn^{2+}, on the germination and seedling growth of mustard seed. The term mustard refers to a group of plants of the Cruciferae family, which belongs to the genus Brassica. Mainly three species of mustard are cultivated worldwide for their gastronomic value: yellow or white mustard (*Sinapis alba*), oriental mustard (*Brassica juncea*), and black mustard (*Brassica nigra*). Usually, mustard plants are consumed as edible oils, condiments, sauces, fermented vegetables, or salad greens [4]. These plants have been reported for their high nutritional value and richness in bioactive compounds such as glucosinolates, polyphenols, dietary fiber, β-carotene, and ascorbic acid. The cultivation and investigation of mustard revolve around its culinary use, agricultural applications, soil improvement, potential medicinal properties, and biofumigation effects [5, 6, 7, 8, 9]. Mustard was chosen to be studied because in literature, it has been proposed as a crop model to investigate soil management practices on crop growth and the effects of climate changes [10].

In Agriculture, encapsulation technology offers benefits such as the protection and controlled release of nutrients, pesticides, and fertilizers, leading to enhanced crop productivity and reduced environmental impact [11]. Alg has been used for agriculture beads development, as a sustainable delivery system, effectively preserve and deliver active compounds to plants, preventing their environmental degradation and enabling controlled release over extended periods. Alg beads have been especially applied for crop protection against pests and illnesses, which pose a significant risk to farmers. When encapsulated within the Alg matrix, pesticides and biocontrol agents can be released in a controlled manner with targeted action. This enables the optimization of pesticide efficiency, reduces the frequency of applications, minimizes waste, enhances user safety, and mitigates phytotoxicity and environmental pollution [12, 13, 14, 15, 16, 17]. Additionally, the use of Alg beads improves nutrient utilization, guarantees a regular supply of nutrients, reduces the risk of undernourishment and enhances fertilizer efficiency. Alg beads may also be employed for the encapsulation of beneficial microorganisms [18, 19], thereby increasing their survivability and enhancing their biological activity [20, 21] Alg beads may be utilized as well to encapsulate seeds, promoting increased germination rates and root ball growth [22], while enhancing seed tolerance to environmental conditions such as diseases, salinity, and drought [11]. Therefore, Alg beads provide organic compounds that contribute to extended soil fertility and sustainability. Moreover, the composition of beads can be optimized attending to factors such as the crop variety, development stage and environmental conditions. Furthermore, the employed crosslinkers can have beneficial effects on plant development. For instance, as depicted in Chapter 1, Cu^{2+} is an essential micronutrient for early stages of plant growth, for the photosynthetic and respiratory electron transport chains, cell wall metabolism, etc. . . [19, 23]. Furthermore, Cu^{2+} is used to treat a wide variety of bacterial and fungal infections [19]. Similarly, Zn^{2+} is also necessary for proper plant growth [24]. In addition, Ca^{2+} is an essential macronutrient with important functions in cell wall structure and permeability, plant cell division and elongation, signal transduction and absorption of nutrients [25]. Thus, the controlled release of these micronutrients through encapsulation offers advantages over standard applications to protect plants. As a matter of example, Vinceković et al. [19] proved the encapsulation of *Trichoderma* species within Alg beads crosslinked with Cu^{2+} to be a potential alternative to conventional plant protection methods. Likewise, Shaban et al. [26] and Qi et al. [27] conducted investigations on the encapsulation of *Trichoderma* species within alginate beads crosslinked with Ca^{2+}. Furthermore, both Ca^{2+} and Cu^{2+} have been used for encapsulation of plant

growth regulators [28], while fertilizer encapsulation through Alg crosslinking with Cu^{2+} and Zn^{2+} has been studied by Ekanayake and Godakumbura [29].

5.3   Agriculture results

As it is described in Chapter 2, to investigate the effect of the encapsulated cations on the plants, two type of tests were carried out: mustard germination tests and mustard seedling growth tests. In these studies, Ca-, Cu- and Zn- based Alg beads prepared by polymeric solution extrusion dropwise into a crosslinking bath containing 0.5% (w/w) of $CaCl_2$, $CuCl_2$ and $ZnCl_2$, respectively (Table 5.1), were used.

As it is described in Chapter 2, mustard germination tests were carried out using a soil solution (SScontrol) mixed with the beads (SS-Ca, SS-Cu and SS-Zn), while mustard seedling growth tests were performed using soil (Scontrol) mixed with beads (S-Ca, S-Cu and S-Zn) during 7 or 14 days incubation time.

5.3.1   Kinetics of cations release from beads

In order to understand the influence of cations released from beads to soil or to soil solution on mustard plants, it was crucial to investigate the cations concentration in the soil and soil solution. The concentrations of cations released from the beads (characterized in Chapter 3, section 3.2.6) were studied by ICP, according to the time of beads incubation in soil solution or in bulk soil. Table 5.2 displays the concentrations of soluble cations in soil solutions incubated with the beads for 3, 6 and 9 days, and cations available for plants in soil incubated with the beads for 7 and 14 days. It can be observed that in the control samples (SControl and SSControl) the content of available Ca^{2+}, Cu^{2+} or Zn^{2+} did not change neither in the soil solution nor in the soil during whole time of incubation.

Table 5.2: Concentration of a) soluble elements in soil solutions incubated for 3, 6 and 9 days and b) available elements for plants in soil incubated for 7 and 14 days with the corresponding beads. Means followed by the same letter do not differ significantly according to DMRT at p = 0.05

	Days of incubation of soil solutions		
a) Samples	3	6	9
	Ca^{2+} (mg/L)		
SSControl	110.7 c	112.0	113.0 c
SS-Ca	168.3 b	170.0 b	200.7 a
SS-Zn	90.7 e	88.5 e	77.2 f
SS-Cu	106.7 d	104.0 d	71.6 g
	Zn^{2+} (mg/L)		
SSControl	0.01 c	0.01 c	0.01 c
SS-Ca	0.36 c	0.06 c	0.37 c
SS-Zn	92.60 b	94.80 b	123.20a
SS-Cu	0.08 c	0.07 c	0.08 c
	Cu^{2+} (mg/L)		
SSControl	0.02 c	0.01 c	0.01 c
SS-Ca	0.20 c	0.02 c	0.16 c
SS-Zn	0.84 c	0.80 c	0.66 c
SS-Cu	46.50b	50.00b	73.20 a

	Days of incubation of soil	
b) Samples	7	14
	Ca^{2+} (mg/L)	
SControl	837.3 c	768.0 d
S-Ca	1006.7 a	877.3 b
S-Zn	828.0 c	705.7 e
S-Cu	823.0 c	760.7 d
	Zn^{2+} (mg/L)	
SControl	11.6 c	10.5 c
S-Ca	8.7 c	9.5 c
S-Zn	1369.0 b	1501.7 a
S-Cu	9.2 c	9.8 c
	Cu^{2+} (mg/L)	
SControl	2.2 c	3.0 c
S-Ca	1.5 c	2.0 c
S-Zn	2.1 c	1.9 c
S-Cu	914.9 b	977 a

When Ca-, Cu- and Zn-beads were added to the soil solution, the concentration of the respective cations significantly increased (53%, 926%, 232%, respectively, Table 5.2a) after three days of incubation, in regard to the control sample. After next three days of incubation (day 6) the concentrations of these cations in the amended solutions did not increase. However, a significant increase of the studied cations concentrations was recorded after 9 days. It was also observed that application of beads with Zn^{2+} also resulted in an increment of the concentration of available Cu^{2+}, and opposite, application of Cu-beads caused increased amount of available Zn^{2+} (Table 5.2a). McBride and Bouldin carried out studies based on ion-selective electrode data, and they reported that at least 99.5% of Cu^{2+} in soil solution is in an organically complexed form [30], while Hazra et al. reported that more than 84% of total Zn^{2+} in soils occurs as structurally lattice bound; about 13% as sesquioxide bound; 1.6% as organically complexed; and about 1% as exchangeable and water soluble forms [31]. According to Draszawka-Bołzan [32], the pH value of the soil system is a very important parameter, directly influencing sorption/desorption, precipitation/dissolution, complex formation, cation exchange capacity and oxidation-reduction reactions. In general, maximum retention of cationic metals by soil active sides occurs at pH>7. Indeed, Gong and Donahoe [33] reported that Cu^{2+} and Zn^{2+} became mobile in soil solution by decreasing its pH value. Thus, very low concentrations of Cu^{2+} and Zn^{2+} cations detected in SSControl soil solution (0.02 and 0.01 mg/L, respectively) could be explained by its pH value of 7.7. At this pH values Cu^{2+} and Zn^{2+} cations can be retained by complexes. Whereas, when the SS-Zn and SS-Cu beads were added, the pH values of these soils solutions decreased from pH 7.7 to 7.1 and 6.3, respectively. It seems that these pH changes caused Cu^{2+} and Zn^{2+} cations released and, as a consequence, they were detected in the investigated soil solutions. A similar increase of soluble Cu^{2+} and Zn^{2+} concentration in soil solution was noted after application of Ca-beads (soil solution pH 7.2). However, the addition of Zn- and Cu-beads to the soil solutions reduced the availability of Ca^{2+} presented in the stock solution by approximately 32% and 36%, respectively, after 9 days of incubation. In the case of Zn-beads, the reduction of Ca^{2+} availability was significant during the first 3 days of incubation. This phenomena could be explained by Ca^{2+} and Zn^{2+} exchangeability and adsorption processes [34, 35].

In bulk soil, just like in the soil suspension, incubation time was not the factor changing the concentration of available cations. In fact, the addition of beads to the soil mixture with perlite resulted in significant growth of soluble cations amount compared to control soil (SControl) not supplemented with the beads (Table 5.2b). For Cu-beads, after 7 days of soil incubation, the concentration of this element increased more than 400-times compared to control, and successively rose after 14 days of incubation. To a lower extend, the concentration of soluble Zn^{2+} increased as well (about 100-times after 7 days), but also in the case of this ion progressed availability was observed with incubation. On the contrary, Ca^{2+} concentration increased, although significant after the addition of beads, was lower compared to Cu^{2+} and Zn^{2+}. Moreover, in the case of Ca^{2+} added with the beads, its availability decreased with time of incubation and was significantly lower after 14 days than after 7 days.

5.3.2 Effects of encapsulated cations on mustard seeds germination and sprouts biomass

Figure 5.1 shows the effect of the cations released from beads into soil solution on mustard sprouts development, in regard to germination (Figure 5.1a), total weight (Figure 5.1b), radicle length (Figure 5.1c), radicle weight (Figure 5.1d) and cotyledon weight (Figure 5.1e). Released Ca^{2+}, Cu^{2+} and Zn^{2+} affected significantly seeds germination and biomass of mustard sprouts in *in vitro* tests. Seed germination was the most influenced by Cu^{2+}, especially after treatment with the 9-th day-incubated soil solution (Figure 5.1a), where mustard germination was inhibited by about 50% compared to control. Similar effects were observed by Rather et al. [36] who exposed Indian Mustard seeds (*Brassica juncea* L.) to 3.0 mM Cu^{2+} aqueous solution for 3 days as well as by Gautam et al. [37] who investigated the changes in the Safflower (*Carthamus tinctorius* L.) growth during its exposure to different concentrations of Cu^{2+} (25, 50 and 100 M) for 20 days. In our studies we also observed that in excess of its permissible concentration, Cu^{2+} can lead to a significant reduction of seed germination and seedling growth, while Ca^{2+} and Zn^{2+} did not affected mustard germination significantly. A similar effect was observed during evaluation of total sprouts weight, which was significantly reduced by Cu^{2+} released form the Cu-beads (Figure 5.1c). Indeed, Zhao et al. [38] and Xia et al. [39] indicated that high concentration of Cu^{2+} can have negative impact on seeds germination and plant growth. While, in the studies of Baczek-Kwinta et al. [40], it was found that Zn^{2+} unaffected germination of broccoli (*Brassica oleracea* var. *botrytis italic*), sunflower (*Helianthus annuus* L.), and pea (*Pisum sativum* L.) seeds. In our studies, total

149

biomass of the sprouts was not affected by Ca^{2+} nor Zn^{2+} released from beads. However, the cations had different effects on the ratio of radicle to cotyledons weight. The strongest effect of the cations released to soil solution was observed in the case of sprout radicles. Cu^{2+} and Zn^{2+} released from Cu- and Zn-beads, respectively, greatly reduced mustard radicles, especially their length (Figure 5.1c and d). In the case of Cu^{2+}, radicle development was almost completely reduced regardless of the incubation time of soil solution with Cu-beads. Zn^{2+} also reduced the radicle development but its effect was enhanced proportionally with increased incubation time of Zn-beads in soil solution: 38%, 70%, 94% for 3, 6 and 9 days of beads incubation, respectively. In opposite, Ca^{2+} significantly stimulated sprouts radicle elongation (Figure 5.1c), and its effect was positively proportional to the time of its release from the Ca-beads. When the soil solution incubated with the Ca-beads for 9 days was used, the mustard radicles were 39% longer compared to control sprouts. Actually, Li et al. [41] reported that the treatment of wheat seeds (*Triticum aestivum*) with aqueous solution of heptahydrate $ZnSO_4 \cdot 7H_2O$ (concentration range from 0.5 mM to 3 mM) did not affect seed germination, but reduced root length, while Takahaski et al. [42] reported that Ca^{2+} at 10 or 20 mM, significantly stimulated root elongation in pea (*Pisum sativum* L.) and corn (*Zea mays* L.) seedlings.
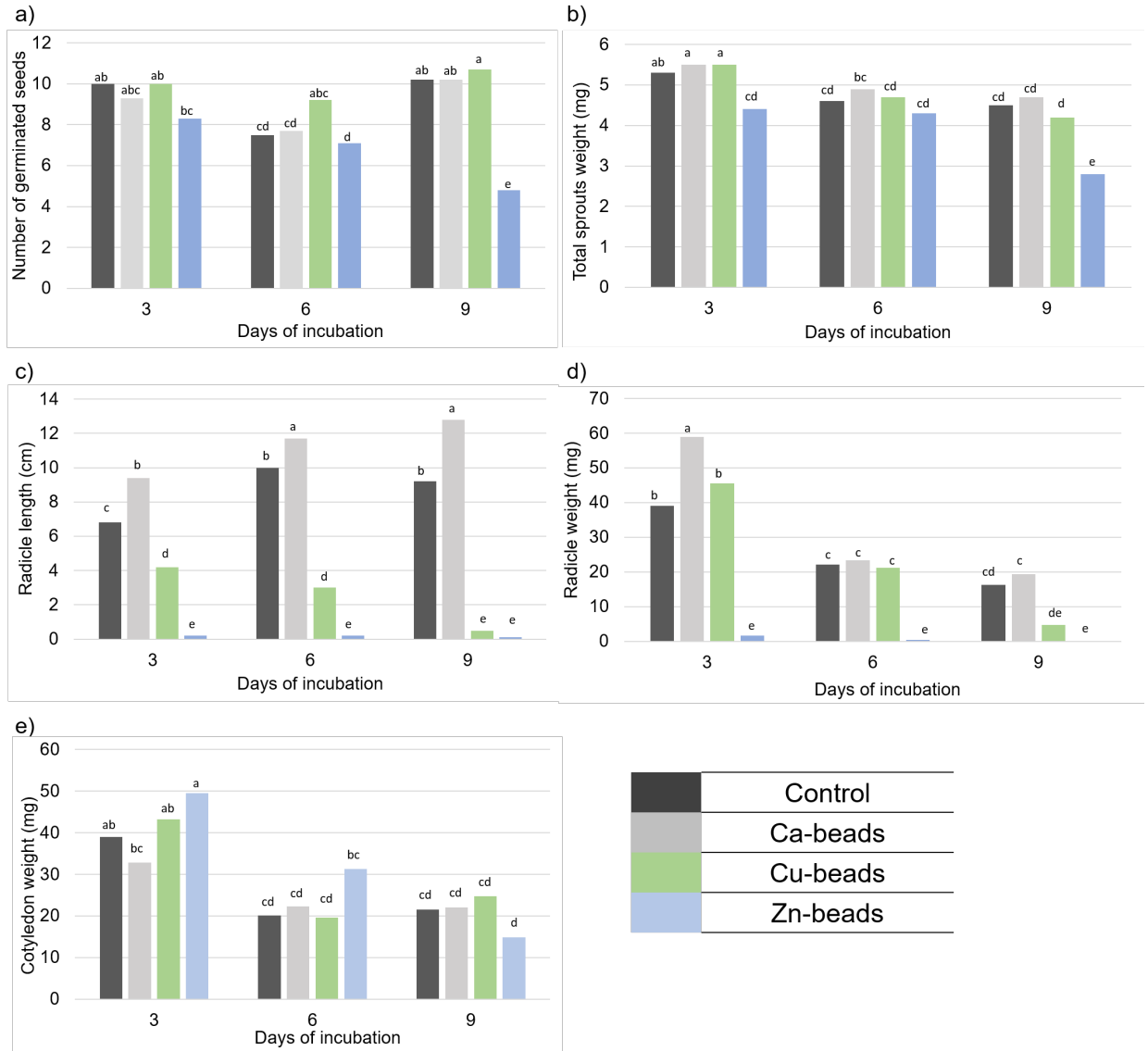
Figure 5.1: Effect of the ions released from beads into soil solution on mustard sprouts development: a) germination; b) total weight; c) radicle length; d) radicle weight; and e) cotyledon weight. The same letters above the bars indicate that means are not significantly differentiated according to DMRT at p = 0.05

A different response to the ions applied with beads was found on cotyledons. In this case, Cu^{2+} released to the soil solution stimulated weight of this part for 27% and 55% after 3 and 6 days of incubation respectively, compared to control (Figure 5.1e). However, the differences were not significant. After 9 days of incubation in soil solution, the concentration of Cu^{2+} released from the beads was phytotoxic. Ca^{2+} and Zn^{2+} released from the Ca- and Zn-beads had no significant effect on cotyledons biomass.

5.3.3   Effects of encapsulated cations on mustard seedling growth

The effect of the cations released from beads to the soil on mustard seedling growth, in regard to germination, total seedlings weight, root length, root weight and shoot weight, are shown in Figure 5.2. Thus, the cations had not any significant effect on mustard seeds germination in Phytotoxkit tests. The germination was comparable for all treatments in both incubation times (Figure 5.2a). However, the seedling weight was significantly enhanced by Ca^{2+} released to the soil from the beads (Figure 5.2b). Stronger, positive effect of Ca^{2+} on mustard growth was observed in soil incubated for 14 days, where the seedlings from soil with Ca-beads were by 106% bigger than in control. This positive effect of Ca^{2+} was mostly related to the greater roots development: length and weight (Figures 5.2c and 5.2d). The average length of the roots in soil amended with Ca-beads was 29% and 58% higher than in control for plants grown in soil incubated for 7 and 14 days respectively. Similarly, the weight of mustard roots treated with released Ca^{2+} was 29% and 70% greater than for control plants grown in soil incubated for 7 and 14 days respectively. Moreover, Ca^{2+} released from the beads stimulated also the growth of the above-ground parts of mustard seedlings of (Figure 5.2e), despite the differences were not significant.

In the case of Cu^{2+} and Zn^{2+}, the release of these elements to the soil during incubation significantly decreased roots elongation (Figure 5.2c). However, these cations did not affect significantly the weight of the young roots (Figure 5.2d). In those experiments, Zn^{2+} also significantly inhibited the development of the above-ground parts of the seedlings (Figure 5.2e), what resulted in decreased total seedlings weight (Figure 5.2b). Cu^{2+} had no marked influence on mustard seedling growth, regardless the duration of the beads incubation in soil.
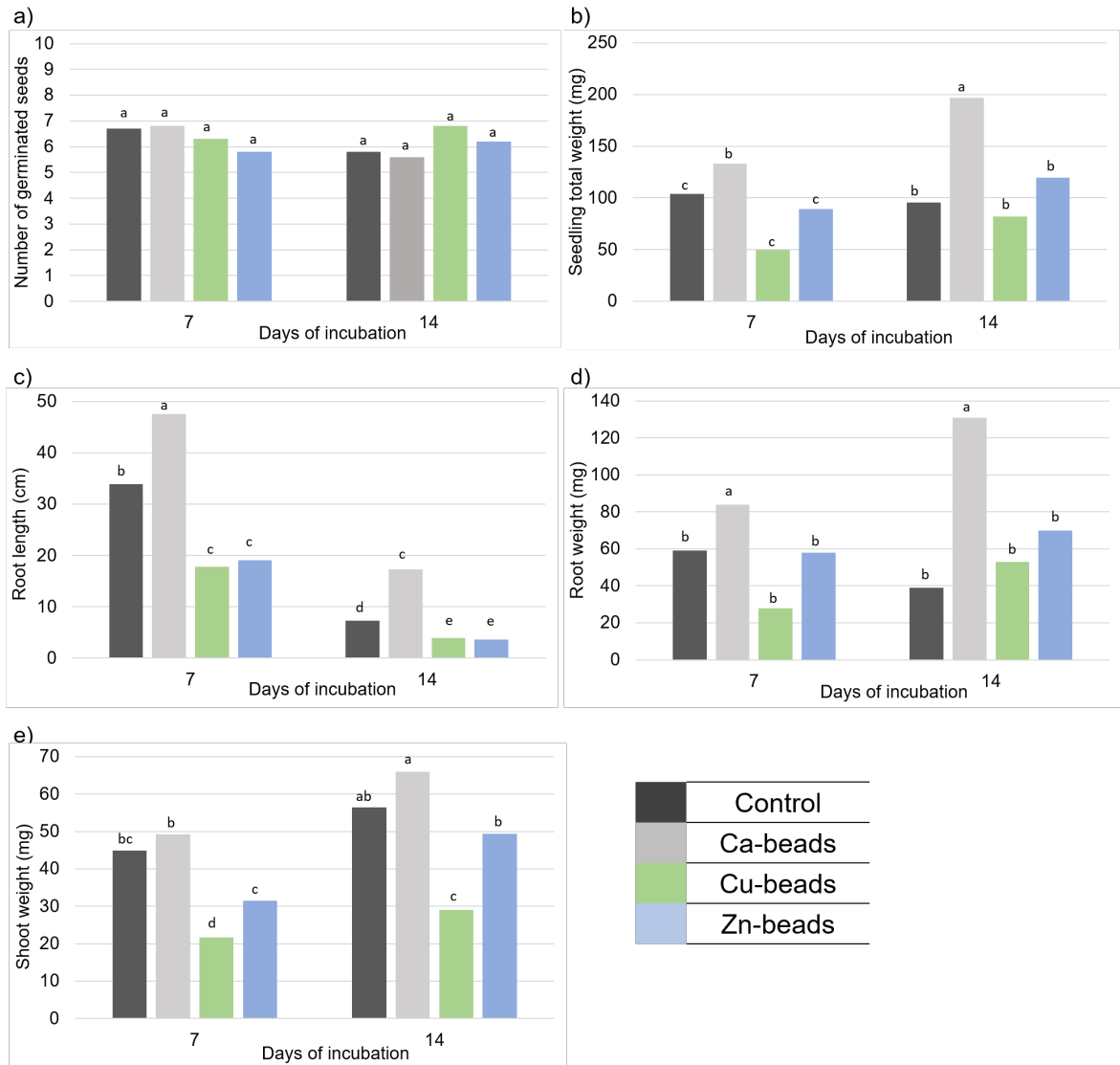
Figure 5.2: Effect of the ions released from beads on mustard seedling growth in treated soil: a) seeds germination; b) total seedlings weight; c) root length; d) root weight; and e) shoot weight. The same letters above the bars indicate that means are not significantly differentiated according to DMRT at p = 0.05

5.4   Conclusions Agriculture application

- The application of Ca-, Cu- or Zn-beads to the soil solution resulted in a significant increase in the concentrations of the respective cations. The application of Zn-based beads led to an increase in the concentration of available Cu^{2+} and vice versa. However, the addition of Zn- and Cu-based beads reduced the availability of Ca^{2+} in the soil solution, suggesting ion exchange and adsorption processes. In literature, the pH of the soil system has been indicated to be an important parameter for the retention of cationic metals, being maximum at pH values above 7.

- Incubation time of Alg beads in soil did not significantly affect the concentration of available cations. Nevertheless, the addition of perlite led to a significant increase of the amount of soluble cations compared to the control soil. Cu^{2+} showed the highest increase, followed by Zn^{2+}, whereas Ca^{2+} concentration not only displayed the lowest increase but also decreased over time when Ca-based beads were added to the soil mixture.

- The release of Cu^{2+} had the greatest impact on seed germination and sprout biomass, inhibiting germination and reducing sprout weight. Differently, Ca^{2+} and Zn^{2+} did not significantly affect mustard germination nor total biomass of the sprouts.

- The release of Cu^{2+} and Zn^{2+} from the beads hindered radicle development. Cu^{2+} almost completely inhibited radicle development, while Zn^{2+} had a progressive inhibitory effect with increased incubation time. In contrast, Ca^{2+} stimulated radicle elongation.

- Cu^{2+} stimulated the weight of cotyledons. However, after 9 days of incubation, the concentration of Cu^{2+} released from the beads exhibited phytotoxic effects. Ca^{2+} and Zn^{2+} did not have a significant effect regarding the biomass of cotyledon.

5.5   Introduction to applications of alginate beads in Biomedicine

The second part of this chapter describes the investigation carried out in collaboration with the research group of Professor Anna Bajek from the Collegium Medicum, Nicolaus Copernicus University in Torun, Poland. During this work, cytotoxicity and anti-cancer properties of the Alg-based delivery systems were studied and assessed by MTT assays using:

- 3T3 NIH cell line, which are mouse embryonic fibroblasts, recommended by the ISO norm 10993-5. 3T3 cells are commonly employed as a model system to study cell proliferation, differentiation and migration due to their high growth rate and ability to grow in culture media containing antibiotics, making them easy to cultivate;

- SV-HUC-1 uroepitelium cells, which are a non-cancerous cell lines derived from human epithelial cells isolated from the uroepithelium; and

- T24 cell line, which is a highly characterized human cancer cell line derived from urinary bladder carcinoma. It is often used as a model system for investigating cellular processes and evaluating the effects of different compounds and treatments. T24 cells are notable for their aggressive behaviour associated to a rapid proliferation, resistance to apoptosis and a propensity for invasion and metastasis.

The samples to which the cells were exposed in order to measure the effects on their metabolical activity through the MTT assays are summarized in Table 5.1. Cellular toxicity towards the extracts of BACs-loaded beads prepared with $CuCl_2$ and $CaCl_2$ 2% (w/w) was tested to assess the cytotoxicity of beads and to evaluate the potential health benefits of BACs. The extracts were studied at increasing concentrations (0.1%, 1%, 10%, 100%) to determine the initial dose for cytotoxicity assessment. Additionally, the potential anticancer properties of Alg-based delivery systems prepared with $CuCl_2$, $CaCl_2$ and $ZnCl_2$ 2% (w/w), with and without BACs, were evaluated in SV-HUC-1 and T24 cells. The cell line SV-HUC-1 was employed as a control for the assessment of the anticancer properties whereas 3T3 cells were employed as a benchmark cell line, frequently employed in the field of biomaterial science [43].

155

Generally, nature is a valuable source of therapeutic compounds as well as one of the best reservoirs of novel bioactive structures. Numerous studies have demonstrated the anti-obesity activity of polyphenols, which help to prevent or mitigate oxidative stress, inflammation and diabetes while aiding in the regulation of blood glucose levels [44]. Moreover, other phenolic extracts such as the obtained from black rice exhibited inhibitory effects on cancer cell proliferation *in vitro* [45], a high protection against oxidative stress on endothelial cells [46] and substantial suppression of angiogenesis induced by vascular endothelial growth factor [47]. *In vivo* studies in rat models have further demonstrated that pigmented rice varieties reduce the risk of atherosclerosis and efficiently decrease total cholesterol, low-density cholesterol and total triacyl-glycerol blood levels [48]. Furthermore, previous encapsulation of polyphenols from *Clitoria ternatea* petal flower extract in Alg hydrogel proved to enhance stability and maintained biological activity under simulated gastrointestinal conditions [49].

Additionally, Alg beads have been extensively employed for diverse Biomedical applications, especially in drug delivery, wound healing and tissue engineering. Alg-based systems are commonly employed as carriers for the controlled and targeted release of drugs, proteins and nucleic acids [50, 51, 52]. Alg-based beads facilitate targeted therapeutic levels within the organism, which in turn reduce dosage frequency and enhance patient compliance.

The biological and physicochemical properties of Alg hydrogels, combined with their high-water content, closely resemble the characteristics of natural extracellular matrices in biological tissues. Hence, Alg-beads are used for the encapsulation and immobilization of living cells, such as pancreatic islet cells for diabetes treatment, stem cells for regenerative therapies or genetically modified cells for the therapeutic agents synthesis [53, 54]. Indeed, encapsulated cells offer a sustained supply of active compounds and more complex release profiles [55, 56]. Additionally, Alg hydrogels serve as scaffolds in tissue engineering, providing a 3D polymeric network that supports the growth and development of cells and tissues [57, 58]. Physicochemical characteristics can be tailored to meet the requirements of particular cell types [58].

Alg-based hydrogels have gained significant importance in modern wound dressings due to their excellent moisture-retention properties [59]. The incorporation of additional compounds within Alg-based systems has the potential to enhance the beneficial properties of the hydrogel, promoting a faster healing and preventing infections [44, 60, 61].

Moreover, Alg hydrogels can be functionalized with specific molecules, such as metals, antibodies or enzymes, enabling the capture or detection of biomarkers in diagnostic tests [62]. Furthermore, Alg-based systems can be loaded with contrast agents for imaging purposes, enabling the visualization of specific tissues or structures during surgery procedures [63] or medical imaging techniques like computed tomography (CT) [64] or magnetic resonance imaging (MRI) [65].

5.6 Biomedicine results

5.6.1 Evaluation of beads cytotoxicity

5.6.1.1 BACs 10% beads prepared with $CaCl_2$ 2% (w/w)

The cell viability results regarding the extracts of BACs 10% beads prepared with $CaCl_2$ and $CuCl_2$ 2% (w/w), after 24h incubation with 3T3 and T24 cells are exhibited in Figure 5.3a and b, respectively. As mentioned in Chapter 2, section 2.2.1.2, BACs 10% refers to the relative concentration of BACs in regard to Alg, which are 0.17% and 1.7% (w/w), respectively (Table 5.1). The findings of BACs 10% Ca-beads reveal that the extracts derived were non-toxic to 3T3 cells. In fact, the effect of Ca-Alg beads on cells has been previously evaluated by other authors. For instance, Bohari et al. investigated the impact of Ca^{2+} and high M-content Alg on viability and proliferation of encapsulated 3T3 cells at different concentrations [66]. The tested concentrations of Na Alg polymeric solutions were: 0.5%, 1%, 2% and 5% (w/v). 3T3 cells were seeded at intermediate (0.76×10^6 cells/ml) and low (0.76×10^5 cells/ml) densities and transferred into a sterile $CaCl_2$ solution 100 mM. The utilized culture media was DMEM. Although there was an initial loss of cells after being cultured, the cell population eventually recovered and it maintained the proper morphology. High levels of cell viability were observed under all conditions, indicating that the Alg matrix was biocompatible and supported cell growth and proliferation of 3T3 cells. Likewise, our experiments were based on high M-content Alg, 3T3 cells were seeded at a density of 0.5×10^5 cells/mL and the employed concentration of $CaCl_2$ was 180 mM - 2% (w/w). The culture media that we utilized was DMEM/F12K and contained 10% (v/v) FBS.
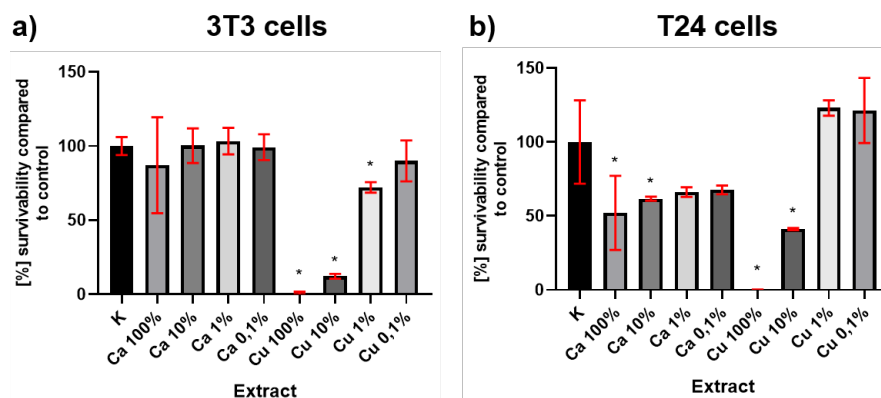
Figure 5.3: Metabolic activity of 3T3 cells (left) and T24 cells (right) after 24h of incubation with diluted extracts obtained from BACs 10% Alg beads prepared with $CaCl_2$ and $CuCl_2$ 2% (w/w)

Otherwise, Ca^{2+} concentration could exert significant effects on 3T3 fibroblasts, as it is involved in numerous cellular processes, signalling pathways and regulation of gene expression. However, our findings demonstrated that neither cell growth nor proliferation of 3T3 cells were adversely affected by Ca^{2+} released from BACs 10% Ca-beads after 24h of incubation (Figure 5.3a).

The cytotoxicity of polyphenols is highly dependent on the specific compound and its concentration. In our study, neither the concentration of BACs in the extract (100%) nor the BACs composition in BACs 10% Ca-beads exhibited cytotoxic effects on 3T3 cells after 24h.

According to the obtained results (Figure 5.3a), the cellular viability of T24 cells was compromised by the extracts derived from BACs 10% Ca-beads after 24h of incubation. In fact, polyphenols have been recognized for their potential anti-cancer properties, as demonstrated by investigations on bladder cancer cells [67, 68, 69]. Furthermore, Marchetti et al. revealed that polyphenols, namely epigallocatechin gallate (EGCG), inhibited the proliferation of prostate cancer cells by inducing an increase in intracellular Ca^{2+} concentration, which was dependent on extracellular Ca^{2+} availability [70]. The dysregulation of cytosolic Ca^{2+} was directly associated with the induction of cellular apoptosis (programmed cell death) in cancerous cells. Therefore, a synergistic interaction between the polyphenols and Ca^{2+} might be possible [71]. Nonetheless, further studies are required to prove this hypothesis.

158

Results reported by Ransato et al. evidenced the inhibitory effect of EGCG on various types of cancerous cells, including bladder carcinoma [72]. Their findings revealed that EGCG induced cancer cell apoptosis at lower doses and necrosis at higher doses, while exerting a selective cytotoxic effect towards cancerous cells compared to normal mesothelial cells. Similar experiments involving EGCG and T24 cells were carried by Ke-Wang Luo et al. [73], in which EGCG inhibited proliferation, migration and invasion of T24 cancerous cells through the induction of apoptosis, without causing apparent toxicity to normal bladder SV-HUC-1 cells. The results displayed in Figure 5.3 evidenced this selectivity as well. Furthermore, Luo et al. demonstrated that EGCG enhanced the anti-tumour, anti-migration and anti-proliferation effects of doxorubicin in T24 cells [74].

Other polyphenols, such as resveratrol and its derivatives [75, 76] have also demonstrated selective anti-cancer effects on mesothelioma and breast cancerous cells, respectively. Results pointed at the activation of pro-apoptotic Ca^{2+} signalling pathways to induce the influx and elevation of intracellular Ca^{2+} levels. Curcumin and carnosic acid have shown as well synergistic anti-proliferative effects towards metastatic prostate cancer cells [77]. In addition, both compounds synergistically induced selective apoptosis in acute myeloid leukemia cells, but not in normal hematopoietic and non-hematopoietic cells, through sustained cytosolic Ca^{2+} overload [78]. The rise in cytosolic Ca^{2+} levels, coupled with the defective oxidative phosphorylation and mitochondrial dysfunction, contributed to the cell cycle arrest.

Notably, the use of curcumin and carnosic acid at non-toxic concentrations was possible due to their synergistic effects. However, achieving proliferation arrest and/or inducing cancer cells death may demand significantly high concentrations of polyphenols, which can be challenging to attain *in vivo* or may even lead to cytotoxicity. An alternative approach is the use of polyphenols-rich extracts, as the formula of these may comprise elements that enhance anticancer activity through interactions with other bioactive compounds, which can target multiple pathways involved in cancer development and progression. For instance, tea extracts rich in catechins have demonstrated anti-cancer effects on bladder cancer T24 cells [79]. Other polyphenol-rich extracts that have displayed anti-cancer properties on T24 cells include a methanolic extract of *A. baetica* and *A. paucinervis* roots (high flavonoid content) [80], *C. spinosa* [81] and olive extract [82].

In addition, Ca-Alg nanoparticles loaded with curcumin and resveratrol were prepared and tested *in vitro* on DU145 prostate carcinoma. Both polyphenols were added in powder form. The employed Alg concentration was 0.6 mg/mL and $CaCl_2$ at 0.052% (w/v). The blank (empty Ca-Alg nanoparticles) and the drug-loaded nanoparticles were found to be safe for intravenous administration and both exhibited cytotoxic effects specifically on prostate cancer cells. However, at high concentrations, the drug solution showed higher cytotoxicity compared to nanoparticles.

5.6.1.2 BACs 10% beads prepared with $CuCl_2$ 2% (w/w)

The cytotoxic effects of Cu^{2+} in 3T3 cells shown in Figure 5.3b are evident even at the lowest concentration of extract. In the case of T24 cells, cellular viability was significantly compromised when exposed to the concentrated extract of BACs 10% Cu-beads and the 10% dilution showed poor or negligible cell viability. Interestingly, at lower concentrations, cell viability exceeded the control value. Cu^{2+} plays a crucial role in various cellular processes associated with cell growth, proliferation and differentiation. As previously discussed in Chapter 1, section 1.2.2.2, the range of therapeutic Cu^{2+} concentration is narrow and it results in potent biological responses [83]. Nevertheless, excessive levels of Cu^{2+} can be toxic to cells and induce oxidative stress.

Cu^{2+} completely abolished the potential anti-cancer properties of the extract. In fact, Cu^{2+} has been proved to drop the cytotoxic effect of wedelolactone, a plant polyphenolic derivative of coumestan and a promising anticancer agent, through the formation of a coordination complex [84]. Simultaneously, the interaction between wedelolactone and Cu^{2+} is essential for therapeutic accomplishment and selectivity towards cancerous cells. That is particularly relevant as increased or altered levels of intratumoral Cu^{2+} are a common feature which is shared by several cancer types [85].

Elevated levels of Cu^{2+} in cancer cells are known to contribute to angiogenesis, proliferation and metastasis [86]. In fact, as it can be observed in Figure 5.3b, the most concentrated extract displayed a toxic effect towards both cell types, although T24 cells seemed to have a higher tolerance limit for Cu^{2+} concentration compared to 3T3 fibroblasts. Interestingly, at lower concentrations, the Cu^{2+} extract not only was non-toxic but also promoted metabolic activity of cancerous cells.

5.6.2   Evaluation of beads anti-cancer properties

5.6.2.1   Empty beads prepared with $CaCl_2$ 2% (w/w)

Figure 5.4 shows the cytotoxicity results of T24 and SV-HUC-1 cells towards the extracts derived from Alg beads prepared with $CaCl_2$ 2% (w/w) after 24h incubation. It can be observed that both, the most concentrated extract and the 10% dilution, exhibited cytotoxic effects on SV-HUC-1 cells. Nevertheless, the lowest concentration of extract (0.1%) promoted metabolic activity. Figure 5.5 displays images of these cells captured after 24h of incubation with extraction media (control) or Ca-beads extract by means of an inverted, phase contrast microscope. It reveals that, although the morphology of SV-HUC-1 cells was not altered, the extract seemed to induce cell cycle arrest.

Although previous reports of Alg cytotoxicity in SV-HUC-1 cells are still limited, its safety profile has been extensively investigated and Alg is generally considered as biocompatible. Nevertheless, it is important to note that the Ca^{2+} concentration may have an impact on SV-HUC-1 cells, considering that it is involved in numerous cellular processes such as cell adhesion.

As evidenced in section 5.5.1.1., the extracts derived from BACs-loaded Ca-beads did not exhibit cytotoxicity towards 3T3 cells at any tested concentration (Figure 5.3a). In case of SV-HUC-1 cells, the inhibitory effect on cell growth increased with the concentration of the Ca-beads extract (Figure 5.4). Hence, SV-HUC-1 cells were inhibited by high concentrations of extract, whereas for 3T3 cells the extract of BACs-loaded Ca-beads was not cytotoxic. To further investigate this phenomenon, we hypothesised whether the observed differences in cell viability could be attributed to the presence of Ca^{2+} or BACs in the extracts. It is also possible that these divergent outcomes were influenced by the specific cell types employed, which represented healthy cells but of different origins. Otherwise, the presence of BACs may be a contributing factor enhancing cellular viability.

A relevant consideration during the preparation of both extracts of Ca-beads, with and without BACs, was the observation of the colour of the pH indicator in the extraction media (Data not shown). The pH of both DMEM and F-12 culture media was determined by the concentration of hydrogen ions (H^+) present in the solution. Both media formulations incorporated $CaCl_2$ along with buffering agents, such as bicarbonate (HCO_3^-) and phosphate (HPO_4^-). Consequently, alterations in the concentration of Ca^{2+} could indirectly affect the pH value by reducing the

buffering capacity of the media. For instance, Ca^{2+} may interact with phosphate ions to form insoluble $Ca_3(PO_4)_2$, which could result in the removal of phosphate ions from the solution and a decrease in the buffering capacity. Similarly, Ca^{2+} might react with bicarbonate ions to form $CaCO_3$, which could also lead to a reduction in the buffering capacity of the media.

Therefore, the colour of the extract was yellowish when empty Ca-beads were utilized, indicating a more acidic pH compared to BACs-loaded Ca-beads. The observed decrease in cell viability of SV-HUC-1 cells when exposed to the Ca-beads extract could be attributed to a lower pH value of the extract, which may be suboptimal for the incubation of SV-HUC-1 cells and thus impeded their survivability. In contrast, the pH of the BACs extract appeared to be more neutral and closer to the optimal range, which might explain why cell survivability was not compromised in this case. We postulated two hypotheses to explain these contrasting effects: first, that the presence of Ca^{2+} in the extraction media acidified the environment, leading to reduced growth of SV-HUC-1 cells; and second, that BACs in the extract neutralized the acidic effect of Ca^{2+} and promoted metabolic activity of 3T3 cells. It is important to note that the culture requirements for SV-HUC-1 cells might be more complex compared to those of 3T3 cells, demanding additional requisitions for their optimal growth.

The findings revealed the potential cytotoxicity of the empty Ca-beads extract towards T24 cells (Figure 5.4). Both concentrated and 10% diluted extract exhibited cytotoxic effects on T24 cells, suggesting that the observed cytotoxicity could be attributed to the presence of Ca^{2+} in the extract. The effects of Ca^{2+} on cell growth and proliferation are known to be influenced by the concentration of Ca^{2+} and specific cellular conditions, such as the stage of cell growth and differentiation. Interestingly, our results indicated that SV-HUC-1 cells exhibited lower cytotoxicity to higher concentrations of Ca^{2+} compared to T24 cells. The inhibitory effect of the extract was more pronounced in T24 cells than in SV-HUC-1 cells at higher Ca^{2+} concentrations. However, at lower extract concentration, SV-HUC-1 cells viability was more compromised. Metabolic activity of SV-HUC-1 cells was promoted at the lowest extract concentration (0.1%) compared to T24 cells.

Figure 5.4: Diluted extracts obtained from Alg beads prepared with $CaCl_2$ 2% (w/w) tested on SV-HUC-1 cells (purple) and T24 cancer cells (blue) after 24h of incubation

Figure 5.5: Images of SV-HUC-1 and T24 cells captured after 24h of incubation with extraction media (control) or Ca-beads extract using an inverted, phase contrast microscope

5.6.2.2 Empty beads prepared with $ZnCl_2$ 2% (w/w)

The cell viability results regarding the extracts of Zn-beads prepared with $ZnCl_2$ 2% (w/w) after 24h incubation with SV-HUC-1 and T24 cells are exhibited in Figure 5.6. Hence, citotoxicity of SV-HUC-1 cells towards the extracts of Zn-beads was evidenced to be poor or negligible, with only the lowest concentrations of extract (1% and 0.1%) demonstrating slightly harmful effects. Similarly, the cellular viability of T24 cells was also impaired or non-existent across all the extract concentrations tested, except for the lowest concentration (0.1%) where metabolic activity surpassed that of the control (Figure 5.6). In fact, this response has been previously reported and it is known as "hormesis". Hormesis refers to the phenomenon designated by a "low-dose stimulation and high-dose inhibition". Therefore, it occurs when cells are exposed to a mild environmental stress, which leads to adaptive stress. It gives rise to increased cell growth and development in order to compensate the imbalance in homeostasis caused by the exposure to feeble doses of stressor stimuli [87].

It is worth noting that the cytotoxicity of Zn^{2+} has been proved to be more pronounced in rapidly dividing cells, such as cancerous cells, in comparison to quiescent or normal cells [88]. Our results aligned with this finding as SV-HUC-1 cells survived under the extract 1% concentration, whereas T24 cells did not. However, the lowest concentration of Zn^{2+} enhanced the viability of T24 cells over that of the control sample (without extract).
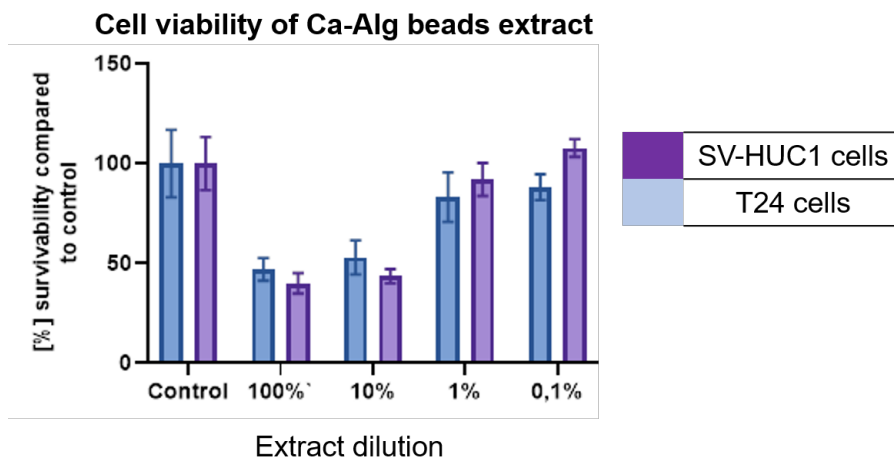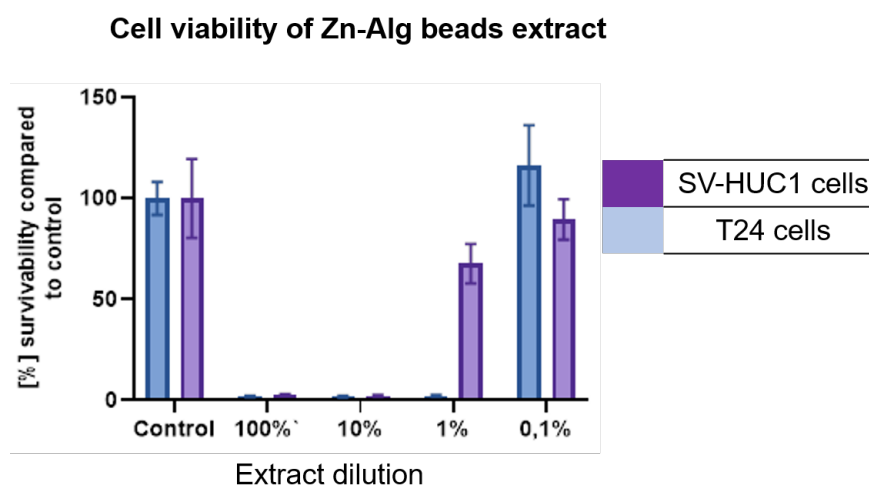
Figure 5.6: Diluted extracts obtained from Alg beads prepared with $ZnCl_2$ 2% (w/w) tested on SV-HUC-1 cells (purple) and T24 cells (blue) after 24h of incubation

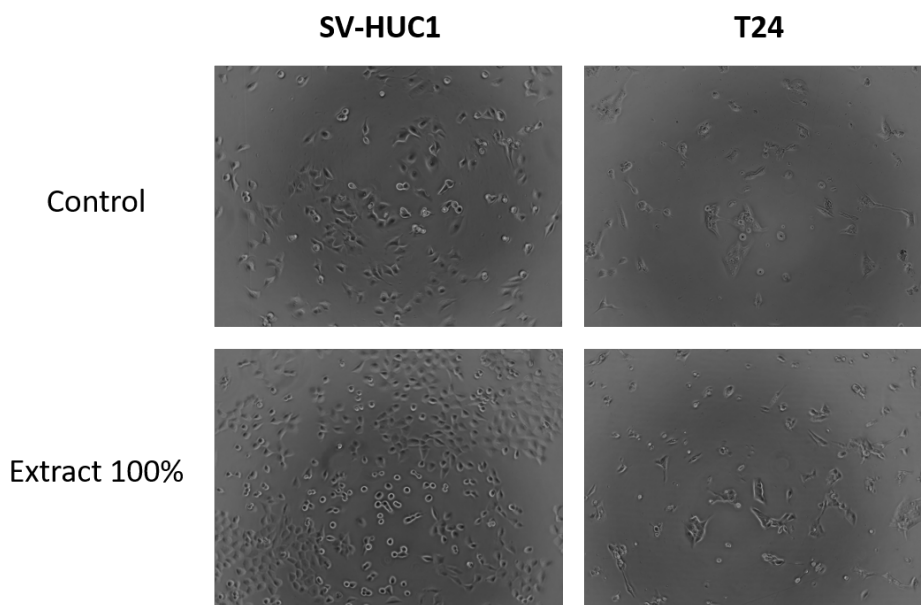### 5.6.2.3   BACs 10% beads prepared with $ZnCl_2$ 2% (w/w)

Figure 5.7 exposes MTT results of T24 and SV-HUC-1 cells towards the extracts derived from BACs 10% beads prepared with $ZnCl_2$ 2% (w/w) after 24h incubation. Figure 5.8 displays images of these cells captured after 24h of incubation with extraction media (control), Zn-beads extract and BACs-loaded Zn-beads extract by means of an inverted, phase contrast microscope.

The results in Figure 5.7 and Figure 5.8a revealed similar outcomes regardless of the presence of BACs in the extracts of Zn-beads. Hence, cellular viability of SV-HUC-1 cells was also negligible when BACs were included in the extract formulation. Only the lowest concentration (0.1%) allowed for a limited survival of cells compared to the control.

Likewise, cellular viability of T24 cells was null regardless of the extract concentration (Figure 5.7 and 8b). However, at the lowest extract concentration (0.1%), cell viability exceeded that of the control value, likely as a result of hormesis. Moreover, the presence of BACs in the extract further promoted cellular metabolic activity compared to Zn^{2+} alone.

Zn^{2+} exhibited more pronounced cytotoxicity in T24 carcinoma than in SV-HUC-1 cells, although the lowest concentration of BACs-loaded Zn-beads enhanced T24 cells viability over the control sample (Figures 5.7-5.8). Similarly, the effects of Zn^{2+} on T24 cell viability were comparable to the ones that Cu^{2+} displayed (Figure 5.3).

The anti-cancer effects of Zn^{2+} in combination with polyphenols have been investigated, yielding in diverse and contradictory results. Some studies have evidenced Zn^{2+} anti-cancer effects, whereas others have suggested that it promotes cancer progression as explained in the following lines. For instance, it is known that the Zn^{2+} uptake and cellular accumulation is particularly diminished in liver, pancreas and prostate cancerous cells, which are intolerant to physiological concentrations of Zn^{2+} [89]. Thus, any approach that leads to an increase in Zn^{2+} levels in cancer cells may be a potentially effective cancer treatment.

Conversely, Bobrowska et al. determined that the supplementation of resveratrol and Zn^{2+} in rats with induced mammary cancer resulted in accelerated tumorigenesis [90]. Supplementation with resveratrol and Zn^{2+} remarkably increased the rate of carcinogenesis and the number of mammary tumours [91]. Additionally, co-supplementation of Zn^{2+} with apigenin, epicatechin and naringenin (flavonoids) promoted the progress of carcinogenesis [92].

The synergistic effect of EGCG and Zn^{2+} on PC-3 prostate carcinoma has been proved by Sun et al. and Yang et at. [93, 94]. Moreover, EGCG may enable Zn^{2+} transport across cell membrane and Zn^{2+}-EGCG complex might damage proteins more effectively [95, 96]. In addition, Zn^{2+}-curcumin complexes exhibited enhanced antioxidant, anti-inflammatory and anti-cancer properties [97]. The anti-cancer activity of Zn^{2+}-curcumin complexes on T-24 cells has been proved and attributed to mitochondrial dysfunction [98]. Zn^{2+}-quercetin complexes have shown both anti-cancer and anti-metastatic effects on human bladder BFTC-905 carcinoma [99].

It is important to notice that the effects of polyphenols on cancerous cells exhibit variability based on the specific compound and concentration. Consequently, the anti-cancer effects of Zn^{2+} can also vary depending on the cancer type and the concentration employed, considering both the polyphenol under investigation and the Zn^{2+} itself.

Likewise, if BACs also promoted Zn^{2+} transport and accumulation on SV-HUC-1 cells, leading to protein damage, it was plausible that the low cellular viability observed is a result of the tolerance of these cells towards Zn^{2+} [95]. Hence, additional MTT assays could be performed using distinct cell lines such as 3T3 cells in order to determine whether the extract of Zn-beads exhibited general toxicity towards healthy cells or only specifically towards SV-HUC-1 cells.
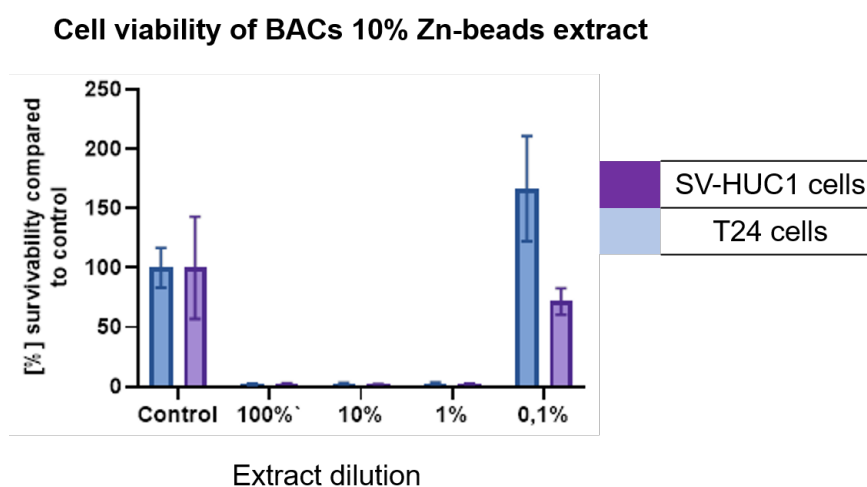

Figure 5.7: Diluted extracts from BACs 10% beads prepared with $ZnCl_2$ 2% (w/w) tested on SV-HUC-1 cells (purple) and T24 cells (blue) for 24h
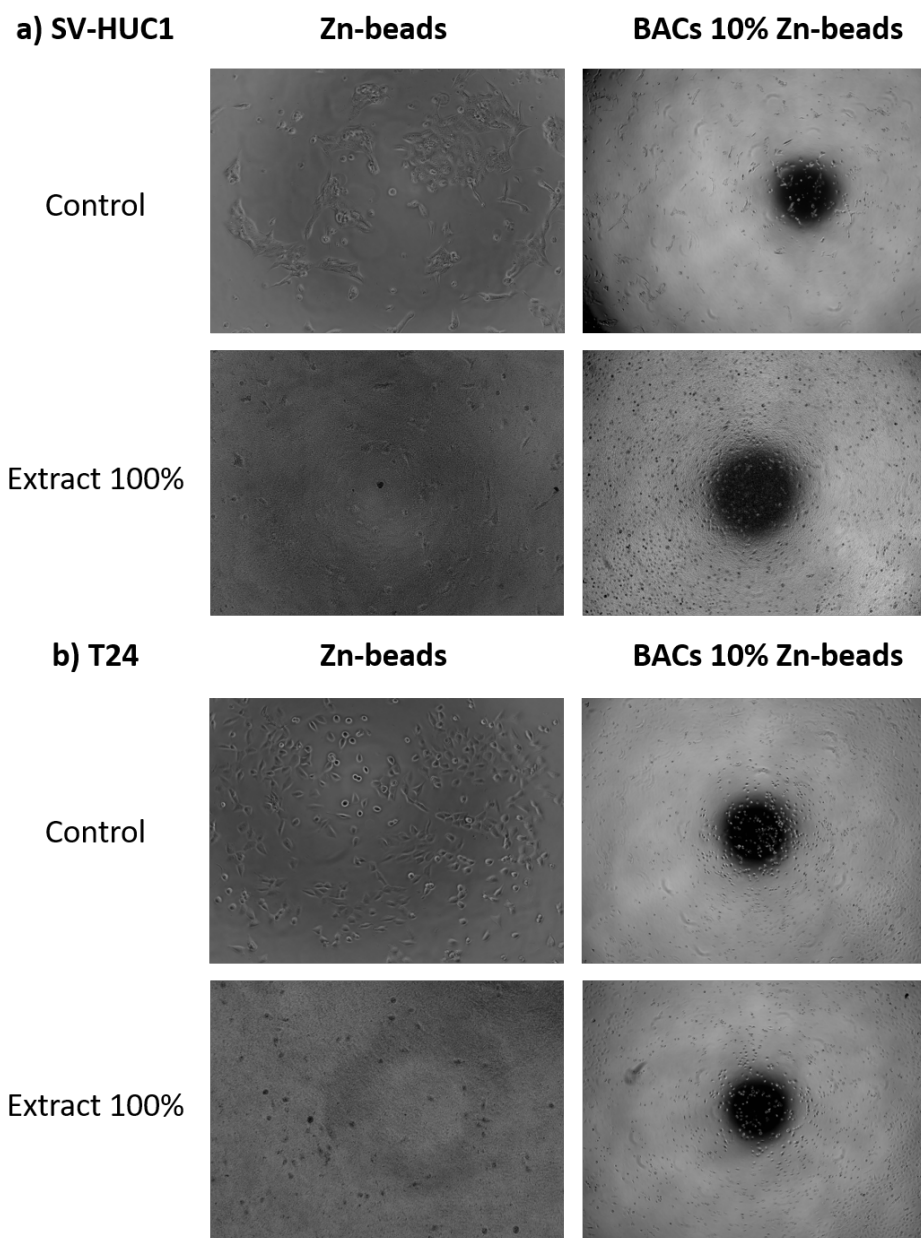
Figure 5.8: Images of a) SV-HUC-1 and b) T24 cells captured after 24h of incubation with Zn-beads extract, BACs 10% Zn-beads extract or with extraction media (control) using an inverted, phase contrast microscope

5.7   Conclusions Biomedical application

- In regard to *in vitro* studies with cell cultures, neither the cell growth nor proliferation of 3T3 cells were adversely affected by the presence of Ca^{2+} or BACs after 24h, although the cytotoxicity of polyphenols was highly dependent on the specific compound and its concentration. The concentrated extract of Ca-beads and the 10% dilution demonstrated cytotoxic effects on SV-HUC-1 cells. The inhibitory effect on cell growth increased with higher concentrations of Ca-beads extract. Nevertheless, the lowest concentration of both extracts (0.1%) promoted cellular metabolic activity. The observed decrease in cell viability of SV-HUC-1 cells when exposed to the Ca-beads extract could be attributed to the lower pH value of the extract, which may not be optimal for the incubation of SV-HUC-1 cells and thus, impeded their survivability.

- The viability of T24 cells was compromised by both extracts, derived from Ca-beads and from BACs 10% Ca-beads after 24h of incubation. The presence of BACs did not lead to a higher cytotoxicity. The possibility of a synergistic interaction between the polyphenols and Ca^{2+} was suggested although Ca-beads extract reduced T24 cells viability itself. The cytotoxicity towards T24 cells was more pronounced with increasing Ca^{2+} concentrations, indicating that the observed cytotoxicity may be attributed to the presence of Ca^{2+}. The cytotoxic action was selective towards cancerous cells in case of BACs 10% beads. However, SV-HUC-1 cells viability also decreased at high concentrations of empty Ca-beads extract likely due to the pH value of the extract.

- The viability of 3T3 cells was highly compromised at the lowest concentration of BACs 10% Cu-beads extract. Interestingly, at lower concentrations, cell viability exceeded the control value, likely led by the hormesis phenomenon. T24 cells exhibited a higher tolerance limit for Cu^{2+} concentration compared to 3T3 fibroblasts. Remarkably, at lower concentrations, the Cu^{2+} extract not only lacked toxicity but also promoted metabolic activity of cancerous cells. Indeed, Cu^{2+} was already known to contribute to angiogenesis, proliferation and metastasis of cancer cells [86].

- The viability of SV-HUC-1 cells was highly compromised at the lowest concentration of Zn-beads extract, diminishing further in the presence of BACs. When utilized as crosslinking agent, Zn^{2+} displayed greater toxicity than Ca^{2+} but less than Cu^{2+} towards healthy, non-cancerous cells. Similarly, the metabolic

activity of T24 cells was low or negligible, except at the lowest concentration (0.1%) where metabolic activity surpassed that of the control. The presence of BACs in the extract further promoted cellular metabolic activity compared to Zn^{2+} alone. Additionally, Zn^{2+} exerted greater toxic effects toward cancerous T24 cells compared to SV-HUC-1 cells. These findings aligned with the fact that cytotoxicity of Zn^{2+} had been proved to be more pronounced in rapidly dividing cells, such as cancerous cells, in comparison to quiescent or normal cells [100].

- Generally, when employed as crosslinking cation, Zn^{2+} displayed greater cyto-toxicity toward cancerous T24 cells compared to Ca^{2+} and Cu^{2+}. Notably, the presence of Cu^{2+} in the extract resulted in increased viability of cancer cells in regard to healthy cells, whereas Zn^{2+} exhibited the same effect just at the lowest concentration. The potential anti-cancer effects of Zn^{2+} in combination with polyphenols should be further investigated, as already existing studies yielded contradictory conclusions. Hence, additional MTT assays could be performed using distinct cell lines such as 3T3 cells in order to determine whether the extract from Zn-beads exhibits general toxicity towards healthy cells or specif-ically affects SV-HUC-1 cells. This would contribute to a better understanding of the overall cytotoxicity profile and selectivity of the Zn-beads extract.

Bibliography

[1] Affairs, United Nations Department for Economic and Social, *World Population Prospects 2022: Summary of results.* [S.l.]: UNITED NATIONS, 2023.

[2] J. Gao, J. M. Karp, R. Langer, and N. Joshi, "The future of drug delivery," *Chemistry of Materials*, vol. 35, no. 2, pp. 359–363, 2023.

[3] G. St. J. Perrott and D.F. Holland, "Population trends and problems of public health," *The Milbank quarterly*, vol. 83, no. 4, pp. 569–608, 2005.

[4] M. Rahman, A. Khatun, L. Liu, and B. J. Barkla, "Brassicaceae Mustards: Traditional and Agronomic Uses in Australia and New Zealand," *Molecules (Basel, Switzerland)*, vol. 23, no. 1, 2018.

[5] R. Dang, H. Guan, and C. Wang, "Sinapis semen: A review on phytochemistry, pharmacology, toxicity, analytical methods and pharmacokinetics," *Frontiers in pharmacology*, vol. 14, p. 1113583, 2023.

[6] J. Lietzow, "Biologically active compounds in mustard seeds: A toxicological perspective," *Foods (Basel, Switzerland)*, vol. 10, no. 9, 2021.

[7] S. W. Cui, M. A. N. Eskin, Y. Wu, and S. Ding, "Synergisms between yellow mustard mucilage and galactomannans and applications in food products–a mini review," *Advances in colloid and interface science*, vol. 128-130, pp. 249–256, 2006.

[8] B. Krasnodebska-Ostrega, M. Sadowska, E. Biaduń, R. Mazur, and J. Kowalska, "Sinapis alba as a useful plant in bioremediation - studies of defense mechanisms and accumulation of as, tl and pges," *International journal of phytoremediation*, vol. 24, no. 14, pp. 1475–1490, 2022.

[9] P. Chhetri, L. M. Dandurand, and I. Popova, "Control of globodera pallida using sinapis alba or 4-hydroxybenzyl alcohol with the trap crop solanum sisymbriifolium or the biofumigant brassica juncea seed meal extract," *Plant disease*, vol. 107, no. 5, pp. 1491–1498, 2023.

[10] K. Boomiraj, B. Chakrabarti, P. K. Aggarwal, R. Choudhary, and S. Chander, "Assessing the vulnerability of Indian mustard to climate change," *Agriculture, Ecosystems & Environment*, vol. 138, no. 3-4, pp. 265–273, 2010.

[11] V. A. de Castro, V. G. O. Duarte, D. A. C. Nobre, G. H. Silva, V. R. L. Constantino, F. G. Pinto, W. R. Macedo, and J. Tronto, "Plant growth regulation by seed coating with films of alginate and auxin-intercalated layered double hydroxides," *Beilstein journal of nanotechnology*, vol. 11, pp. 1082–1091, 2020.

[12] F. Artusio, D. Casà, M. Granetto, T. Tosco, and R. Pisano, "Alginate nanohydrogels as a biocompatible platform for the controlled release of a hydrophilic herbicide," *Processes*, vol. 9, no. 9, p. 1641, sep 2021.

[13] N. Işıklan, "Controlled release study of carbaryl insecticide from calcium alginate and nickel alginate hydrogel beads," *Journal of Applied Polymer Science*, vol. 105, no. 2, pp. 718–725, 2007.

[14] Y.-L. Xie, W. Jiang, F. Li, Y. Zhang, X.-Y. Liang, M. Wang, X. Zhou, S.-Y. Wu, and C.-H. Zhang, "Controlled release of spirotetramat using starch-chitosan-alginate-encapsulation," *Bulletin of environmental contamination and toxicology*, vol. 104, no. 1, pp. 149–155, 2020.

[15] C. Fan, Y. Liu, M. Dang, Y. Liang, P. Feng, F. Wei, L. Fu, C. Xu, and B. Lin, "Polysaccharides synergistic boosting drug loading for reduction pesticide dosage and improve its efficiency," *Carbohydrate polymers*, vol. 297, p. 120041, 2022.

[16] Y. Du, Q. Zhang, M. Yu, B. Jiao, F. Chen, and M. Yin, "Sodium alginate-based composite microspheres for controlled release of pesticides and reduction of adverse effects of copper in agricultural soils," *Chemosphere*, vol. 313, p. 137539, 2023.

[17] S. Babaei, D. Kahrizi, I. Nosratti, N. Karimi, E. Arkan, and M. B. Tahir, "Preparation and characterization of chloridazon-loaded alginate/chitosan

nanocapsules," *Cellular and molecular biology (Noisy-le-Grand, France)*, vol. 68, no. 3, pp. 34–42, 2022.

[18] Y. Bashan, L. E. de Bashan, S. R. Prabhu, and J.-P. Hernandez, "Advances in plant growth-promoting bacterial inoculant technology: formulations and practical perspectives (1998–2013)," *Plant and Soil*, vol. 378, no. 1-2, pp. 1–33, 2014.

[19] M. Vinceković, S. Jurić, E. Đermić, and S. Topolovec-Pintarić, "Kinetics and mechanisms of chemical and biological agents release from biopolymeric microcapsules," *Journal of agricultural and food chemistry*, vol. 65, no. 44, pp. 9608–9617, 2017.

[20] R. Saberi Riseh, Y. A. Skorik, V. K. Thakur, M. Moradi Pour, E. Tamanadar, and S. S. Noghabi, "Encapsulation of plant biocontrol bacteria with alginate as a main polymer material," *International journal of molecular sciences*, vol. 22, no. 20, 2021.

[21] E. N. Shcherbakova, A. V. Shcherbakov, P. Rots, L. N. Gonchar, S. A. Mulina, L. M. Yahina, Y. Lactionov, and V. K. Chebotar, "Inoculation technology for legumes based on alginate encapsulation: 554.0kb," 2018.

[22] D. Skrzypczak, Ł. Jarzembowski, G. Izydorczyk, K. Mikula, V. Hoppe, K. A. Mielko, N. Pudełko-Malik, P. Młynarz, K. Chojnacka, and A. Witek-Krowiak, "Hydrogel alginate seed coating as an innovative method for delivering nutrients at the early stages of plant growth," *Polymers*, vol. 13, no. 23, 2021.

[23] K. Mikula, D. Skrzypczak, B. Ligas, and A. Witek-Krowiak, "Preparation of hydrogel composites using Ca^{2+} and Cu^{2+} ions as crosslinking agents," *SN Applied Sciences*, vol. 1, no. 6, 2019.

[24] A. S. Prasad, *Biochemistry of Zinc*, ser. Biochemistry of the Elements Ser. New York, NY: Springer, 2013, vol. 11. [Online]. Available: https://ebookcentral.proquest.com/lib/kxp/detail.action?docID=6583565

[25] P. K. Hepler, "Calcium: a central regulator of plant growth and development," *The Plant cell*, vol. 17, no. 8, pp. 2142–2155, 2005.

[26] G. M. Shaban and H. M. El-Komy, "Survival and proliferation of alginate encapsulated Trichoderma spp. in Egyptian soil in comparison with allyl alcohol soil fumigation," *Mycopathologia*, vol. 151, no. 3, pp. 139–146, 2001.

[27] Q. Qi, C. Fan, H. Wu, L. Sun, and C. Cao, "Preparation of trichoderma asperellum microcapsules and biocontrol of cucumber powdery mildew," *Microbiology spectrum*, vol. 11, no. 3, p. e0508422, 2023.

[28] D. Kudasova, B. Mutaliyeva, K. Vlahoviček-Kahlina, S. Jurić, M. Marijan, S. V. Khalus, A. V. Prosyanik, S. Šegota, N. Španić, and M. Vinceković, "Encapsulation of synthesized plant growth regulator based on copper(ii) complex in chitosan/alginate microcapsules," *International journal of molecular sciences*, vol. 22, no. 5, 2021.

[29] S. A. Ekanayake and P. I. Godakumbura, "Synthesis of a dual-functional nanofertilizer by embedding zno and cuo nanoparticles on an alginate-based hydrogel," *ACS omega*, vol. 6, no. 40, pp. 26 262–26 272, 2021.

[30] M. B. McBride and D. R. Bouldin, "Long-term reactions of copper(ii) in a contaminated calcareous soil," *Soil Science Society of America Journal*, vol. 48, no. 1, pp. 56–59, 1984.

[31] Hazra, G.C., Mandal, P. and Mandal, L.N, "Distribution of zinc fractions and their transformation in rice soils," *Plant and Soil*, vol. 104, no. 2, pp. 175–181, 1987. [Online]. Available: http://www.jstor.org/stable/42936869

[32] Beata Draszawka-Bołzan, *World news of Natural Sciences*, 2017.

[33] C. Gong and R. J. Donahoe, "An experimental study of heavy metal attenuation and mobility in sandy loam soils," *Applied Geochemistry*, vol. 12, no. 3, pp. 243–254, 1997.

[34] J. Kónya, N. M. Nagy, and K. Szabó, "The study of ion exchange processes in systems of zinc(II)-calcium-soils by a radioisotopic tracer method," *Reactive Polymers, Ion Exchangers, Sorbents*, vol. 7, no. 2-3, pp. 203–209, 1988.

[35] R. Prasad, Y. Shivay, and D. Kumar, "Interactions of Zinc with Other Nutrients in Soils and Plants -A Review," vol. 12, pp. 16–26, 2016.

[36] B. A. Rather, I. R. Mir, A. Masood, N. A. Anjum, and N. A. Khan, "Nitric Oxide Pre-Treatment Advances Seed Germination and Alleviates Copper-Induced Photosynthetic Inhibition in Indian Mustard," *Plants (Basel, Switzerland)*, vol. 9, no. 6, 2020.

[37] S. Gautam, K. Anjani, and N. Srivastava, "*In vitro* evaluation of excess copper affecting seedlings and their biochemical characteristics in *Carthamus tinctorius* L. (variety PBNS-12)," *Physiology and molecular biology of plants*, vol. 22, no. 1, pp. 121–129, 2016.

[38] X. Zhao, Y. Guo, and E. G. Papazoglou, "Screening flax, kenaf and hemp varieties for phytoremediation of trace element-contaminated soils," *Industrial Crops and Products*, vol. 185, p. 115121, 2022.

[39] X. Xin, F. Zhao, J. Y. Rho, S. L. Goodrich, B. S. Sumerlin, and Z. He, "Use of polymeric nanoparticles to improve seed germination and plant growth under copper stress," *The Science of the total environment*, vol. 745, p. 141055, 2020.

[40] R. Baczek-Kwinta, A. Baran, M. Simlat, J. Lang, M. Bieniek, and B. Florek, "Enrichment of different plant seeds with zinc and assessment of health risk of zn-fortified sprouts consumption," *Agronomy*, vol. 10, no. 7, p. 937, 2020.

[41] X. Li, Y. Yang, J. Zhang, L. Jia, Q. Li, T. Zhang, K. Qiao, and S. Ma, "Zinc induced phytotoxicity mechanism involved in root growth of triticum aestivum l," *Ecotoxicology and environmental safety*, vol. 86, pp. 198–203, 2012.

[42] H. Takahashi, T. K. Scott, and H. Suge, "Stimulation of root elongation and curvature by calcium," *Plant physiology*, vol. 98, no. 1, pp. 246–252, 1992.

[43] M. Monavari, S. Homaeigohar, R. Medhekar, Q. Nawaz, M. Monavari, K. Zheng, and A. R. Boccaccini, "A 3d-printed wound-healing material composed of alginate dialdehyde-gelatin incorporating astaxanthin and borate bioactive glass microparticles," *ACS applied materials & interfaces*, 2023.

[44] Z. Zheng, J. Qi, L. Hu, D. Ouyang, H. Wang, Q. Sun, L. Lin, L. You, and B. Tang, "A cannabidiol-containing alginate based hydrogel as novel multifunctional wound dressing for promoting wound healing," *Biomaterials advances*, vol. 134, p. 112560, 2022.

[45] P.-N. Chen, W.-H. Kuo, C.-L. Chiang, H.-L. Chiou, Y.-S. Hsieh, and S.-C. Chu, "Black rice anthocyanins inhibit cancer cells invasion via repressions of mmps and u-pa expression," *Chemico-biological interactions*, vol. 163, no. 3, pp. 218–229, 2006.

[46] A. C. Pedro, D. Granato, and N. D. Rosso, "Extraction of anthocyanins and polyphenols from black rice (*Oryza sativa* L.) by modeling and assessing their reversibility and stability," *Food Chemistry*, vol. 191, pp. 12–20, 2016.

[47] J. Tanaka, S. Nakamura, K. Tsuruma, M. Shimazawa, H. Shimoda, and H. Hara, "Purple rice (*Oryza sativa* L.) extract and its constituents inhibit VEGF-induced angiogenesis," *Phytotherapy research : PTR*, vol. 26, no. 2, pp. 214–222, 2012.

[48] X. Xia, W. Ling, J. Ma, M. Xia, M. Hou, Q. Wang, H. Zhu, and Z. Tang, "An anthocyanin-rich extract from black rice enhances atherosclerotic plaque stabilization in apolipoprotein e-deficient mice," *The Journal of nutrition*, vol. 136, no. 8, pp. 2220–2225, 2006.

[49] P. Pasukamonset, O. Kwon, and S. Adisakwattana, "Alginate-based encapsulation of polyphenols from *Clitoria ternatea* petal flower extract enhances stability and biological activity under simulated gastrointestinal conditions," *Food Hydrocolloids*, vol. 61, pp. 772–779, 2016.

[50] B. Reig-Vano, B. Tylkowski, X. Montané, and M. Giamberini, "Alginate-based hydrogels for cancer therapy and research," *International journal of biological macromolecules*, vol. 170, pp. 424–436, 2021.

[51] H. Yuan, C. Guo, L. Liu, L. Zhao, Y. Zhang, T. Yin, H. He, J. Gou, B. Pan, and X. Tang, "Progress and prospects of polysaccharide-based nanocarriers for oral delivery of proteins/peptides," *Carbohydrate polymers*, vol. 312, p. 120838, 2023.

[52] S. L. Tomić, M. M. Babić Radić, J. S. Vuković, V. V. Filipović, J. Nikodinovic-Runic, and M. Vukomanović, "Alginate-Based Hydrogels and Scaffolds for Biomedical Applications," *Marine drugs*, vol. 21, no. 3, 2023.

[53] M. G. Funaro, K. V. Nemani, Z. Chen, Z. M. Bhujwalla, K. E. Griswold, and B. Gimi, "Effect of alginate microencapsulation on the catalytic efficiency andiin vitro/ienzyme-prodrug therapeutic efficacy of cytosine deaminase and of recombinantie. coli/iexpressing cytosine deaminase," *Journal of Microencapsulation*, vol. 33, no. 1, pp. 64–70, dec 2015. [Online]. Available: https://doi.org/10.3109%2F02652048.2015.1115902

[54] Y. Xie, S. C. R. Kollampally, M. Jorgensen, and X. Zhang, "Alginate microfibers as therapeutic delivery scaffolds and tissue mimics," *Experimental biology and medicine (Maywood, N.J.)*, vol. 247, no. 23, pp. 2103–2118, 2022.

[55] S. V. Bhujbal, P. de Vos, and S. P. Niclou, "Drug and cell encapsulation: Alternative delivery options for the treatment of malignant brain tumors," *Advanced Drug Delivery Reviews*, vol. 67-68, pp. 142–153, apr 2014.

[56] J. K. Gandhi, E. C. Opara, and E. M. Brey, "Alginate-based strategies for therapeutic vascularization," *Therapeutic Delivery*, vol. 4, no. 3, pp. 327–341, mar 2013.

[57] K. Y. Lee and D. J. Mooney, "Alginate: Properties and biomedical applications," *Progress in Polymer Science*, vol. 37, no. 1, pp. 106–126, jan 2012.

[58] A. Gonzalez-Pujana, G. Orive, J. L. Pedraz, E. Santos-Vizcaino, and R. M. Hernandez, "Alginate microcapsules for drug delivery," in *Alginates and their biomedical applications, Springer Series in Biomaterials Science and Engineering*. Elsevier Ltd, 2012, vol. 11, pp. 67–100.

[59] A. Froelich, E. Jakubowska, M. Wojtyłko, B. Jadach, M. Gackowski, P. Gadziński, O. Napierała, Y. Ravliv, and T. Osmałek, "Alginate-based materials loaded with nanoparticles in wound healing," *Pharmaceutics*, vol. 15, no. 4, 2023.

[60] L. Wei, J. Tan, L. Li, H. Wang, S. Liu, J. Chen, Y. Weng, and T. Liu, "Chitosan/Alginate Hydrogel Dressing Loaded FGF/VE-Cadherin to Accelerate Full-Thickness Skin Regeneration and More Normal Skin Repairs," *International journal of molecular sciences*, vol. 23, no. 3, 2022.

[61] P. Qin, J. Tang, D. Sun, Y. Yang, N. Liu, Y. Li, Z. Fu, Y. Wang, C. Li, X. Li, Y. Zhang, Y. Liu, S. Wang, J. Sun, Z. Deng, L. He, Y. Wang, and X. Yang, "Zn^{2+} Cross-Linked Alginate Carrying Hollow Silica Nanoparticles Loaded with RL-QN15 Peptides Provides Promising Treatment for Chronic Skin Wounds," *ACS applied materials & interfaces*, vol. 14, no. 26, pp. 29 491–29 505, 06 2022.

[62] L. Zhao, S. Yin, and Z. Ma, "Ca^{2+}-Triggered pH-Response Sodium Alginate Hydrogel Precipitation for Amplified Sandwich-Type Impedimetric Immunosensor of Tumor Marker," *ACS sensors*, vol. 4, no. 2, pp. 450–455, 2019.

[63] S. S. Lee, H. Kim, D. K. Sohn, J. B. Eom, Y. S. Seo, H. M. Yoon, and Y. Choi, "Indocyanine green-loaded injectable alginate hydrogel as a marker for precision cancer surgery," *Quantitative Imaging in Medicine and Surgery*, vol. 10, no. 3, pp. 779–788, 2020.

[64] M. Danesh-Doust, R. Irajirad, F. Vaziri Nezamdoust, S. Khademi, and A. Montazerabadi, "Triptorelin peptide conjugated alginate coated gold nanoparticles as a new contrast media for targeted computed tomography imaging of cancer cells," *Cell journal*, vol. 25, no. 2, pp. 126–134, 2023.

[65] X.-H. Do, T. D. Nguyen, T. T. H. Le, T. T. To, T. V. K. Bui, N. H. Pham, K. Lam, T. M. N. Hoang, and P. T. Ha, "High Biocompatibility, MRI Enhancement, and Dual Chemo- and Thermal-Therapy of Curcumin-Encapsulated Alginate/Fe$_3$O$_4$ Nanoparticles," *Pharmaceutics*, vol. 15, no. 5, 2023.

[66] S. P. M. Bohari, D. W. L. Hukins, and L. M. Grover, "Effect of calcium alginate concentration on viability and proliferation of encapsulated fibroblasts," *Biomedical materials and engineering*, vol. 21, no. 3, pp. 159–170, 2011.

[67] A. Hazafa, M. O. Iqbal, U. Javaid, M. B. K. Tareen, D. Amna, A. Ramzan, S. Piracha, and M. Naeem, "Inhibitory effect of polyphenols (phenolic acids, lignans, and stilbenes) on cancer by regulating signal transduction pathways: a review," *Clinical & translational oncology: official publication of the Federation of Spanish Oncology Societies and of the National Cancer Institute of Mexico*, vol. 24, no. 3, pp. 432–445, 2022.

[68] L. Shen, F. Zhang, R. Huang, J. Yan, and B. Shen, "Honokiol inhibits bladder cancer cell invasion through repressing SRC-3 expression and epithelial-mesenchymal transition," *Oncology letters*, vol. 14, no. 4, pp. 4294–4300, 2017.

[69] A. Hazafa, K.-U. Rehman, N. Jahan, and Z. Jabeen, "The role of polyphenol (flavonoids) compounds in the treatment of cancer cells," *Nutrition and cancer*, vol. 72, no. 3, pp. 386–397, 2020.

[70] C. Marchetti, P. Gavazzo, and B. Burlando, "Epigallocatechin-3-gallate mobilizes intracellular Ca^{2+} in prostate cancer cells through combined Ca^{2+} entry and Ca^{2+}-induced Ca^{2+} release," *Life sciences*, vol. 258, p. 118232, 2020.

[71] A. Esteban-Fernández, I. Zorraquín-Peña, M. D. Ferrer, A. Mira, B. Bartolomé, D. González de Llano, and M. V. Moreno-Arribas, "Inhibition of oral pathogens adhesion to human gingival fibroblasts by wine polyphenols alone and in combination with an oral probiotic," *Journal of agricultural and food chemistry*, vol. 66, no. 9, 2018.

[72] E. Ranzato, S. Martinotti, V. Magnelli, B. Murer, S. Biffo, L. Mutti, and B. Burlando, "Epigallocatechin-3-gallate induces mesothelioma cell death via H_2O_2-dependent t-type Ca^{2+} channel opening," *Journal of cellular and molecular medicine*, vol. 16, no. 11, pp. 2667–2678, 2012.

[73] K.-W. Luo, W.-Y. Lung, Chun-Xie, X.-L. Luo, and W.-R. Huang, "EGCG inhibited bladder cancer T24 and 5637 cell proliferation and migration via PI3K/AKT pathway," *Oncotarget*, vol. 9, no. 15, pp. 12 261–12 272, 2018.

[74] K.-W. Luo, X.-H. Zhu, T. Zhao, J. Zhong, H.-C. Gao, X.-L. Luo, and W.-R. Huang, "EGCG Enhanced the Anti-tumor Effect of Doxorubicine in Bladder Cancer via NF-kB/MDM2/p53 Pathway," *Frontiers in cell and developmental biology*, vol. 8, p. 606123, 2020.

[75] C. Marchetti, S. Ribulla, V. Magnelli, M. Patrone, and B. Burlando, "Resveratrol induces intracellular Ca^{2+} rise via t-type Ca^{2+} channels in a mesothelioma cell line," *Life sciences*, vol. 148, pp. 125–131, 2016.

[76] J. A. Peterson, H. P. Doughty, A. J. Eells, T. A. Johnson, J. P. Hastings, C. M. Crowther, M. B. Andrus, and J. D. Kenealey, "The effects of 4'-esterified resveratrol derivatives on calcium dynamics in breast cancer cells," *Molecules (Basel, Switzerland)*, vol. 22, no. 11, 2017.

[77] S. Ossikbayeva, M. Khanin, Y. Sharoni, A. Trachtenberg, S. Tuleukhanov, R. Sensenig, S. Rom, M. Danilenko, and Z. Orynbayeva, "Curcumin and carnosic acid cooperate to inhibit proliferation and alter mitochondrial function of metastatic prostate cancer cells," *Antioxidants (Basel, Switzerland)*, vol. 10, no. 10, 2021.

[78] S. Pesakhov, M. Nachliely, Z. Barvish, N. Aqaqe, B. Schwartzman, E. Voronov, Y. Sharoni, G. P. Studzinski, D. Fishman, and M. Danilenko, "Cancer-selective cytotoxic Ca^{2+} overload in acute myeloid leukemia cells and attenuation of disease progression in mice by synergistically acting polyphenols curcumin and carnosic acid," *Oncotarget*, vol. 7, no. 22, pp. 31 847–31 861, 2016.

[79] B. J. Philips, C. H. Coyle, S. N. Morrisroe, M. B. Chancellor, and N. Yoshimura, "Induction of apoptosis in human bladder cancer cells by green tea catechins," *Biomedical research (Tokyo, Japan)*, vol. 30, no. 4, pp. 207–215, 2009.

[80] M. Bourhia, F. E. Laasri, S. I. Moussa, R. Ullah, A. Bari, S. Saeed Ali, A. Kaoutar, A. A. Haj Said, M. El Mzibri, G. Said, N. Khlil, and L. Benbacer, "Phytochemistry, Antioxidant Activity, Antiproliferative Effect, and Acute Toxicity Testing of Two Moroccan *Aristolochia* Species," *Evidence-based complementary and alternative medicine : eCAM*, vol. 2019, p. 9710876, 2019.

[81] T. Bacchetti, R. Campagna, D. Sartini, M. Cecati, C. Morresi, L. Bellachioma, E. Martinelli, G. Rocchetti, L. Lucini, G. Ferretti, and M. Emanuelli, "*C. spinosa* L. subsp. *rupestris* Phytochemical Profile and Effect on Oxidative Stress in Normal and Cancer Cells," *Molecules (Basel, Switzerland)*, vol. 27, no. 19, 2022.

[82] A. Bermúdez-Oria, G. Rodríguez-Gutiérrez, F. Rubio-Senent, M. Sánchez-Carbayo, and J. Fernández-Bolaños, "Antiproliferative activity of olive extract rich in polyphenols and modified pectin on bladder cancer cells," *Journal of medicinal food*, vol. 23, no. 7, pp. 719–727, 2020.

[83] D. C. Bassett, I. Madzovska, K. S. Beckwith, T. B. Melø, B. Obradovic, and P. Sikorski, "Dissolution of copper mineral phases in biological fluids and the controlled release of copper ions from mineralized alginate hydrogels," *Biomed. Mater.*, vol. 10, no. 1, 2014.

[84] T. Kučírková, M. Stiborek, M. Dúcka, J. Navrátilová, J. Bogdanović Pristov, A. Popović-Bijelić, S. Vojvodić, J. Preisler, V. Kanický, J. Šmarda, I. Spasojević, and P. Beneš, "Anti-cancer effects of wedelolactone: interactions with copper and subcellular localization," *Metallomics : integrated biometal science*, vol. 10, no. 10, pp. 1524–1531, 2018.

[85] D. Denoyer, S. Masaldan, S. La Fontaine, and M. A. Cater, "Targeting copper in cancer therapy: 'copper that cancer'," *Metallomics : integrated biometal science*, vol. 7, no. 11, pp. 1459–1476, 2015.

[86] Y. Li, "Copper homeostasis: Emerging target for cancer treatment," *Journal IUBMB life*, 2020.

[87] D. Bhakta-Guha and T. Efferth, "Hormesis: Decoding two sides of the same coin," *Pharmaceuticals (Basel, Switzerland)*, vol. 8, no. 4, pp. 865–883, 2015.

[88] S. Parveen, F. Arjmand, and D. K. Mohapatra, "Zinc(II) complexes of Pro-Gly and Pro-Leu dipeptides: synthesis, characterization, *in vitro* DNA binding and cleavage studies," *Journal of Photochemistry and Photobiology B: Biology*, vol. 126, pp. 78–86, 2013.

[89] P. Samutprasert, K. Chiablaem, C. Teeraseranee, P. Phaiyarin, P. Pukfukdee, P. Pienpinijtham, J. Svasti, T. Palaga, K. Lirdprapamongkol, and S. Wanich-wecharungruang, "Epigallocatechin gallate-zinc oxide co-crystalline nanoparticles as an anticancer drug that is non-toxic to normal cells," *RSC advances*, vol. 8, no. 14, pp. 7369–7376, 2018.

[90] B. Bobrowska-Korczak, D. Skrajnowska, K. Seidel, W. Bielecki, and B. Gadzinski, "Effect of zinc, copper and resveratrol supplementation on the urinary level of 15-hydroxyeicosatetraenoic acid at the early stage of breast cancer in rats," *Journal of biological regulators and homeostatic agents*, vol. 33, no. 1, pp. 19–28, 2019.

[91] B. Bobrowska-Korczak, D. Skrajnowska, and A. Tokarz, "The effect of dietary zinc-and polyphenols intake on DMBA-induced mammary tumorigenesis in rats," *Journal of biomedical science*, vol. 19, no. 1, p. 43, 2012.

[92] M. Jastrzebska, J. Giebułtowicz, A. K. Ciechanowicz, R. Wrzesień, W. Bielecki, and B. Bobrowska-Korczak, "Effect of polyphenols and zinc co-supplementation on the development of neoplasms in rats with breast cancer," *Foods (Basel, Switzerland)*, vol. 12, no. 2, 2023.

[93] S.-L. Sun, G.-Q. He, H.-N. Yu, J.-G. Yang, D. Borthakur, L.-C. Zhang, S.-R. Shen, and U. N. Das, "Free Zn^{2+} enhances inhibitory effects of EGCG on the growth of PC-3 cells," *Molecular nutrition & food research*, vol. 52, no. 4, pp. 465–471, 2008.

[94] J. Yang, H. Yu, S. Sun, L. Zhang, U. N. Das, H. Ruan, G. He, and S. Shen, "Mechanism of free Zn^{2+} enhancing inhibitory effects of EGCG on the growth of PC-3 cells: interactions with mitochondria," *Biological trace element research*, vol. 131, no. 3, pp. 298–310, 2009.

[95] A. E. Hagerman, R. T. Dean, and M. J. Davies, "Radical chemistry of epigallo-catechin gallate and its relevance to protein damage," *Archives of biochemistry and biophysics*, vol. 414, no. 1, pp. 115–120, 2003.

[96] H. Dabbagh-Bazarbachi, G. Clergeaud, I. M. Quesada, M. Ortiz, C. K. O'Sullivan, and J. B. Fernández-Larrea, "Zinc ionophore activity of quercetin and epigallocatechin-gallate: from Hepa 1-6 cells to a liposome model," *Journal of agricultural and food chemistry*, vol. 62, no. 32, pp. 8085–8093, 2014.

[97] S. Prasad and R. Lall, "Zinc-curcumin based complexes in health and diseases: An approach in chemopreventive and therapeutic improvement," *Journal of trace elements in medicine and biology : organ of the Society for Minerals and Trace Elements (GMS)*, vol. 73, p. 127023, 2022.

[98] L.-Q. Qin, C.-J. Liang, Z. Zhou, Q.-P. Qin, Z.-Z. Wei, M.-X. Tan, and H. Liang, "Mitochondria-localizing curcumin-cryptolepine Zn(II) complexes and their antitumor activity," *Bioorganic & medicinal chemistry*, vol. 30, p. 115948, 2021.

[99] Y.-H. Lee and P.-T. Tuyet, "Synthesis and biological evaluation of quercetin-zinc (ii) complex for anti-cancer and anti-metastasis of human bladder cancer cells," *In vitro cellular & developmental biology. Animal*, vol. 55, no. 6, pp. 395–404, 2019.

[100] B. J. Grattan and H. C. Freake, "Zinc and cancer: implications for LIV-1 in breast cancer," *Nutrients*, vol. 4, no. 7, pp. 648–675, 2012.

Chapter 6

General conclusions

- The preparation process of Alg hydrogels was optimized in regard to the concentration of Alg and metal chloride in the crosslinking bath, extrusion rate and set up. The time employed for beads maturation - 48h, was remarkably longer than the time employed in the most part of previous studies - 3-24h. Given that cations' diffusion towards the beads and the evolution of these systems is quite slow, we consider longer times to be necessary to reach the steady-state equilibrium.

- M-rich Alg was crosslinked with Ca^{2+}, Cu^{2+} or Zn^{2+} cations at diverse concentrations - 0.5%, 2% and 10% (w/w). The resulting hydrogels were characterized in terms of morphology (ESEM, SAXS and EXAFS), composition (TGA and WAXRD), mechanical properties and interactions between U and different cations (FT-IR).

- Based on the pH values of the crosslinking baths, when Ca^{2+} and Zn^{2+} are employed as crosslinking agents, only ionotropic gelation gives rise to beads' formation. Nevertheless, in case of Cu^{2+}, a hybrid system of ionotropic gelation and acid precipitation is proposed to lead to beads formation when $CuCl_2$ concentration is higher than 2% (w/w).

- The ESEM images revealed the wide variety of surfaces and inner morphologies of cryofractured beads, consistent with the distinct gelation mechanisms of each crosslinking cation. In all cases, Alg gelation was conditioned by both, the stiffness and permeability of the outer wall, as well as by the concentration of the crosslinker in the coagulation bath. Notably, Zn-based beads displayed a more defined core-shell structure, which enhanced their potential for future encapsulation applications.

- Ca-beads resulted to be the less resistant and the most ductile hydrogels. This elastoplastic behaviour, which progressively diminished with rising the metal load, was attributed to the ionic nature of Ca^{2+} interactions with Alg residues. Alternatively, Cu- and Zn-beads were the same resistant. Indeed, both have been proved to coordinate with Alg by the formation of strong covalent bonds. Zn-beads resulted to be more resistant than Ca-beads probably due to the employed Alg. Normally, Zn^{2+} displays the lowest Alg affinity. However, Ca^{2+} exhibits high affinity only toward G-rich Alg chains while Zn^{2+} interaction is unspecific. Zn^{2+} binds randomly to GG-blocks, MM-blocks and MG-blocks. Therefore, the interaction of Zn^{2+} with M-rich Alg was more favourable compared to Ca^{2+} due to the lack of Ca crosslinking points. Otherwise, the M/G ratio does not concern the level of crosslinking nor Zn^{2+} crosslinking points. Alternatively, Cu^{2+} complexation is always going to be strong due to the high Alg affinity and the lack of selectivity for the diverse U. The observations with ESEM supported the results of the mechanical analysis and pointed Cu- and Zn-based systems to have in general better mechanical properties than Ca-based ones. In the case of Zn-based hydrogels, increasing Zn^{2+} concentration led to a rise in rigidity and eventually on the strength. However, the highly inhomogeneous inner structure of Zn 10% beads resulted in scattered values of E and σ_b.

- In the instance of Cu-beads, increasing the Cu^{2+} concentration resulted in a greater E although the ultimate σ_b did not certainly change. As the pH value of the coagulation bath was under the Alg pKa, the interpretation of this hybrid acidic-ionic system may be challenging.

- The calculated number of uronic residues per Zn^{2+} ion was 2 regardless of the studied concentration. This evidences a homogenous coordination between Alg and this cation. The composition of Ca- and Cu-beads, on the other hand, was influenced by the concentration of the crosslinker. In the case of Ca-beads, the variation of beads' composition could be attributed to alterations in the Alg denticity as well as in the number of water molecules surrounding Ca^{2+} ions. In regard to Cu-beads, it is likely that the number of uronic residues per cation increased due to the combination of ionotropic and acidic gelation.

- The nature of cation-Alg interactions was studied by means of FT-IR. It was based on the comparison of the diverse $\Delta\nu$, which is the difference between the asymmetric and symmetric vibrational modes of carboxyl groups, of the crosslinked and uncrosslinked Na Alg. Therefore, the resulting values of $\Delta\nu(COO^-)_{complex} < \Delta\nu(COO^-)_{Na}$ pointed, according to the literature, to a "pseudo-bridged" unidentate interaction, in which one oxygen in the carboxyl interacts with the cation whereas the other oxygen establishes a hydrogen bond with a neighbouring hydroxyl group.

- SAXS research revealed that only the beads formed at lower cation concentrations had pristine gel rod-like structure. The degree of crystallinity was correlated to bead's size. Thus, the most crystalline structure was identified for the most compact Zn-beads.

- EXAFS technique was applied to analyse the coordination environment of Cu- and Zn-beads and determined that no oxide particles were generated during the beads manufacturing procedure. The coordination number was 4.3 ± 0.4 for Cu 0.5% beads, whereas each Zn^{2+} ion could coordinate 4 oxygens from an uronic residue as well as one molecule of water. These results are supported by Density Functional Calculations (DFT) on Cu^{2+} or Zn^{2+} and dimannuronate complexes, as well as by ICP results, which indicate that the optimal coordination state - the number of Alg units per mol of Zn^{2+}, is 2 regardless the $ZnCl_2$ concentration.

- These findings suggest that Zn-based hydrogels display features that might be useful for future innovative applications. Zn^{2+} gave rise to beads with superior mechanical qualities and a core-shell structure, which is very suitable for the microencapsulation of active compounds. Nonetheless, when compared to Ca^{2+} and Cu^{2+}, the gelation mechanism of Zn^{2+} has not been as frequently studied. Firstly, the lack of selectivity and creation of strong coordination interactions with the carboxyl groups of the Alg residues result in stronger and more stable hydrogels, in contrast with Ca^{2+}. In addition, the reduced affinity of Alg for Zn^{2+} may be seen as a benefit as the crosslinking process could be tuned more easily, potentially allowing the formation of more complex structures. Moreover, Zn^{2+} is an essential element, which is involved in many cellular processes such as cell growth, differentiation, and enhancement of wound healing.

- The stability of the grape seed phenolic extract (BACs) was evaluated under different conditions, including the exposure to an inert atmosphere and light. Neither the presence of an inert atmosphere nor light exposure demonstrated a significant impact on the stability of BACs.

- The HPLC method employed to determine the encapsulation efficiency (EE) of BACs demonstrated inconsistency. It revealed the formation of chelates between GA and $ZnCl_2$ at a concentration of 10% (w/w).

- EE xalculations based on thermogravimetric analysis (TGA) data led to an overestimation of the Alg content. This overestimation was attributed to the excess of cations that did not interact with the polymeric chains. Consequently, accurate calculation of the EE was not achievable.

- It is crucial to invest additional efforts in finding alternatives to accurately quantify the amount of BACs entrapped within the Alg beads, considering their complexation with Ca^{2+}, Cu^{2+} and Zn^{2+} in the crosslinking bath. Furthermore, investigating how BACs' complexation affects their encapsulation, whether it enhances or inhibits it, would be of significant interest.

- Release assays aimed to examine the behavior of BACs-loaded Ca-beads and the release tendencies. MS primarily identified small molecules. Peaks with m/z values greater than 350 were challenging to identify and were presumed to correspond to complex compositions of various BACs with water molecules, along with Na^+, Ca^{2+}, K^+ or NH_4^+ cations. As a result, the release of BACs was impeded and only small molecules, which have lower tendencies to form complexes and are easier to be released from the Alg matrix, were detected.

- Due to the complexation of BACs with cations, Alg may not be the ideal material for their encapsulation as the presence of crosslinking cations is necessary for the production of Alg beads.

- The application of Ca-, Cu- or Zn-beads to the soil solution resulted in a significant increase in the concentrations of the respective cations. The application of Zn-based beads led to an increase in the concentration of available Cu^{2+} and vice versa. However, the addition of Zn- and Cu-based beads reduced the availability of Ca^{2+} in the soil solution, suggesting ion exchange and adsorption processes. In literature, the pH of the soil system has been indicated to be an

important parameter for the retention of cationic metals, being maximum at pH values above 7.

- Incubation time of Alg beads in soil did not significantly affect the concentration of available cations. Nevertheless, the addition of perlite led to a significant increase of the amount of soluble cations compared to the control soil. Cu^{2+} showed the highest increase, followed by Zn^{2+}, whereas Ca^{2+} concentration not only displayed the lowest increase but also decreased over time when Ca-based beads were added to the soil mixture.

- The release of Cu^{2+} had the greatest impact on seed germination and sprout biomass, inhibiting germination and reducing sprout weight. Differently, Ca^{2+} and Zn^{2+} did not significantly affect mustard germination nor total biomass of the sprouts.

- The release of Cu^{2+} and Zn^{2+} from the beads hindered radicle development. Cu^{2+} almost completely inhibited radicle development, while Zn^{2+} had a progressive inhibitory effect with increased incubation time. In contrast, Ca^{2+} stimulated radicle elongation.

- Cu^{2+} stimulated the weight of cotyledons. However, after 9 days of incubation, the concentration of Cu^{2+} released from the beads exhibited phytotoxic effects. Ca^{2+} and Zn^{2+} did not have a significant effect regarding the biomass of cotyledons.

- In regard to *in vitro* studies with cell cultures, neither the cell growth nor proliferation of 3T3 cells were adversely affected by the presence of Ca^{2+} or BACs after 24h, although the cytotoxicity of polyphenols was highly dependent on the specific compound and its concentration. The concentrated extract of Ca-beads and the 10% dilution demonstrated cytotoxic effects on SV-HUC-1 cells. The inhibitory effect on cell growth increased with higher concentrations of Ca-beads extract. Nevertheless, the lowest concentration of both extracts (0.1%) promoted cellular metabolic activity. The observed decrease in cell viability of SV-HUC-1 cells when exposed to the Ca-beads extract could be attributed to the lower pH value of the extract, which may not be optimal for the incubation of SV-HUC-1 cells and thus, impeded their survivability.

187

- The viability of T24 cells was compromised by both extracts, derived from Ca-beads and from BACs 10% Ca-beads after 24h of incubation. The presence of BACs did not lead to a higher cytotoxicity. The possibility of a synergistic interaction between the polyphenols and Ca^{2+} was suggested although Ca-beads extract reduced T24 cells viability itself. The cytotoxicity towards T24 cells was more pronounced with increasing Ca^{2+} concentrations, indicating that the observed cytotoxicity may be attributed to the presence of Ca^{2+}. The cytotoxic action was selective towards cancerous cells in case of BACs 10% beads. However, SV-HUC-1 cells viability also decreased at high concentrations of empty Ca-beads extract likely due to the pH value of the extract.

- The viability of 3T3 cells was highly compromised at the lowest concentration of BACs 10% Cu-beads extract. Interestingly, at lower concentrations, cell viability exceeded the control value, likely led by the hormesis phenomenon. T24 cells exhibited a higher tolerance limit for Cu^{2+} concentration compared to 3T3 fibroblasts. Remarkably, at lower concentrations, the Cu^{2+} extract not only lacked toxicity but also promoted metabolic activity of cancerous cells. Indeed, Cu^{2+} was already known to contribute to angiogenesis, proliferation and metastasis of cancer cells.

- The viability of SV-HUC-1 cells was highly compromised at the lowest concentration of Zn-beads extract, diminishing further in the presence of BACs. When utilized as crosslinking agent, Zn^{2+} displayed greater toxicity than Ca^{2+} but less than Cu^{2+} towards healthy, non-cancerous cells. Similarly, the metabolic activity of T24 cells was low or negligible, except at the lowest concentration (0.1%) where metabolic activity surpassed that of the control. The presence of BACs in the extract further promoted cellular metabolic activity compared to Zn^{2+} alone. Additionally, Zn^{2+} exerted greater toxic effects toward cancerous T24 cells compared to SV-HUC-1 cells. These findings aligned with the fact that cytotoxicity of Zn^{2+} had been proved to be more pronounced in rapidly dividing cells, such as cancerous cells, in comparison to quiescent or normal cells.

- Generally, when employed as crosslinking cation, Zn^{2+} displayed greater cytotoxicity toward cancerous T24 cells compared to Ca^{2+} and Cu^{2+}. Notably, the presence of Cu^{2+} in the extract resulted in increased viability of cancer cells in regard to healthy cells, whereas Zn^{2+} exhibited the same effect just at the lowest concentration. The potential anti-cancer effects of Zn^{2+} in combination with polyphenols should be further investigated, as already existing studies yielded contradictory conclusions. Hence, additional MTT assays could be performed using distinct cell lines such as 3T3 cells in order to determine whether the extract from Zn-beads exhibits general toxicity towards healthy cells or specifically affects SV-HUC-1 cells. This would contribute to a better understanding of the overall cytotoxicity profile and selectivity of the Zn-beads extract.

Bibliography

UNIVERSITAT ROVIRA I VIRGILI
UNVEILING THE POTENTIAL: EXPLORING GELATION MECHANISMS IN ALGINATE BEADS CROSSLINKED WITH CALCIUM,
COPPER AND ZINC AND THEIR VERSATILE APPLICATIONS IN AGRICULTURE AND BIOMEDICINE
Belén Reig Vañó

UNIVERSITAT
ROVIRA i VIRGILI